From AUDITOR tractor experiment to WARTK fundamentals and IonSAT-tools

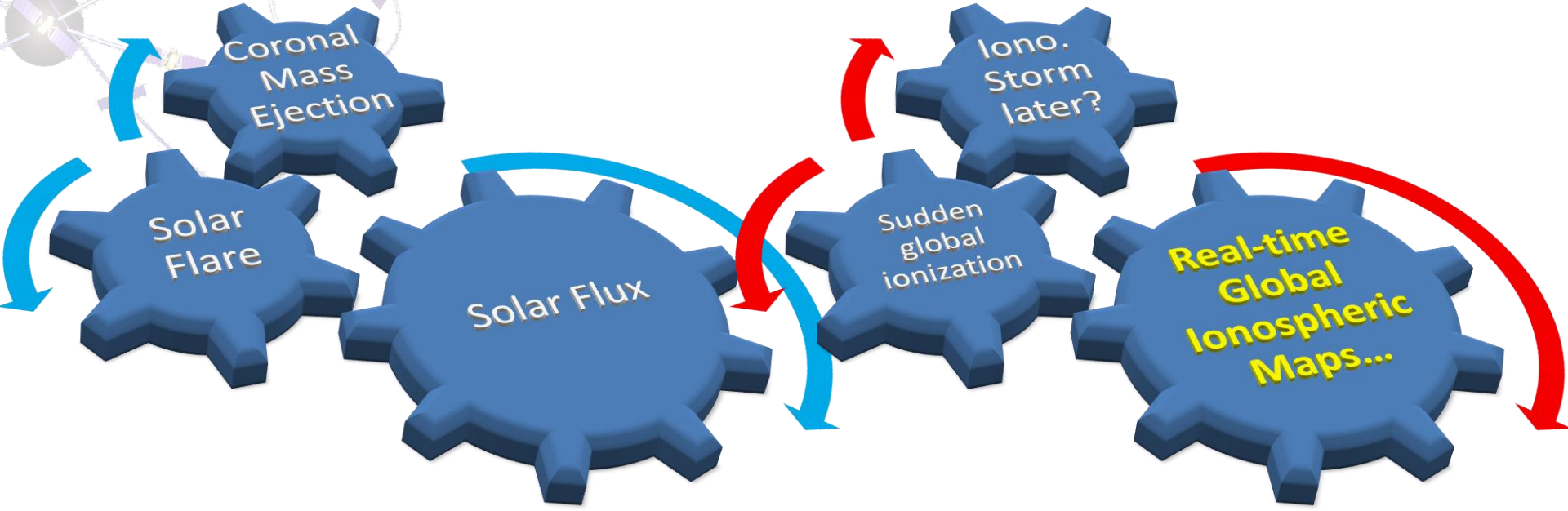

SIRGAS workshop, Mendoza, Argentina, Nov. 2017

Manuel Hernández-Pajares(1), Victoria Graffigna(2), David Roma-Dollase(3,1), Alberto García-Rigo(1)

(1) UPC-IonSAT, Barcelona, Spain
(2) UNLP, La Plata, Argentina
(3) UB-Dept. Electronics, Barcelona, Spain

[contact e-mail : manuel.hernandez@upc.edu]

Outline

Three on-going applications of the dual-frequency GNSS measurements available in real-time from hundreds of IGS permanent receivers will be presented and supported with new learning tools and exercises.

The corresponding synergic objectives are in the fields of Precise Farming, Space Weather and Real-Time Global Ionospheric Maps.

On-going applications of RT-IGS datastreams @ UPC-IonSAT

A) Space Weather: RT detection and estimation of the solar EUV flux rate, during solar flares with SISTED and GSFLAI GNSS indices. Maps of ionospheric scintillation (ROTI) and Medium Scale Travelling Ionospheric Disturbances (MSTID) activity proxies are also produced (started under MONITOR ESA project –see oral presentation of Alberto García-Rigo in ionospheric subsession-).

B) Precise farming: Improvement of precise RT positioning with Wide Area RTK technique and open-source software user receivers for the agriculture improvement in South Europe, where ionospheric modelling challenges, sparse GNSS networks and less funding availability for farmers coincide (ongoing AUDITOR H2020 EC project).

C) RT-GIMs: opportunities for combined IGS product

Layout:

1) [**Motivation**] Precise Agriculture (PA) presentation (EU AUDITOR experiment)

2) [**Background**]: Brief introduction to main identified points of the presentation:
   a) GPS fundamentals: pseudoranges and carrier phases (optional)
   b) Ionospheric electron content
   c) Wide Area Real-Time Kinematic
   d) The International GNSS Service (*optional*)

3) [**One efficient operative system**] Quick introduction to Linux (*optional*)

4) [**New tools for learning and research**] IonSAT Tools (IT), emulating Real-Time (RT) as much as possible (presented on the PA AUDITOR experiment):
   a) *gim2vtec.v2.scr*
   b) *gimrnx2stec.v2.scr*

5) [**IT application to ECLIPSE, FLARE & GSTORM scenarios**] (*optional*).

6) [**Example of RT GPS-ionospheric system**]: UPC-IonSAT since 2012.

7) [**Monitoring of co-seismic generated ionospheric signals]:** Application of RT ionospheric sounding for potential Tsunami warnings), with GNSS dense (Tohoku and mid earthquakes, EQ) and sparse networks (Chile 2015 EQ).

8) [**Conclusions**]

Layout:

1) [**Motivation**] Precise Agriculture (PA) presentation (EU AUDITOR experiment)

2) [**Background**]: Brief introduction to main identified points of the presentation:
   a) GPS fundamentals: pseudoranges and carrier phases (optional)
   b) Ionospheric electron content
   c) Wide Area Real-Time Kinematic
   d) The International GNSS Service (*optional*)

3) [**One efficient operative system**] Quick introduction to Linux (*optional*)

4) [**New tools for learning and research**] IonSAT Tools (IT), emulating Real-Time (RT) as much as possible (presented on the PA AUDITOR experiment):
   a) *gim2vtec.v2.scr*
   b) *gimrnx2stec.v2.scr*

5) [**IT application to ECLIPSE, FLARE & GSTORM scenarios**] (*optional*).

6) [**Example of RT GPS-ionospheric system**]: UPC-IonSAT since 2012.

7) [**Monitoring of co-seismic generated ionospheric signals]:** Application of RT ionospheric sounding for potential Tsunami warnings), with GNSS dense (Tohoku and mid earthquakes, EQ) and sparse networks (Chile 2015 EQ).

8) [**Conclusions**]

AUDITOR

ADVANCED MULTI-CONSTELLATION EGNSS AUGMENTATION AND MONITORING NETWORK AND ITS APPLICATION IN PRECISION AGRICULTURE

Analysis of AUDITOR experiment "170613" in RT-mode with TOMION (@Netherlands, 13th June 2017)

Manuel Hernández-Pajares, Alberto García-Rigo & Victoria Graffigna on behalf of UPC-IonSAT

Mid-Term Review meeting

Barcelona, 24/07/2017

ACORDE CTTC UPC DGFI TUM Alpha consult DRAXIS ENVIRONMENTAL TECHNOLOGIES WAGENINGEN UR For quality of life

European Global Navigation Satellite Systems Agency

HORIZON 2020

AUDITOR

Exp. 170613: Overview

Presentation content

- ✓Brief experiment description
- ✓Relative dual-frequency real-time GPS positioning with TOMION

AUDITOR

Scenario and Problem

Scenario:

- ✓In Europe (typically at the South):
  1) The **permanent GNSS networks can be sparse** (up to hundreds of kilometers of distance).
  2) The **ionospheric delays can be large**.
  3) The economy is not going so well.

Problem:

- ✓Precise farming in South of Europe will, then, require:
  1) Prompt decimeter-error level real-time GNSS positioning at more than 100 km from the nearest GNSS reference site => **Wide Area RTK**
  2) Precise real-time ionospheric modelling from the measurements of the GNSS permanent networks => **Dual-layer tomography + Iono. wave modelling** (TOMION).
  3) Open source GNSS source receiver, combining flexibility for new GNSS algorithms and affordability.

Exper. 170613: Goal & Characteristics

Experiment:

- ✓Precise Farming activity: GNSS receiver (TOPCON GP-DX1) logging data for **several hours while spraying with a tractor**, which data has been kindly provided by Dirk De Hoog, WUR.
- ✓Place: Experimental farm in Wageningen, The Netherlands, with **reference receiver BORJ at 190 km** far.
- ✓Time: Day 13 June 2017 (doy 164), 06:11:39 to 13:30:59 GPS time.

Goal:

- ✓To analyze such recent AUDITOR experiment "170613" performed in actual precise farming conditions, **emulating Wide Area RTK processing in real-time**.

Exp. 170613: Tractor & permanent network

Rec. Id.	Distance to BORJ / km
HELG	104
IJMU	**188**
TPSD	**190**
VLIS	316
EIJS	321
DILL	468
OSLS	722
INVR	811
BRMF	882

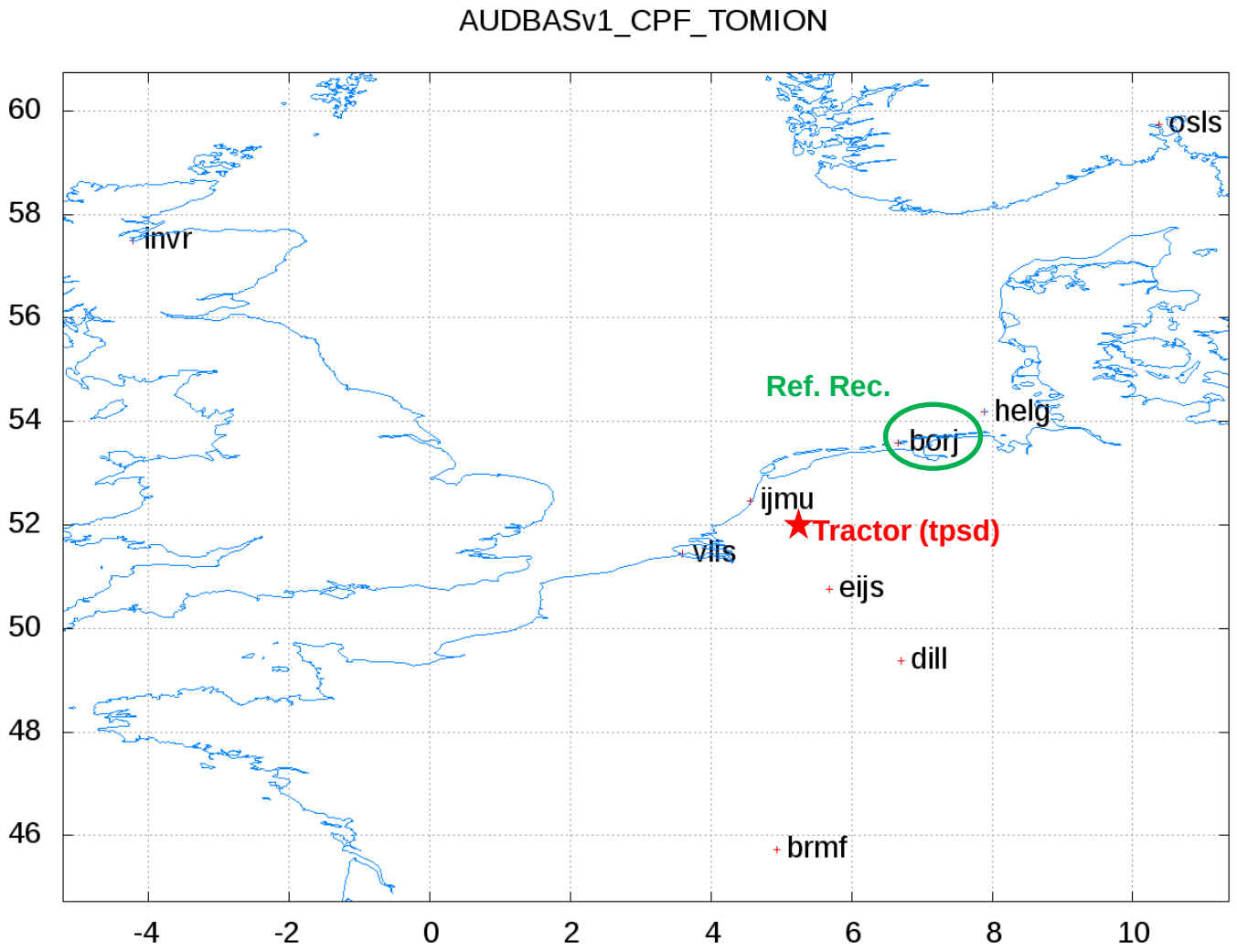

Wide Area RTK in a nutshell: The independent DD phase ambiguities of two physical carriers

DDBw (widelane from Melbourne-Wubbenna combination, Lw-Pn)

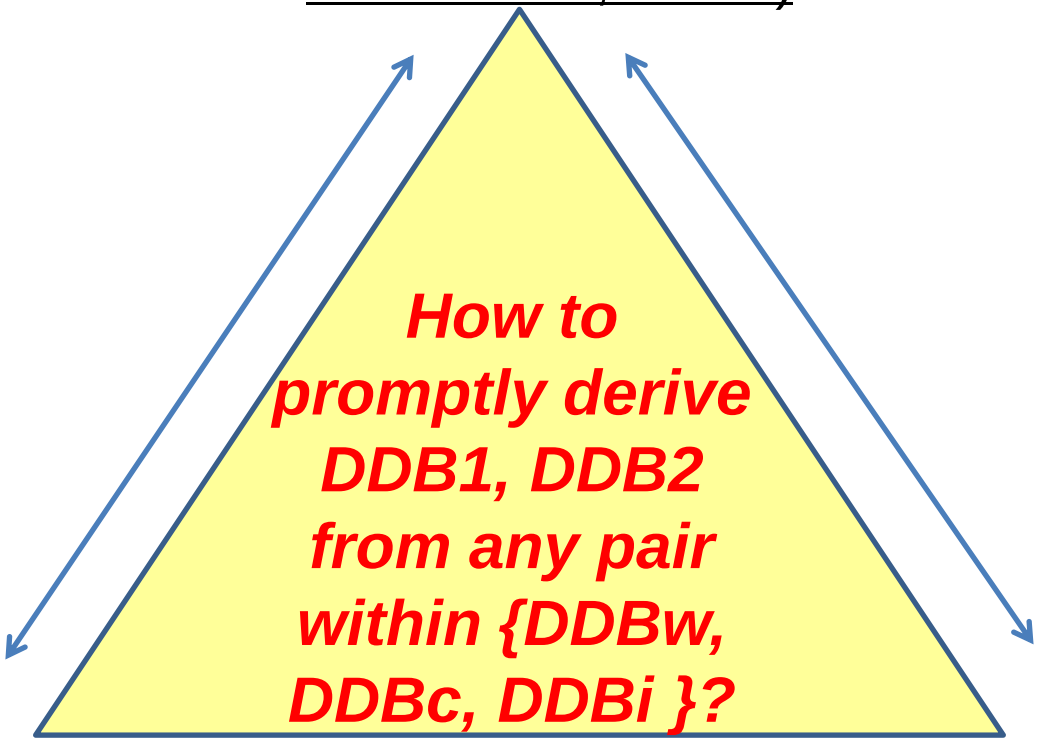

DDBc (from ionospheric-free combination Lc - precise geometric modelling)

DDBi (from ionospheric combination LI - precise ionospheric modelling)

Wide Area RTK in a nutshell: How to improve the DD phase ambiguity fixing

Geometry- & Ionospheric- free way
(Melbourne-Wubbenna combination, Lw-Pn)

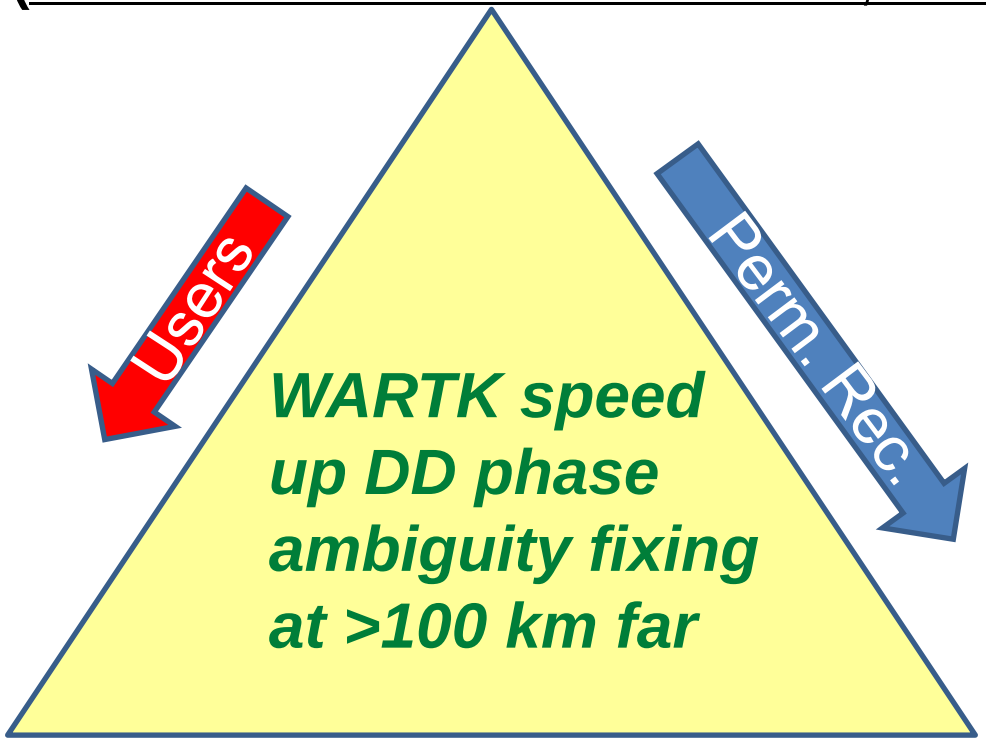

Ionospheric- free way
(Ionospheric-free combination Lc - precise geometric modelling)

Perm. Rec.

Users

Geometry- free way
(Ionospheric combination LI - precise ionospheric modelling)

AUDITOR

Wide Area RTK in a nutshell: Basic equations on DDamb

Once $\nabla\Delta N_\delta$ is fixed, it is possible to fix the L_1 and L_2 double-differenced integer ambiguities N_1 and N_2 for the reference stations, using a sufficiently accurate determination of the double-differenced ambiguity $\nabla\Delta B_c$ of the ionospheric free combination $L_c = (f_1^2 L_1 - f_2^2 L_2)/(f_1^2 - f_2^2)$. The following relationships illustrate these steps:

$$\begin{aligned}
\nabla\Delta B_c &= 0.5[\lambda_\delta \nabla\Delta N_\delta + \lambda_n \nabla\Delta(N_1 + N_2)] \\
\nabla\Delta(N_1 + N_2) &= \mathrm{NI}[(2\nabla\Delta B_c - \lambda_\delta \nabla\Delta N_\delta)/\lambda_\nu] \\
\nabla\Delta N_1 &= 0.5[\nabla\Delta N_\delta + \nabla\Delta(N_1 + N_2)] \\
\nabla\Delta N_2 &= \nabla\Delta N_1 - \nabla\Delta N_\delta
\end{aligned} \tag{3}$$

being $\lambda_n = c/(f_1 + f_2) \simeq 10.7\mathrm{cm}$ and NI the nearest integer. Hence, from $\nabla\Delta N_1$ and $\nabla\Delta N_2$, the unambiguous double-differenced ionospheric slant total electron content, STEC, can be computed for the reference stations:

$$\alpha\nabla\Delta STEC = \nabla\Delta(L_1 - L_2) - (\lambda_1 \nabla\Delta N_1 - \lambda_2 \nabla\Delta N_2) \tag{4}$$

(Extracted from *Hernández-Pajares, M., Juan, J. M., Sanz, J., & Colombo, O. L. (2000). Application of ionospheric tomography to real-time GPS carrier-phase ambiguities resolution, at scales of 400–1000 km and with high geomagnetic activity. Geophysical Research Letters, 27(13), 2009-2012).*

T5.2 - GNSS network prefit module

Hybrid ionospheric-geodetic approach

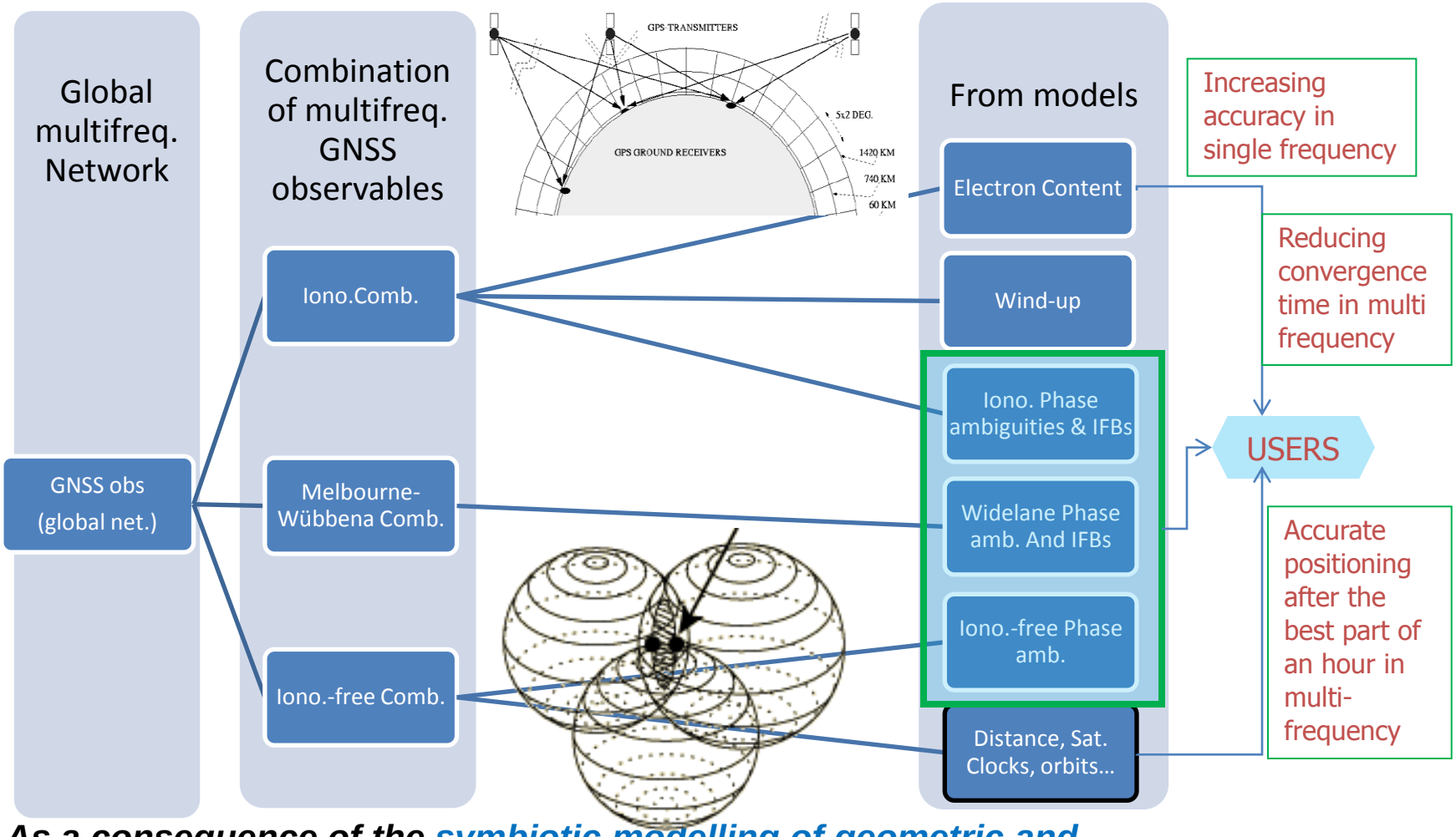

As a consequence of the symbiotic modelling of geometric and ionospheric delay dependences of the GPS, Galileo, GLONASS & Beidou signals: a better positioning service is obtained (cm-accuracy in real-time after short convergence time), and better ionospheric sounding

T5.2 - GNSS network prefit module

Hybrid ionospheric-geodetic approach

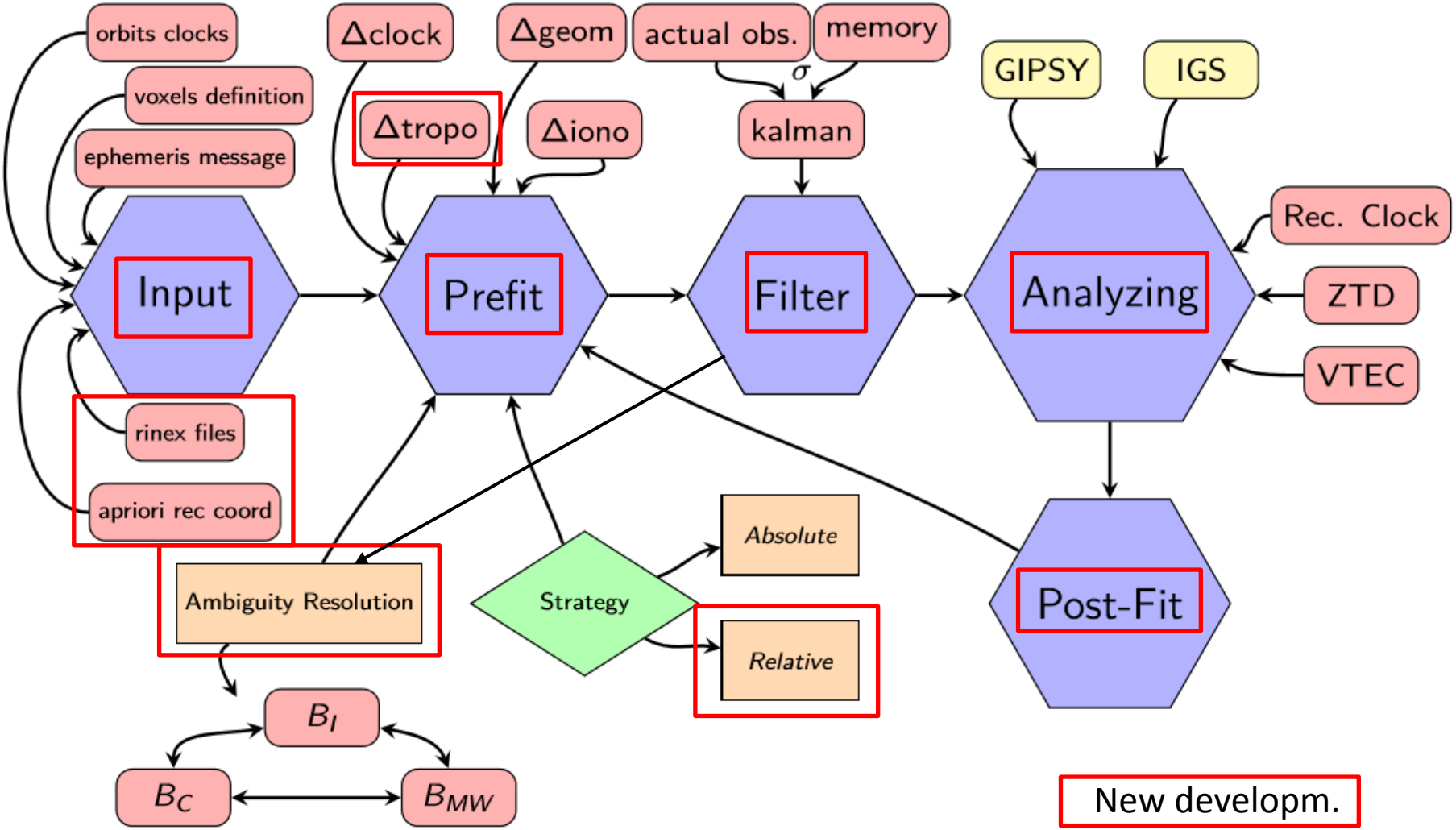

New developm.

Exp. 170613: Relative RT-mode dual-frequency positioning of Tractor (tpsd) vs Ref. Rec. (borj) with TOMION (1 of 4)

AUDITOR

Rec. Id.	Distance to BORJ / km
IJMU	188
TPSD	190

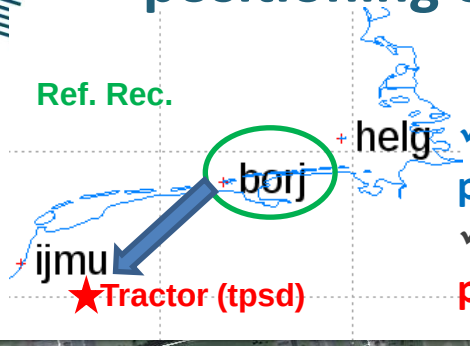

✓**Consistency of the most part of positions over the paths compatible with 10cm-error level RT positioning.**

✓ But a **cloud of apparently very noisy estimated positions appear**. **Why**? Cold start? Other reasons?

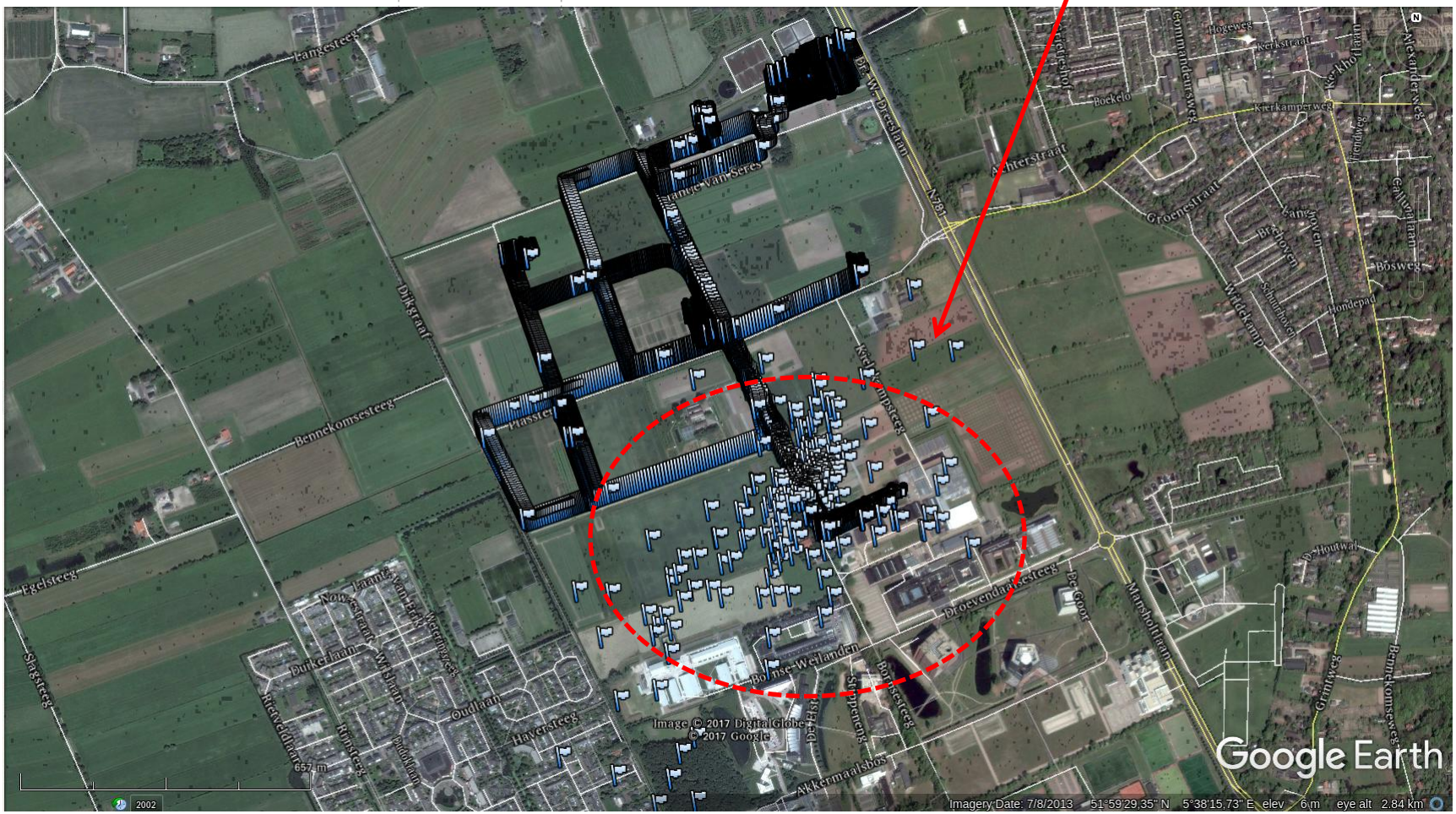

Exp. 170613: Relative RT-mode dual-frequency positioning of Tractor (tpsd) vs Ref. Rec. (borj) with TOMION (2 of 4)

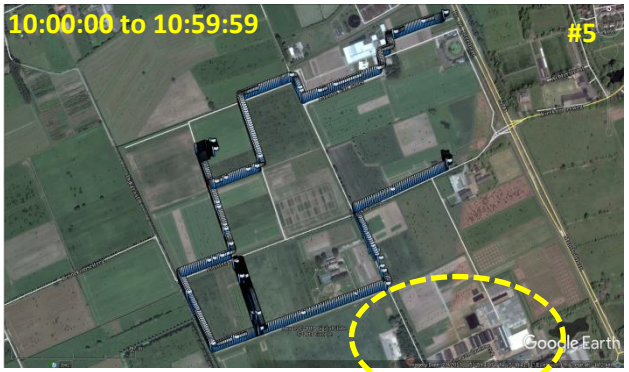

✓The big positioning errors are NOT concentrated on the initial convergence phase of the tractor navigation (beginning of time-frame #1): **they appear when the tractor moves through one part of the path** (red arrow)

✓ Which can be the potential explanation?

Exp. 170613: Relative RT-mode dual-frequency positioning of Tractor (tpsd) vs Ref. Rec. (borj) with TOMION (3 of 4)

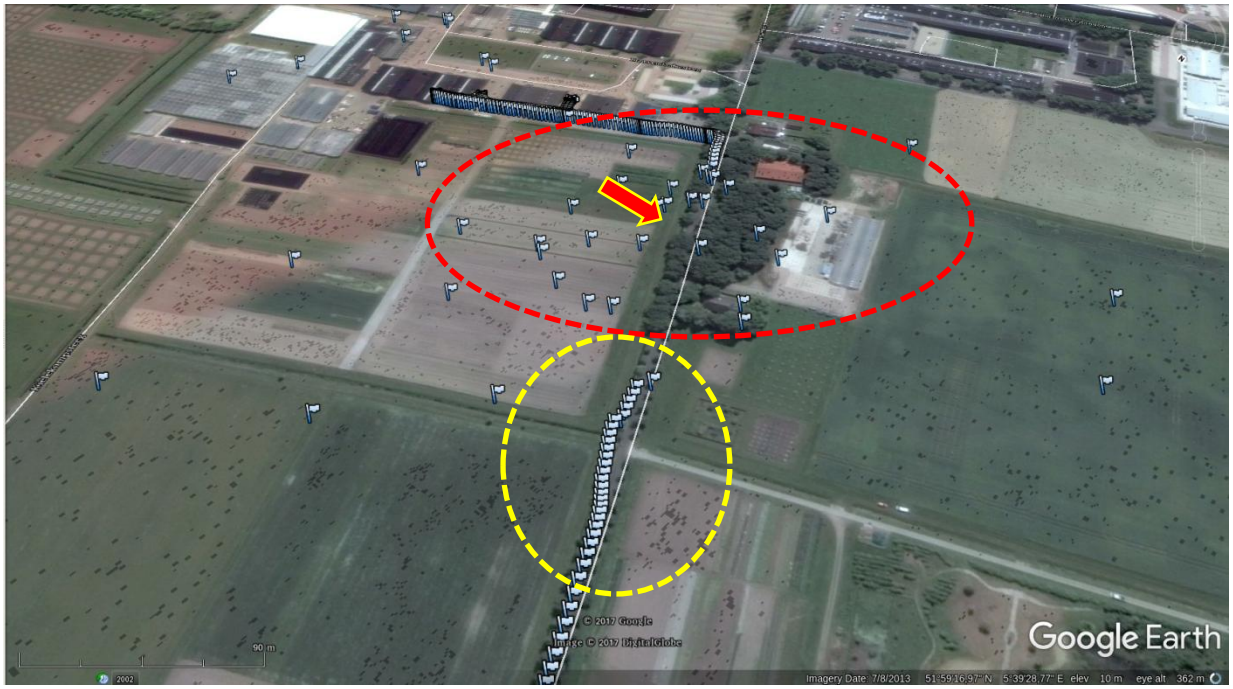

✓The potential reason of such very large positioning error when moving during the same path (marked by the red arrow) is strongly suggested when the 3D representation is activated at google-earth: **THE CANOPY** (trees densely distributed in such part of the path).

✓The **trees**, affecting to this part of the path, are likely **blocking the signal of many GPS satellites generating cycle-slips and the corresponding re-initialization** of the carrier phase ambiguity estimation.

✓The **convergence phase of the positioning can be clearly seen** (within yellow ellipse), lasting for about ~25 seconds.

Exp. 170613: Relative RT-mode dual-frequency positioning of Tractor (tpsd) vs Ref. Rec. (borj) with TOMION (4 of 4)

✓The **association of the precise positioning outage with the canopy** and **not with the initial cold start of the tractor movement**, during the very first minutes (starting on 06:11:39) can be seen in the Way Points number labels (equivalent to time in seconds since tractor receiver starting): the erroneous positions happen within the range 1637-1658 and beyond (red arrow), while previous epochs are well located in previous path (**yellow arrow**).

Exp. 170613: Relative RT-mode dual-frequency positioning of IJMU vs Ref. Rec. (borj) with licted satellite clocks & orbits, IGU)

AUDITOR

Rec. Id.	Distance to BORJ / km
IJMU	188
TPSD	190

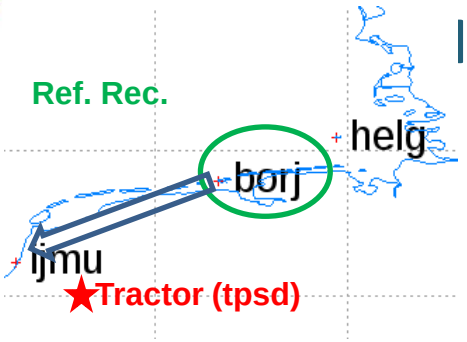

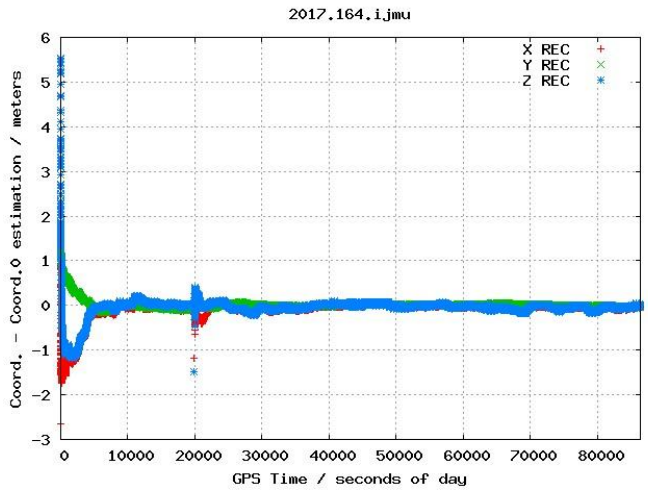

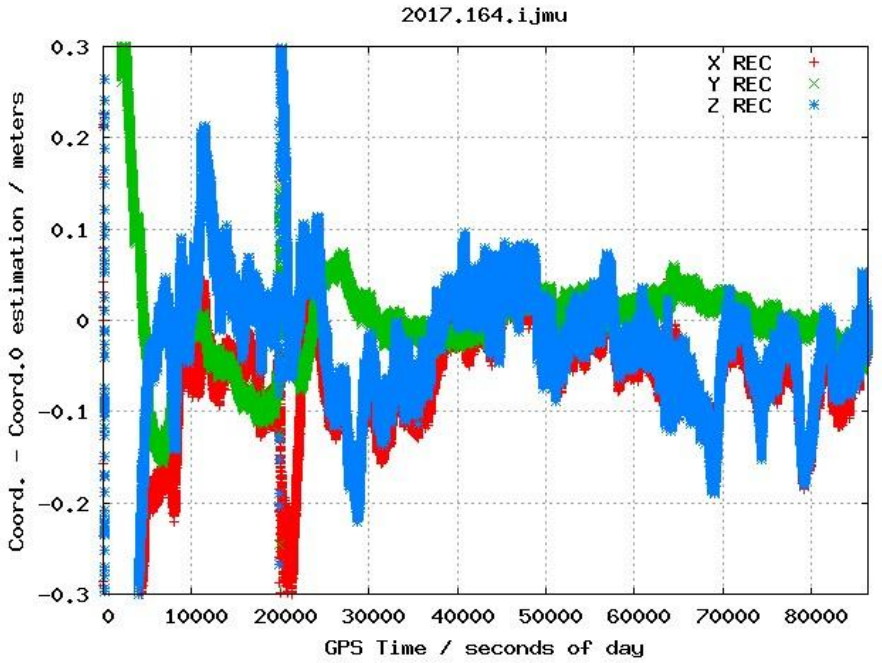

✓Among the good fitting with the paths shown by google-earth, a more consistency indication of the decimeter error level navigation achieved by the relative dual-frequency carrier-phase based positioning on the tractor, has been obtained.

✓We have processed the permanent receiver IJMU, also @ 1Hz, forming a similar baseline, in distance (188 km vs 190 km) and orientation (SW), than the Tractor (TPSD), comparing the IJMU RT-kinematic positioning, performed with the strategy than the one previously performed to TPSD, with the precise final PPP coordinates of IJMU, computed with postprocessing (rapid IGS) products, which can be taken as ground truth at centimeter error level: Errors up to +/- 20 cm, after the cold start (~4000 sec).

Exp. 170613: Relative RT-mode dual-frequency positioning of IJMU vs Ref. Rec. (borj) with TOMION (rapid satellite clocks & orbits, IGR)

Rec. Id.	Distance to BORJ / km
IJMU	188
TPSD	190

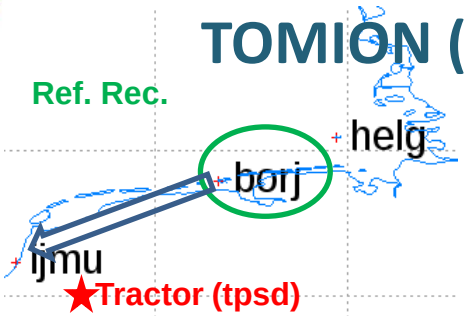

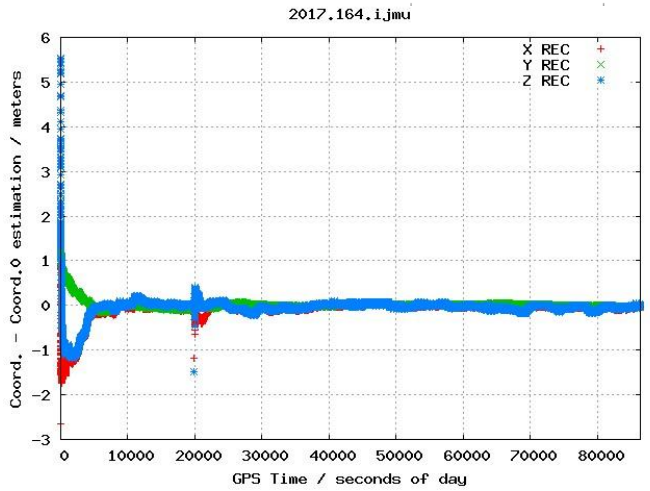

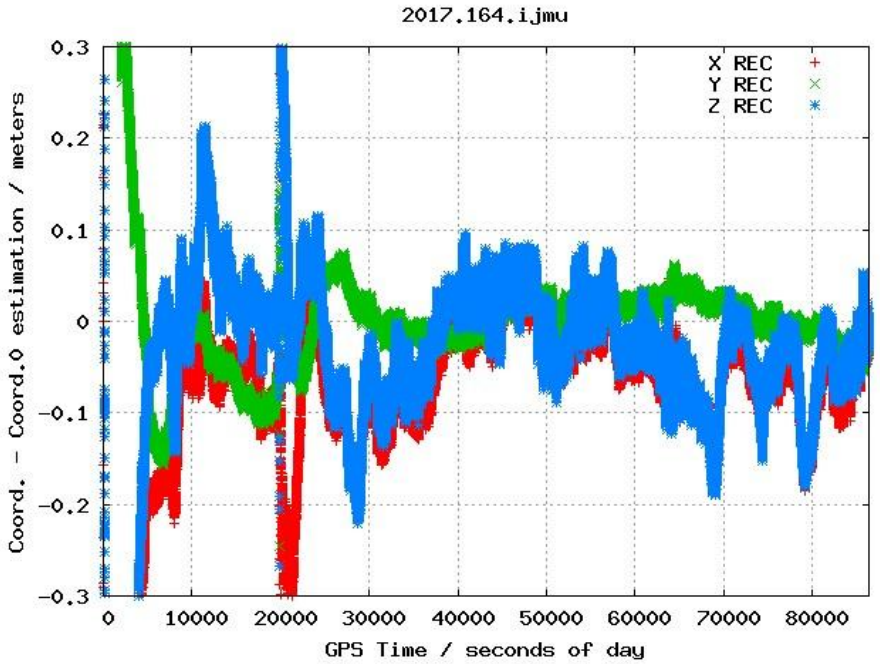

✓The result is almost the same when the predicted ("ultrarapid") IGS products (IGU), available in real-time, are used (previous slide) and the postprocessing "rapid" IGS products (IGR) are used (this slide).

✓This is the expected result when the relative RT approach is used (see modelling details in first slides).

Exp. 170613: Relative RT-mode dual-frequency positioning of Tractor (tpsd) vs Ref. Rec. (borj) with TOMION: equivalent under IGU & IGR

AUDITOR

Rec. Id.	Distance to BORJ / km
IJMU	188
TPSD	190

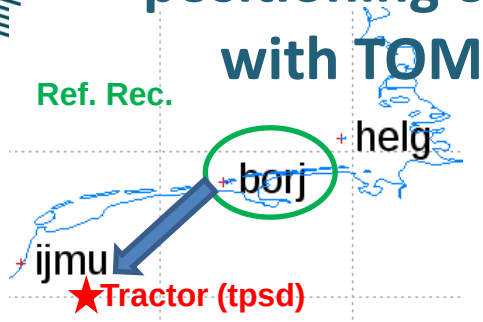

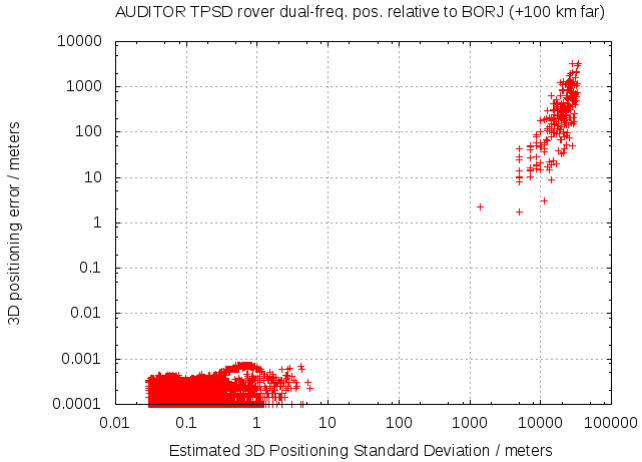

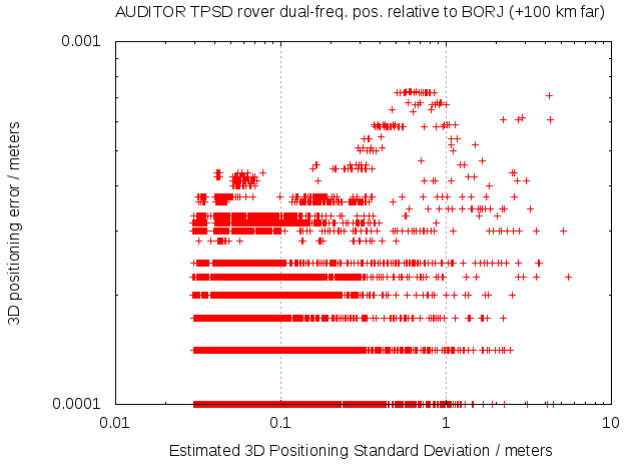

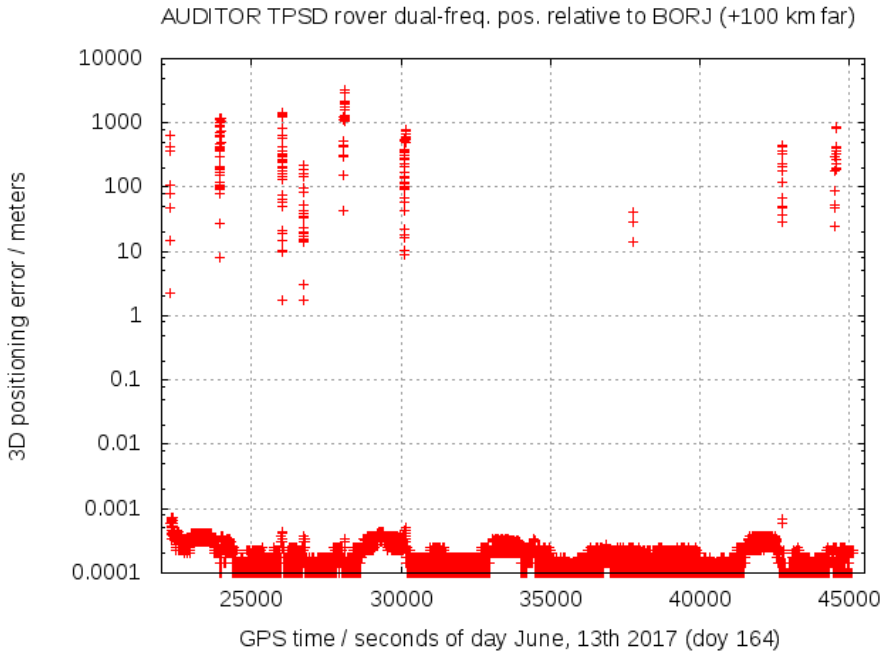

✓As expected, the result is almost the same for the Tractor positioning (sub-mm discrepancies), when the predicted ("ultrarapid") IGS products (IGU), available in real-time, are used (previous slide) and the postprocessing "rapid" IGS products (IGR) are used (this slide).

✓The exceptions happen when a very large error happen (mostly on the canopy-affected part of the Tractor path studied before), when the precise real-time processing is interrupted.

Exp. 170613, PPP static processing@15 min.: IGU (predicted clocks & orbits) vs IGR (rapid postprocessed clocks and orbits)

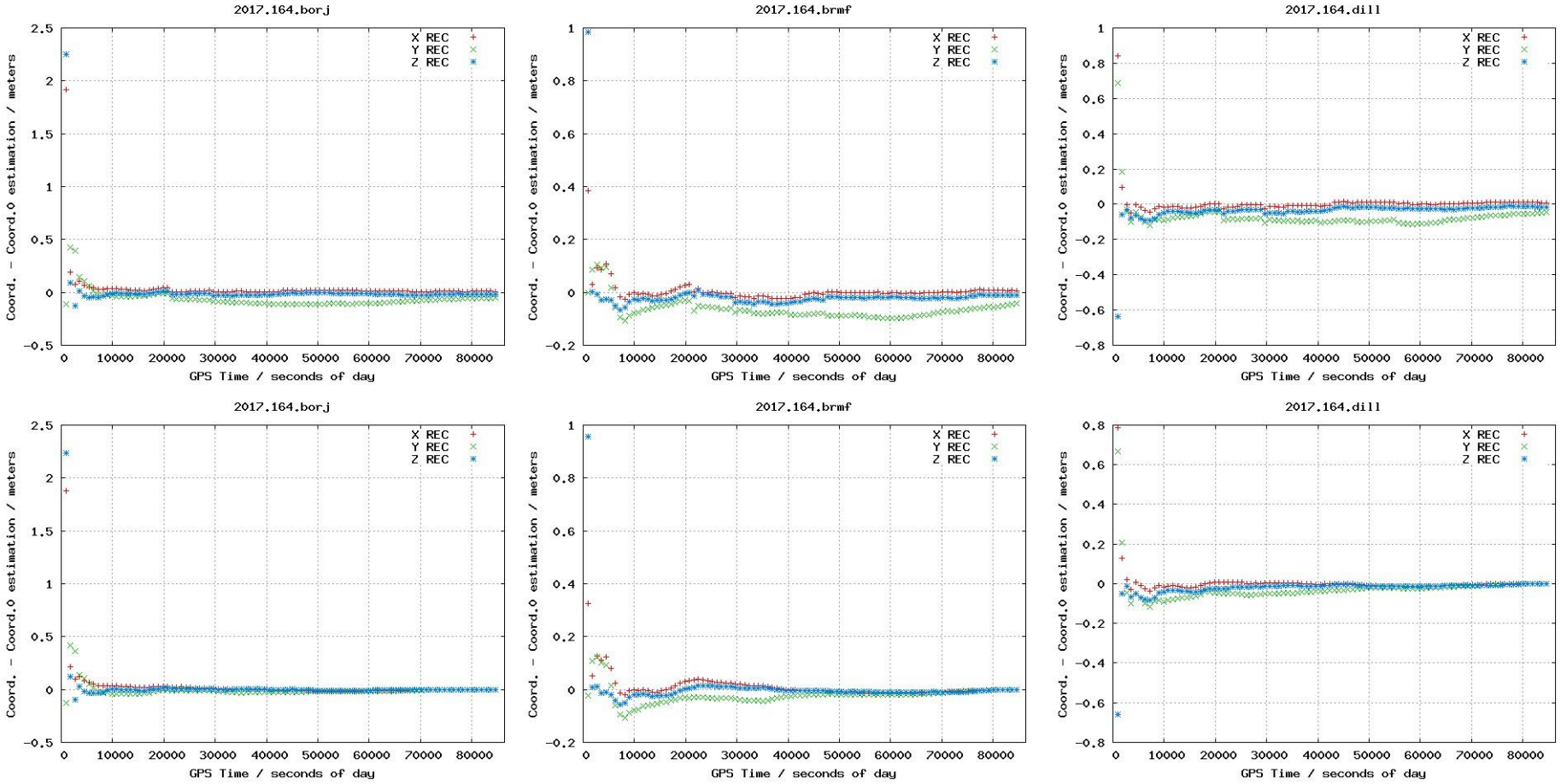

✓The influence of the degradation of (mainly) the predicted satellite clocks errors (IGU, first row) makes the PPP processing significantly worser than with postprocessed rapid (IGR) satellite clocks and orbits (second row), as expected.

Exp. 170613: RT Relative dual-frequency positioning of IJMU vs. Ref. Rec. (borj) with TOMION (same time period than Tractor): No Iono. + floating ambiguities

AUDITOR

Rec. Id.	Distance to BORJ / km
IJMU	188
TPSD	190

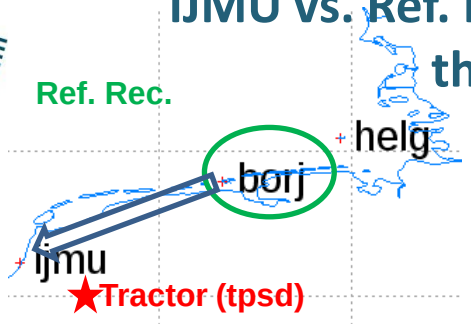

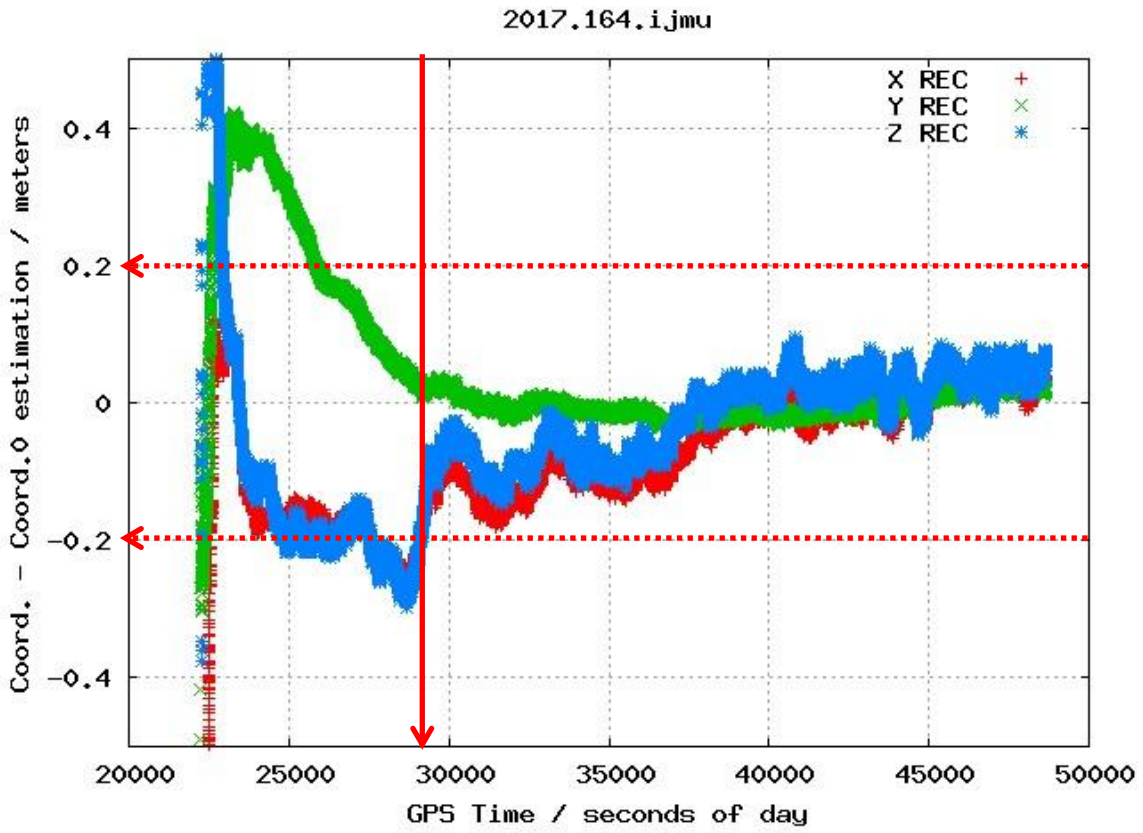

✓Convergence time of ~7000 sec (No Iono. + floating ambiguities)

Exp. 170613: Tractor & permanent network

Rec. Id.	Distance to BORJ / km
HELG	104
IJMU	**188**
TPSD	**190**
VLIS	316
EIJS	321
DILL	468
OSLS	722
INVR	811
BRMF	882

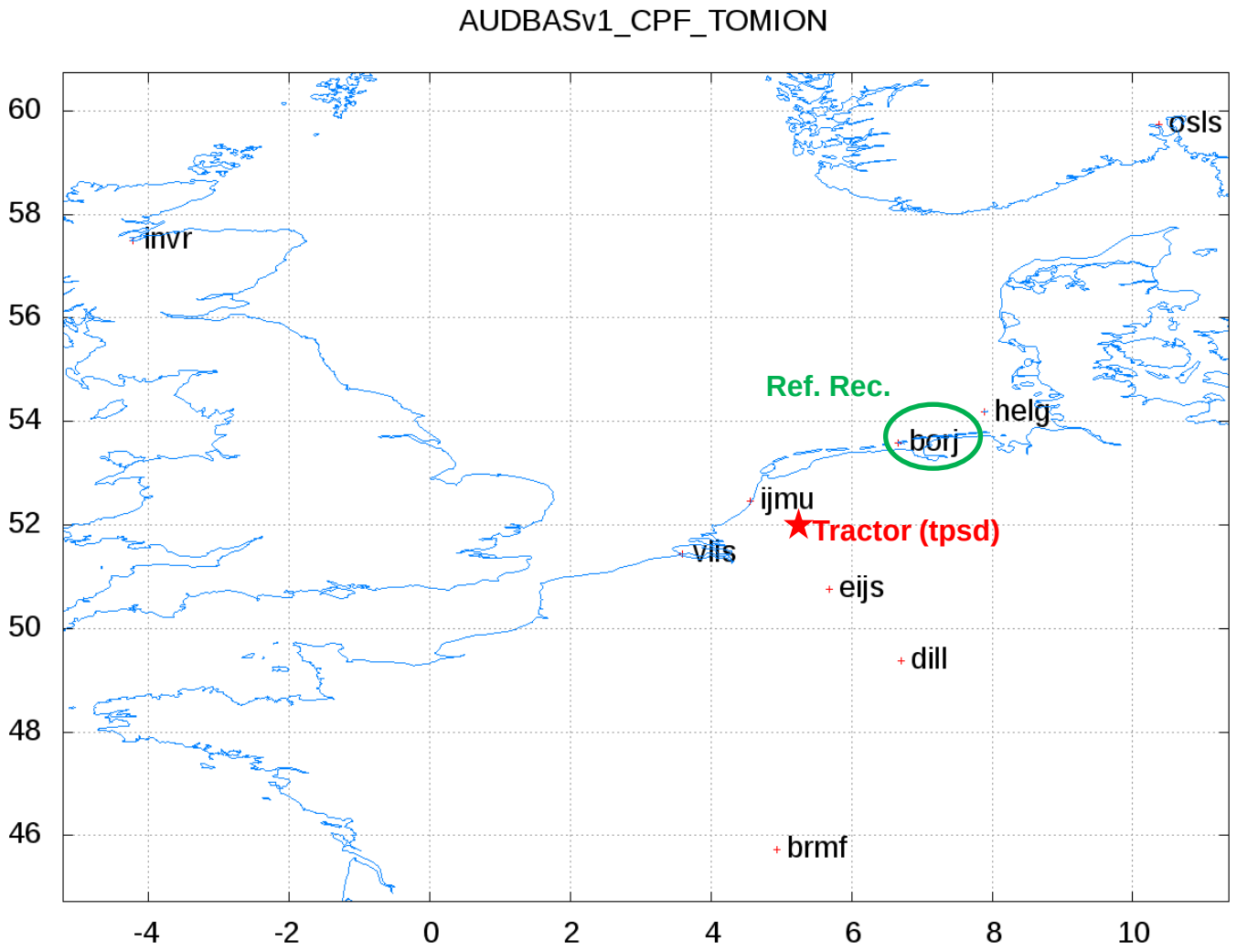

AUDITOR

Exp. 170613: RT Relative dual-frequency positioning of
f. Rec. (borj) with TOMION (same time period
Tractor): ambiguities constrained by RT iono.

Rec. Id.	Distance to BORJ / km
IJMU	188
TPSD	190

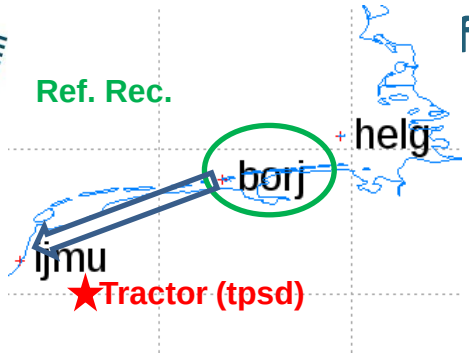

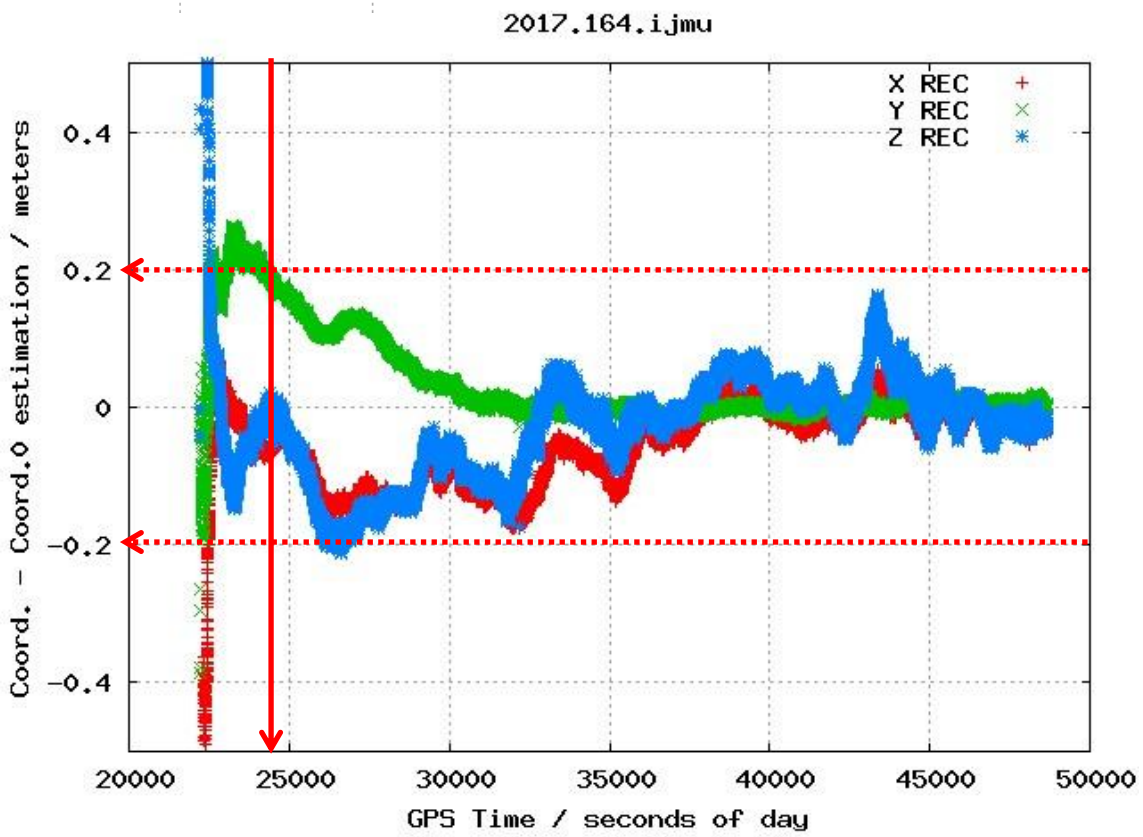

✓Convergence time of ~2000 sec (ambiguities constrained by RT iono)

AUDITOR

Exp. 170613: RT Relative dual-frequency positioning of IJMU vs. Ref. Rec. (borj) with TOMION (same time period than Tractor): *hybrid* amb. constrained & fixed by RT-iono

Rec. Id.	Distance to BORJ / km
IJMU	188
TPSD	**190**

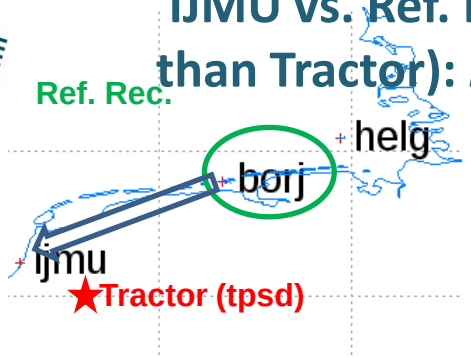

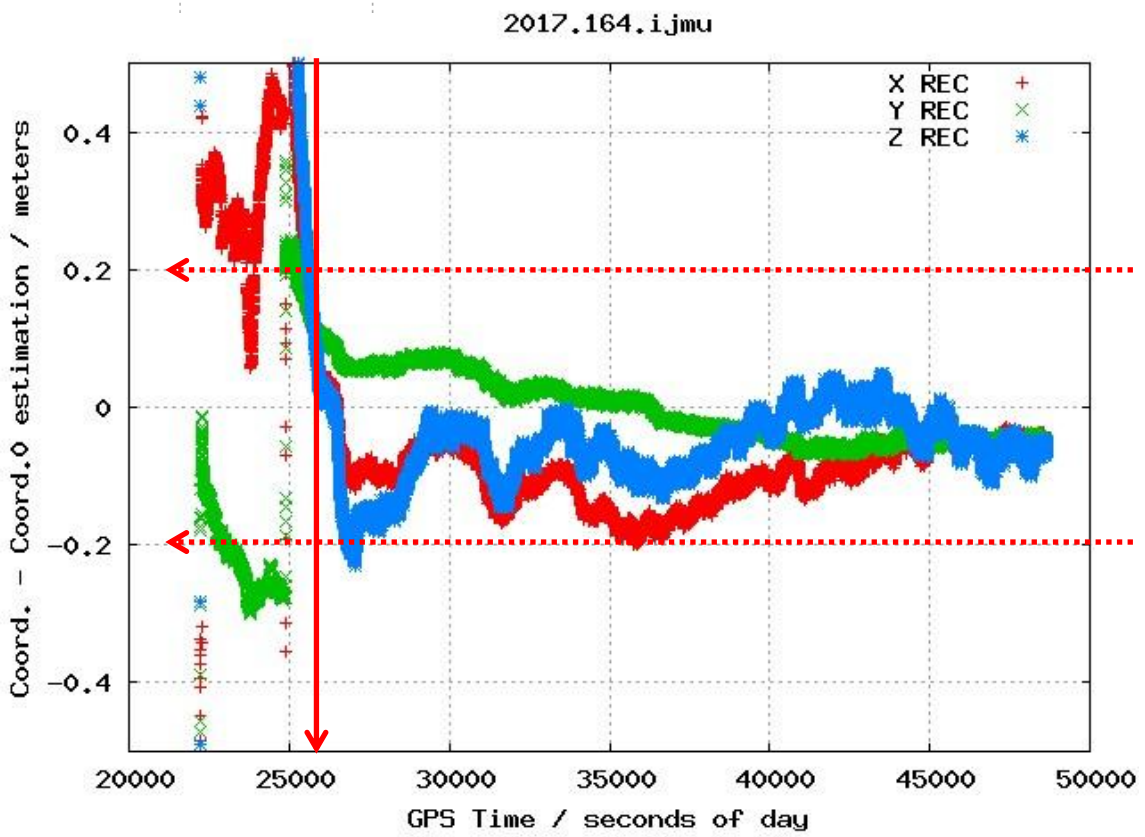

✓Convergence time of ~4000 sec (hybrid amb. constrained & fixed by RT-iono, working CPF from 00h)

Exp. 170613, RT-iono performance (PRN12) during full cold-start (compared with calibrated STEC in postprocess)

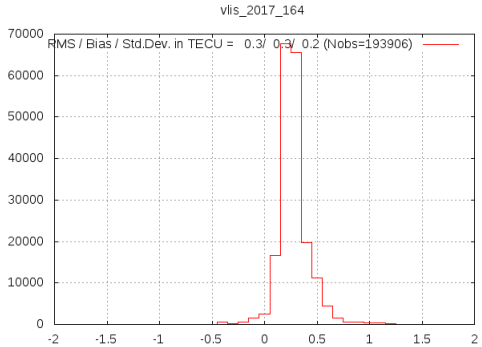

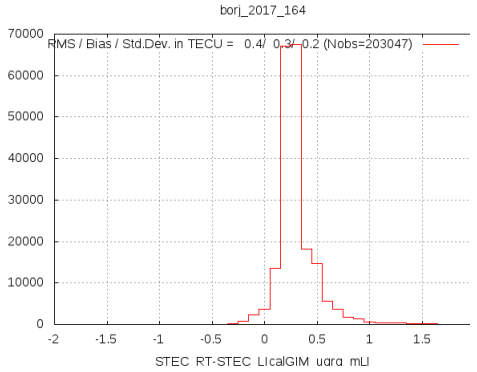

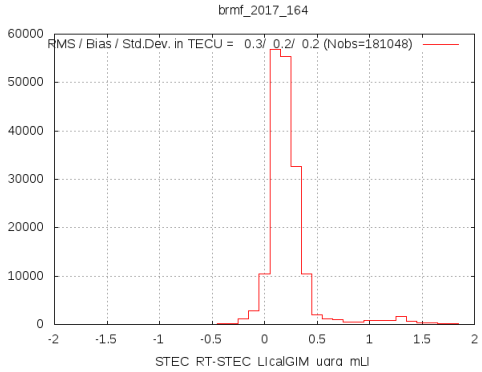

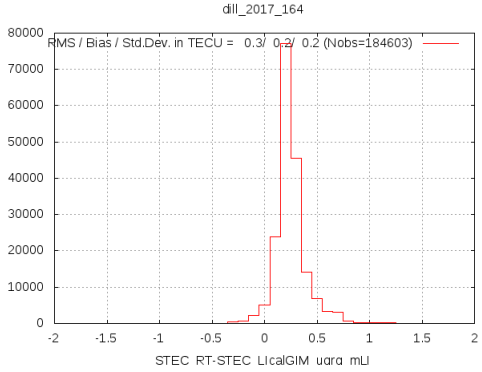

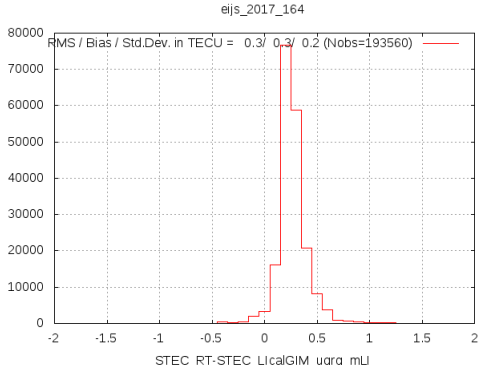

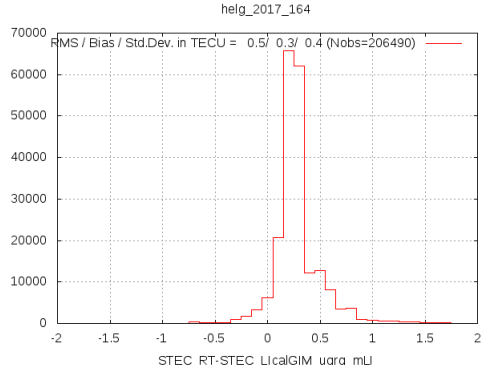

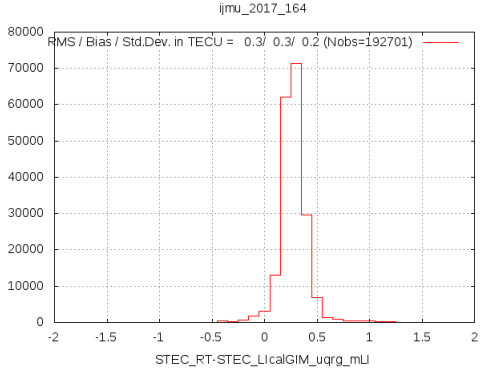

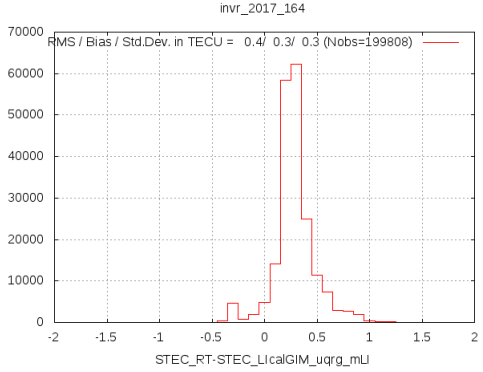

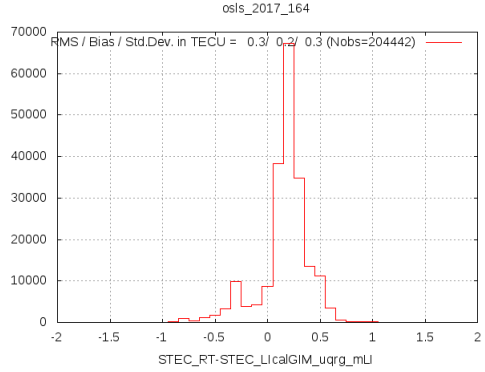

Exp. 170613, Zenith Tropospheric Delay : RT relative processing @ 30sec vs postpr. (IGR) PPP processing@15 min.

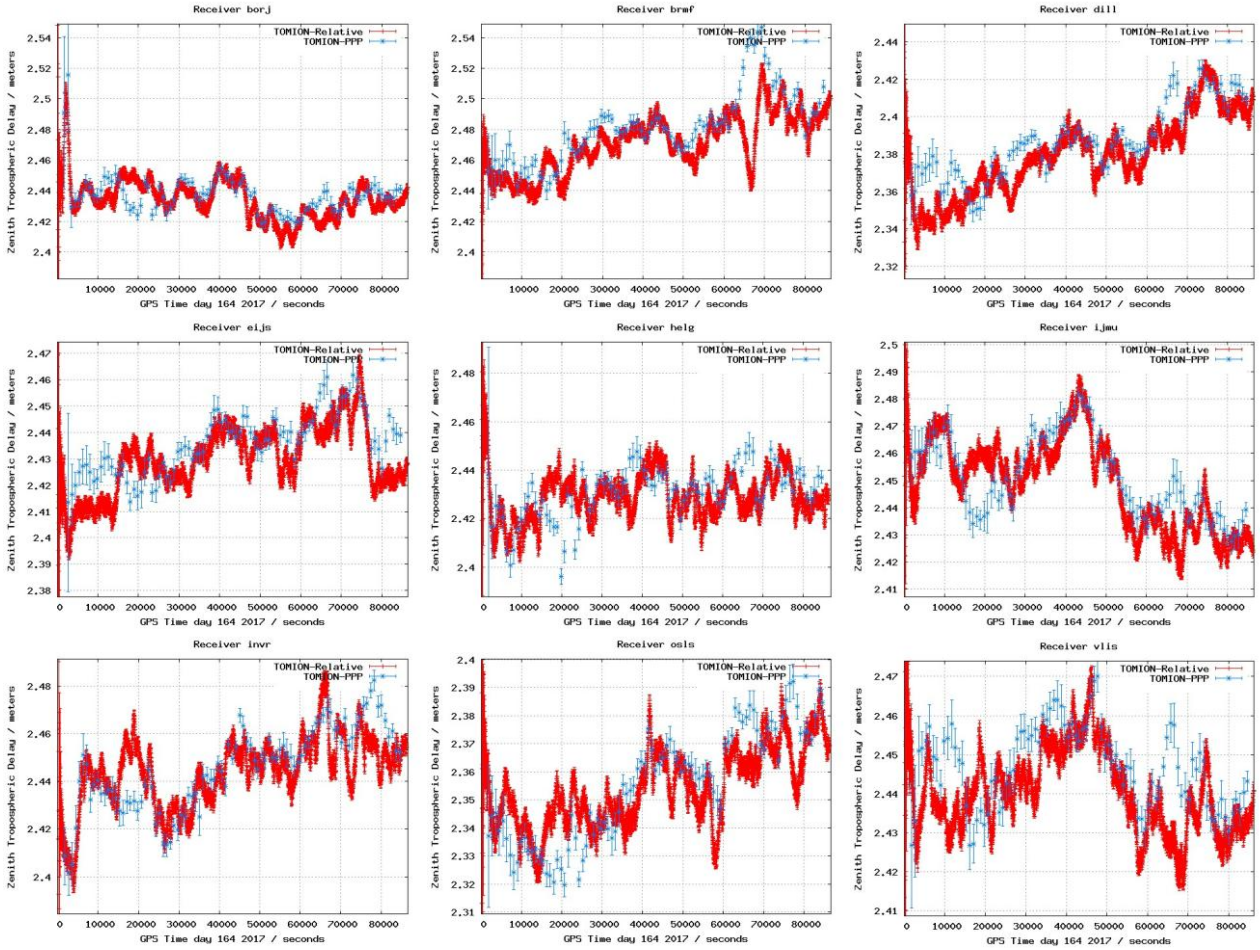

✓Another test of consistency of the same RT relative dual-frequency GPS processing is looking at the associated ZTD @ 30 sec., comparing them with the results with post-processed (IGR) PPP @ 15 min.

✓The results are mostly in agreement under 1 cm level, with some deviations up to 3 cm for two given periods and for two stations.

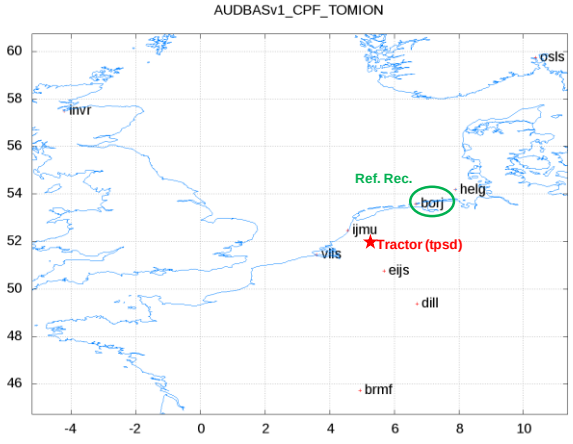

Exp. 170613, Zenith Tropospheric Delay : RT relative processing @ 30sec vs postpr. (IGR) PPP processing@15 min. vs first results of relative processing fixing DD ambiguities from filter

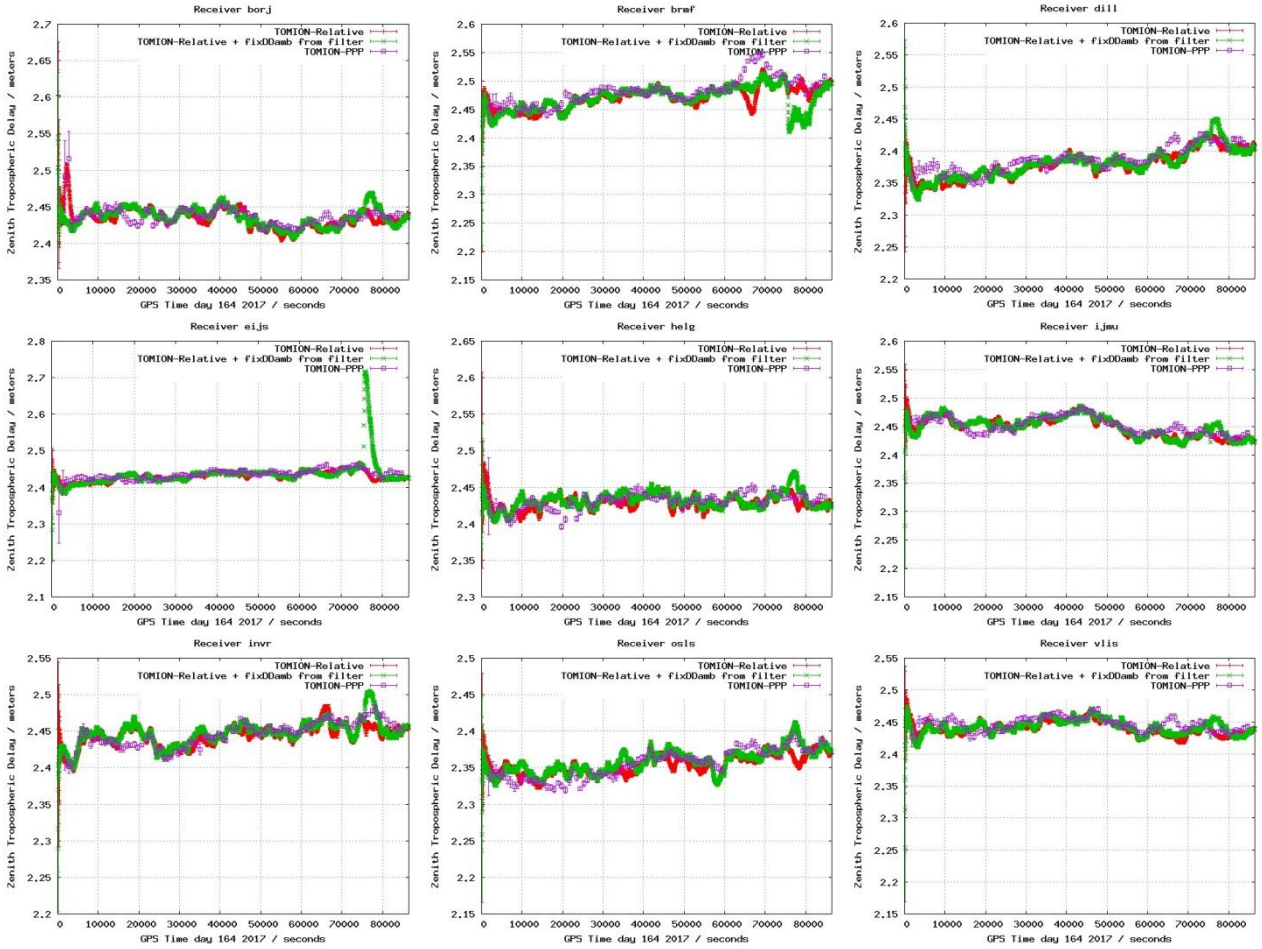

✓The first results of the relative precise positioning after ambiguity fixing are very similar to the floated-ambiguities ones (at cm-level), excepting for the period [75000,80000] sec (likely due to a wrong ambiguity fixing).

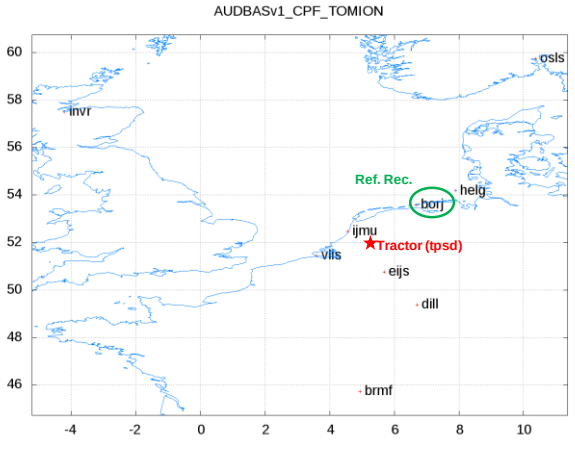

AUDITOR

Conclusions

✓The GPS data gathered from a tractor working 6 hours in a Netherlands farm, has been processed with the in-house UPC-IonSAT software, RT-TOMION.

✓The analysis has been done emulating RT from dual-frequency carrier phase and pseudorange measurements, in relative processing approach, taking the reference station (BORJ) at around 190 km NE.

✓The results show characteristics compatible with decimeter-error level RT-positioning (from fitting with exiting paths, equivalent analysis of IJMU, and ZTD results), excepting for an small sector under canopy.

✓The satellite-clocks-proof in the quality of the relative processing, vs. undifference (PPP) one, has been exemplified as well during this experiment.

✓The precise analysis of this farming exp. reinforces the need of looking for mitigation strategies of GNSS precise positioning under canopy (such as the one of Soloviev & Dickman, 2011), which might be considered in the soft. receiver.

✓When Wide Area RTK, involving precise ionospheric corrections, is applied, the convergence time under full cold start is reduced to less than one third.

Thank you

Soloviev, A., & Dickman, J. (2011). Extending GPS carrier phase availability indoors with a deeply integrated receiver architecture. IEEE Wireless Communications, 18(2).

Two slides previously shown contain main terms to clarify or summarize if needed:

- *Global Navigation Satellite Systems (GNSS)*
- *Ionospheric delays*
- *Wide Area Real Time Kinematic (WARTK)*
- *Ionospheric waves*
- *TOMION*
- *Double-difference carrier phase ambiguities*

AUDITOR

Scenario and Problem

Scenario:

- ✓In Europe (typically at the South):
  1) The **permanent GNSS networks can be sparse** (up to hundreds of kilometers of distance).
  2) The **ionospheric delays can be large**.
  3) The economy is not going so well.

Problem:

- ✓Precise farming in South of Europe will, then, require:
  1) Prompt decimeter-error level real-time GNSS positioning at more than 100 km from the nearest GNSS reference site => **Wide Area RTK**
  2) Precise real-time ionospheric modelling from the measurements of the GNSS permanent networks => **Dual-layer tomography + Iono. wave modelling** (TOMION).
  3) Open source GNSS source receiver, combining flexibility for new GNSS algorithms and affordability.

Wide Area RTK in a nutshell: The independent DD phase ambiguities of two physical carriers

DDBw (widelane from Melbourne-Wubbenna combination, Lw-Pn)

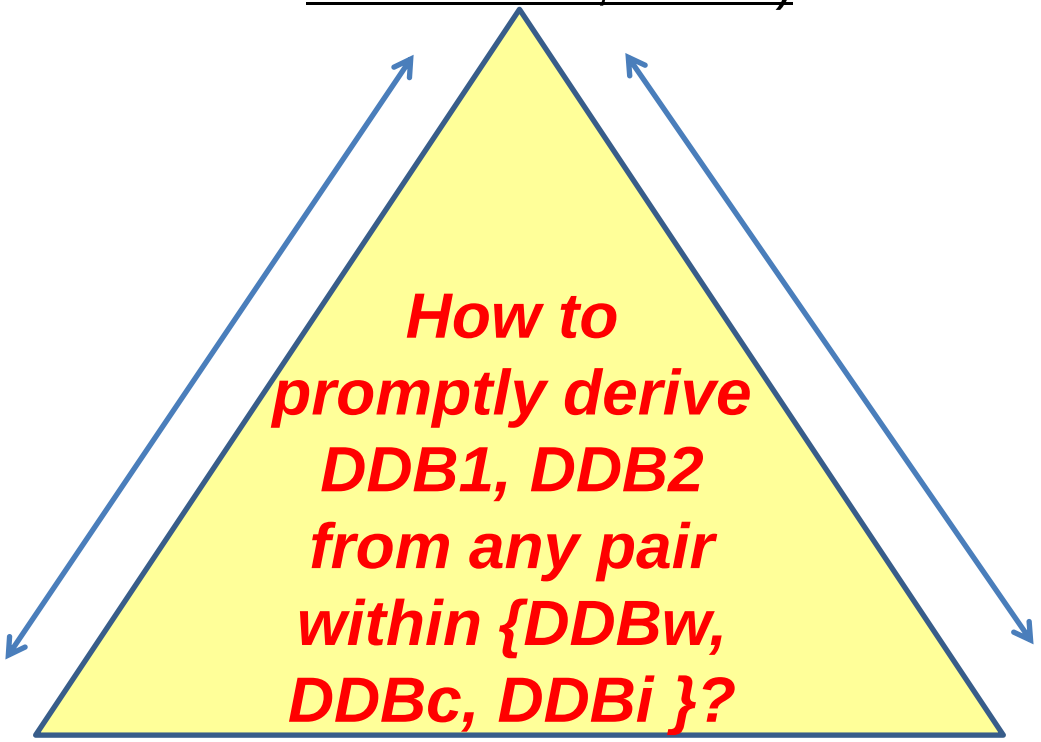

DDBc (from ionospheric-free combination Lc - precise geometric modelling)

DDBi (from ionospheric combination LI - precise ionospheric modelling)

Layout:

1) [**Motivation**] Precise Agriculture (PA) presentation (EU AUDITOR experiment)

2) [**Background**]: Brief introduction to main identified points of the presentation:
   a) GPS fundamentals: pseudoranges and carrier phases (*optional*)
   b) Ionospheric electron content
   c) Wide Area Real-Time Kinematic
   d) The International GNSS Service (*optional*)

3) [**One efficient operative system**] Quick introduction to Linux (*optional*)

4) [**New tools for learning and research**] IonSAT Tools (IT), emulating Real-Time (RT) as much as possible (presented on the PA AUDITOR experiment):
   a) *gim2vtec.v2.scr*
   b) *gimrnx2stec.v2.scr*

5) [**IT application to ECLIPSE, FLARE & GSTORM scenarios**] (*optional*).

6) [**Example of RT GPS-ionospheric system**]: UPC-IonSAT since 2012.

7) [**Monitoring of co-seismic generated ionospheric signals]:** Application of RT ionospheric sounding for potential Tsunami warnings), with GNSS dense (Tohoku and mid earthquakes, EQ) and sparse networks (Chile 2015 EQ).

8) [**Conclusions**]

How GPS Works

(the most madure GNSS)

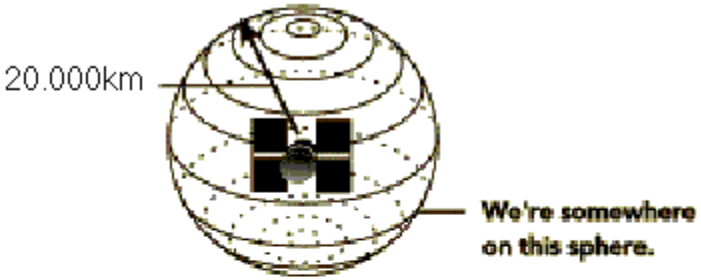

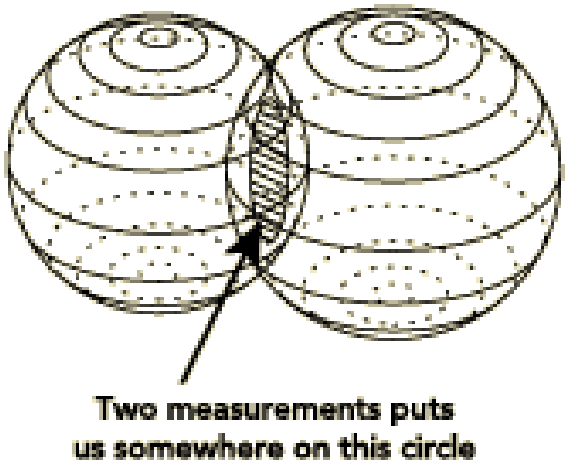

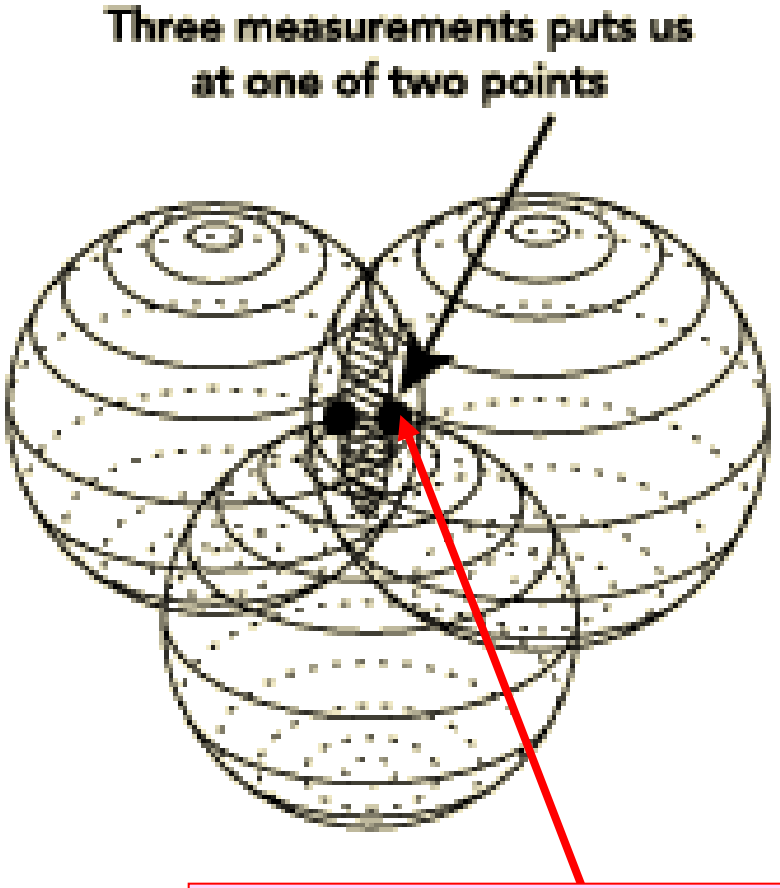

One of the solutions is not on the Earth surface.

How GPS Works

Satellites broadcast orbit and clock data

➔Satellite coordinates and clock offset

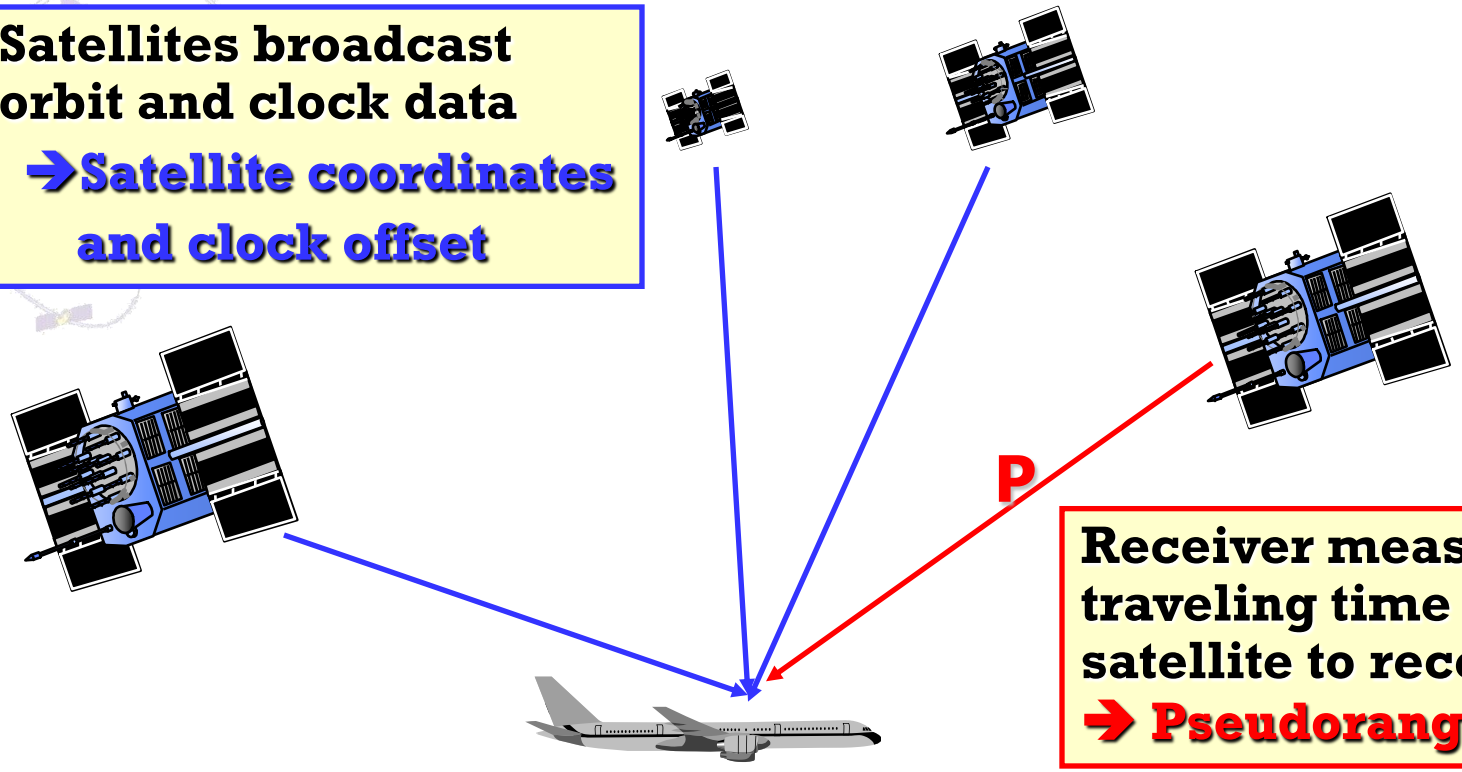

Receiver measures traveling time from satellite to receiver

➔ Pseudorange (P)

Thence, the receiver coordinates are found **solving a geometrical problem**: from sat. coordinates and ranges

How GPS Works

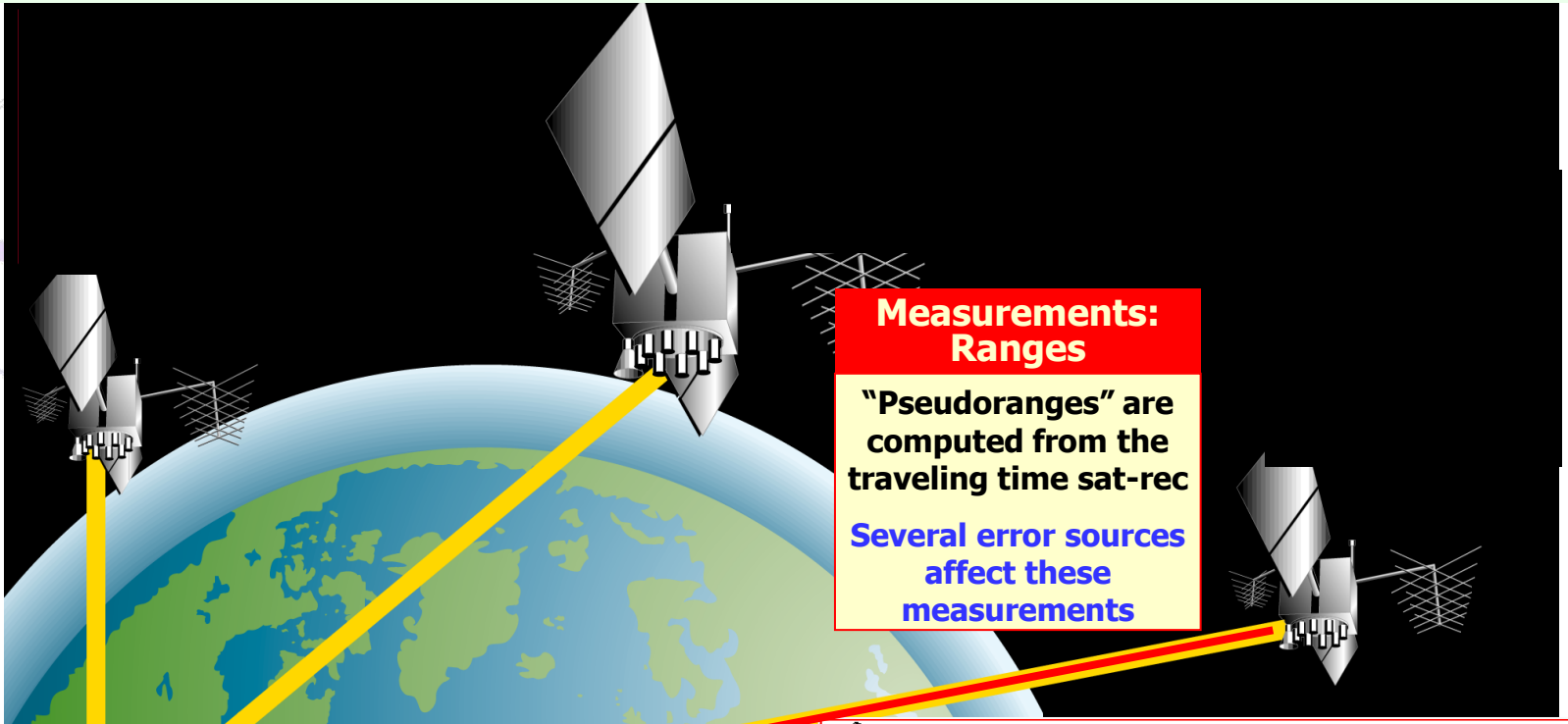

Measurements: Ranges

"Pseudoranges" are computed from the traveling time sat-rec

Several error sources affect these measurements

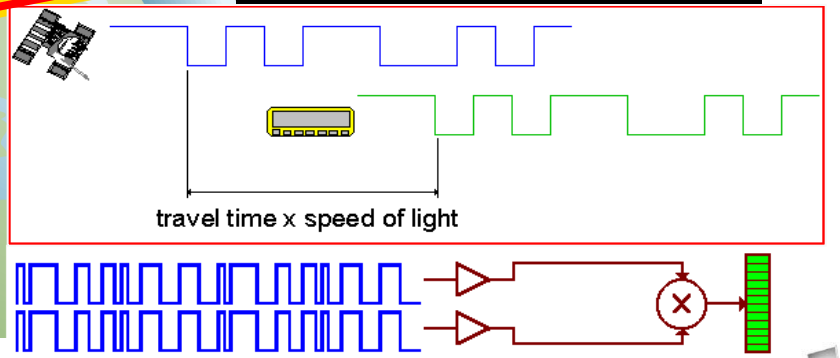

1. Code or pseudorange: This measurement is given by the apparent travel time τ of the EM signal propagated from GPS transmitter to receiver, scaled by the speed of light in the vacuum, c. This value can be partially considered as a range, i.e., a pseudorange $\tilde{\rho}$:

$$P \equiv c\tau = \tilde{\rho} \tag{3}$$

2. Carrier phase: This measurement is computed in the receiver by continuously integrating the frequency Doppler shift, primarily due to the relative velocity, clocks, and tropospheric and ionospheric drifts. This value is scaled in unit lengths in such a way that it represents the pseudorange $\tilde{\rho}$ and basically refers to the last time the carrier phase was locked by the receiver t_L (i.e., the pseudorange change since the last "cycle-slip" or the first acquisition epoch).

$$\int_{t_L}^{t} \dot{\tilde{\rho}}\, \mathrm{d}t = -\frac{c}{f} \int_{t_L}^{t} \delta f \cdot \mathrm{d}t. \qquad (5)$$

Thus, the carrier phase is finally defined as:

$$L \equiv -\lambda \int_{t_L}^{t} \delta f \cdot \mathrm{d}t = \tilde{\rho}(t) - \tilde{\rho}(t_L) = \tilde{\rho} + B_f, \qquad (6)$$

where B_f is the carrier phase ambiguity for frequency f and $\lambda = c/f$ is the corresponding carrier wavelength.

Carrier phase ambiguity fixing: key for precise navigation

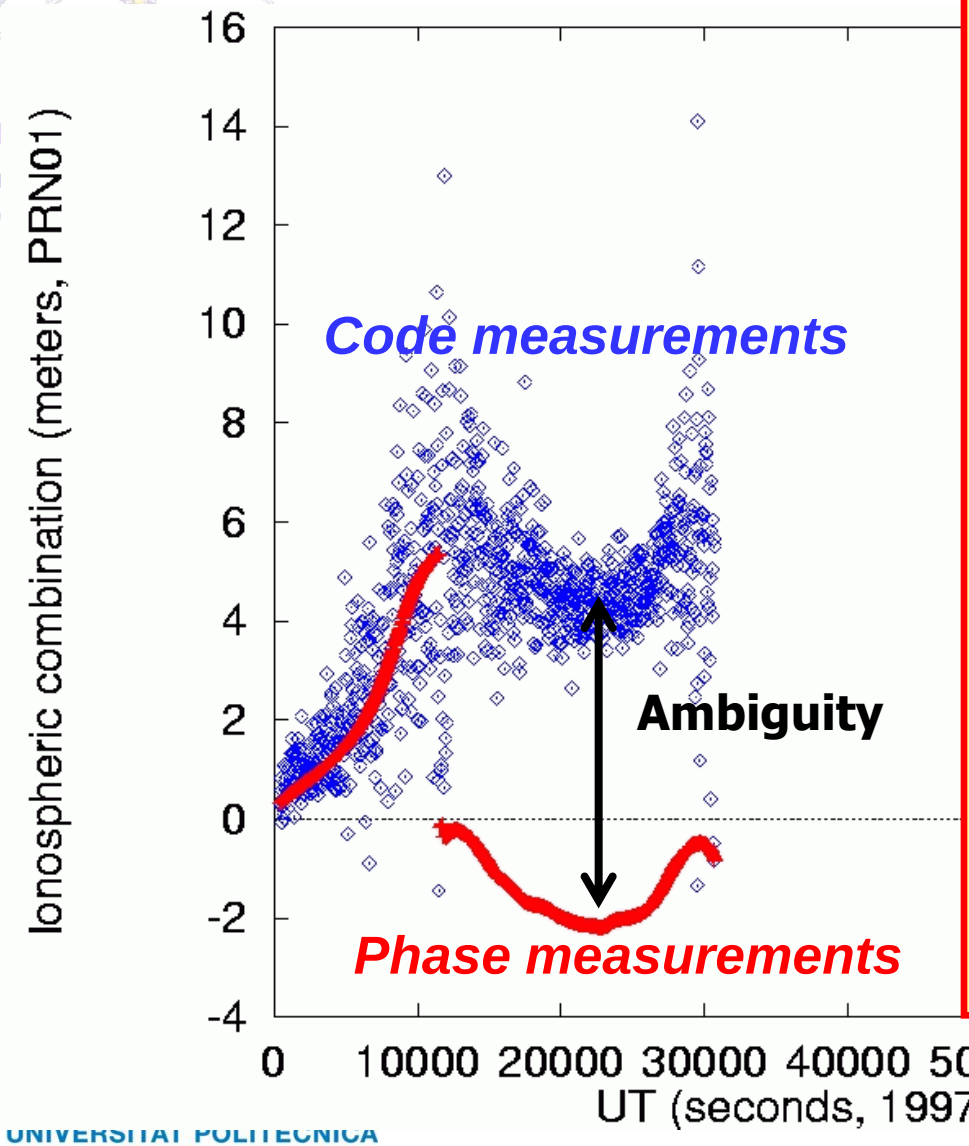

- **The code measurements (such as C/A) are accurate (psedorange) but not precise (measurement noise and multipath >~1 m).**
- **The carrier phase measurements are not accurate (unknown ambiguity = pseudorange at phase lock) but very precise (measurement noise and multipath < 1cm).**
- **To get real-time precise positioning the carrier phase ambiguities should be fixed in real-time.**
- **The differential approach is quite convenient in this task.**

The characteristic wavelengths in GPS are those associated with the corresponding carriers: $f_1 = 154\,f_0$ for L_1 and $f_2 = 120\,f_0$ for L_2, derived from the fundamental frequency $f_0 = 10.23\,\text{MHz}$, i.e., $\lambda_1 \simeq 0.19\,\text{m}$ and $\lambda_2 \simeq 0.24\,\text{m}$. For phase measurements, the error is approximately at millimeter level ($\simeq 0.01\lambda$), between two to three orders of magnitude smaller than the code measurement error. This fact, along with a much smaller multipath (less than $\frac{\lambda}{4} \simeq 0.05\,\text{m}$, typically at the level of few millimeters) due to the beat phase characteristics, makes this observable the most suitable for high-accuracy applications in general and for ionospheric sounding in particular. Indeed, precise navigation and ionospheric determinations are usually made with carrier phase measurements. However, to best utilize the carrier phase, the large associated unknown (carrier phase ambiguity) must be properly solved, typically as an unknown parameter (treated as a Gaussian random variable) in a given continuous arc of data (with no cycle-slips, i.e., with no loss of lock on the signal).

$$P_m = \rho + c(\mathrm{d}t - \mathrm{d}t') + \frac{40.309}{{f_m}^2} S + T + D_m + D'_m \quad (15)$$

and

$$L_m = \rho + c(\mathrm{d}t - \mathrm{d}t') - \frac{40.309}{{f_m}^2} S + T + B_m + \frac{c}{f_m}\phi \quad (16)$$

$$S = \int_{r_T}^{r_R} N_e \mathrm{d}l$$

here, in SI units, P_m and L_m represent the code and phase measurements, respectively, of the transmitter by the receiver at a given time t, after correcting for the corresponding antenna phase center offset and vector; ρ, $\mathrm{d}t$, $\mathrm{d}t'$, S and T are the corresponding distance, receiver and transmitter clock errors, slant total electron content and slant tropospheric delay respectively; f_m refers to the frequency of the carrier "m"; D_m and D'_m are the receiver and transmitter interfrequency differential code biases (DCBs), respectively, for the given frequency also referred to as interfrequency bias, IFB (note that the "prime" symbol represents terms associated with the GNSS transmitter/satellite). Finally, ϕ represents the relative rotation, in cycles, between the transmitter and receiver antennas (the wind-up effect associated with the

The basic relationships defining B_c and B_w ambiguities are:

$$B_c = \frac{f_1^2 B_1 - f_2^2 B_2}{f_1^2 - f_2^2}, \tag{19}$$

$$B_w = \frac{f_1 B_1 - f_2 B_2}{f_1 - f_2} \tag{20}$$

Dual-frequency GPS combinations: The iono.-free (geometric) ones, Lc, Pc, and the iono.- & geom.free one, Melbourne-Wubbena, MW=Lw-Pn

associated with the corresponding ionospheric-free and widelane carrier phase combinations:

$$L_c = \frac{f_1^2 L_1 - f_2^2 L_2}{f_1^2 - f_2^2}, \tag{21}$$

$$L_w = \frac{f_1 L_1 - f_2 L_2}{f_1 - f_2}. \tag{22}$$

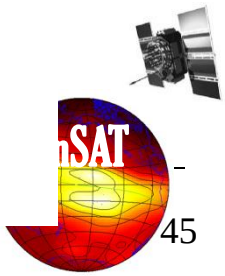

$$P_c = \frac{f_1^2 P_1 - f_2^2 P_2}{f_1^2 - f_2^2}, \qquad (23)$$

$$P_n = \frac{f_1 P_1 + f_2 P_2}{f_1 + f_2}.$$

In this last case, the Melbourne-Wübbena combination $M_w = L_w - P_n$ can be formed. From here on, it is straightforward to deduce that the phase ambiguity B_I of the ionospheric combination of carrier phases $L_I = L_1 - L_2$ (see Eq. 17) can be computed from B_c and B_w (which helps in the determination of the electron content in ionospheric models based on permanent GNSS receiver data; see the corresponding subsection below):

$$B_I \equiv B_1 - B_2 = \frac{\lambda_1 \lambda_2}{\lambda_w \lambda_n}[B_w - B_c] \qquad (25)$$

considering

$$B_w = M_w - \frac{\lambda_w \lambda_n}{\lambda_1 \lambda_2}(D_I + D'_I) \qquad (26)$$

$$P_m = \rho + c(\mathrm{d}t - \mathrm{d}t') + \frac{40.309}{f_m{}^2} S + T + D_m + D'_m \quad (15)$$

and

$$L_m = \rho + c(\mathrm{d}t - \mathrm{d}t') - \frac{40.309}{f_m{}^2} S + T + B_m + \frac{c}{f_m}\phi \quad (16)$$

$$S = \int_{r_T}^{r_R} N_e \mathrm{d}l$$

here, in SI units, P_m and L_m represent the code and phase measurements, respectively, of the transmitter by the receiver at a given time t, after correcting for the corresponding antenna phase center offset and vector; ρ, $\mathrm{d}t$, $\mathrm{d}t'$, S and T are the corresponding distance, receiver and transmitter clock errors, slant total electron content and slant tropospheric delay respectively; f_m refers to the frequency of the carrier "m"; D_m and D'_m are the receiver and transmitter interfrequency differential code biases (DCBs), respectively, for the given frequency also referred to as interfrequency bias, IFB (note that the "prime" symbol represents terms associated with the GNSS transmitter/satellite). Finally, ϕ represents the relative rotation, in cycles, between the transmitter and receiver antennas (the wind-up effect associated with the

*Let's **focus on** the frequency dependent term due to the **ionosphere** (an opportunity as **extra condition for precise RT positioning**, and GNSS as **geophysical RT sounder**)*

More details can be found for instance in:

J Geod
DOI 10.1007/s00190-011-0508-5

ORIGINAL ARTICLE

The ionosphere: effects, GPS modeling and the benefits for space geodetic techniques

Manuel Hernández-Pajares · J. Miguel Juan · Jaume Sanz ·
Àngela Aragón-Àngel · Alberto García-Rigo ·
Dagoberto Salazar · Miquel Escudero

Received: 1 July 2010 / Accepted: 13 August 2011
© Springer-Verlag 2011

What happen with the up to 0.1% of the ionospheric effect not explained in these fundamental GNSS equations? It can be corrected from models (now in a Web service!)

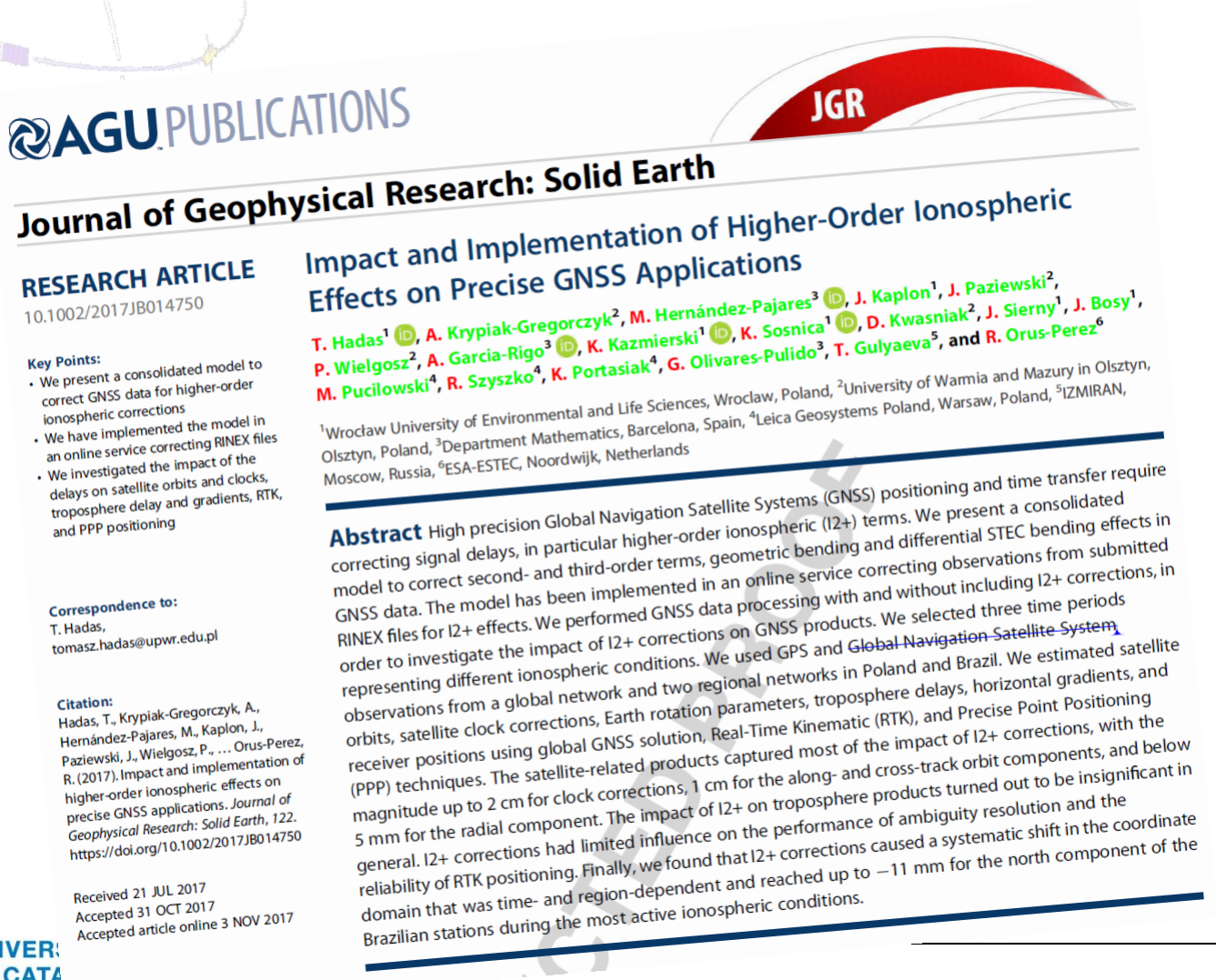

AGU PUBLICATIONS

JGR

Journal of Geophysical Research: Solid Earth

RESEARCH ARTICLE

10.1002/2017JB014750

Key Points:
- We present a consolidated model to correct GNSS data for higher-order ionospheric corrections
- We have implemented the model in an online service correcting RINEX files
- We investigated the impact of the delays on satellite orbits and clocks, troposphere delay and gradients, RTK, and PPP positioning

Correspondence to:
T. Hadas,
tomasz.hadas@upwr.edu.pl

Citation:
Hadas, T., Krypiak-Gregorczyk, A., Hernández-Pajares, M., Kaplon, J., Paziewski, J., Wielgosz, P., … Orus-Perez, R. (2017). Impact and implementation of higher-order ionospheric effects on precise GNSS applications. *Journal of Geophysical Research: Solid Earth*, *122*. https://doi.org/10.1002/2017JB014750

Received 21 JUL 2017
Accepted 31 OCT 2017
Accepted article online 3 NOV 2017

Impact and Implementation of Higher-Order Ionospheric Effects on Precise GNSS Applications

T. Hadas[1], A. Krypiak-Gregorczyk[2], M. Hernández-Pajares[3], J. Kaplon[1], J. Paziewski[2], P. Wielgosz[2], A. Garcia-Rigo[3], K. Kazmierski[1], K. Sosnica[1], D. Kwasniak[2], J. Sierny[1], J. Bosy[1], M. Pucilowski[4], R. Szyszko[4], K. Portasiak[4], G. Olivares-Pulido[3], T. Gulyaeva[5], and R. Orus-Perez[6]

[1]Wrocław University of Environmental and Life Sciences, Wroclaw, Poland, [2]University of Warmia and Mazury in Olsztyn, Olsztyn, Poland, [3]Department Mathematics, Barcelona, Spain, [4]Leica Geosystems Poland, Warsaw, Poland, [5]IZMIRAN, Moscow, Russia, [6]ESA-ESTEC, Noordwijk, Netherlands

Abstract High precision Global Navigation Satellite Systems (GNSS) positioning and time transfer require correcting signal delays, in particular higher-order ionospheric (I2+) terms. We present a consolidated model to correct second- and third-order terms, geometric bending and differential STEC bending effects in GNSS data. The model has been implemented in an online service correcting observations from submitted RINEX files for I2+ effects. We performed GNSS data processing with and without including I2+ corrections, in order to investigate the impact of I2+ corrections on GNSS products. We selected three time periods representing different ionospheric conditions. We used GPS and Global Navigation Satellite System observations from a global network and two regional networks in Poland and Brazil. We estimated satellite orbits, satellite clock corrections, Earth rotation parameters, troposphere delays, horizontal gradients, and receiver positions using global GNSS solution, Real-Time Kinematic (RTK), and Precise Point Positioning (PPP) techniques. The satellite-related products captured most of the impact of I2+ corrections, with the magnitude up to 2 cm for clock corrections, 1 cm for the along- and cross-track orbit components, and below 5 mm for the radial component. The impact of I2+ on troposphere products turned out to be insignificant in general. I2+ corrections had limited influence on the performance of ambiguity resolution and the reliability of RTK positioning. Finally, we found that I2+ corrections caused a systematic shift in the coordinate domain that was time- and region-dependent and reached up to −11 mm for the north component of the Brazilian stations during the most active ionospheric conditions.

PROOF

Layout:

1) [**Motivation**] Precise Agriculture (PA) presentation (EU AUDITOR experiment)

2) [**Background**]: Brief introduction to main identified points of the presentation:
   a) GPS fundamentals: pseudoranges and carrier phases (optional)
   b) Ionospheric electron content
   c) Wide Area Real-Time Kinematic
   d) The International GNSS Service (*optional*)

3) [**One efficient operative system**] Quick introduction to Linux (*optional*)

4) [**New tools for learning and research**] IonSAT Tools (IT), emulating Real-Time (RT) as much as possible (presented on the PA AUDITOR experiment):
   a) *gim2vtec.v2.scr*
   b) *gimrnx2stec.v2.scr*

5) [**IT application to ECLIPSE, FLARE & GSTORM scenarios**] (*optional*).

6) [**Example of RT GPS-ionospheric system**]: UPC-IonSAT since 2012.

7) [**Monitoring of co-seismic generated ionospheric signals]:** Application of RT ionospheric sounding for potential Tsunami warnings), with GNSS dense (Tohoku and mid earthquakes, EQ) and sparse networks (Chile 2015 EQ).

8) [**Conclusions**]

Dual-frequency GPS combinations: The geometry-free (ionospheric) ones: LI, PI

$$L_I \equiv L_1 - L_2 = \alpha \cdot S - \beta \cdot \phi + B_I, \quad (17)$$

$$P_I \equiv P_2 - P_1 = \alpha \cdot S + D_I + D'_I + \epsilon_M + \epsilon_T, \quad (18)$$

where $\alpha = 40.309\left(\frac{1}{f_2^2} - \frac{1}{f_1^2}\right) = 1.05 \cdot 10^{-17}\, m^3$, $\beta = c\left(\frac{1}{f_2} - \frac{1}{f_1}\right) = 0.054\,\text{m}$, $B_I = B_1 - B_2$, $D_I = D_2 - D_1$ and $D'_I = D'_2 - D'_1$.[2] In this case, we also made explicit the two main components of the measurement error, both corresponding to the code: the multipath code error ϵ_M and the thermal noise measurement error ϵ_T. Typically, the wind-up term $\beta \cdot \phi$ is a centimeter-level term. For the permanent receivers, this term can be corrected very accurately from their coordinates and orbital information, and it is not discussed explicitly herein.

Estimating the ionospheric electron content…

The GNSS ionospheric measurements are an excellent input for estimating the ionospheric electron content distribution, for instance performing tomography (layout of its implementation in TOMION UPC-IonSAT software).

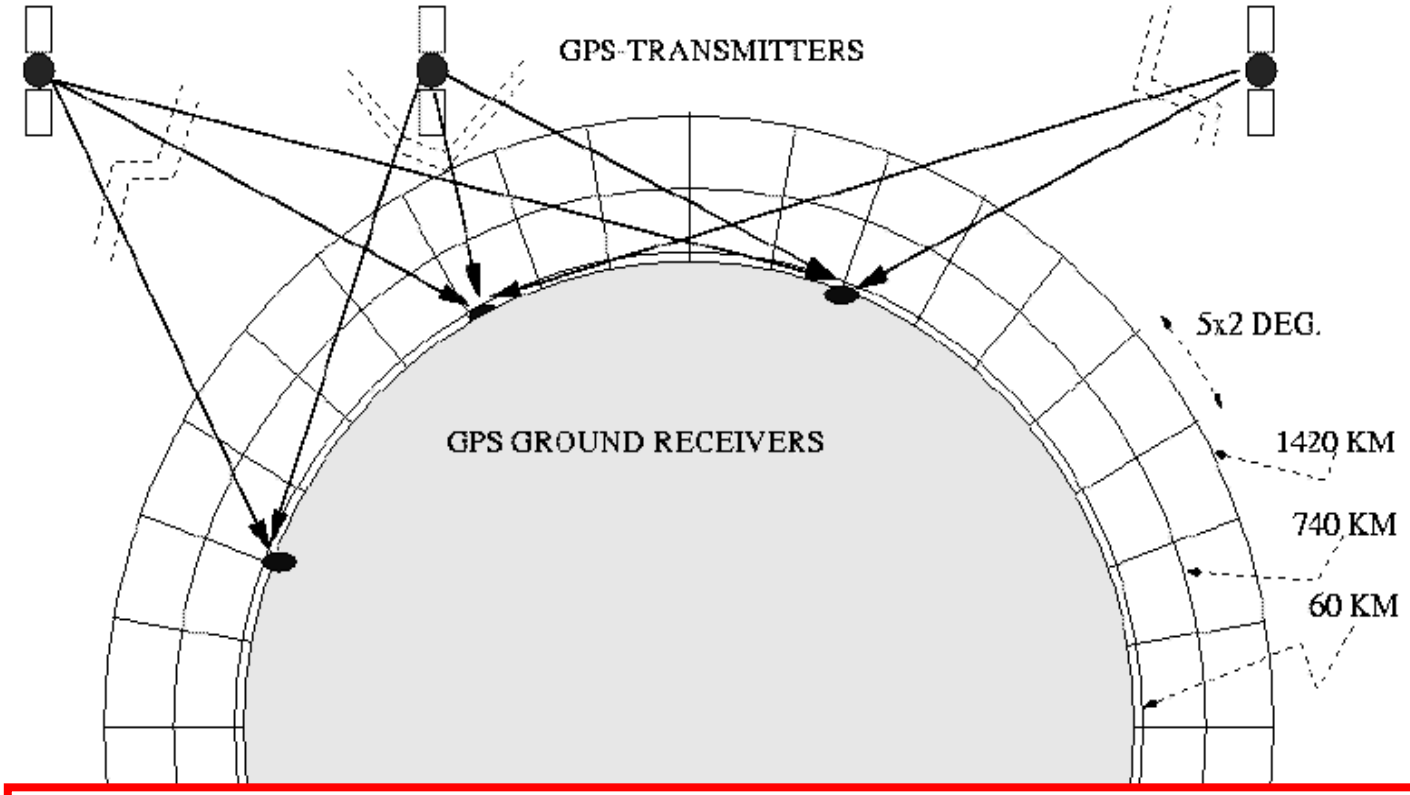

$$L_I = STEC + B_I = \int_{REC}^{SAT} N_e dl + B_I = \sum_i \sum_j \sum_k (N_e)_{i,j,k} \Delta s_{i,j,k} + B_I$$

GPS and the Ionosphere

The GPS signals are affected by the free electrons: carrier phase advance and code/pseudorange delays.

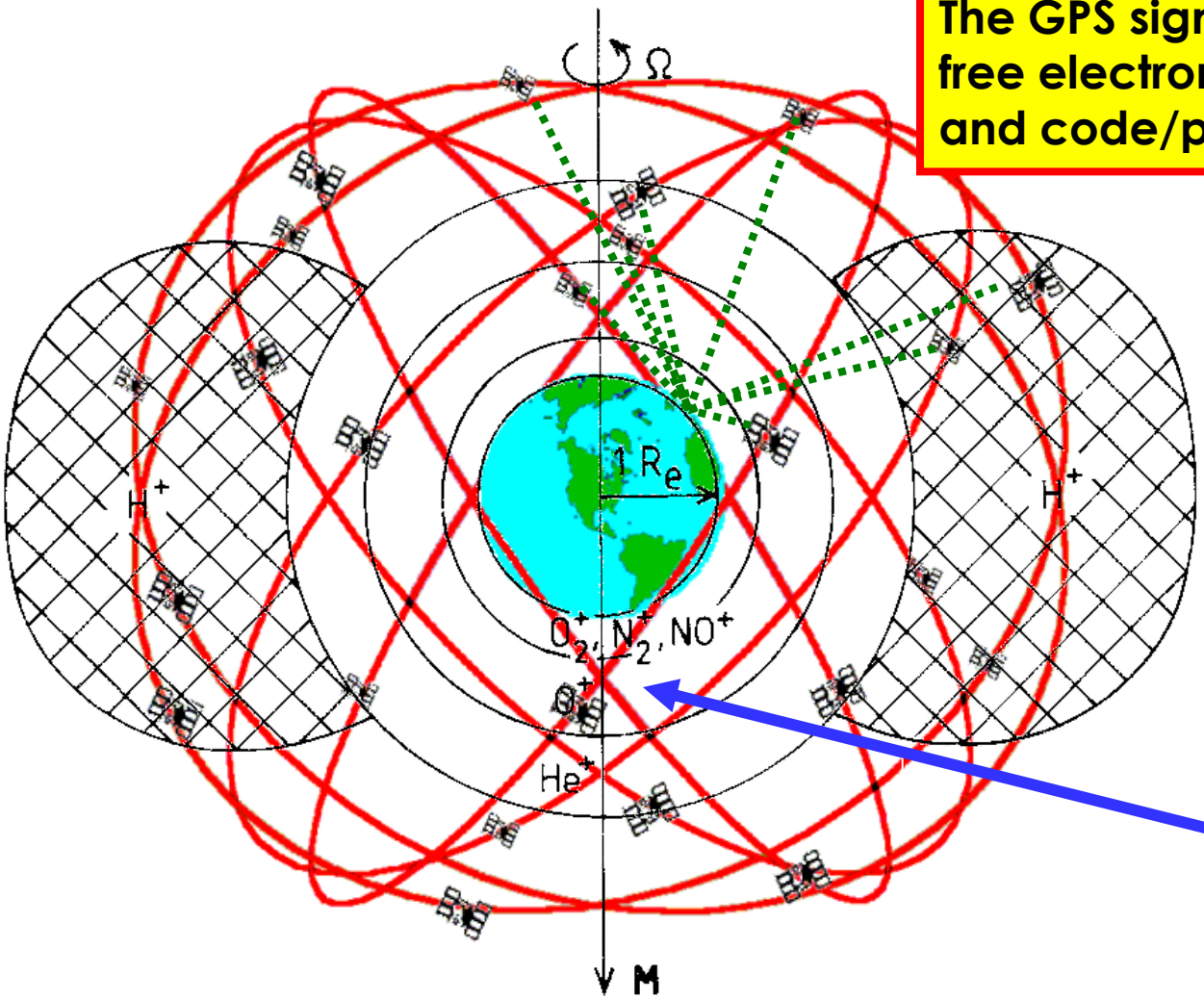

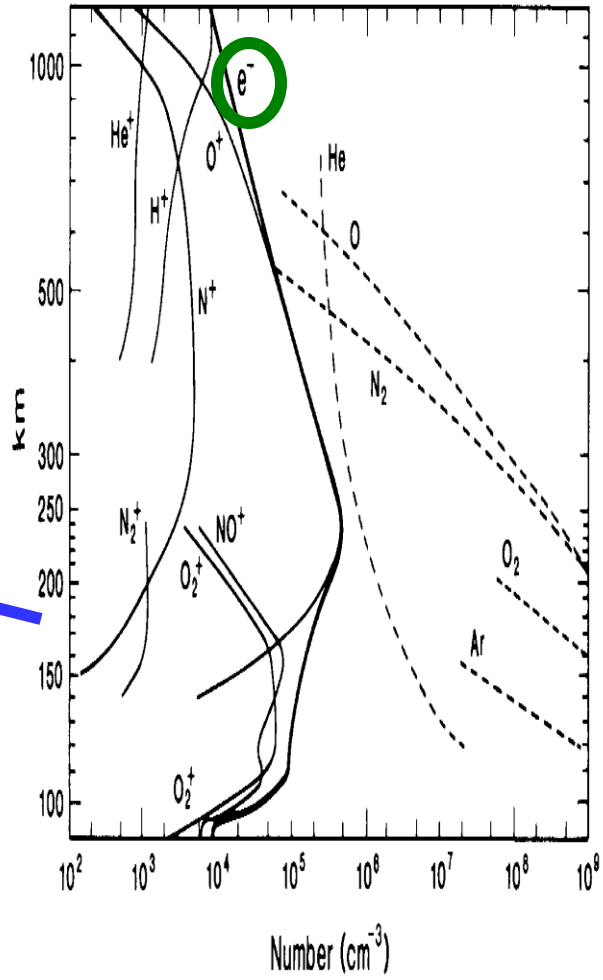

The UV (and X) Solar radiation ionizes the region above 50-100 km: Ionosphere (to 1000 km) and Protonosphere/Plasmasphere (above 1000 km).

Ionospheric delay at a glance

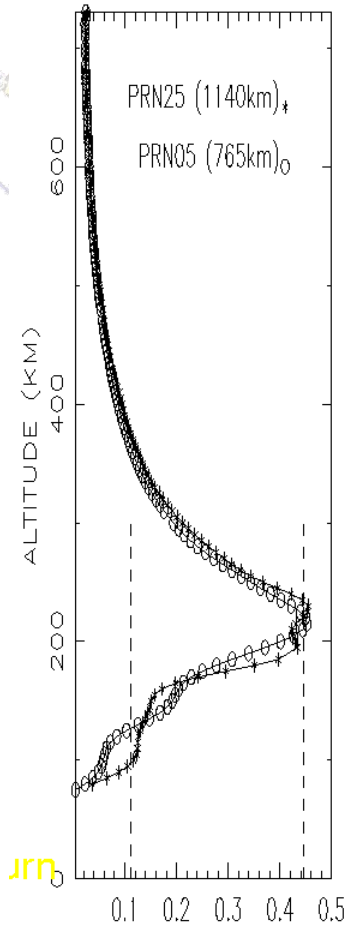

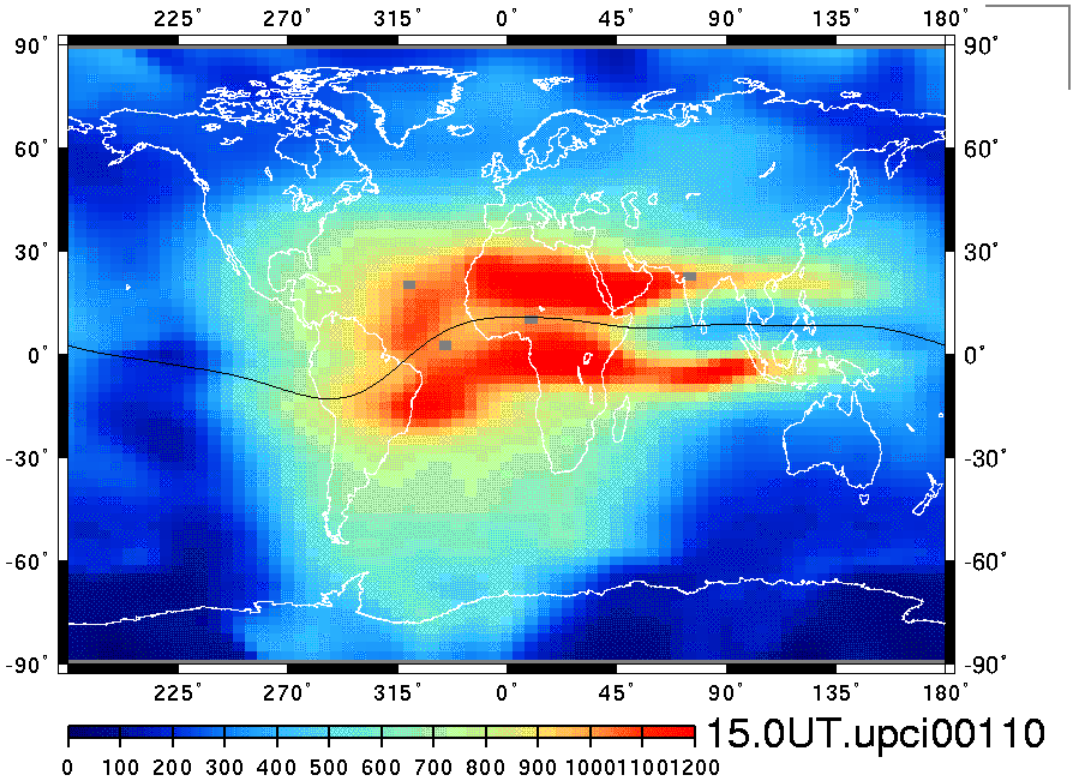

$$\delta R_{IONOSPHERE}[m] \simeq 0.4 \frac{STEC[TECU]}{f^2[GHz^2]}$$

$$1\,TECU = 10^{16} el./m^2 \simeq 15\,cm \simeq 0.5\,ns \text{ in } L_1$$

Typical noon VTEC ionospheric values ranges at mid latitude from 20 to 80 TECU, depending on the Solar cycle and season (3 to 12m in L1, 0.1 to 2 m in C band) (*) 1 TECU=16 cm at L1

Equatorial anomalies and E cross B drift

Assuming only electric and magnetic fields acting on the charged particled, the component of E along B will vanish (it is the only force acting in this direction, generating a polarized field which suppress the external one).

$$\underbrace{\left\langle m\dot{\vec{v}}\right\rangle = q\vec{E} + q\vec{u}_E \times \vec{B} = \vec{0}}_{\times \vec{B}}$$

$$\vec{0} = q\vec{E}\times\vec{B} + q\left[\underbrace{\vec{u}_E \cdot \vec{B}}_{0}\vec{B} - B^2\vec{u}_E\right]$$

$$\vec{u}_E = \frac{1}{B^2}\vec{E}\times\vec{B}$$

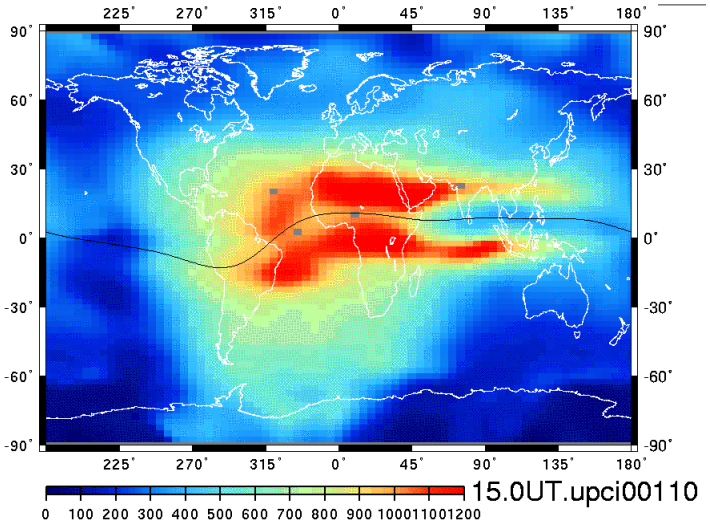

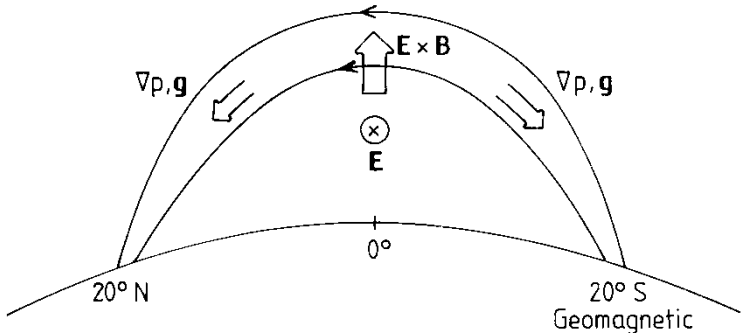

Being u_E the displacement velocity generated by the E cross B drift. For a general force F:

$$\vec{u}_F = \frac{1}{qB^2}\vec{F}\times\vec{B}$$

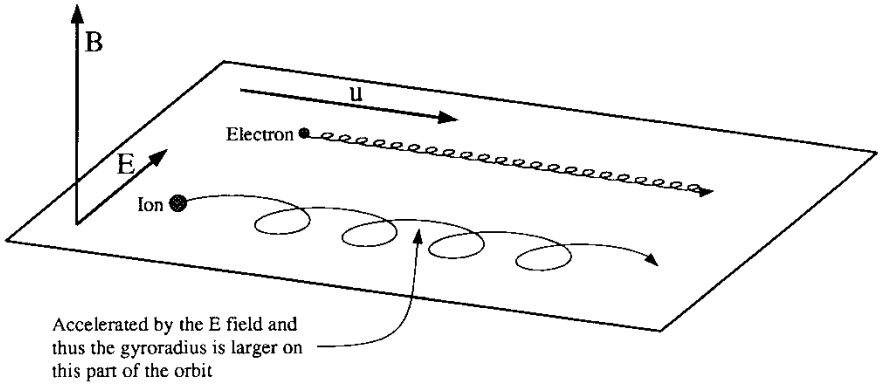

11-years Solar cycle

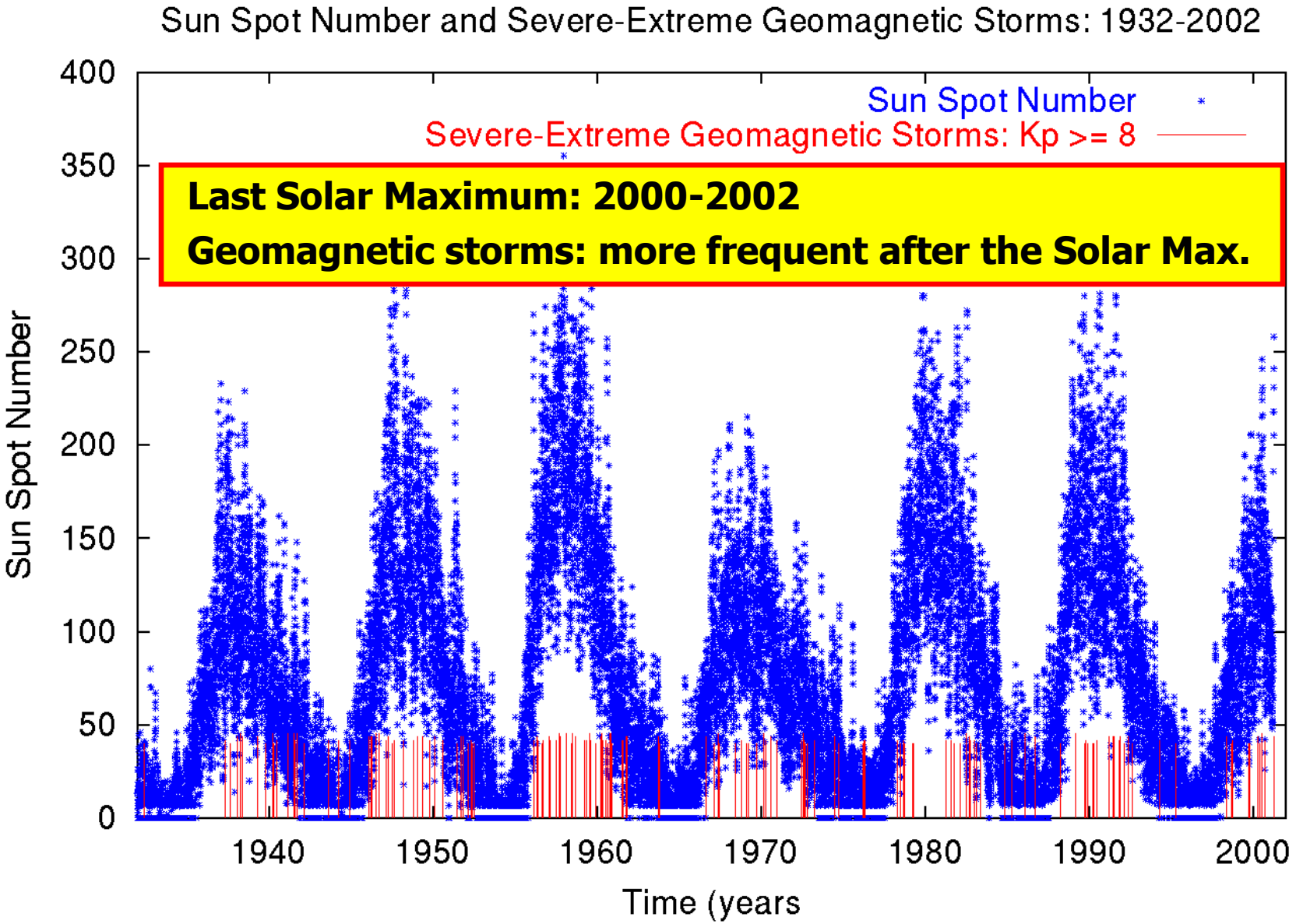

VTEC: Modulated by the Solar Cycle

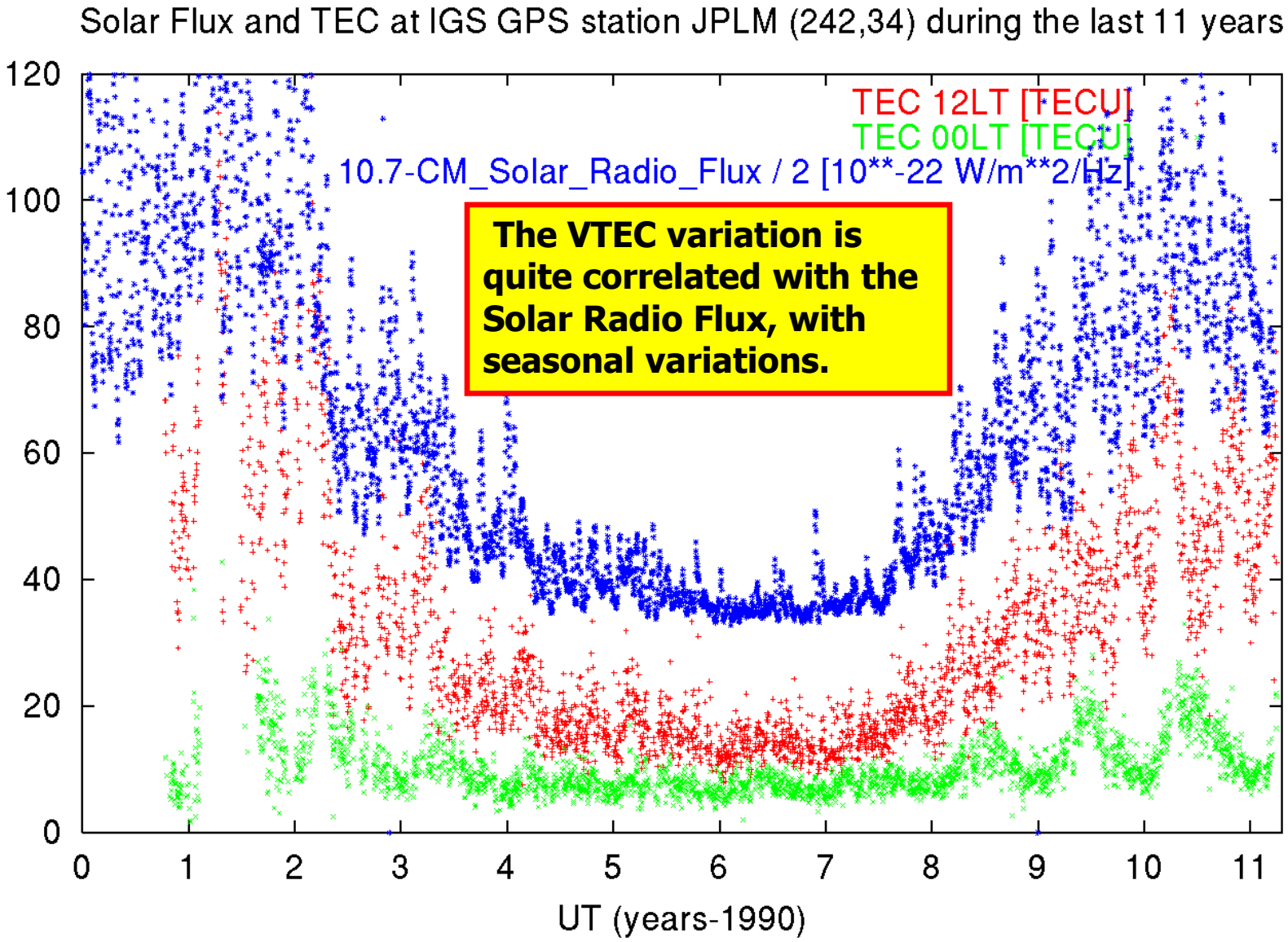

VTEC modulated by the Season

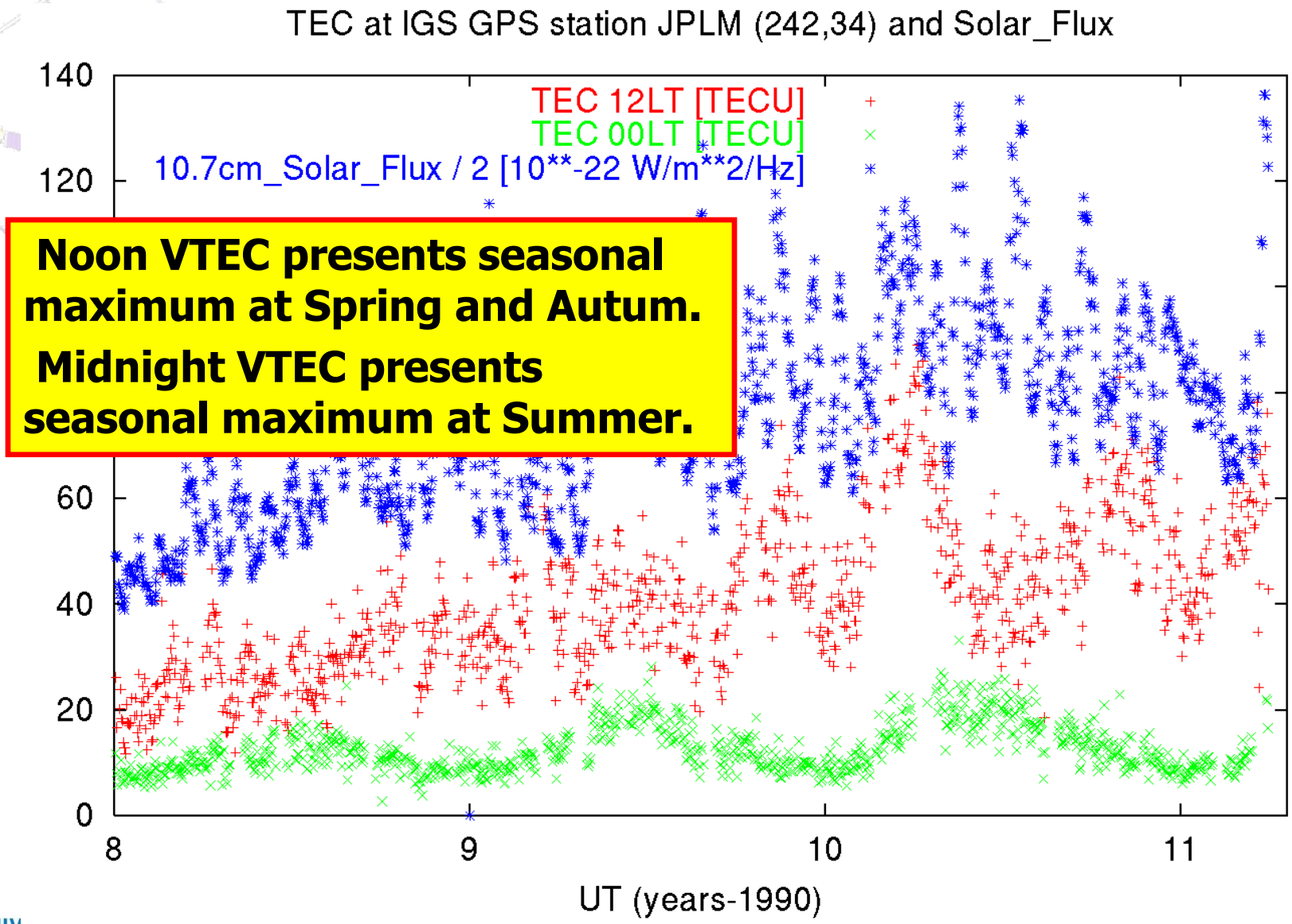

Noon VTEC presents seasonal maximum at Spring and Autum.

Midnight VTEC presents seasonal maximum at Summer.

VTEC can change during geomagnetic storms

During geomagnetic storms the VTEC can experience enhancements or decreases of 100%

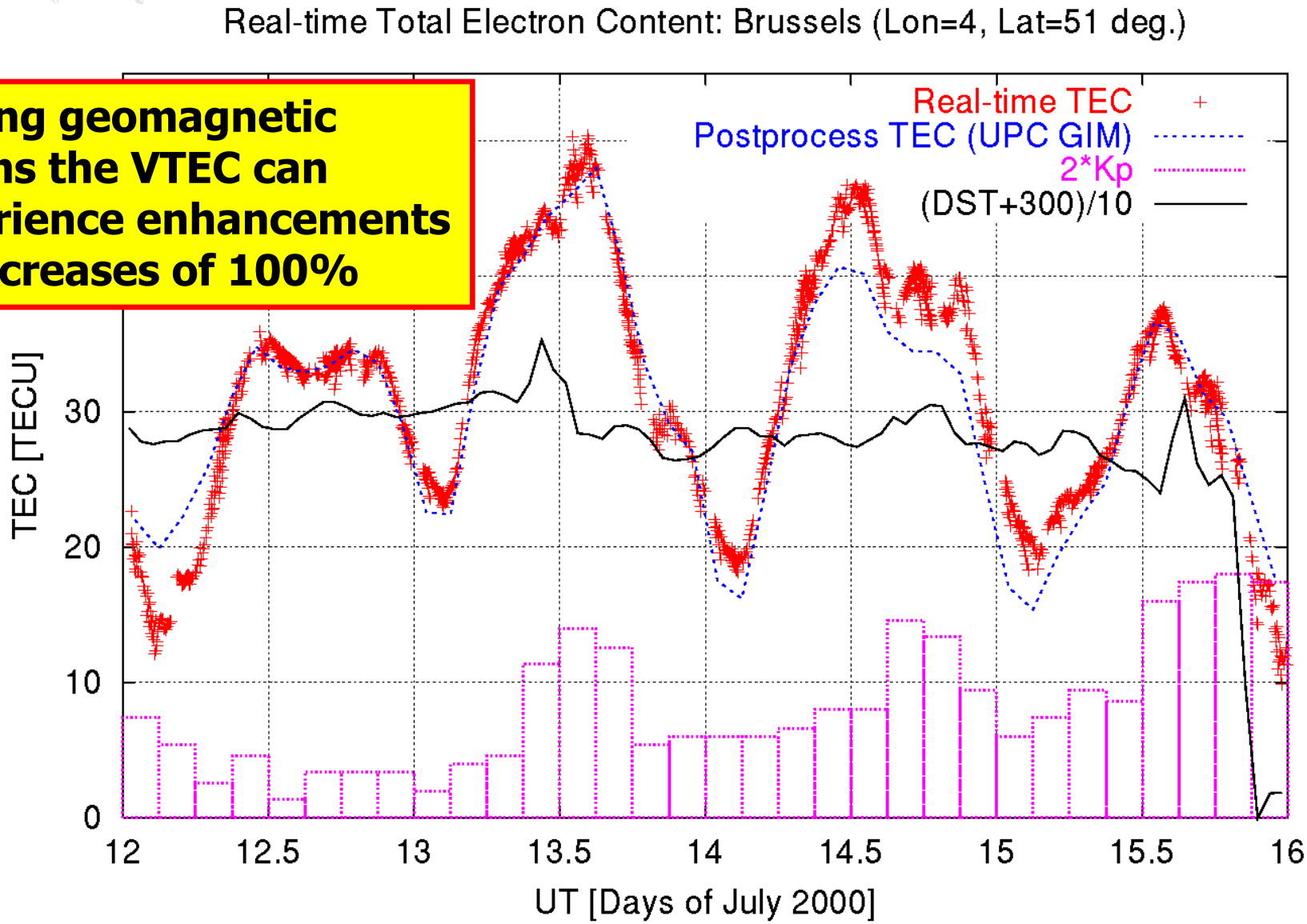

Scintillation: Very rapid VTEC variations

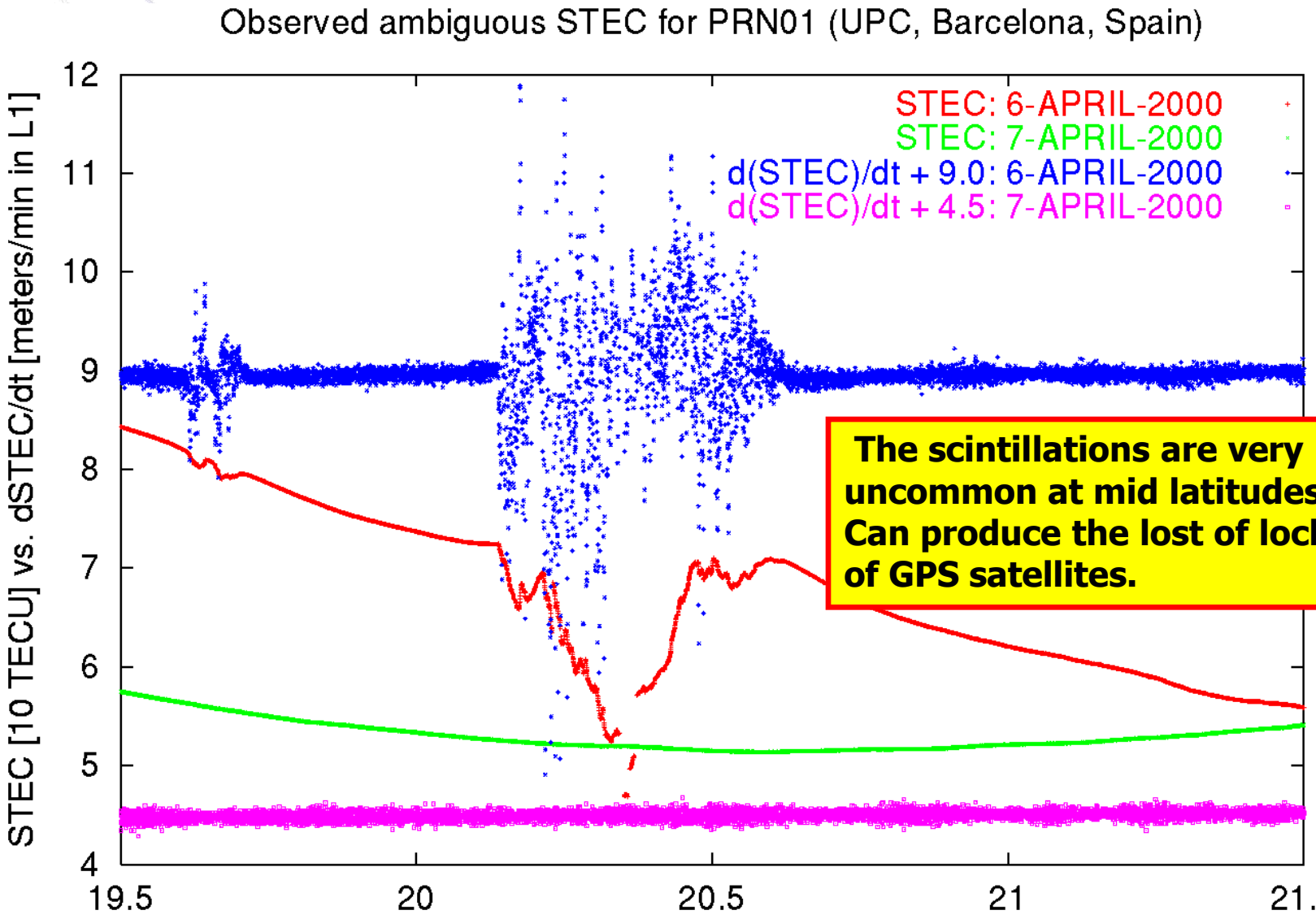

The scintillations are very uncommon at mid latitudes. Can produce the lost of lock of GPS satellites.

AGU PUBLICATIONS

Space Weather

RESEARCH ARTICLE
10.1002/2017SW001674

Midlatitude postsunset plasma bubbles observed over Europe during intense storms in April 2000 and 2001

Zama Thobeka Katamzi-Joseph[1,2], **John Bosco Habarulema**[1,2], **and Manuel Hernández-Pajares**[3]

[1]South African National Space Agency, Space Science, Hermanus, South Africa, [2]Department of Physics and Electronics, Rhodes University, Grahamstown, South Africa, [3]Department of Mathematics, UPC-IonSAT, Barcelona, Spain

Key Points:
- Midlatitude postsunset plasma bubbles observations with GNSS TEC during severe storms in 2000 and 2001
- Results indicate that the plasma bubbles were migrating north from low latitudes at virtual speed of 400 m/s
- Evidence of postsunset plasma enhancement and EIA extension to European midlatitudes presented

Correspondence to:
Z. T. Katamzi-Joseph,
zkatamzi@sansa.org.za

Citation:
Katamzi-Joseph, Z. T., J. B. Habarulema, and M. Hernández-Pajares (2017), Midlatitude postsunset plasma bubbles observed over Europe during intense storms in April 2000 and 2001, *Space Weather*, *15*, doi:10.1002/2017SW001674.

Received 1 JUN 2017
Accepted 8 AUG 2017
Accepted article online 14 AUG 2017

Abstract Plasma bubbles are prevalent features of the equatorial/low-latitude ionosphere which are seldom observed at middle and high latitudes. Understanding the influence of geomagnetic storms on plasma bubbles' migration to higher latitudes is an important space weather topic, since a geomagnetic storm is an important phenomenon of space weather. This paper reports on the first observations of postsunset/evening midlatitude plasma bubbles in the European sector during the main phase of severe storms ($Dst \leq -200$ nT) on 6 April 2000 and 11 April 2001. Plasma depletions observed in Global Navigation Satellite System total electron content measurements are confirmed with those observed from in situ Defense Meteorological Satellite Program ion density measurements. The results show that the plasma bubbles were migrating north at virtual speeds of 400 m/s and on each of the storm days they extended as far north as ~42° (geographic latitude). It is estimated that the plasma bubbles may have grown to a maximum apex height of approximately 4000 km. During the time of bubble occurrence, the evening midlatitude plasma was enhanced and the equatorial ionization anomaly extended to European midlatitudes. In addition, evidence of the upward plasma motion was found in ionosonde h_mF_2 and h′F measurements, while the interplanetary electric field E_y was enhanced. This was found to suggest that the possible mechanism for the enhancement of midlatitude plasma and subsequent midlatitude plasma bubbles occurrence was the eastward penetration electric field associated with B_z southward turning.

STEC can be affected by Travelling Ionospheric Disturbances

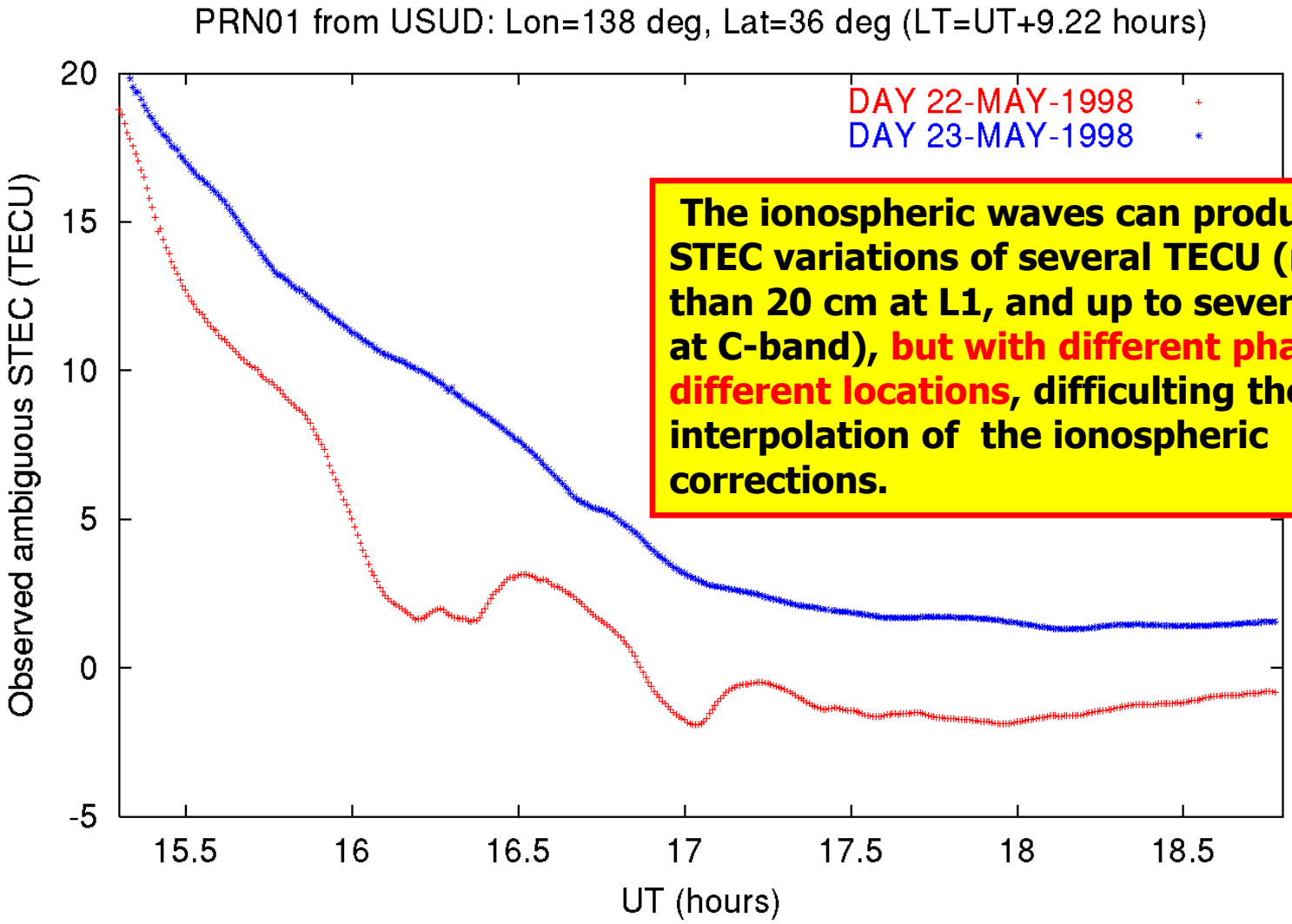

The ionospheric waves can produce STEC variations of several TECU (more than 20 cm at L1, and up to several cm at C-band), but with different phases at different locations, difficulting the interpolation of the ionospheric corrections.

AGU PUBLICATIONS

Radio Science

RESEARCH ARTICLE

10.1002/2016RS006159

Direct MSTID mitigation in precise GPS processing

Manuel Hernández-Pajares[1], Pawel Wielgosz[2], Jacek Paziewski[2], Anna Krypiak-Gregorczyk[2], Marta Krukowska[2], Katarzyna Stepniak[2], Jan Kaplon[3], Tomasz Hadas[3], Krzysztof Sosnica[3], Jaroslaw Bosy[3], Raul Orus-Perez[4], Enric Monte-Moreno[1], Heng Yang[1], Alberto Garcia-Rigo[1], and Germán Olivares-Pulido[1]

[1]Department Mathematics, UPC-IonSAT, Barcelona, Spain, [2]University of Warmia and Mazury in Olsztyn, Olsztyn, Poland, [3]Wroclaw University of Environmental and Life Sciences, Wroclaw, Poland, [4]ESA-ESTEC, Noordwijk, Netherlands

Key Points:
- Direct and simple MSTID mitigation technique (dGII) for GPS observations
- dGII is applicable to differential GPS processing (just one baseline is needed)
- Precise positioning is improved by means of dGII, in terms of ambiguity fixing and convergence time

Correspondence to:
M. Hernández-Pajares,
manuel.hernandez@upc.edu

Citation:
Hernández-Pajares, M., et al. (2017), Direct MSTID mitigation in precise GPS processing, *Radio Sci.*, *52*, doi:10.1002/2016RS006159.

Received 9 SEP 2016
Accepted 29 JAN 2017
Accepted article online 2 FEB 2017
Corrected 5 APR 2017

This article was corrected on 5 APR 2017. See the end of the full text for details.

Abstract In this paper, the authors summarize a simple and efficient approach developed to mitigate the problem in precise Global Navigation Satellite Systems (GNSS) positioning originated by the most frequent ionospheric wave signatures: the medium-scale traveling ionospheric disturbances (MSTIDs). The direct GNSS Ionospheric Interferometry technique (hereinafter dGII), presented in this paper, is applied for correcting MSTID effects on precise Real Time Kinematic (RTK) and tropospheric determination. It consists of the evolution of the former climatic Differential Delay Mitigation Model for MSTIDs (DMTID), for real-time conditions, using ionospheric data from a single permanent receiver only. The performance is demonstrated with networks of GNSS receivers in Poland, treated as users under real-time conditions, during two representative days in winter and summer seasons (days 353 and 168 of year 2013). In range domain, dGII typically reduces the ionospheric delay error up to 10–90% of the value when the MSTID mitigation model is not applied. The main dGII impact on precise positioning is that we can obtain reliable RTK position faster. In particular, the ambiguity success rate parameter increases, from 74% to 83%, with respect to the original uncorrected observations. The average of time to first fix is shortened from 30 s to 13 s. The improvement in troposphere estimaton, due to any potential impact of the MSTID mitigation model, was most difficult to demonstrate.

VTEC: Modulated by the Solar Cycle

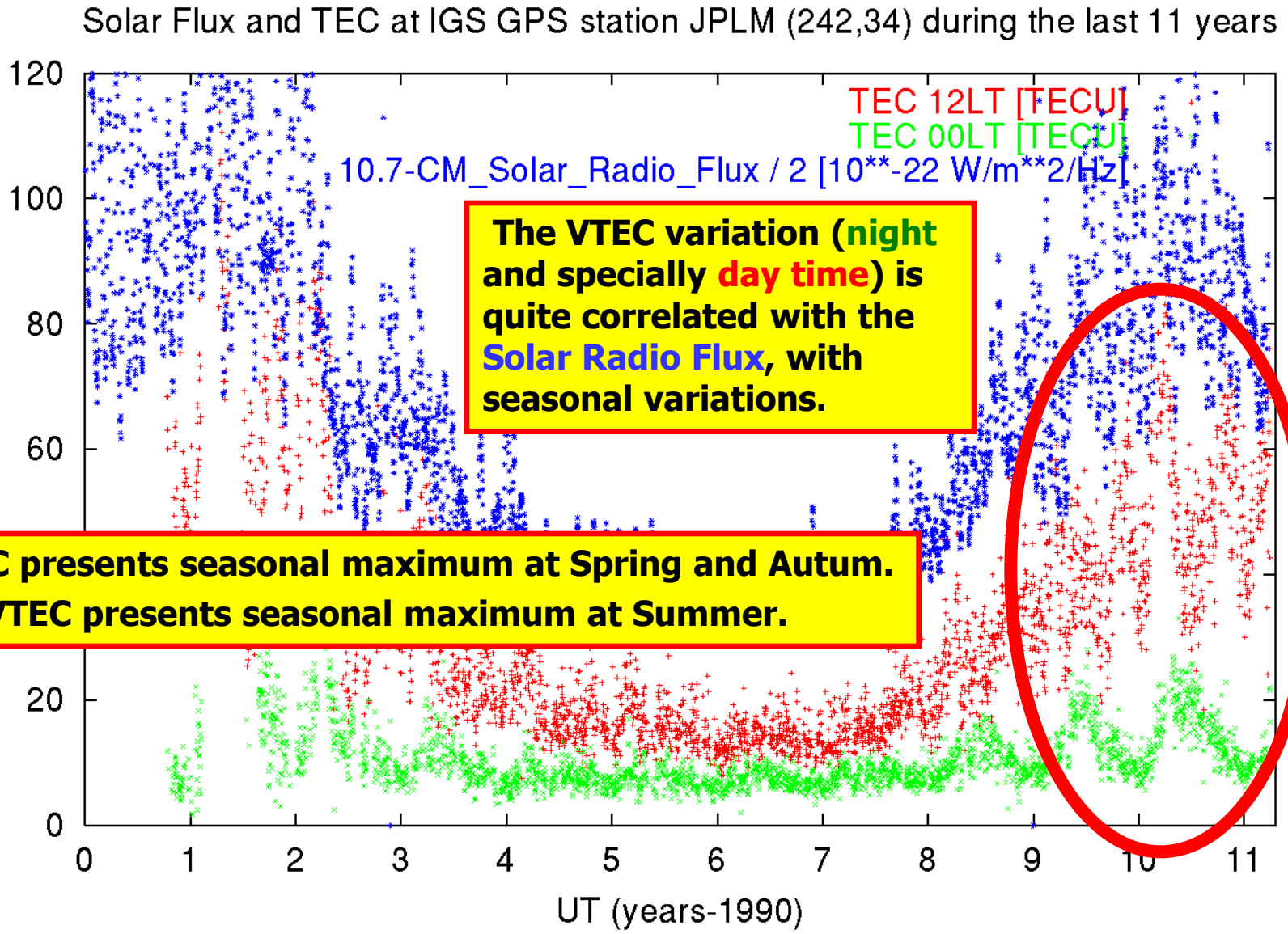

The VTEC variation (night and specially day time) is quite correlated with the Solar Radio Flux, with seasonal variations.

Noon VTEC presents seasonal maximum at Spring and Autum.
Midnight VTEC presents seasonal maximum at Summer.

Effects on single-frequency navigation based on broadcasted iono corrections (EGNOS Test Bed)

Ionospheric Storm during October 30th,2003

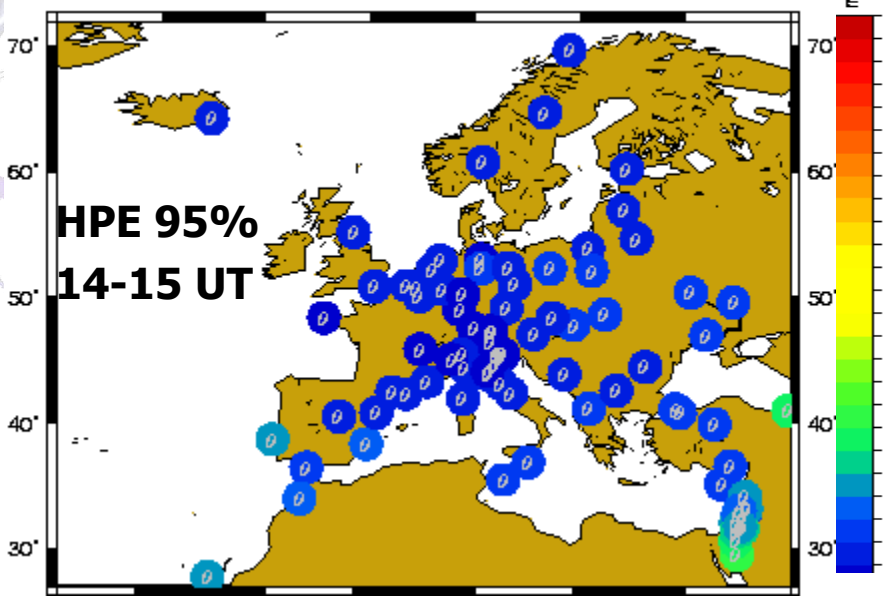

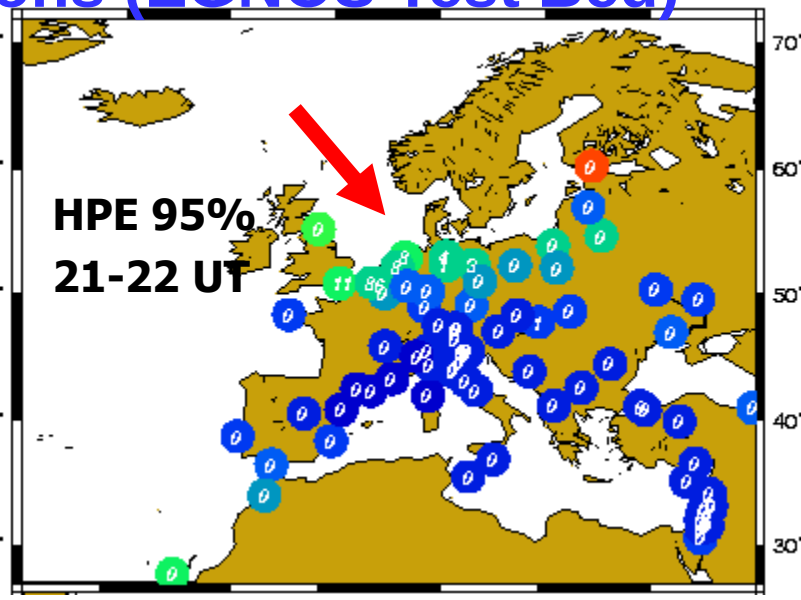

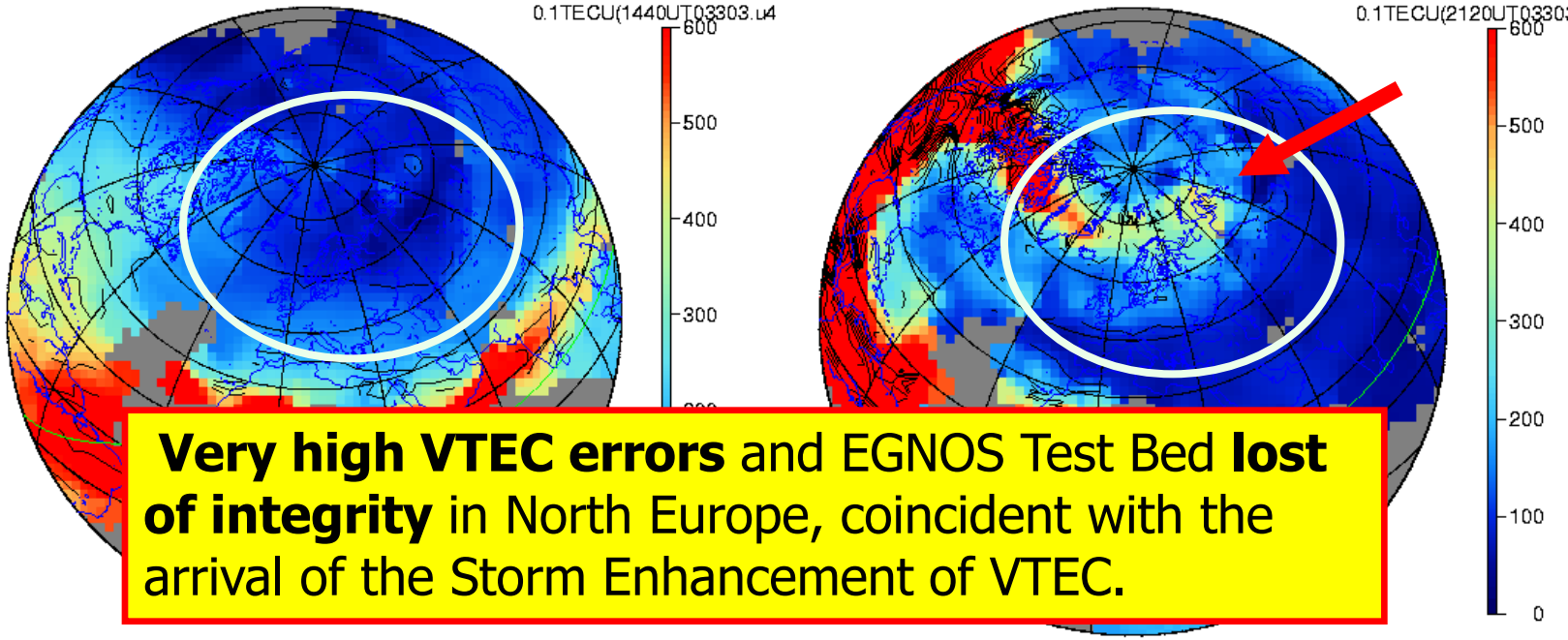

Very high VTEC errors and EGNOS Test Bed **lost of integrity** in North Europe, coincident with the arrival of the Storm Enhancement of VTEC.

Ann. Geophys., 35, 377–391, 2017
www.ann-geophys.net/35/377/2017/
doi:10.5194/angeo-35-377-2017
© Author(s) 2017. CC Attribution 3.0 License.

Annales Geophysicae Open Access EGU

MONITOR Ionospheric Network: two case studies on scintillation and electron content variability

Yannick Béniguel[1], Iurii Cherniak[2], Alberto Garcia-Rigo[3], Pierrick Hamel[1], Manuel Hernández-Pajares[3], Roland Kameni[4], Anton Kashcheyev[5], Andrzej Krankowski[2], Michel Monnerat[8], Bruno Nava[5], Herbert Ngaya[4], Raül Orus-Perez[6], Hughes Secrétan[7], Damien Sérant[8], Stefan Schlüter[9], and Volker Wilken[10]

[1]Informatique, Electromagnétisme, Electronique, Analyse numérique (IEEA), Courbevoie, 92400, France
[2]University of Warmia and Mazury, Olsztyn, Poland
[3]UPC-IonSat, Universitat Politècnica de Catalunya, Barcelona, 08034, Spain
[4]Agence pour la sécurité de la navigation aérienne en Afrique et à Madagascar (ASECNA), Dakar, Senegal
[5]International Center for Theoretical Physics (ICTP), Trieste, 34014, Italy
[6]European Space Agency/European Space Research and Technology Center (ESA/ESTEC), Noordwijk, 2201 AZ, the Netherlands
[7]Centre National d'Etudes Spatiales (CNES), Toulouse, 31401, France
[8]Thales Alenia Space France, Toulouse, 31037, France
[9]European Space Agency/EGNOS Project Office (ESA/EPO), Toulouse, 31401, France
[10]Deutsches Zentrum für Luft- und Raumfahrt (DLR), Neustrelitz, 17235, Germany

Correspondence to: Yannick Béniguel (beniguel@ieea.fr)

Received: 31 July 2016 – Revised: 23 January 2017 – Accepted: 1 February 2017 – Published: 13 March 2017

Global and sudden STEC increase in the day hemisphere due to Solar X-flares

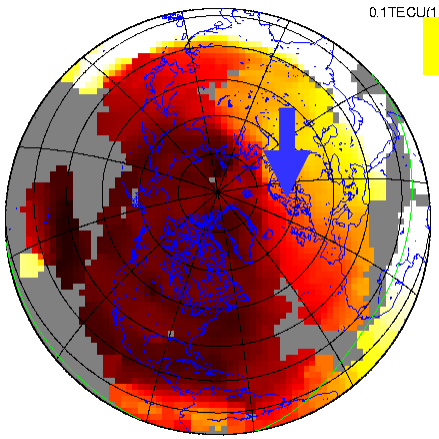

1000UT

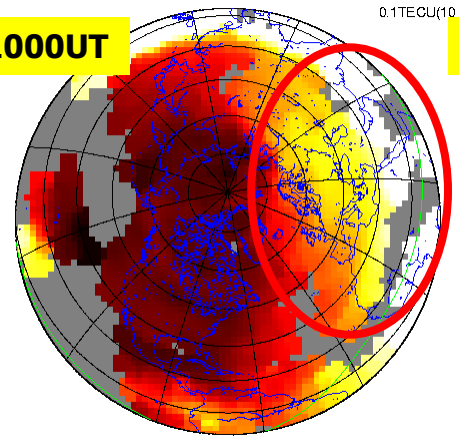

1040UT

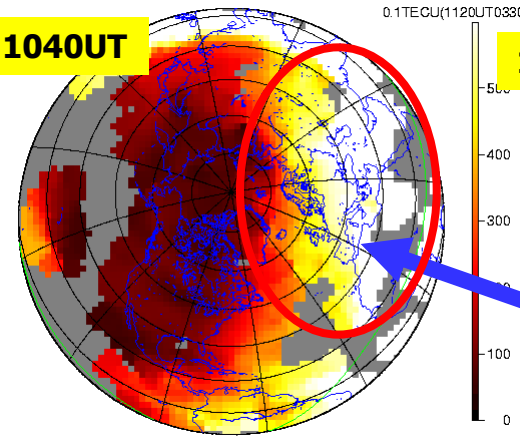

1120UT

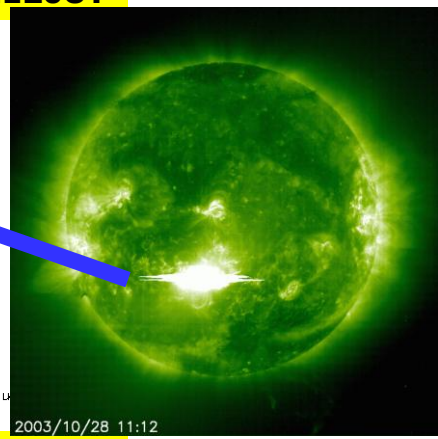

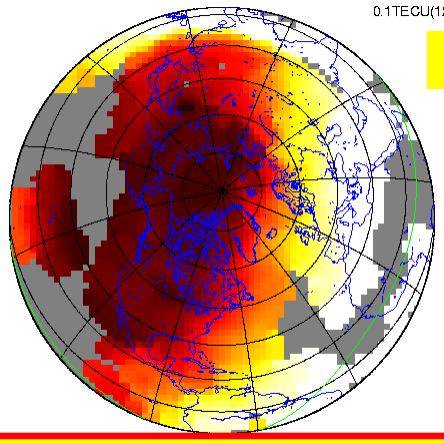

1200UT

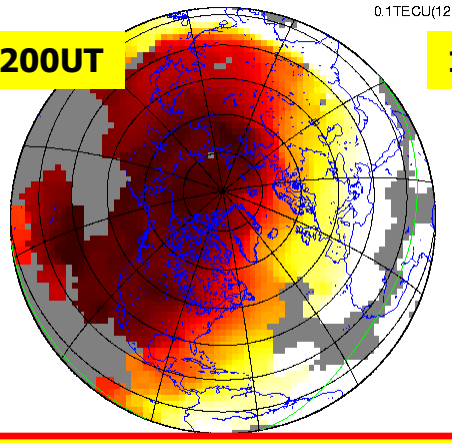

1240UT

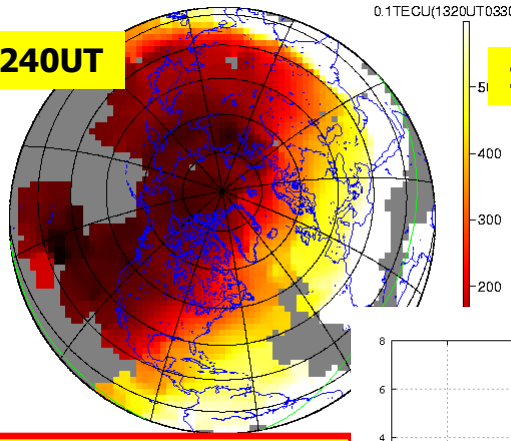

1320UT

1103UT

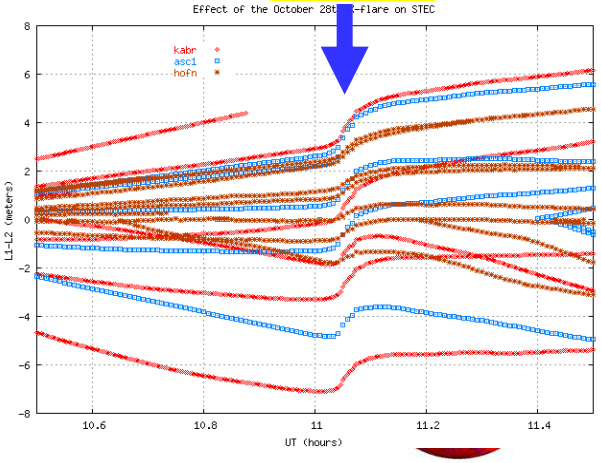

High and sudden STEC variations are experienced in the day hemisphere GPS receivers due to the arrival of the X-rays extra radiation due to Solar X-flares (example: event during 28 Oct. 2003, 11UT approx, preceding the previous mentioned superstorm).

AGU PUBLICATIONS

JGR

Journal of Geophysical Research: Space Physics

RESEARCH ARTICLE

10.1002/2015JA021824

GPS as a solar observational instrument: Real-time estimation of EUV photons flux rate during strong, medium, and weak solar flares

Talwinder Singh[1], Manuel Hernandez-Pajares[2], Enric Monte[3], Alberto Garcia-Rigo[2], and Germán Olivares-Pulido[2]

[1]Department of Physics, Indian Institute of Technology (BHU), Varanasi, India, [2]Departament Matemàtica Aplicada IV, IonSAT res. group, Universitat Politcnica de Catalunya, Barcelona, Spain, [3]Departament de Teoria del Senyal i Comunicacions, TALP res. group, Universitat Politcnica de Catalunya, Barcelona, Spain

Key Points:
- It is shown how GPS can be efficiently used as an accurate solar observational tool
- A constant linear EUV photon flux-GSFLAI dependence is found for all kind of solar flares
- GSFLAI present advantages regarding to direct EUV photons flux measurements taken from solar probes

Correspondence to:
M. Hernandez-Pajares,
manuel@ma4.upc.edu

Citation:
Singh, T., M. Hernandez-Pajares, E. Monte, A. Garcia-Rigo, and G. Olivares-Pulido (2015), GPS as a solar observational instrument: Real-time estimation of EUV photons flux rate during strong, medium, and weak solar flares, *J. Geophys. Res. Space Physics*, *120*, doi:10.1002/2015JA021824.

Received 18 AUG 2015
Accepted 19 NOV 2015
Accepted article online 24 NOV 2015

Abstract In this manuscript, the authors show how the Global Navigation Satellite Systems, GNSS (exemplified in the Global Positioning System, GPS), can be efficiently used for a very different purpose from that for which it was designed as an accurate Solar observational tool, already operational from the open global GPS measurements available in real-time, and with some advantages regarding dedicated instruments onboard spacecraft. The very high correlation of the solar extreme ultraviolet (EUV) photon flux rate in the 26–34 mm spectral band, obtained from the solar EUV monitor instrument onboard the SOHO spacecraft during Solar flares, is shown with the GNSS solar flare activity indicator (GSFLAI). The GSFLAI is defined as the gradient of the ionospheric vertical total electron content rate versus the cosine of the Solar zenith angle in the day hemisphere (which filters out nonsolar over ionization), and it is measured from data collected by a global network of dual frequency GPS receivers (giving in this way continuous coverage). GSFLAI for 60 X class flares, 320 M class flares, and 300 C class flares, occurred since 2001, were directly compared with the EUV solar flux rate data to show existing correlations. It was found that the GSFLAI and EUV flux rate present the same linear relationship for all classes of flares, not only the strong and medium intensity ones, X and M class, as in previous works, but also for the weakest C class solar flares, which is a remarkable result.

Snapshots of some ionospheric variations

Scintillation

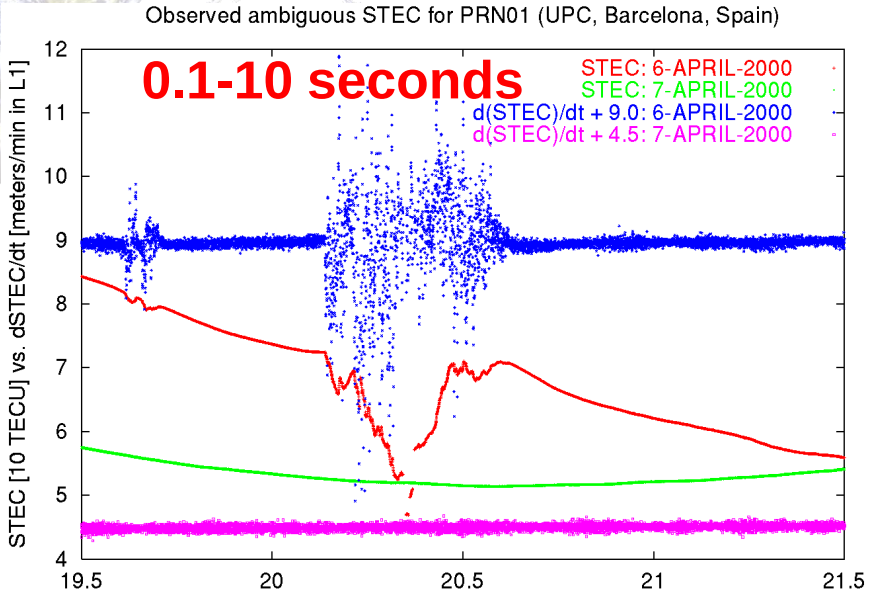

Solar Flare sudden overioniz.

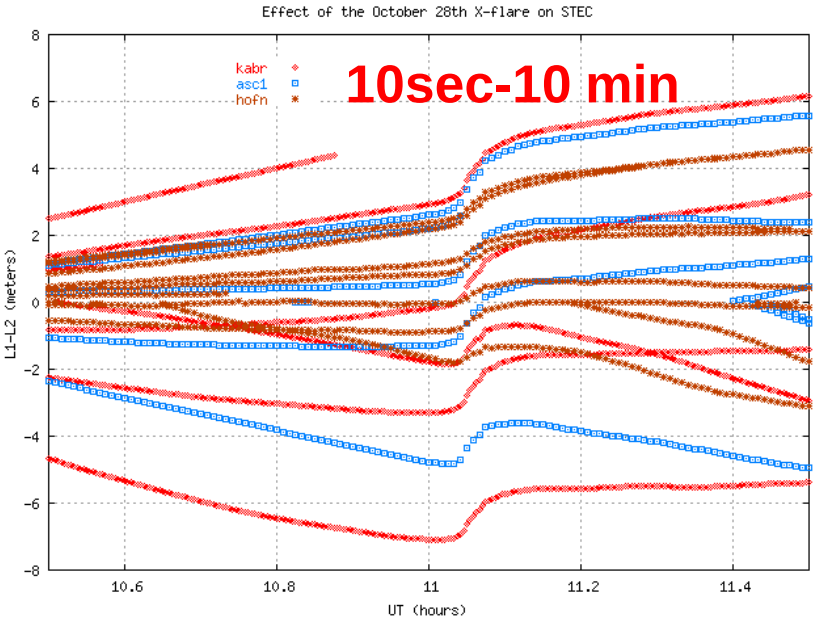

Travelling Ionospheric Disturb.

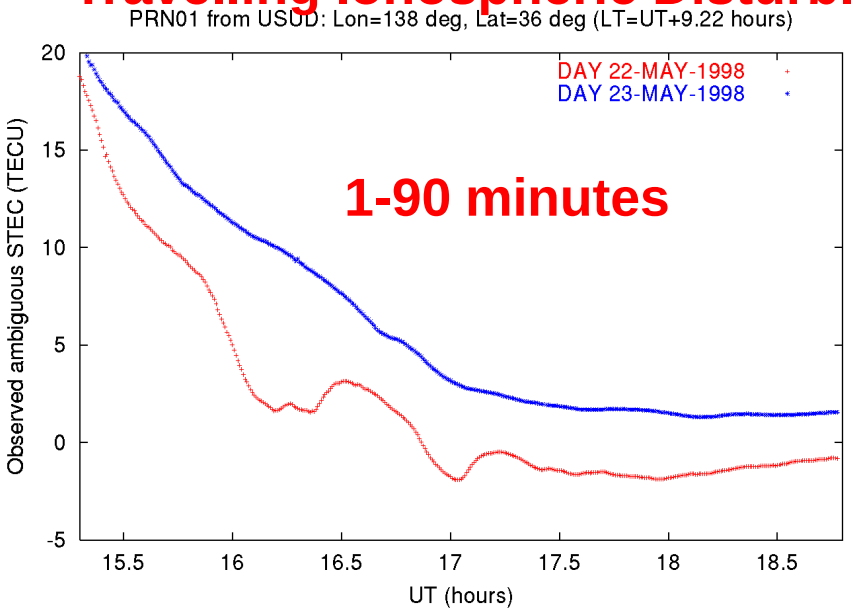

Solar-cycle,seasonal, solar rot.

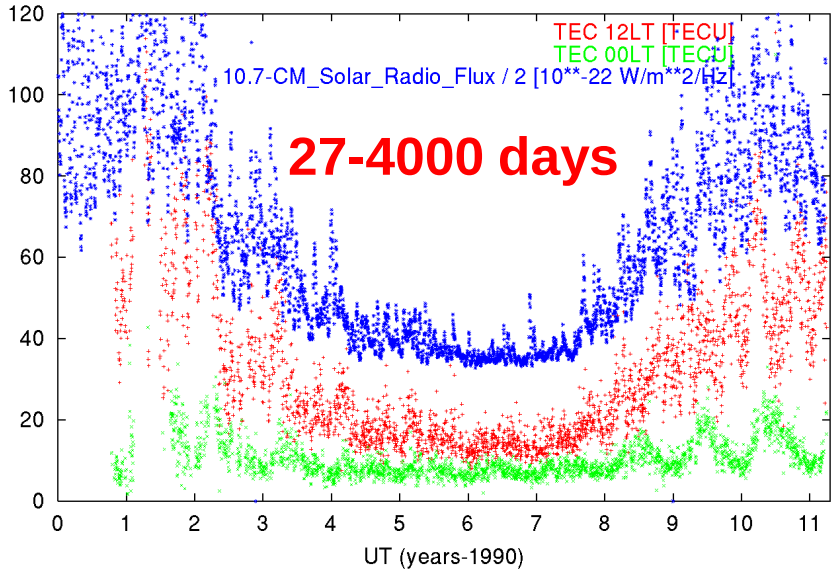

The Ionospheric term in GPS

GPS signal is very sensitive to free electron distribution, which respond to the EM field, oscilating and generating a secondary EM wave which overimposes and change the velocity of the GPS signals (main iono. efect on GPS code and phase).

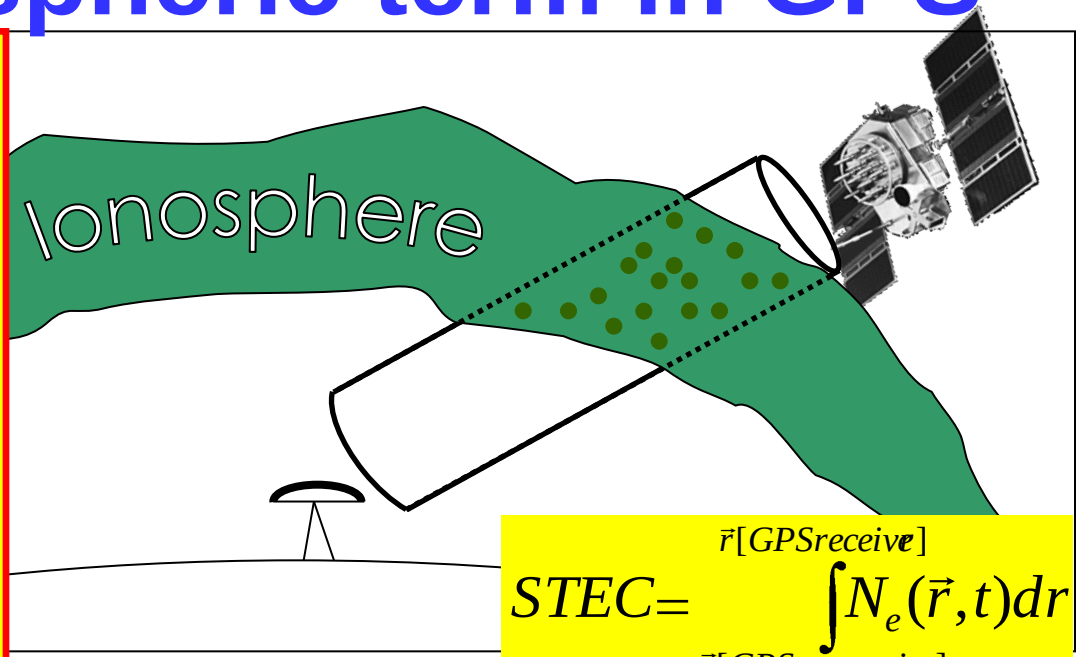

$$STEC = \int_{\vec{r}[GPStransmitter]}^{\vec{r}[GPSreceive]} N_e(\vec{r},t)dr$$

The Slant Total Electron Content (STEC) is defined as the surface electron density along the GPS ray path

The first order iono. term in GPS signal (99.9% of total) is proportional to Slant Total Electron Content (STEC) and to the inverse of the squared frequency (from Appleton equation, neglecting magnetic field and collisions).

$$\delta I_P \equiv \delta I_{PSEUDORANGE} = 40.3\frac{STEC}{f^2}$$

$$\delta I_L \equiv \delta I_{CARRIER-PHASE} = -\delta I_P$$

MKS units

From STEC to VTEC: Single layer model

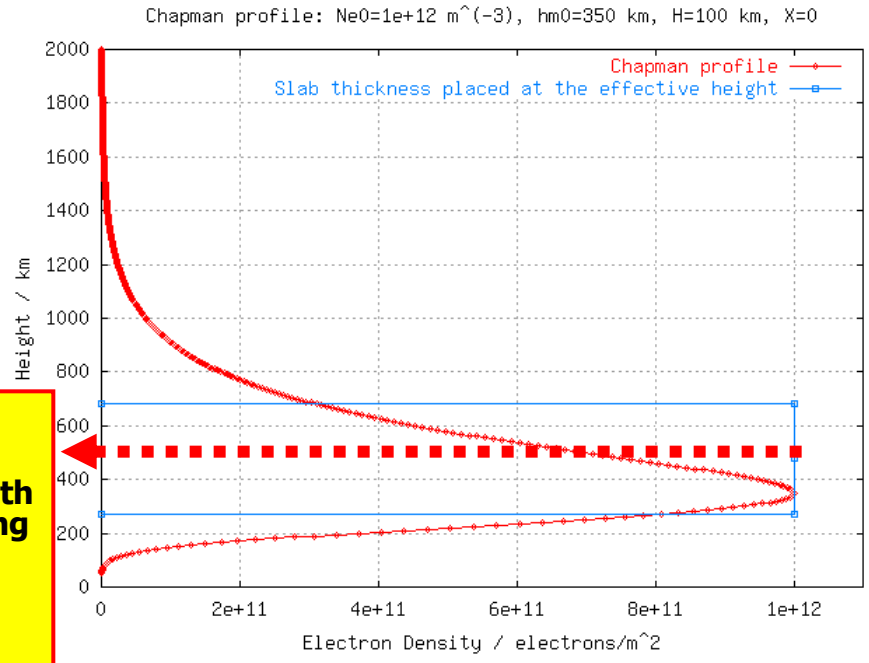

Effective Height (Sun at zenith and assuming the slab thickness width, VTEC/Ne)

One simple way of obtaining the VTEC from STEC is based on the assumption of electron content concentrated at one shell at fixed *effective height* ("single layer model").

But such effective height can change in terms of Local Time (daylight/night), latitude and geomagnetic activity.

You can see at right the effective height change in terms of the Sun-zenith angle predicted by the Chapman model.

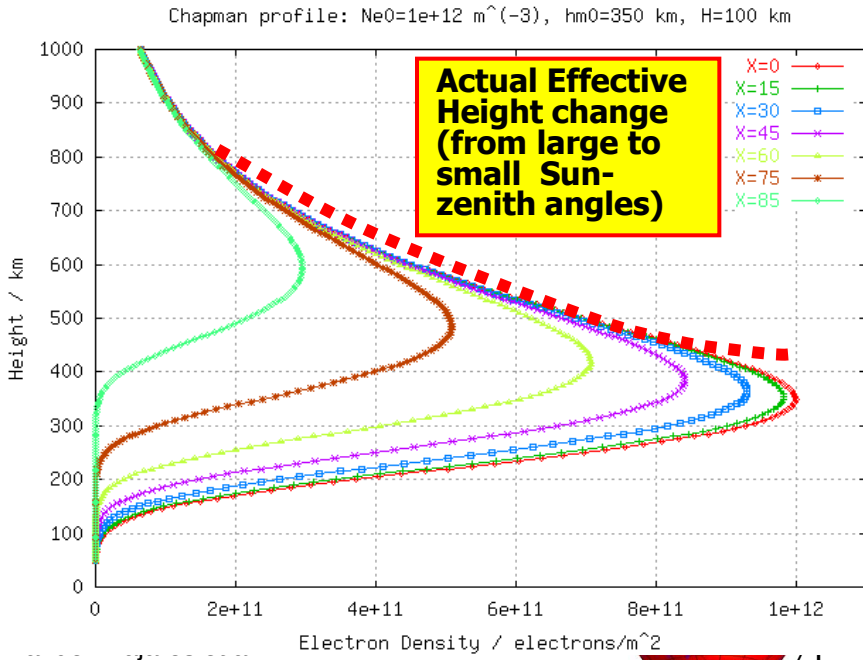

Standard ("Lanyi") Ionospheric Mapping Function

$$STEC = M \cdot VTEC$$

$$\left.\begin{aligned} M &= \frac{1}{\sin E'} \\ r\cos E &= r'\cos E' \end{aligned}\right\} M = \left\{ r = r + h \right\} = \frac{1}{\sqrt{1 - \frac{r^2}{(r+h)^2}\cos^2 E}}$$

$$\left.\begin{aligned} M &= \frac{1}{\sin E'} \\ r\cos E &= r'\cos E' \end{aligned}\right\} M = \left\{ r = r + h \right\} = \frac{1}{\sqrt{1 - \frac{r^2}{(r+h)^2}\cos^2 E}} \Bigg\} VTEC = STEC \cdot \sqrt{1 - \frac{r^2}{(r+h)^2}\cos^2 E} \Rightarrow$$

$$\Rightarrow \underbrace{STEC \cdot \sin E}_{h \to 0^+} < VTEC < \underbrace{STEC}_{h \to +\infty}$$

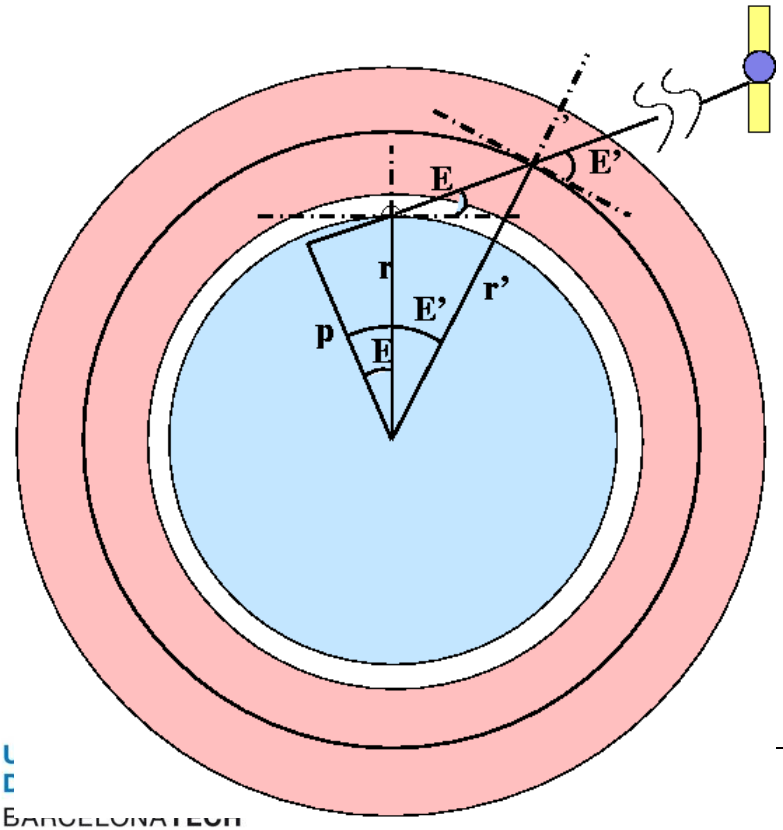

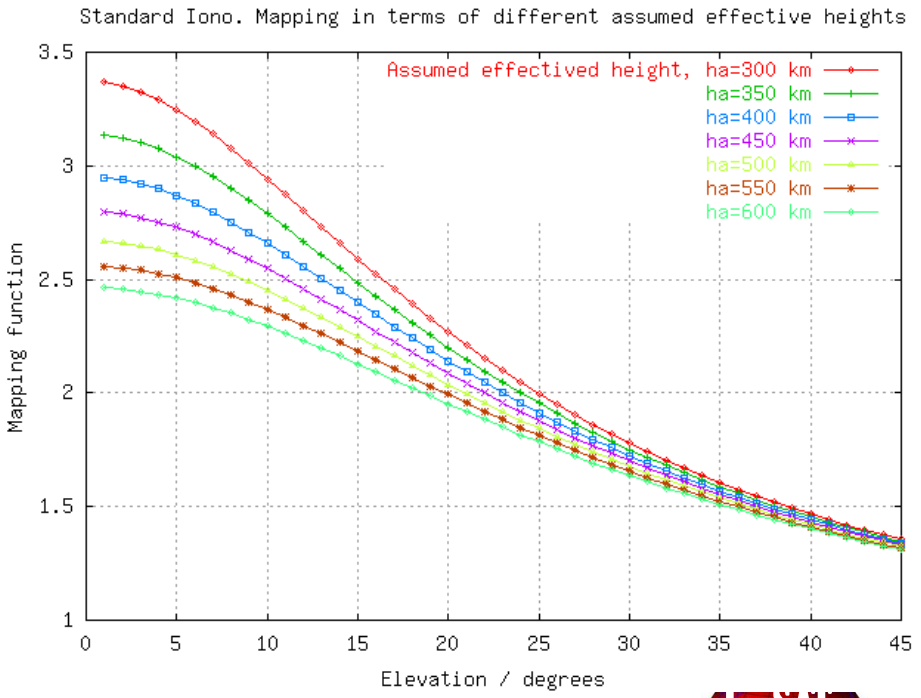

Estimating the ionospheric distribution

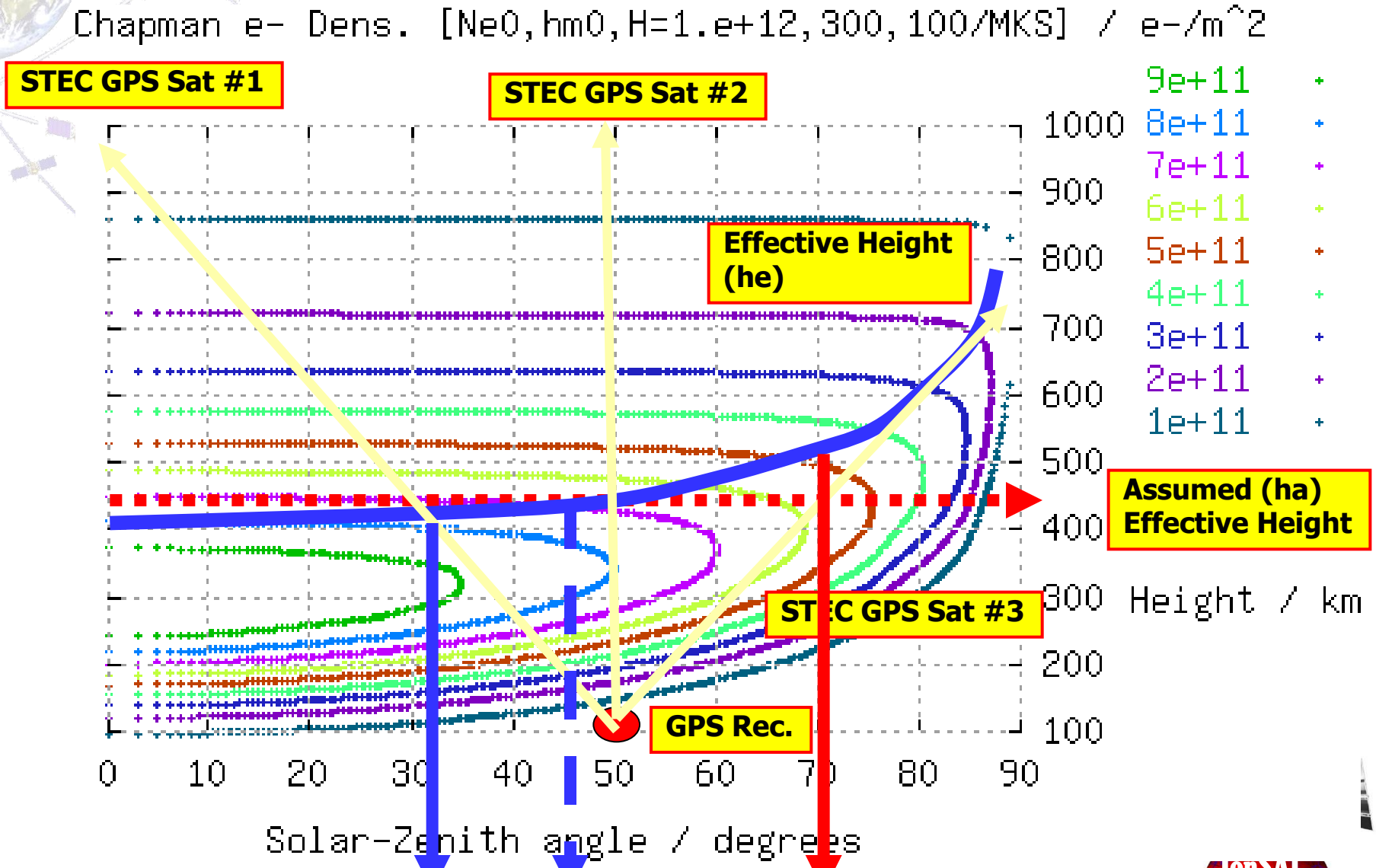

Benefits of combining different kind of Iono. Obs. in a 3D Voxel Model

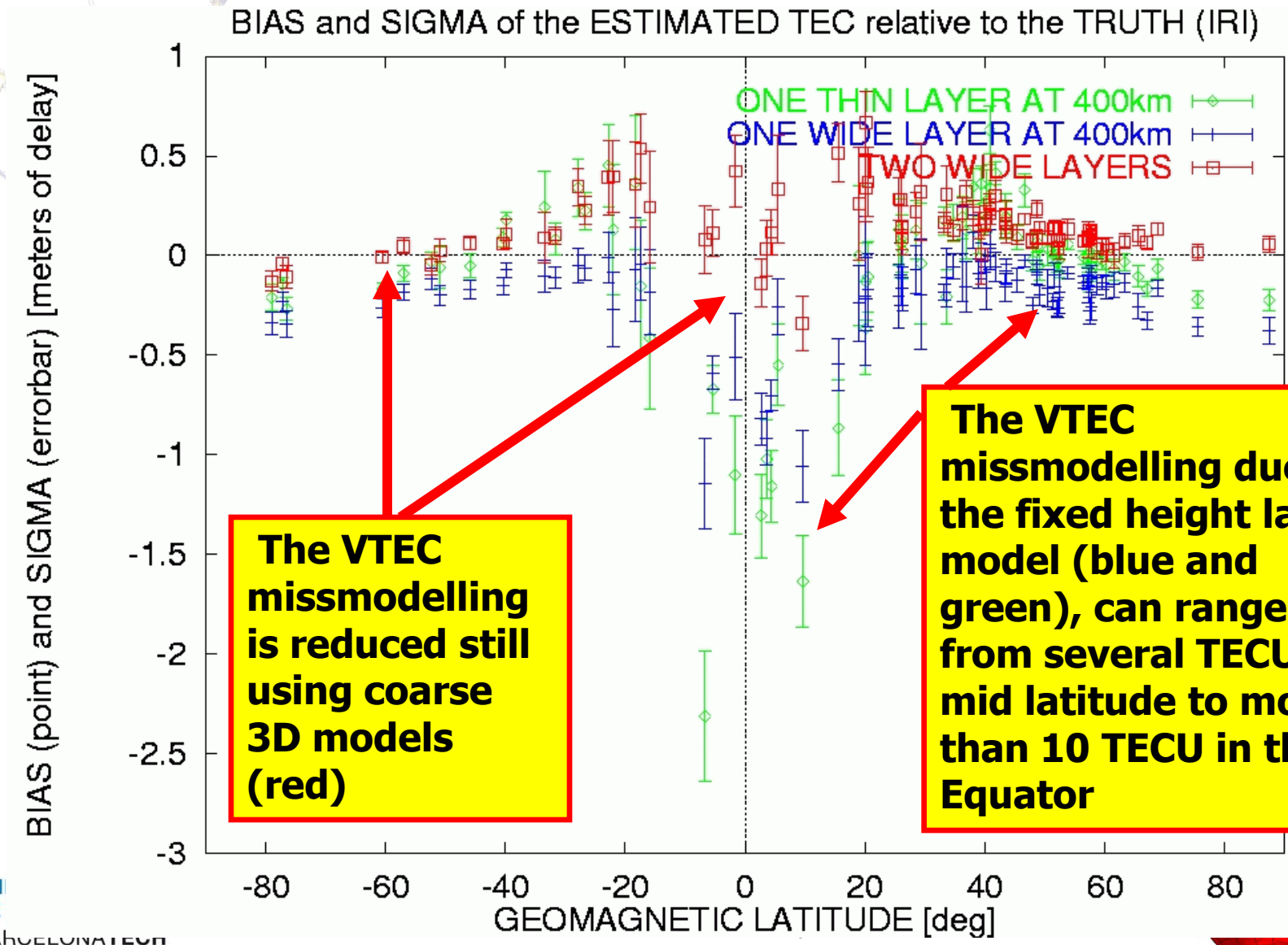

Real-time iono. model

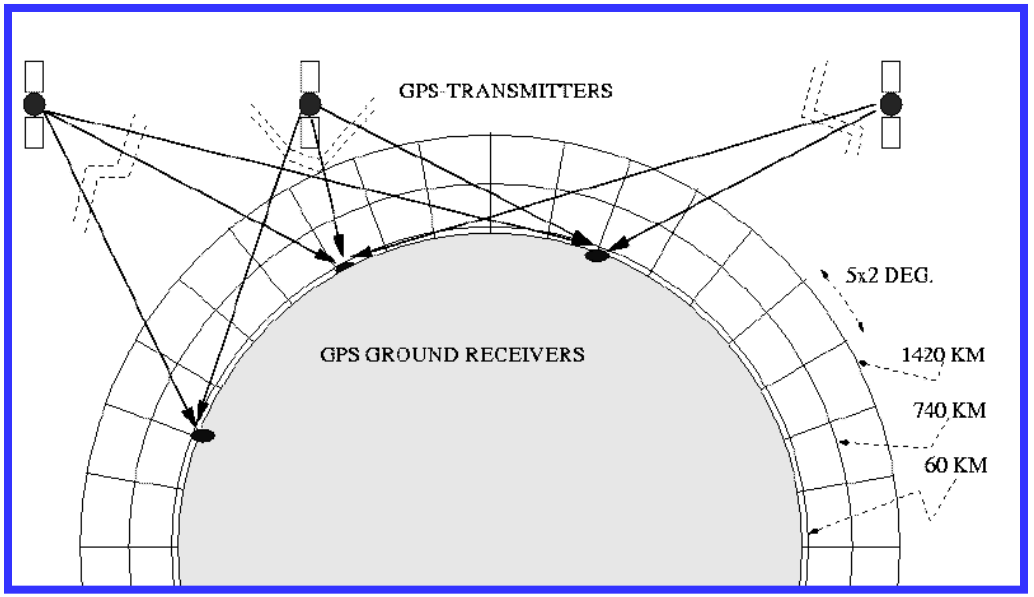

- Only carrier phase data needed
- With tomographic description: more accurate
- DCB's no longer needed
- No affected by pseudorange multipath

$$L_I = STEC + B_I = \int_{REC}^{SAT} N_e dl + B_I = \sum_i \sum_j \sum_k (N_e)_{i,j,k} \Delta s_{i,j,k} + B_I$$

Estimating electron density in a 3D Voxel model (regional/global)

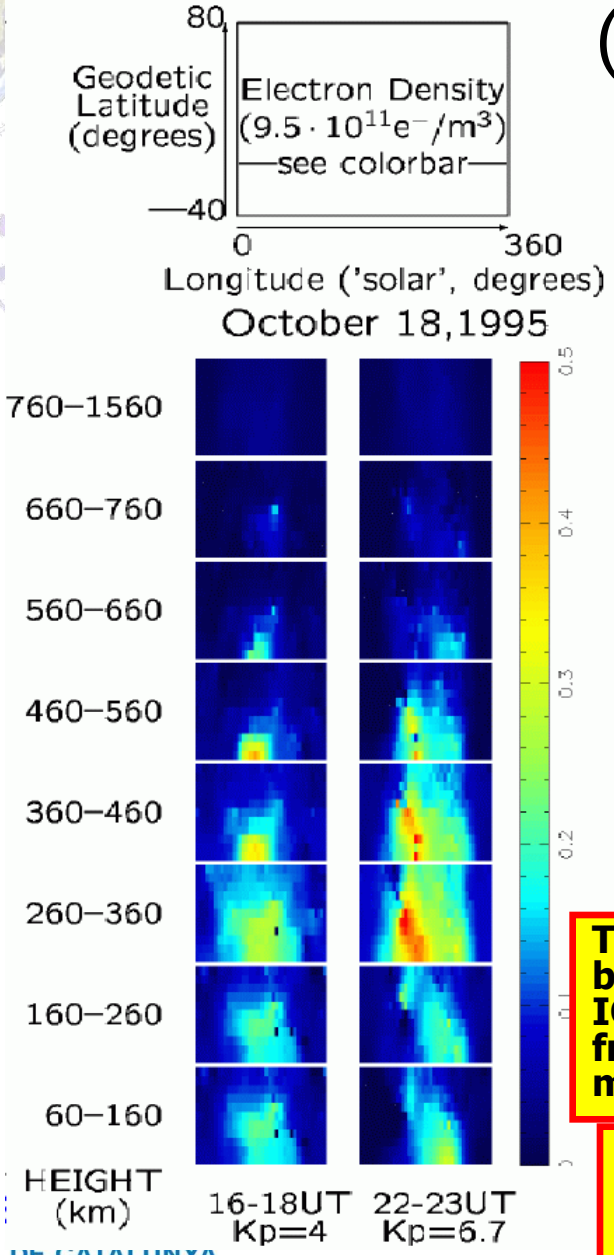

Different kind of data are mixed: occultation and ground GPS data.

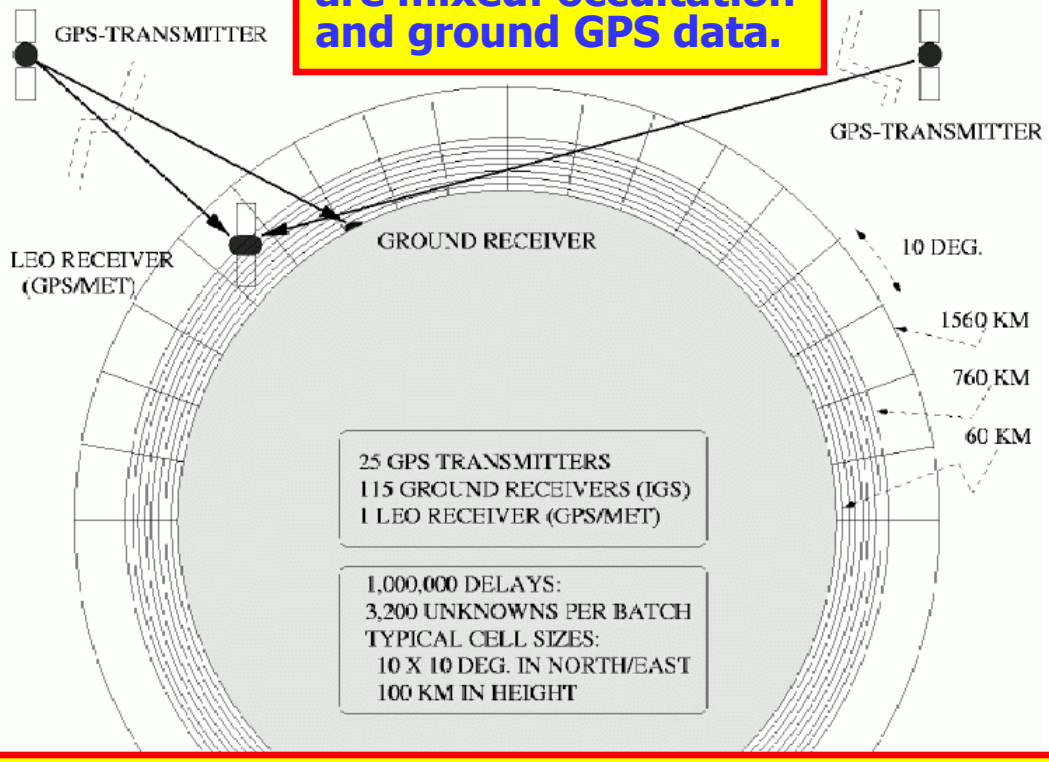

This is an example corresponding to the combination of both complementary type of GPS data (ground-based from IGS network and space-based from GPS/MET LEO) in the framework of a 3D voxel tomographic model solved by means of a Kalman filter (Oct.18, 1995 geomagnetic storm).

More details in: Hernández-Pajares M., J.M. Juan, J. Sanz and J.G. Sole, Global observation of the ionospheric electronic response to solar events using ground and LEO GPS data, *Journal of Geophysical Research-Space Physics*, Vol.61, p.1237-1247, 1998.

Classical Abel transform (independent estimation for each occultation)

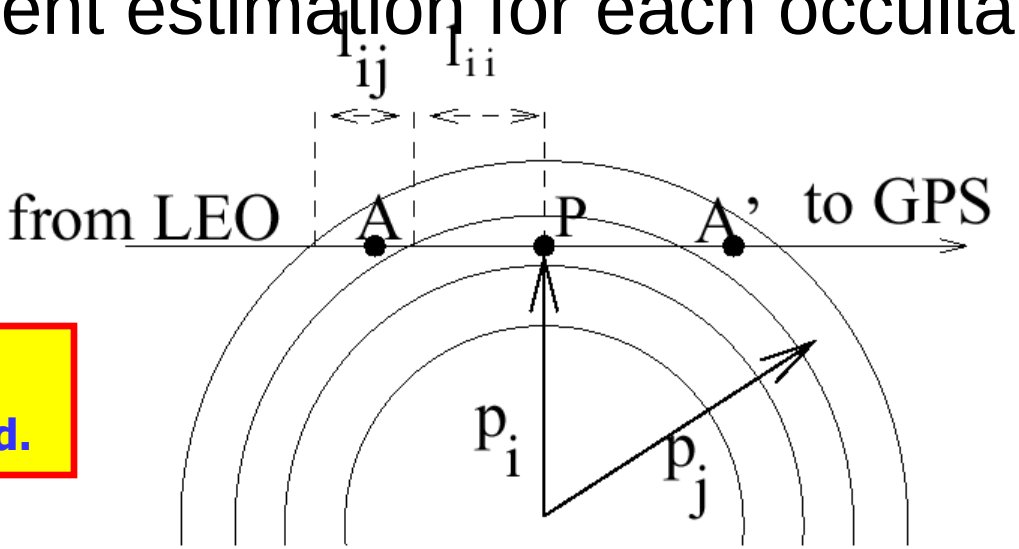

Just the given occultation GPS data are processed.

The classical spherical symmetry hypothesis can be formulatted as:

$$N_e(LT, LAT, H) = \Phi(H)$$

Recursive solution starting from the outer ray. STEC corresponding to the impact parameter p_i:

$$STEC(p_i) = 2 \cdot l_{ii} \cdot N_e(p_i) + \sum_{j=1}^{j=i-1} 2 \cdot l_{ij} \cdot N_e(p_j)$$

Abel Transform vs. 3D-Voxel model

	Abel Transform	3D Voxels
Vertical resolution	$\simeq 1$ km	Tens / hundred km
Computational load	Low ($\simeq 10^2$ unk.)	High ($> 10^3$ unk.)
Sph. Sym. Assump.	Yes	No
Topside mismod.	Yes	No
Assimilation capab.	No	Yes

Our goal: maintaining its other advantages, to avoid these limitations of the classical Abel approach:

- Overcoming the spherical symmetry assumption.
- Overcoming the topside electron content mismodelling.

Separability concept

- $N_e(LT, \ AT, H) = VTEC(LT, LAT) \cdot F(H)$

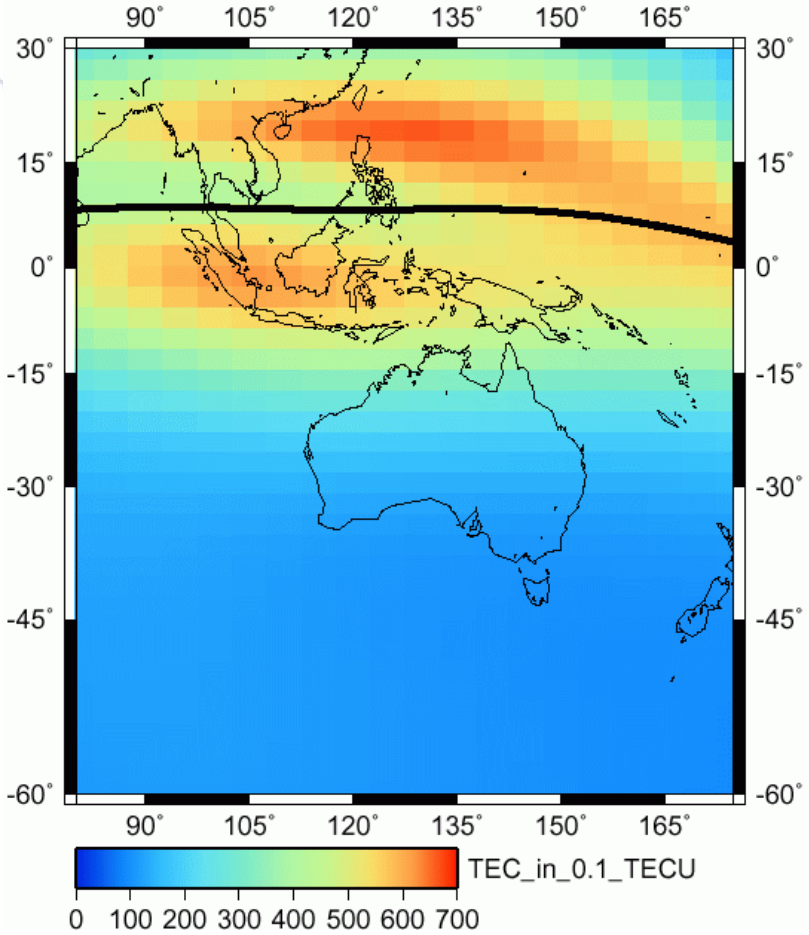

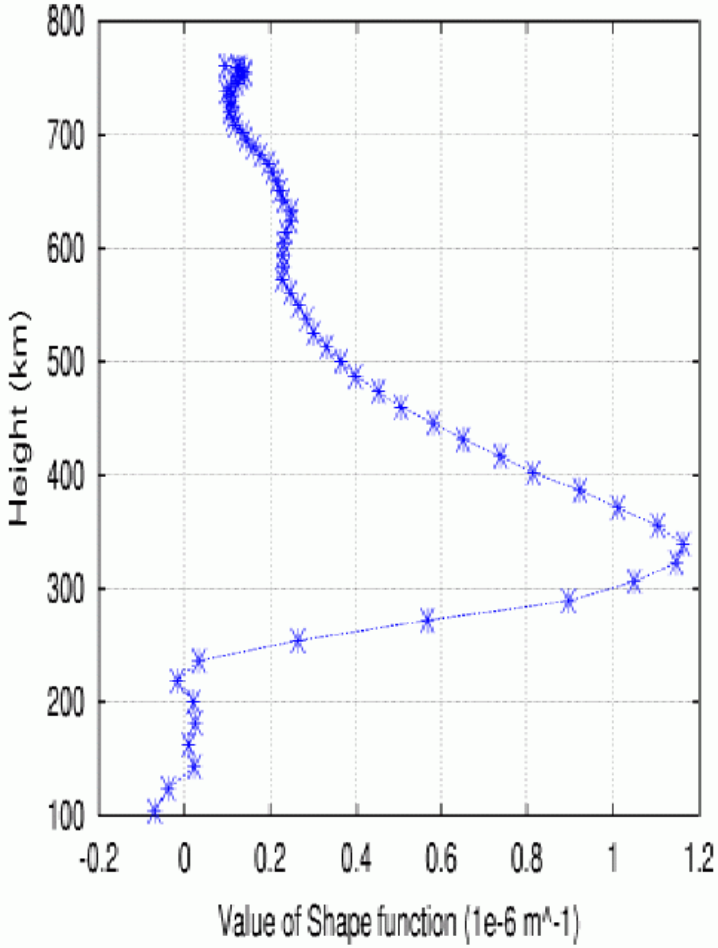

Improved Abel transform

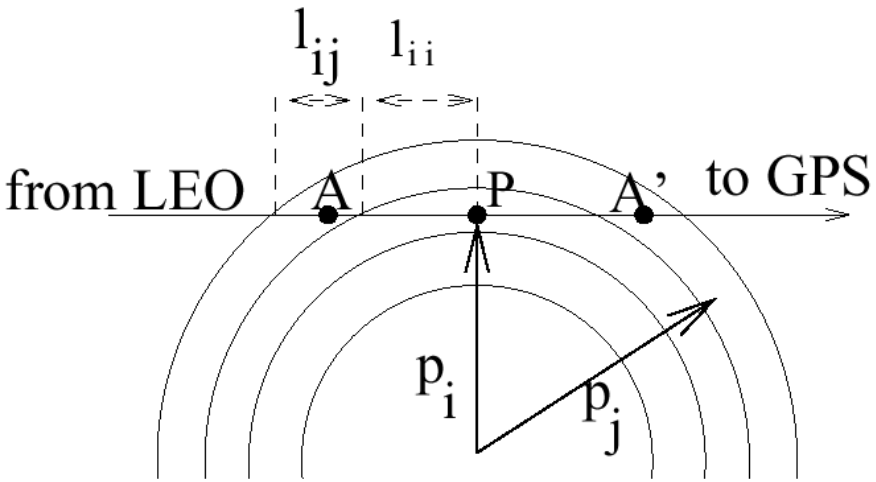

Let's assume a more general hypothesis that just the spherical symmetry:

$$N_e(LT, LAT, H) = VTEC(LT, LAT) \cdot F(H)$$

Starting from the outer ray, the STEC corresponding to the impact parameter p_i can be modeled by:

$$STEC(p_i) = 2 \cdot l_{ii} \cdot VTEC(LT_{ii}, LAT_{ii}) \cdot F(p_i) + \sum_{j=1}^{j=i-1} l_{ij} \cdot \left[VTEC(LT_{ij}, LAT_{ij}) + VTEC(LT'_{ij}, LAT'_{ij})\right] \cdot F(p_j)$$

Benefits of separability hypothesis

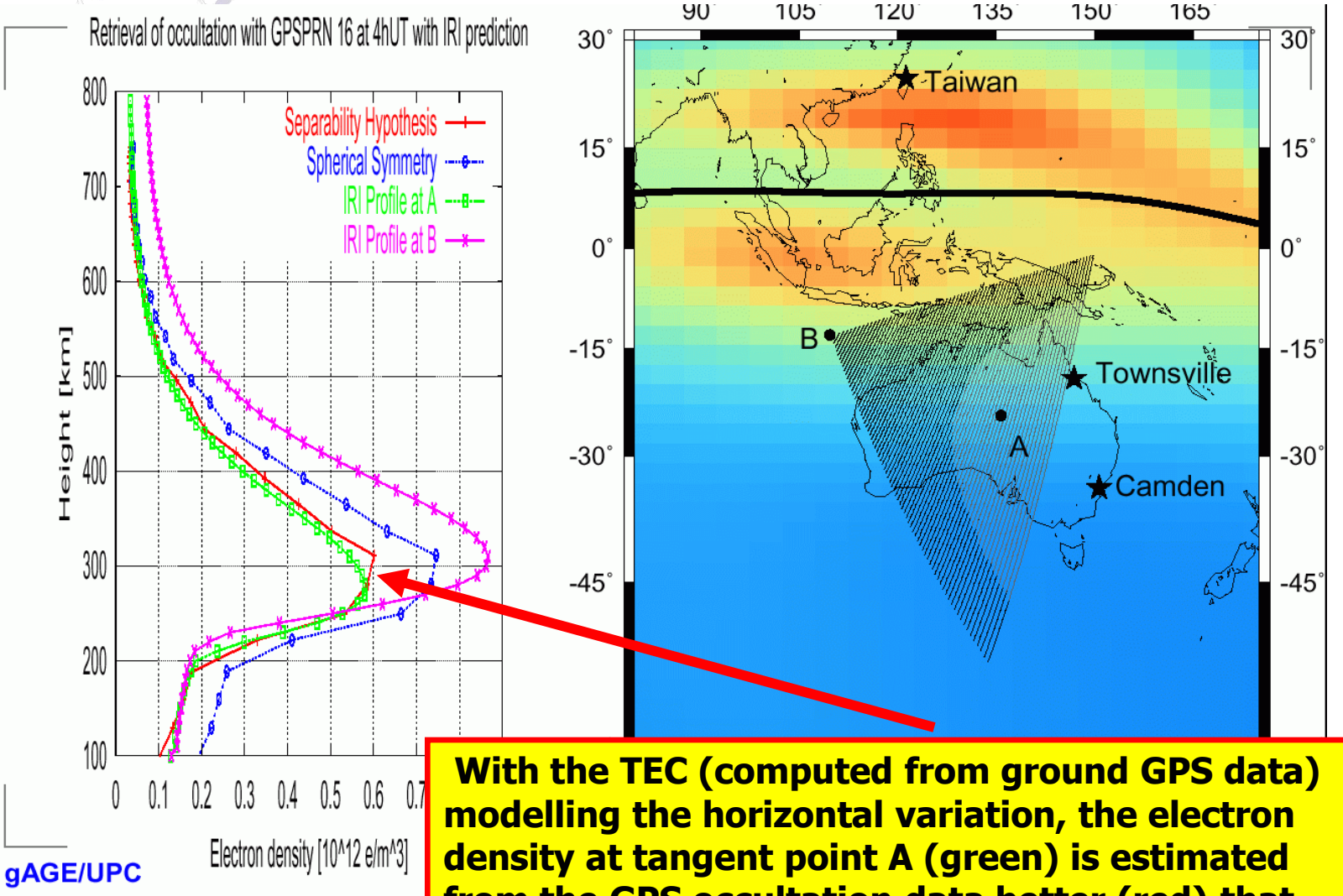

With the TEC (computed from ground GPS data) modelling the horizontal variation, the electron density at tangent point A (green) is estimated from the GPS occultation data better (red) that assuming spherical symmetry (blue).

gAGE/UPC

Separability: improvement in E layer estimation

The improvement in foE estimates reachs to a reduction of 40% in E layer and near 50% in Es layer

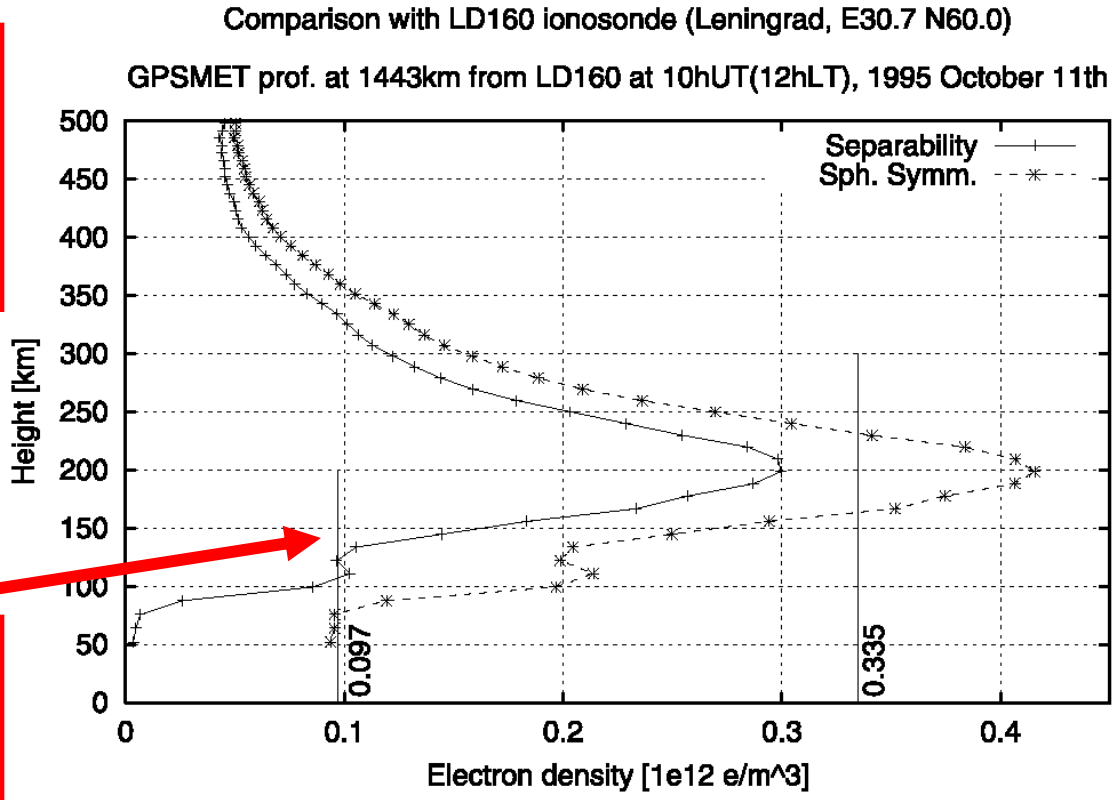

The improved Abel can provide reliable estimates of the NmE value as well (not just NmF2 values).

ble 2. Table of foE Errors With Respect to Ionosonde Value[a]

	N.comp	Sep. Hyp. RMS: MHz [%]	Sph. Symm. RMS: MHz [%]
E layer	135	0.4 [17.1]	0.7 [28.5]
Es layer	35	0.5 [16.2]	1.0 [30.4]

[a]The error is Absolute RMS in MHz and Percentual relative RMS difference in brackets.

AGU PUBLICATIONS

JGR

Journal of Geophysical Research: Space Physics

RESEARCH ARTICLE

10.1002/2017JA023876

Electron density extrapolation above F2 peak by the linear Vary-Chap model supporting new Global Navigation Satellite Systems-LEO occultation missions

Manuel Hernández-Pajares[1], Miquel Garcia-Fernàndez[1,2], Antonio Rius[3], Riccardo Notarpietro[4], Axel von Engeln[4], Germán Olivares-Pulido[1,5], Àngela Aragón-Àngel[6], and Alberto García-Rigo[1]

[1]UPC-IonSAT, Barcelona, Spain, [2]Rokubun, Barcelona, Spain, [3]Instituto de Ciencias del Espacio (CSIC/IEEC), Bellaterra, Spain, [4]EUMETSAT, Darmstadt, Germany, [5]CRC for Spatial Information, Sydney, Australia, [6]European Commission, Joint Research Centre (JRC), Directorate for Space, Security and Migration, Ispra, Italy

Key Points:
- A new electron density profile extrapolation technique (VCET), founded on First Principles, is presented showing a high performance
- VCET is simple and accurate: it is based on the linear behavior of the topside scale height, performing 6-20 times better than Chapman model
- The accuracy and extrapolation range, illustrated with FORMOSAT-3/COSMIC measurements, will be important for new radio-occultation missions like EPS-SG

Correspondence to:
M. Hernández-Pajares,
manuel.hernandez@upc.edu

Citation:
Hernández-Pajares, M., M. Garcia-Fernàndez, A. Rius, R. Notarpietro, A. von Engeln, G. Olivares-Pulido, À. Aragón-Àngel, and A. García-Rigo (2017), Electron density extrapolation above F2 peak by the linear Vary-Chap model supporting new Global Navigation Satellite Systems-LEO occultation missions, *J. Geophys. Res. Space Physics*, *122*, doi:10.1002/2017JA023876.

Received 7 JAN 2017
Accepted 11 JUL 2017
Accepted article online 20 JUL 2017

Abstract The new radio-occultation (RO) instrument on board the future EUMETSAT Polar System-Second Generation (EPS-SG) satellites, flying at a height of 820 km, is primarily focusing on neutral atmospheric profiling. It will also provide an opportunity for RO ionospheric sounding, but only below impact heights of 500 km, in order to guarantee a full data gathering of the neutral part. This will leave a gap of 320 km, which impedes the application of the direct inversion techniques to retrieve the electron density profile. To overcome this challenge, we have looked for new ways (accurate and simple) of extrapolating the electron density (also applicable to other low-Earth orbiting, LEO, missions like CHAMP): a new Vary-Chap Extrapolation Technique (VCET). VCET is based on the scale height behavior, linearly dependent on the altitude above h_mF_2. This allows extrapolating the electron density profile for impact heights above its peak height (this is the case for EPS-SG), up to the satellite orbital height. VCET has been assessed with more than 3700 complete electron density profiles obtained in four representative scenarios of the Constellation Observing System for Meteorology, Ionosphere, and Climate (COSMIC) in the United States and the Formosa Satellite Mission 3 (FORMOSAT-3) in Taiwan, in solar maximum and minimum conditions, and geomagnetically disturbed conditions, by applying an updated Improved Abel Transform Inversion technique to dual-frequency GPS measurements. It is shown that VCET performs much better than other classical Chapman models, with 60% of occultations showing relative extrapolation errors below 20%, in contrast with conventional Chapman model extrapolation approaches with 10% or less of the profiles with relative error below 20%.

Layout:

1) [**Motivation**] Precise Agriculture (PA) presentation (EU AUDITOR experiment)

2) [**Background**]: Brief introduction to main identified points of the presentation:
   a) GPS fundamentals: pseudoranges and carrier phases (optional)
   b) Ionospheric electron content
   c) Wide Area Real-Time Kinematic
   d) The International GNSS Service (*optional*)

3) [**One efficient operative system**] Quick introduction to Linux (*optional*)

4) [**New tools for learning and research**] IonSAT Tools (IT), emulating Real-Time (RT) as much as possible (presented on the PA AUDITOR experiment):
   a) *gim2vtec.v2.scr*
   b) *gimrnx2stec.v2.scr*

5) [**IT application to ECLIPSE, FLARE & GSTORM scenarios**] (*optional*).

6) [**Example of RT GPS-ionospheric system**]: UPC-IonSAT since 2012.

7) [**Monitoring of co-seismic generated ionospheric signals]:** Application of RT ionospheric sounding for potential Tsunami warnings), with GNSS dense (Tohoku and mid earthquakes, EQ) and sparse networks (Chile 2015 EQ).

8) [**Conclusions**]

WARTK: Combining real-time Ionospheric & Geodetic models

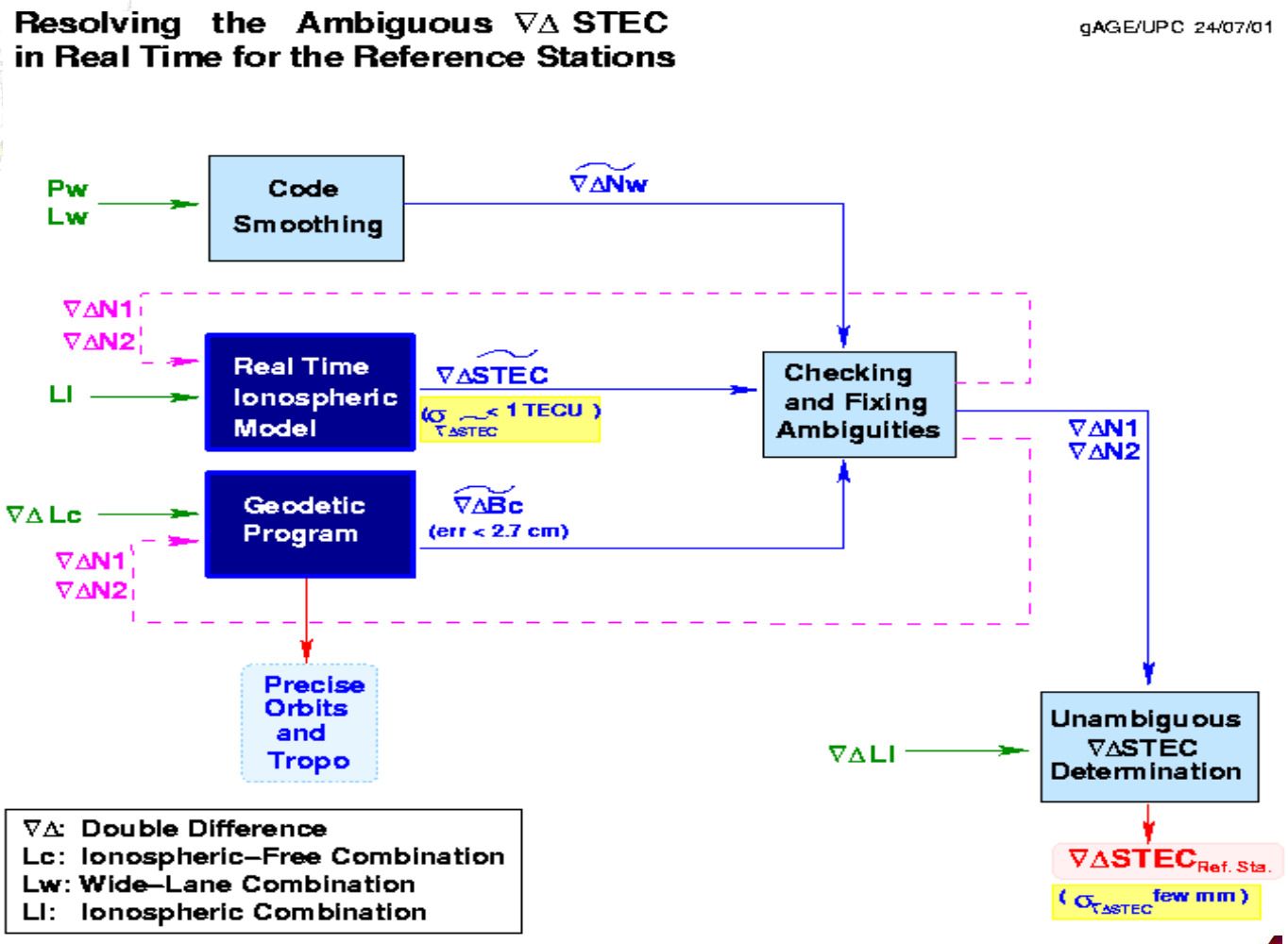

DIFFERENTIAL Positioning concept

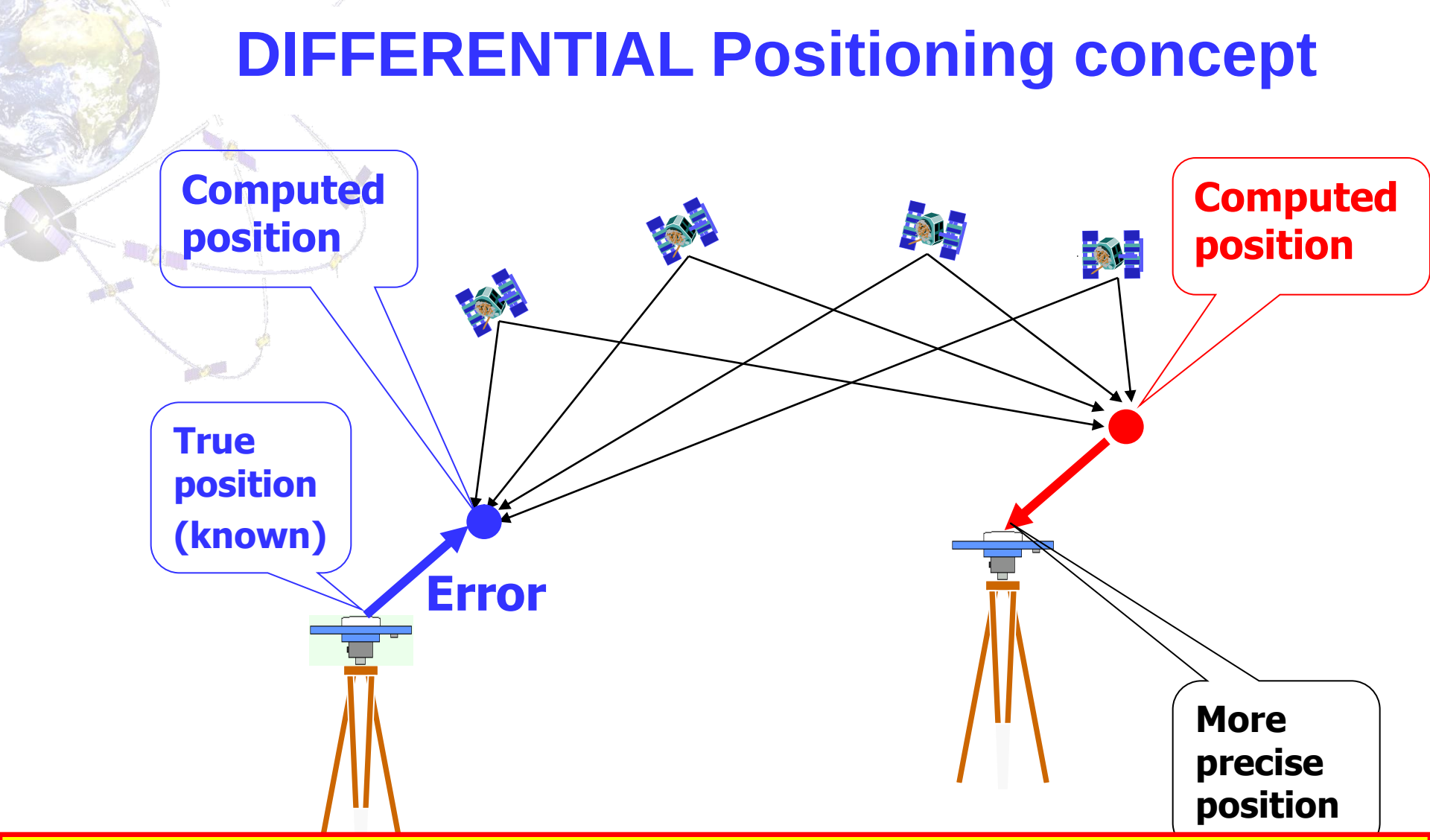

- In baselines shorter than few tens of km, similar errors are expected in differential approach, cancelling-out (exactly for satellite clocks, approximately for GPS orbital errors and for ionospheric error). –
- The extension to longer baselines is a problem specially due to the ionospheric error (quite difficult to predict it accurately).

Wide Area RTK in a nutshell: The independent DD phase ambiguities of two physical carriers

DDBw (widelane from Melbourne-Wubbenna combination, Lw-Pn)

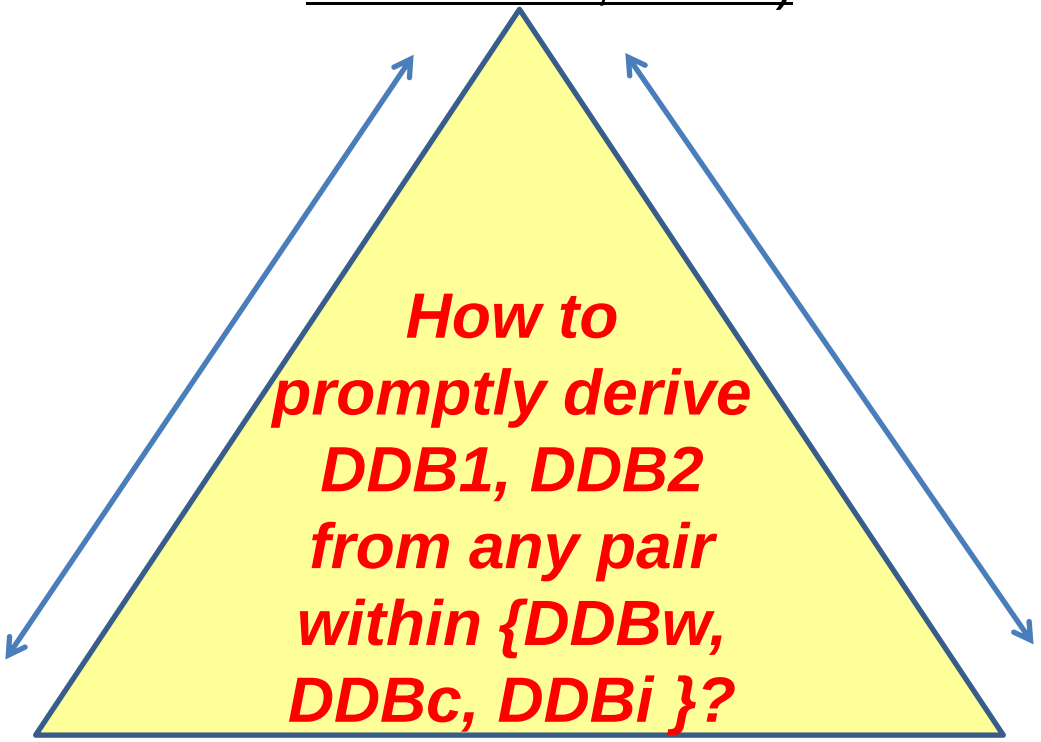

DDBc (from ionospheric-free combination Lc - precise geometric modelling)

DDBi (from ionospheric combination LI - precise ionospheric modelling)

Wide Area RTK in a nutshell: How to improve the DD phase ambiguity fixing

Geometry- & Ionospheric- free way
(Melbourne-Wubbenna combination, Lw-Pn)

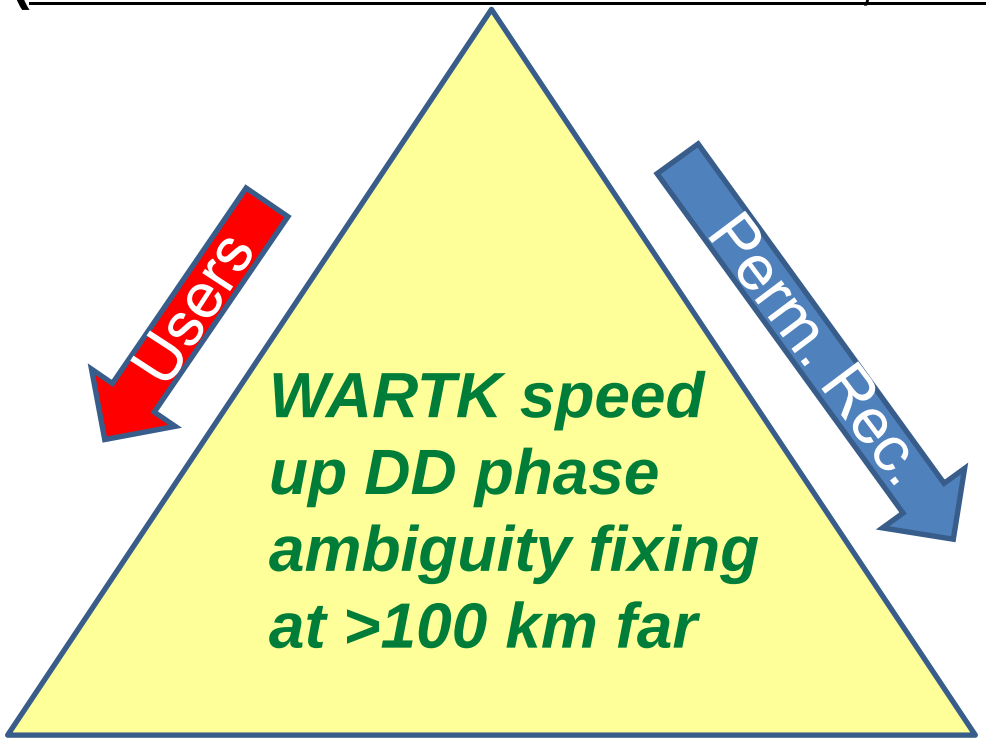

Ionospheric- free way
(Ionospheric-free combination Lc - precise geometric modelling)

Perm. Rec.

Users

Geometry- free way
(Ionospheric combination LI - precise ionospheric modelling)

AUDITOR

Wide Area RTK in a nutshell: Basic equations on DDamb

Once $\nabla\Delta N_\delta$ is fixed, it is possible to fix the L_1 and L_2 double-differenced integer ambiguities N_1 and N_2 for the reference stations, using a sufficiently accurate determination of the double-differenced ambiguity $\nabla\Delta B_c$ of the ionospheric free combination $L_c = (f_1^2 L_1 - f_2^2 L_2)/(f_1^2 - f_2^2)$. The following relationships illustrate these steps:

$$\begin{aligned}
\nabla\Delta B_c &= 0.5[\lambda_\delta \nabla\Delta N_\delta + \lambda_n \nabla\Delta(N_1 + N_2)] \\
\nabla\Delta(N_1 + N_2) &= \mathrm{NI}[(2\nabla\Delta B_c - \lambda_\delta \nabla\Delta N_\delta)/\lambda_\nu] \\
\nabla\Delta N_1 &= 0.5[\nabla\Delta N_\delta + \nabla\Delta(N_1 + N_2)] \\
\nabla\Delta N_2 &= \nabla\Delta N_1 - \nabla\Delta N_\delta
\end{aligned} \tag{3}$$

being $\lambda_n = c/(f_1 + f_2) \simeq 10.7\mathrm{cm}$ and NI the nearest integer. Hence, from $\nabla\Delta N_1$ and $\nabla\Delta N_2$, the unambiguous double-differenced ionospheric slant total electron content, STEC, can be computed for the reference stations:

$$\alpha\nabla\Delta STEC = \nabla\Delta(L_1 - L_2) - (\lambda_1 \nabla\Delta N_1 - \lambda_2 \nabla\Delta N_2) \tag{4}$$

(Extracted from *Hernández-Pajares, M., Juan, J. M., Sanz, J., & Colombo, O. L. (2000). Application of ionospheric tomography to real-time GPS carrier-phase ambiguities resolution, at scales of 400–1000 km and with high geomagnetic activity. Geophysical Research Letters, 27(13), 2009-2012).*

T5.2 - GNSS network prefit module

Hybrid ionospheric-geodetic approach

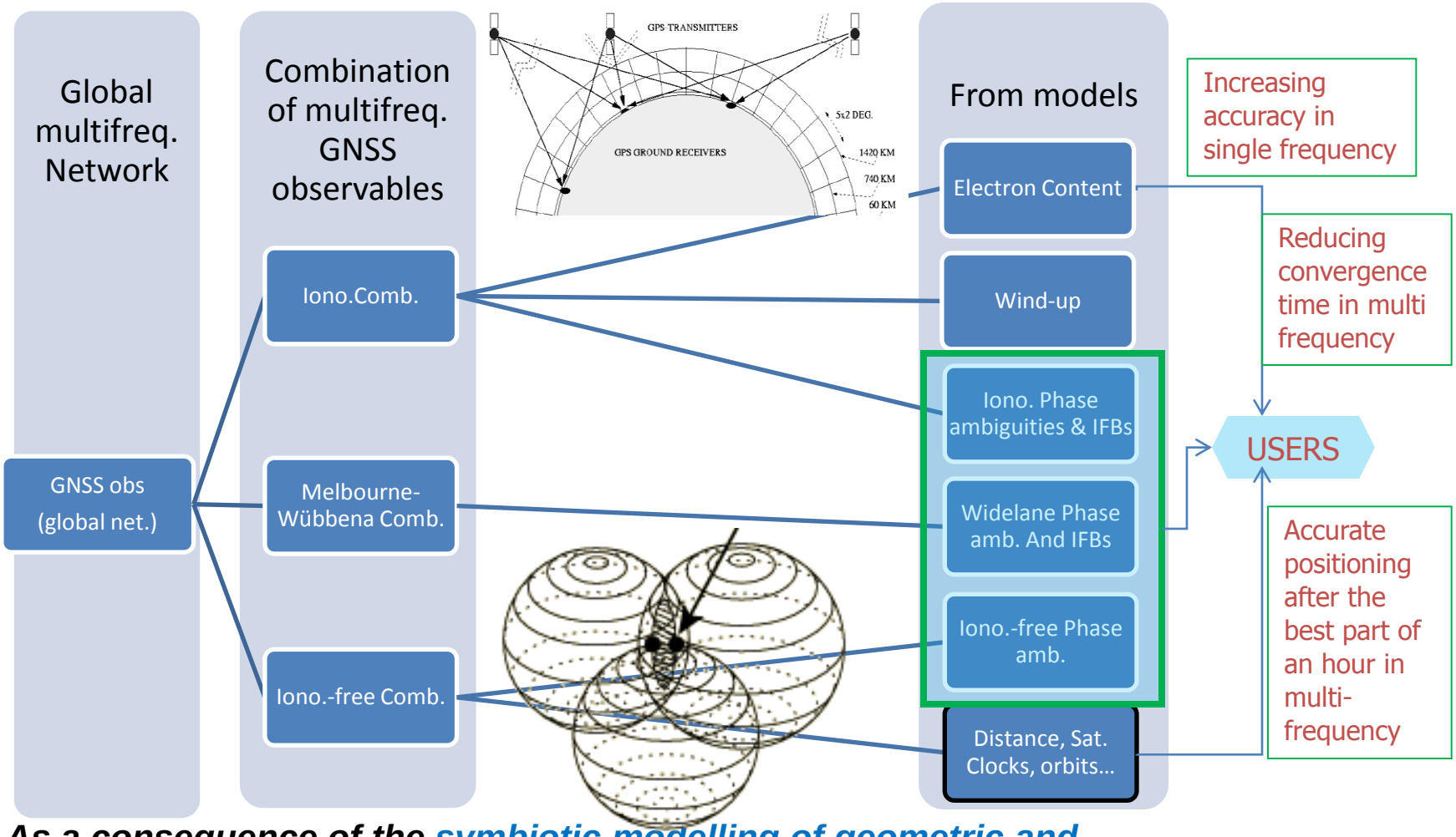

As a consequence of the symbiotic modelling of geometric and ionospheric delay dependences of the GPS, Galileo, GLONASS & Beidou signals: a better positioning service is obtained (cm-accuracy in real-time after short convergence time), and better ionospheric sounding

WARTK

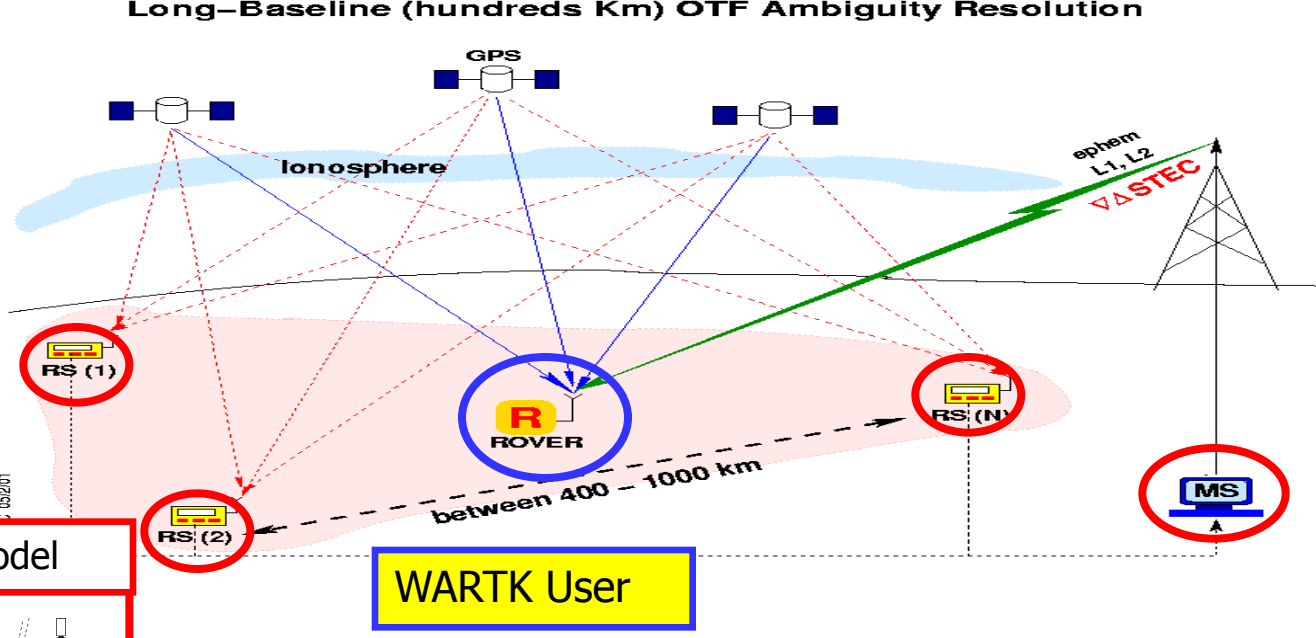

WARTK Central Processing Facility

Real-time Iono. model

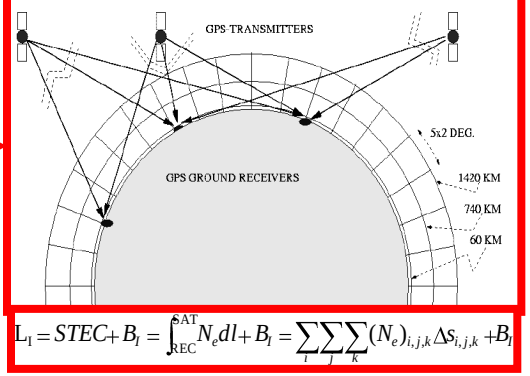

$$L_I = STEC + B_I = \int_{REC}^{SAT} N_e dl + B_I = \sum_i \sum_j \sum_k (N_e)_{i,j,k} \Delta s_{i,j,k} + B_I$$

Real-time geodetic model

WARTK User

- In Wide Area RTK the usual dependence of differential ionospheric refraction can be predicted with errors of few tenths of TECU (few cm in L1), also in difficult scenarios (low latitude, Solar cycle maximum and distances of many hundreds of kilometres, see Hernández-Pajares et al. 2000,2002).
- This allows centimeter-error-level navigation at distancies up to hundreds of kilometers from the nearest GNSS reference site (at single epoch in Galileo and Modernized GPS).
- But "shorter scale" ionospheric perturbations (such as MSTIDs) –from tenths to few TECUs- can affect to GNSS precise positioning at both WARTK & RTK scales.

Layout:

1) [**Motivation**] Precise Agriculture (PA) presentation (EU AUDITOR experiment)

2) [**Background**]: Brief introduction to main identified points of the presentation:
   a) GPS fundamentals: pseudoranges and carrier phases (optional)
   b) Ionospheric electron content
   c) Wide Area Real-Time Kinematic
   d) The International GNSS Service (*optional*)

3) [**One efficient operative system**] Quick introduction to Linux (*optional*)

4) [**New tools for learning and research**] IonSAT Tools (IT), emulating Real-Time (RT) as much as possible (presented on the PA AUDITOR experiment):
   a) *gim2vtec.v2.scr*
   b) *gimrnx2stec.v2.scr*

5) [**IT application to ECLIPSE, FLARE & GSTORM scenarios**] (*optional*).

6) [**Example of RT GPS-ionospheric system**]: UPC-IonSAT since 2012.

7) [**Monitoring of co-seismic generated ionospheric signals]:** Application of RT ionospheric sounding for potential Tsunami warnings), with GNSS dense (Tohoku and mid earthquakes, EQ) and sparse networks (Chile 2015 EQ).

8) [**Conclusions**]

The International GNSS Service (IGS)

- IGS provides continuous measurements of permanent worldwide receivers and derived products of highest quality, openly accesible via anonymous-ftp.

- The multi-frequency measurements are taken from hundreds of permanent GNSS receivers, each 30 seconds or either each second and in real-time, from the Artic to the Antartica, over all the continents, belonging to different contributing institutions.

- The provided products comprise satellite orbits and clocks, tropospheric delay, Global Ionospheric Maps – GIMS, among others.

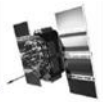

More details on IGS can be found in:

J Geod (2009) 83:191–198
DOI 10.1007/s00190-008-0300-3

INTRODUCTORY PAPER

The International GNSS Service in a changing landscape of Global Navigation Satellite Systems

John M. Dow · R. E. Neilan · C. Rizos

Received: 15 December 2008 / Accepted: 17 December 2008
© Springer-Verlag 2009

GPS+ IGS: Global Iono. scanner

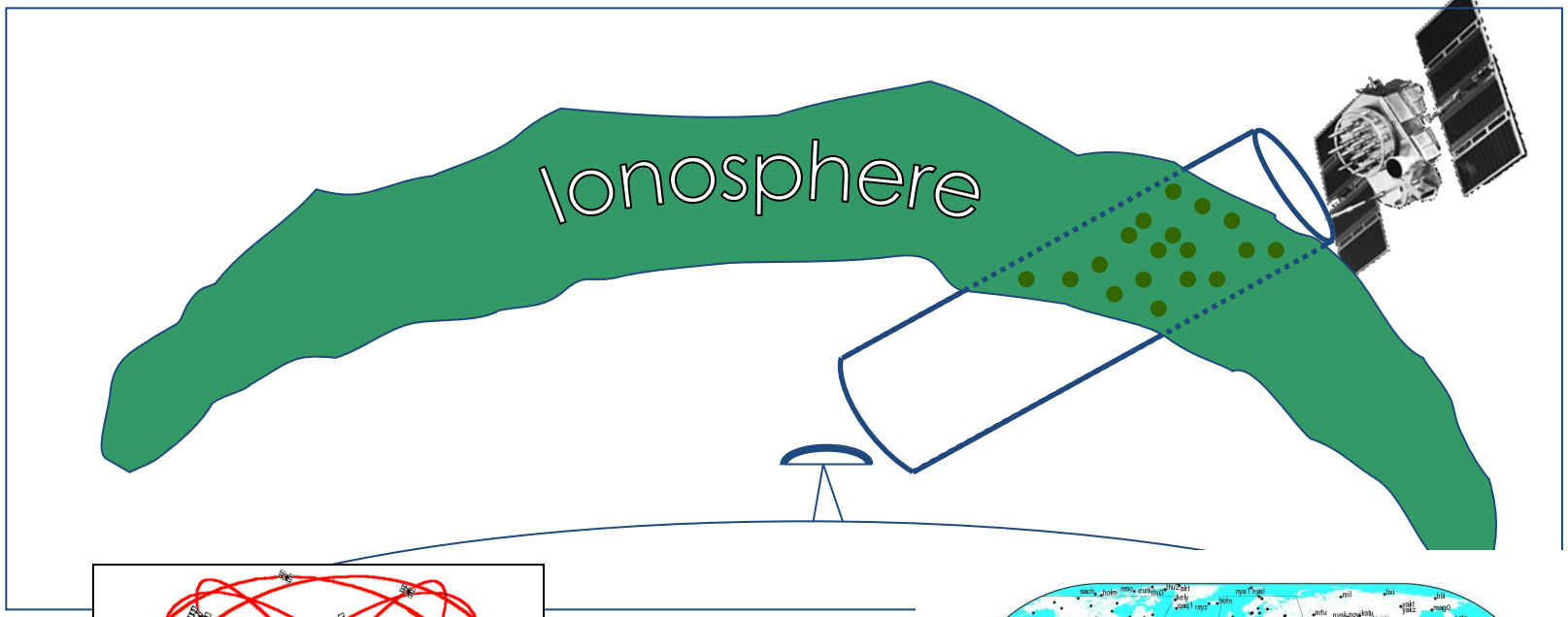

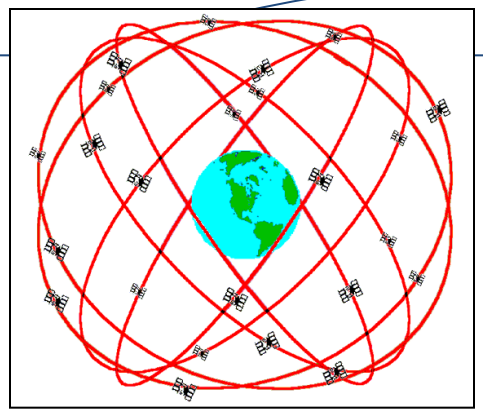

GPS+ IGS

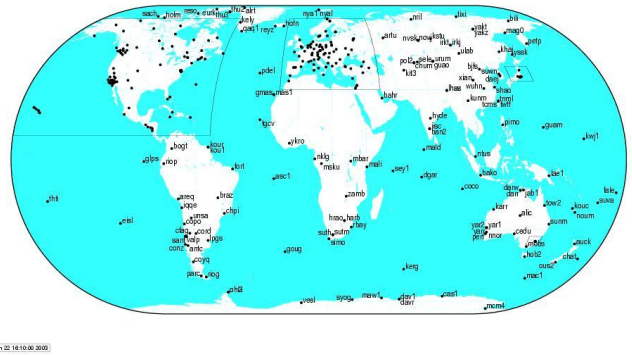

Worldwide *scanner* of the Ionosphere that can be used to generate global VTEC maps

VTEC global maps: the cooperative effort in IGS

The IGS Ionosphere Working group started its activities in June 1998 with the main goal of a routinely producing IGS Global TEC maps (IGTEC). This is being done now with a latency of 11 days (final product –official-) and with a latency of less than 24 hours (rapid product – still unofficial-).

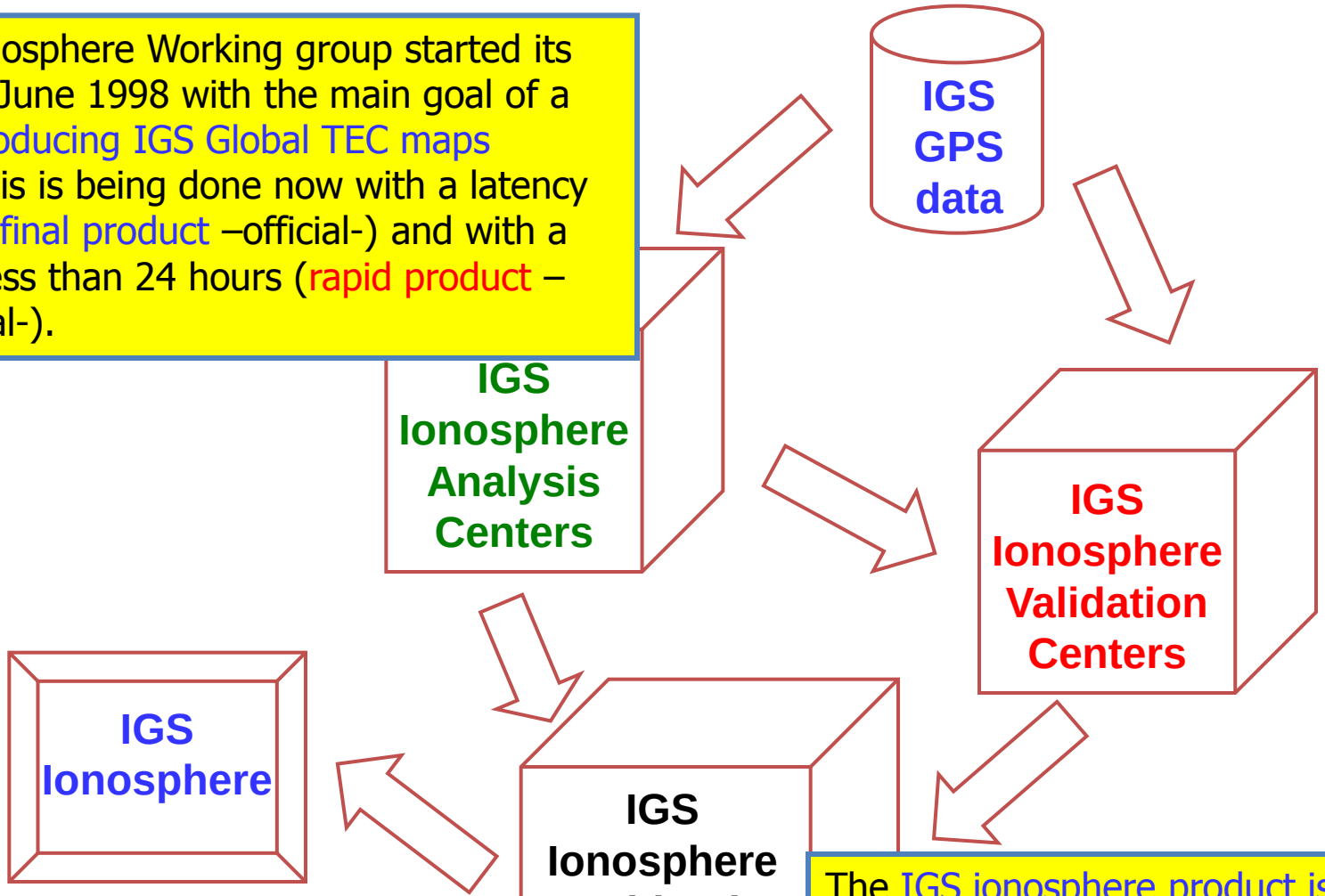

The IGS ionosphere product is a result of the combination of different Analysis Centers TEC maps by using weights computed from GPS data by Validation Centers, in order to get a more accurate product.

IGS Final Ionosphere Flow-Chart

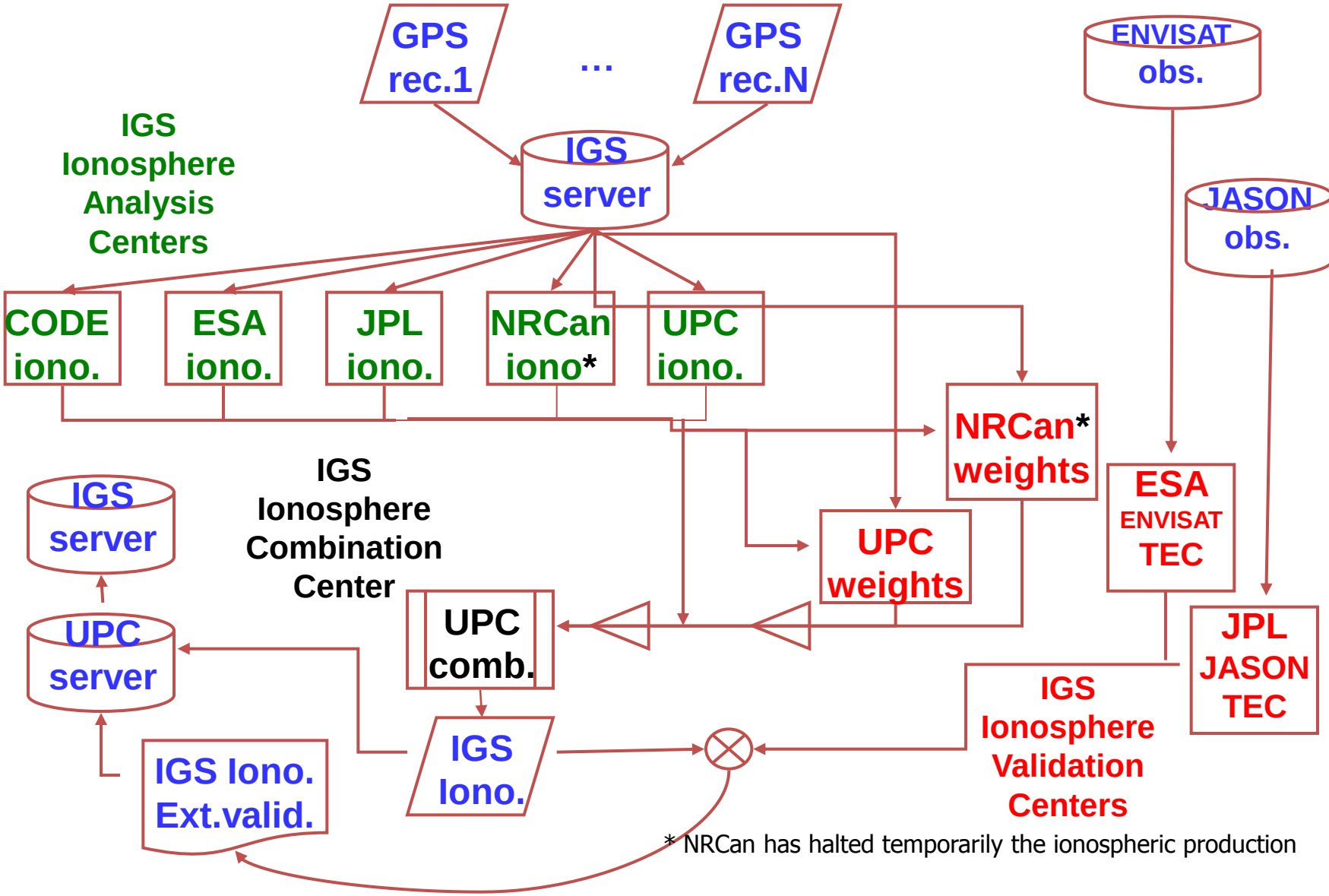

* NRCan has halted temporarily the ionospheric production

… and there is an standard format to distribute the VTEC maps: the IONEX format

The **IONEX** (IONosphere interEXchange) format allows to store the VTEC and its error estimates in a grid format, in consecutive values – at different longitudes- for each latitude grid point.

IONEX header

```
     1.0            IONOSPHERE MAPS     MIX                 IONEX VERSION / TYPE
cmpcmb v1.2         gAGE/UPC            11-may-04 13:10     PGM / RUN BY / DATE
ionex file containing IGS COMBINED Ionosphere maps          COMMENT
global ionosphere maps for day 118, 2004                    DESCRIPTION
IONEX file containing the COMBINED IGS TEC MAPS and DCBs    DESCRIPTION
  2004     4    27     0     0     0                        EPOCH OF FIRST MAP
  2004     4    28     0     0     0                        EPOCH OF LAST MAP
  7200                                                      INTERVAL
    13                                                      # OF MAPS IN FILE
  COSZ                                                      MAPPING FUNCTION
     0.0                                                    ELEVATION CUTOFF
combined TEC calculated as weighted mean of input TEC valuesOBSERVABLES USED
   290                                                      # OF STATIONS
    28                                                      # OF SATELLITES
  6371.0                                                    BASE RADIUS
     2                                                      MAP DIMENSION
   450.0 450.0   0.0                                       HGT1 / HGT2 / DHGT
    87.5 -87.5  -2.5                                       LAT1 / LAT2 / DLAT
  -180.0 180.0   5.0                                       LON1 / LON2 / DLON
    -1                                                      EXPONENT
TEC values in 0.1 tec units;  9999, if no value available   COMMENT
DCB values in nanoseconds, reference is Sum_of_SatDCBs = 0  COMMENT
DIFFERENTIAL CODE BIASES                                    START OF AUX DATA
    01    -2.253     0.035                                  PRN / BIAS / RMS
    03    -1.731     0.035                                  PRN / BIAS / RMS
...
    31    -0.692     0.036                                  PRN / BIAS / RMS
      acor                    -5.773     0.000             STATION / BIAS / RMS
      acu1                    -7.529     0.000             STATION / BIAS / RMS
...
      zwen 12330M001           0.353     0.046             STATION / BIAS / RMS
DIFFERENTIAL CODE BIASES                                    END OF AUX DATA
                                                            END OF HEADER
```

The IONEX format body

The **IONEX** (IONosphere interEXchange) format allows to store the VTEC and its error estimates in a grid format, in consecutive values – at different longitudes- for each latitude grid point.

```
     1                                                      START OF TEC MAP
  2004     4    27     0     0     0                       EPOCH OF CURRENT MAP
    87.5-180.0 180.0   5.0 450.0                           LAT/LON1/LON2/DLON/H
  123  123  123  124  125  125  126  126  126  126  126  126  125  125  125  128
  125  125  125  126  126  125  124  124  124  124  124  123  123  122  122  121
  120  120  119  118  118  118  118  118  117  117  116  116  115  114  114  113
  113  113  114  114  114  114  115  115  115  116  116  117  117  118  119  120
  120  121  121  122  123  123  123  123  123
    85.0-180.0 180.0   5.0 450.0                           LAT/LON1/LON2/DLON/H
  129  129  130  131  132  132  133  133  134  134  134  134  134  134  134  136
  135  136  130  129  129  129  128  128  128  127  126  124  123  122  121  120
  119  118  117  117  117  117  116  116  115  115  114  113  112  111  110  109
  109  110  109  109  109  110  111  111  112  112  113  113  115  116  117  118
  120  122  123  125  126  127  128  129  129
...
   -87.5-180.0 180.0   5.0 450.0                          LAT/LON1/LON2/DLON/H
   87   88   88   90   90   91   92   93   93   94   94   95   94   93   91   89
   87   86   85   84   83   82   81   81   80   80   79   78   78   78   77   77
   76   76   76   75   75   76   77   77   76   79   79   79   80   81   82   83
   83   84   85   85   85   85   85   85   85   86   87   87   87   88   88   87
   87   87   87   88   87   87   87   87   87
     1                                                    END OF TEC MAP
     2                                                    START OF TEC MAP
...
...
    13                                                    END OF TEC MAP
     1                                                    START OF RMS MAP
  2004     4    27     0     0     0                       EPOCH OF CURRENT MAP
    87.5-180.0 180.0   5.0 450.0                           LAT/LON1/LON2/DLON/H
    7    7    7    7    7    7    7    7    7    7    8    8    9    9    9    6
    8    8    8    6    6    7    7    7    7    6    6    6    6    6    6    6
    6    6    7    7    7    6    7    6    6    7    7    7    7    8    8    9
   10    9    8    8    8    8    7    7    8    8    8    8    7    7    7    7
    7    6    6    7    6    7    6    6    7
...
    13                                                    END OF RMS MAP
                                                          END OF FILE
```

International GPS Service, IGS

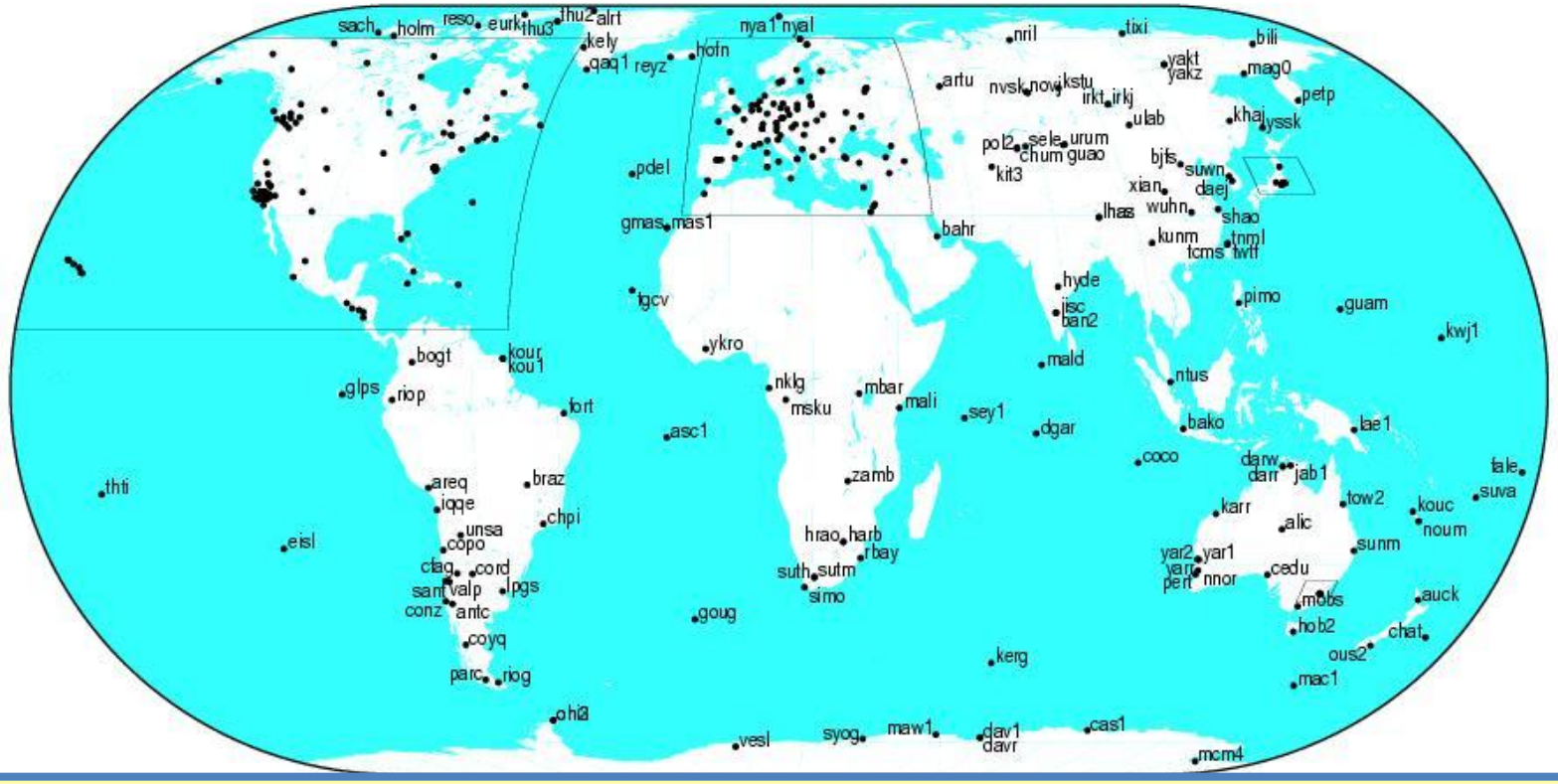

IGS directly manages more than about 350 permanent GPS stations, observing some 4-10 satellites at 30 sec rate: more than 250,000 STEC worldwide observations/hour, but there is lack of stations at the South and over the Seas

Determining VTEC in a global network: main problem of lack of data in South and Seas

It can be seen the typical "holes" appearing in the first stage of the global maps computation (each 2 hours). This requires an optimum spatial-temporal interpolation technique to extend the estimates covering all the Ionosphere.

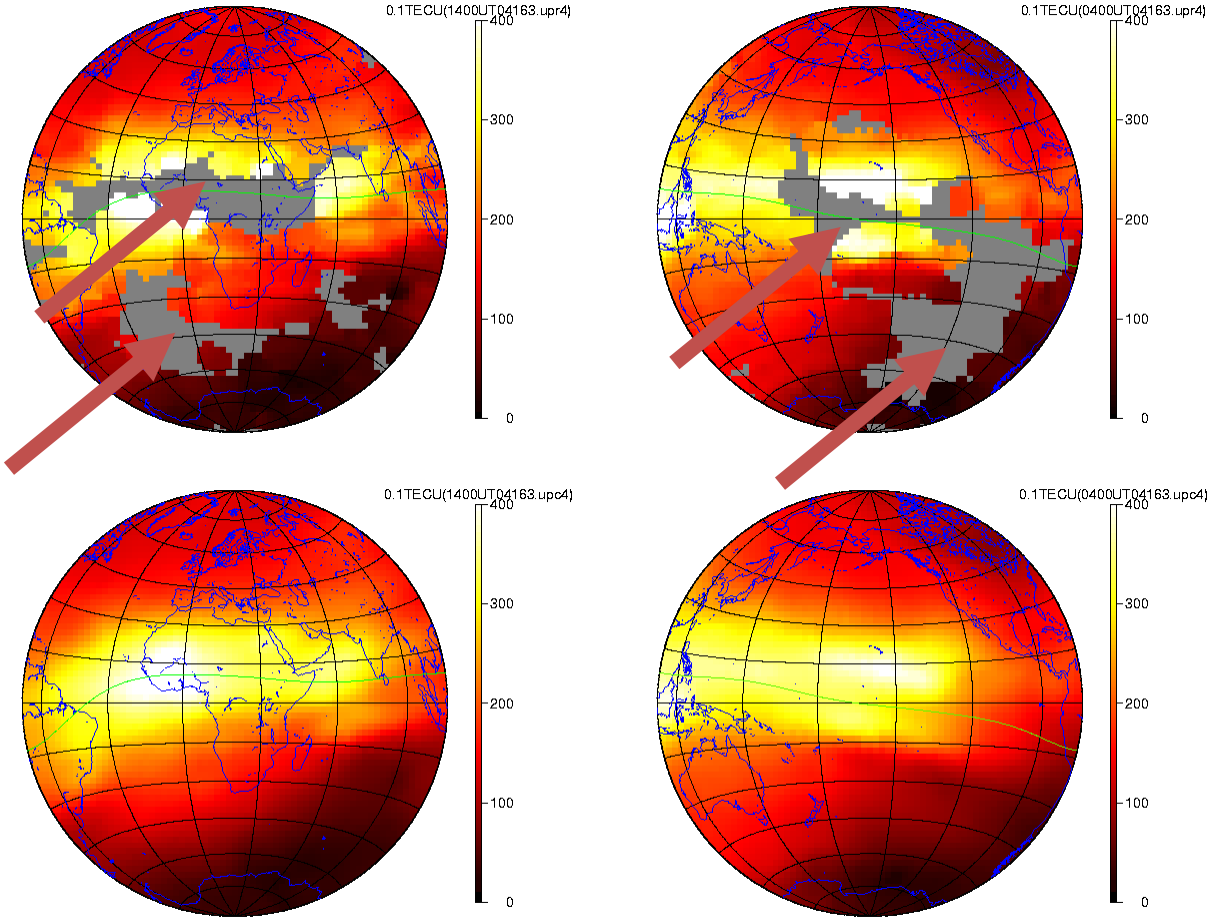

Lack of data in equatorial Africa and Atlantic, and in part of equatorial and southern Pacific, difficulting the detection of the equatorial anomalies (June 13, 2004).

Computing Global VTEC maps: layout

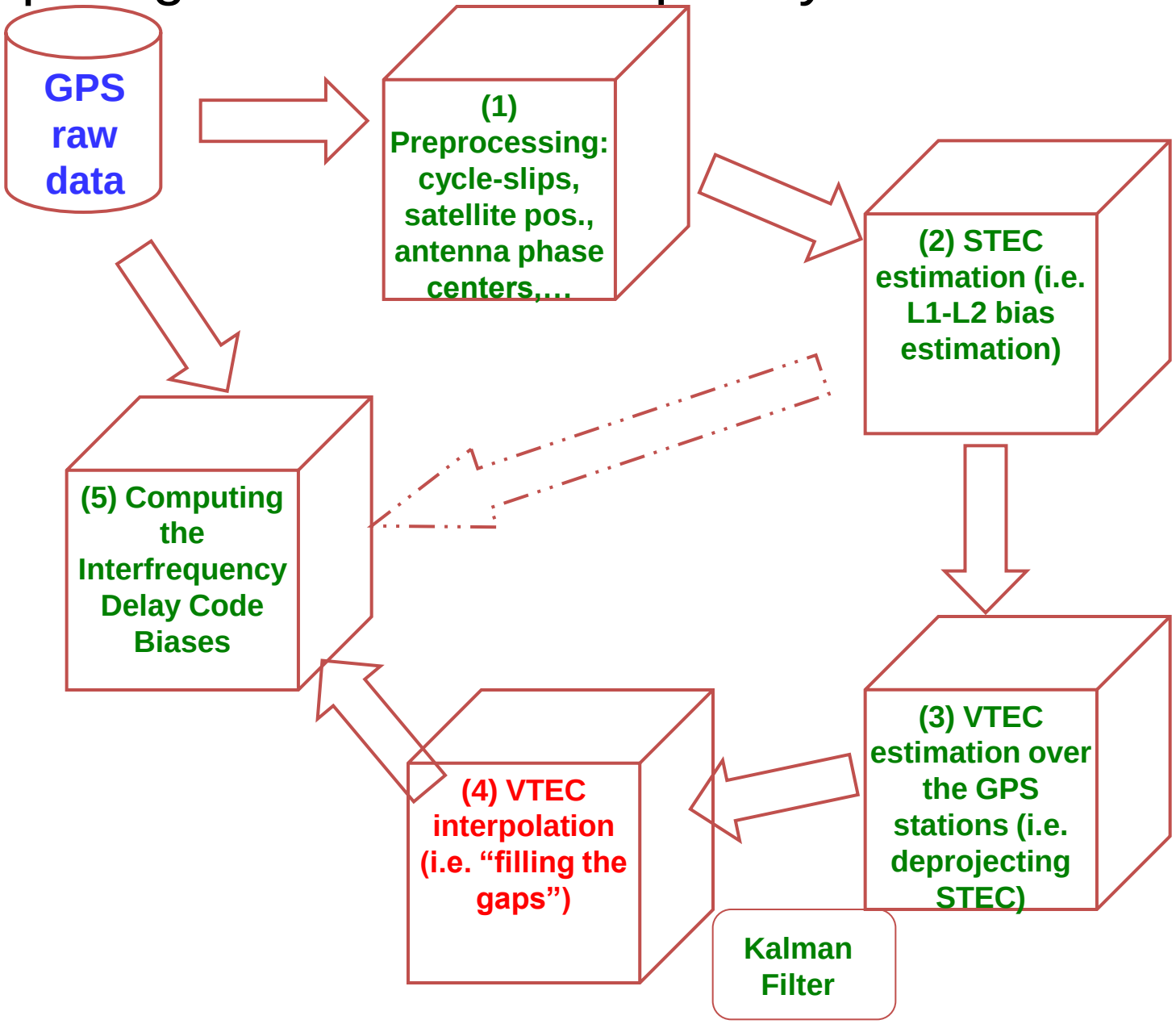

Example of IGS Final TEC map: 2003-347-00UT

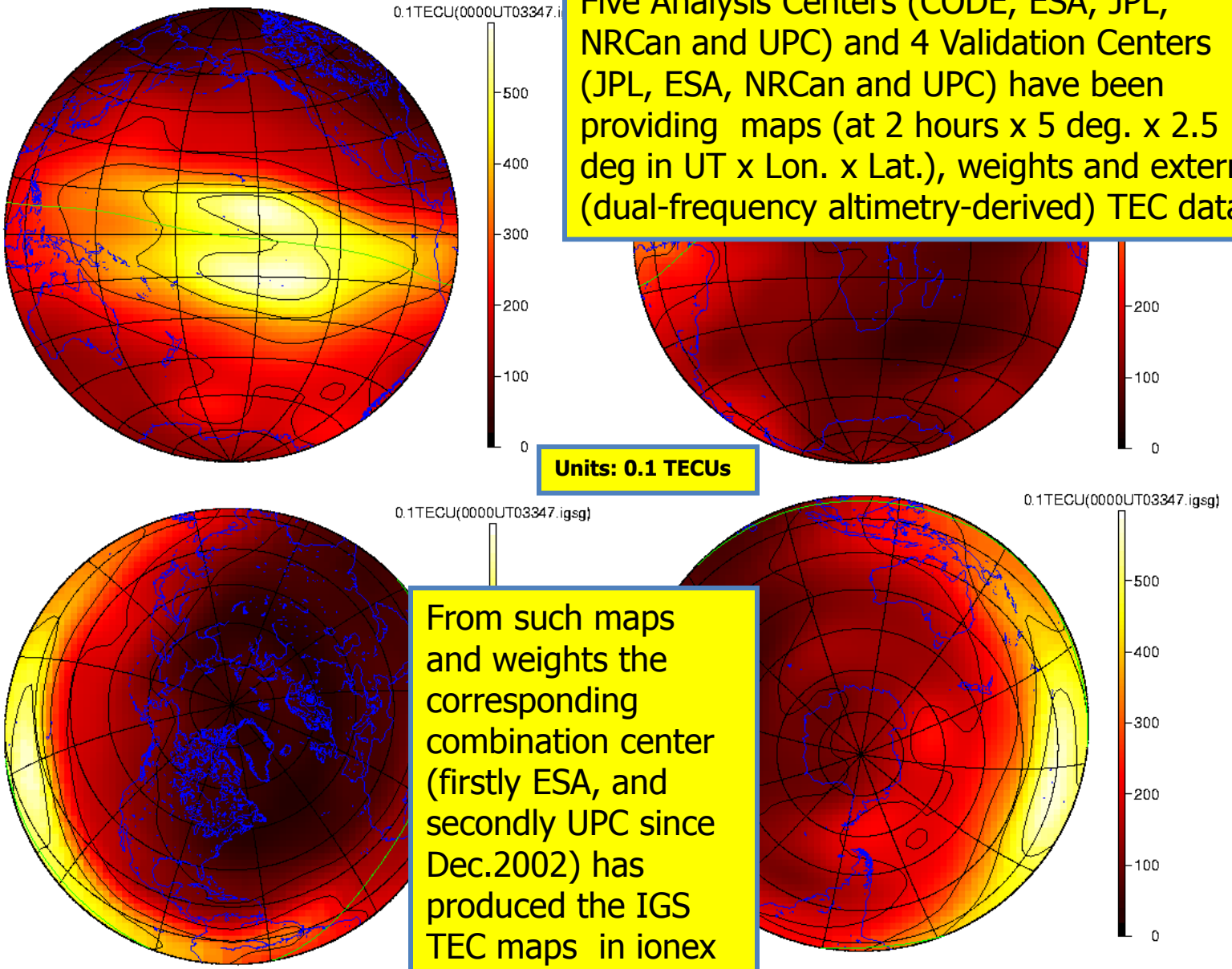

Five Analysis Centers (CODE, ESA, JPL, NRCan and UPC) and 4 Validation Centers (JPL, ESA, NRCan and UPC) have been providing maps (at 2 hours x 5 deg. x 2.5 deg in UT x Lon. x Lat.), weights and external (dual-frequency altimetry-derived) TEC data.

Units: 0.1 TECUs

From such maps and weights the corresponding combination center (firstly ESA, and secondly UPC since Dec.2002) has produced the IGS TEC maps in ionex format.

Example of comparison of IGS vs JASON: 2003-347 each 6 hours

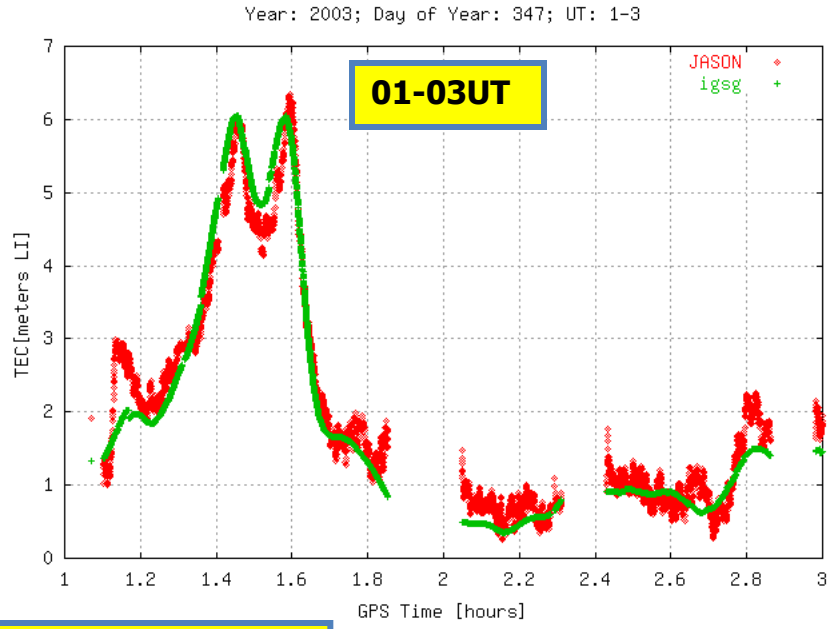

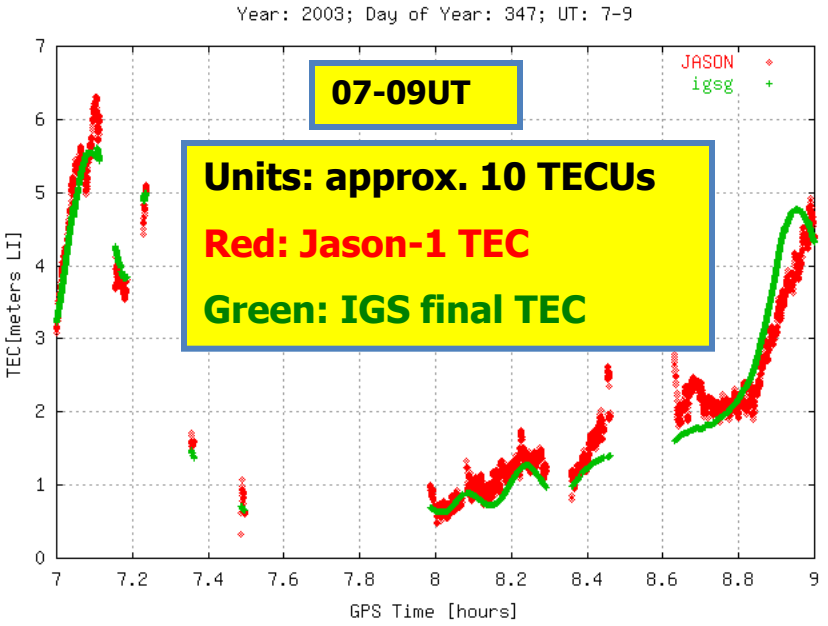

JASON dual frequency altimeter provides a direct and independent VTEC below its orbit (1300 km) and over the oceans (worst case for GPS).

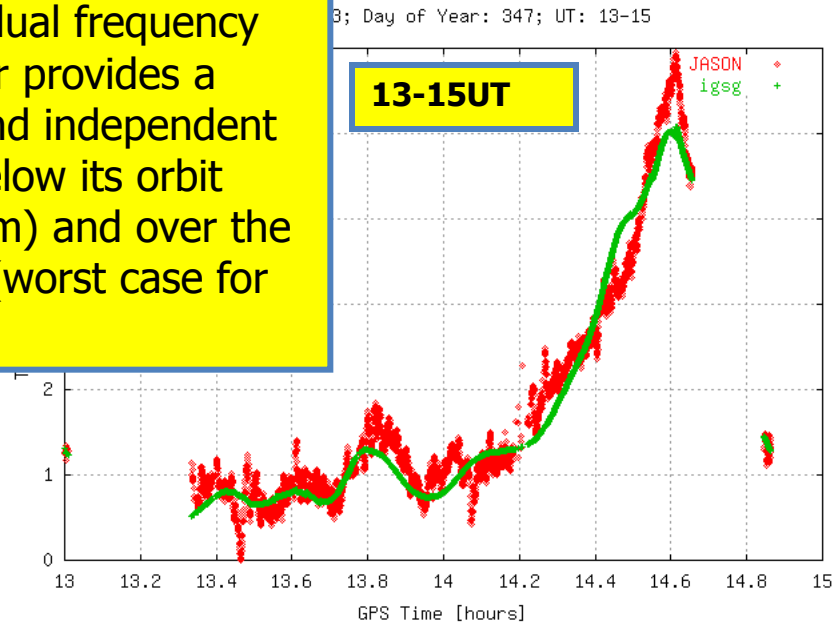

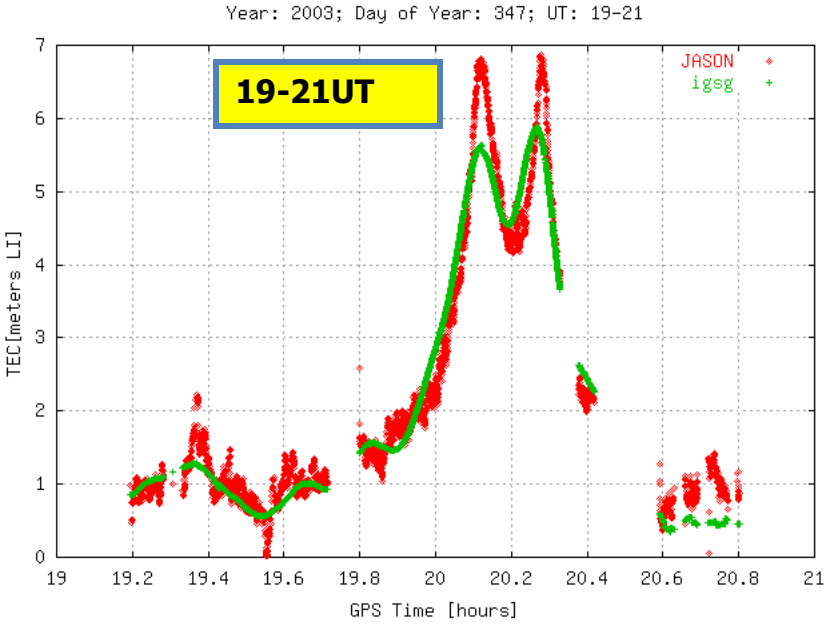

More details on IGS GIMs can be found in:

J Geod (2009) 83:263–275
DOI 10.1007/s00190-008-0266-1

ORIGINAL ARTICLE

The IGS VTEC maps: a reliable source of ionospheric information since 1998

M. Hernández-Pajares · J. M. Juan · J. Sanz ·
R. Orus · A. Garcia-Rigo · J. Feltens · A. Komjathy ·
S. C. Schaer · A. Krankowski

Received: 12 February 2008 / Accepted: 25 August 2008
© Springer-Verlag 2008

And more recently…

J Geod
DOI 10.1007/s00190-017-1032-z

ORIGINAL ARTICLE

Methodology and consistency of slant and vertical assessments for ionospheric electron content models

Manuel Hernández-Pajares[1] · David Roma-Dollase[1,2] · Andrzej Krankowski[3] · Alberto García-Rigo[1] · Raül Orús-Pérez[4]

Received: 28 September 2016 / Accepted: 19 April 2017
© Springer-Verlag Berlin Heidelberg 2017

Journal of Geodesy
https://doi.org/10.1007/s00190-017-1088-9

ORIGINAL ARTICLE

Consistency of seven different GNSS global ionospheric mapping techniques during one solar cycle

David Roma-Dollase[2] · Manuel Hernández-Pajares[1] · Andrzej Krankowski[3] · Kacper Kotulak[3] · Reza Ghoddousi-Fard[4] · Yunbin Yuan[5] · Zishen Li[6] · Hongping Zhang[7] · Chuang Shi[7] · Cheng Wang[7] · Joachim Feltens[8] · Panagiotis Vergados[9] · Attila Komjathy[9] · Stefan Schaer[10] · Alberto García-Rigo[1] · José M. Gómez-Cama[2]

Received: 26 May 2017 / Accepted: 12 November 2017
© Springer-Verlag GmbH Germany, part of Springer Nature 2017

Layout:

1) [**Motivation**] Precise Agriculture (PA) presentation (EU AUDITOR experiment)

2) [**Background**]: Brief introduction to main identified points of the presentation:
   a) GPS fundamentals: pseudoranges and carrier phases (optional)
   b) Ionospheric electron content
   c) Wide Area Real-Time Kinematic
   d) The International GNSS Service (*optional*)

3) [**One efficient operative system**] Quick introduction to Linux (*optional*)

4) [**New tools for learning and research**] IonSAT Tools (IT), emulating Real-Time (RT) as much as possible (presented on the PA AUDITOR experiment):
   a) *gim2vtec.v2.scr*
   b) *gimrnx2stec.v2.scr*

5) [**IT application to ECLIPSE, FLARE & GSTORM scenarios**] (*optional*).

6) [**Example of RT GPS-ionospheric system**]: UPC-IonSAT since 2012.

7) [**Monitoring of co-seismic generated ionospheric signals]:** Application of RT ionospheric sounding for potential Tsunami warnings), with GNSS dense (Tohoku and mid earthquakes, EQ) and sparse networks (Chile 2015 EQ).

8) [**Conclusions**]

Connection to server (from xterm or similar)

- ssh –X –p XXXXX ionsat-tools-userYY@chapman.upc.es

- Where XXXXX is the port number (see blackboard) and YY the UserId # (since 02 to 22), and the password, should be given to you at the beginning of the corresponding laboratory session.

You will find in the next few slides a quick introduction to very basic Linux, the open-source, reliable and high performance operative system.

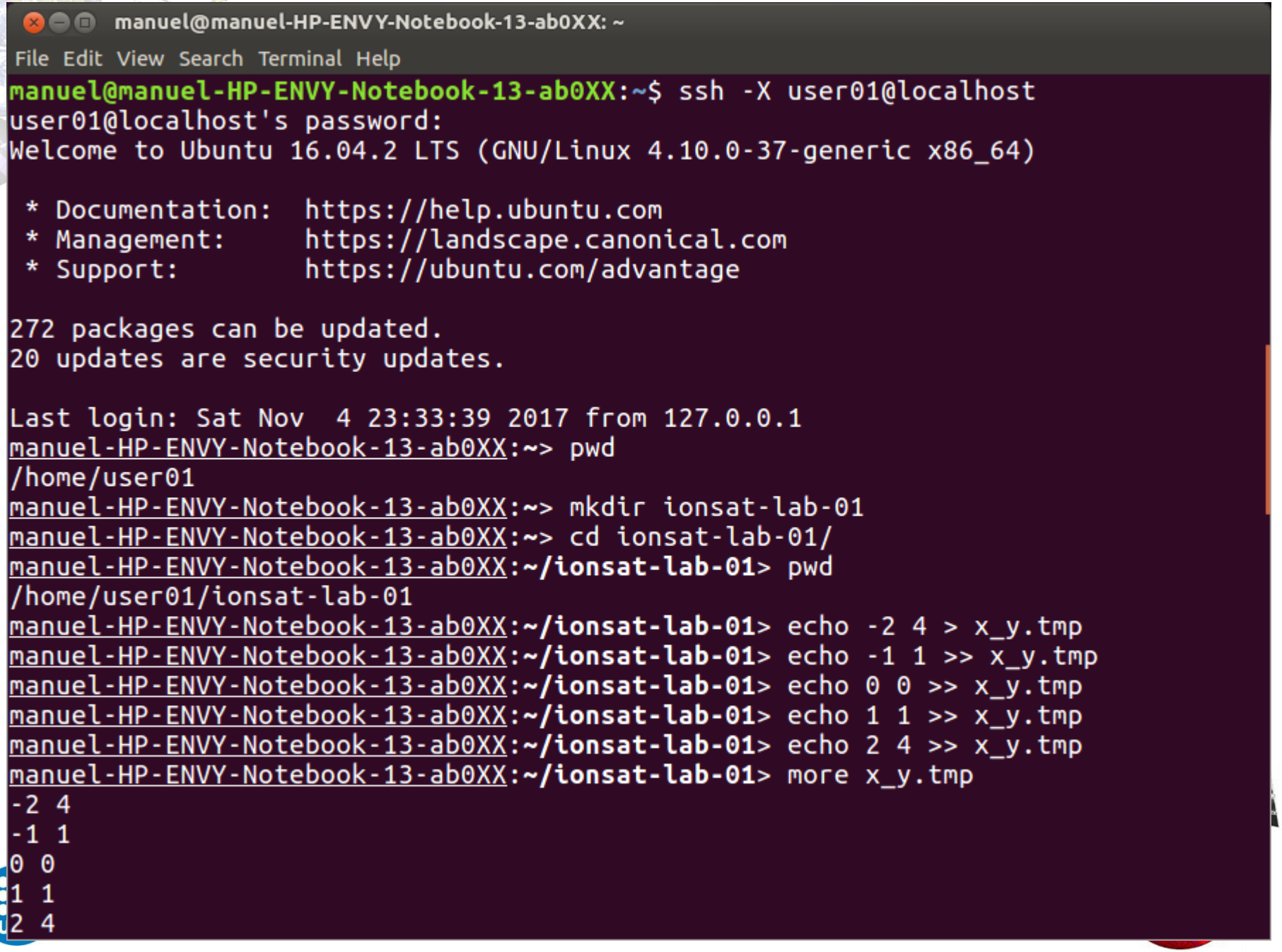
manuel@manuel-HP-ENVY-Notebook-13-ab0XX: ~
File Edit View Search Terminal Help
manuel@manuel-HP-ENVY-Notebook-13-ab0XX:~$ ssh -X user01@localhost
user01@localhost's password:
Welcome to Ubuntu 16.04.2 LTS (GNU/Linux 4.10.0-37-generic x86_64)
* Documentation: https://help.ubuntu.com
* Management: https://landscape.canonical.com
* Support: https://ubuntu.com/advantage
272 packages can be updated.
20 updates are security updates.
Last login: Sat Nov 4 23:33:39 2017 from 127.0.0.1
manuel-HP-ENVY-Notebook-13-ab0XX:~> pwd
/home/user01
manuel-HP-ENVY-Notebook-13-ab0XX:~> mkdir ionsat-lab-01
manuel-HP-ENVY-Notebook-13-ab0XX:~> cd ionsat-lab-01/
manuel-HP-ENVY-Notebook-13-ab0XX:~/ionsat-lab-01> pwd
/home/user01/ionsat-lab-01
manuel-HP-ENVY-Notebook-13-ab0XX:~/ionsat-lab-01> echo -2 4 > x_y.tmp
manuel-HP-ENVY-Notebook-13-ab0XX:~/ionsat-lab-01> echo -1 1 >> x_y.tmp
manuel-HP-ENVY-Notebook-13-ab0XX:~/ionsat-lab-01> echo 0 0 >> x_y.tmp
manuel-HP-ENVY-Notebook-13-ab0XX:~/ionsat-lab-01> echo 1 1 >> x_y.tmp
manuel-HP-ENVY-Notebook-13-ab0XX:~/ionsat-lab-01> echo 2 4 >> x_y.tmp
manuel-HP-ENVY-Notebook-13-ab0XX:~/ionsat-lab-01> more x_y.tmp
-2 4
-1 1
0 0
1 1
2 4

```
manuel@manuel-HP-ENVY-Notebook-13-ab0XX: ~
File  Edit  View  Search  Terminal  Help
2 4
manuel-HP-ENVY-Notebook-13-ab0XX:~/ionsat-lab-01> wc -l x_y.tmp
5 x_y.tmp
manuel-HP-ENVY-Notebook-13-ab0XX:~/ionsat-lab-01> ls -l x_y.tmp
-rw-rw-r-- 1 user01 user01 22 nov  4 23:36 x_y.tmp
manuel-HP-ENVY-Notebook-13-ab0XX:~/ionsat-lab-01> gnuplot

        G N U P L O T
        Version 5.0 patchlevel 3    last

        Copyright (C) 1986-1993, 1998, 20
        Thomas Williams, Colin Kelley and

        gnuplot home:     http://www.gnup
        faq, bugs, etc:   type "help FAQ"
        immediate help:   type "help"  (p

Terminal type set to 'qt'
gnuplot> plot "x_y.tmp"
gnuplot> plot "x_y.tmp" w lp
gnuplot> plot "x_y.tmp" w lp,x**2
gnuplot> set term png
Terminal type set to 'png'
Options are 'nocrop enhanced size 640,480 font "/usr/share/fonts/truetype/libera
tion/LiberationSans-Regular.ttf,12" '
gnuplot> set output "x_y.png"
gnuplot> replot
gnuplot> quit
```

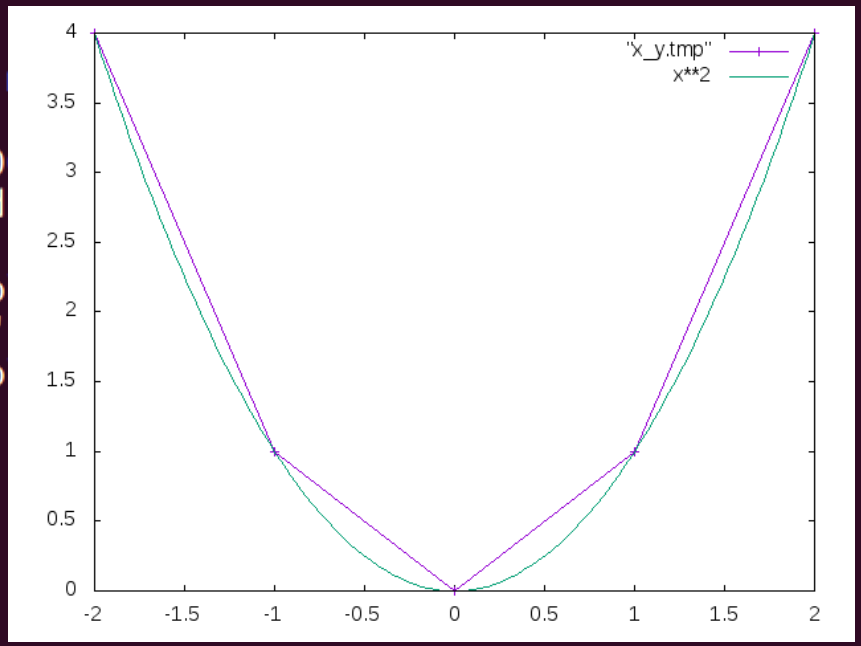

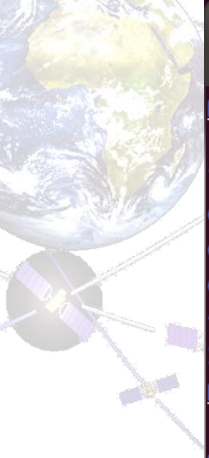

```
manuel@manuel-HP-ENVY-Notebook-13-ab0XX: ~
File  Edit  View  Search  Terminal  Help
manuel-HP-ENVY-Notebook-13-ab0XX:~/ionsat-lab-01> pqiv -i x_y.png

** (pqiv:18405): WARNING **: Couldn't register with accessibility bus: Did not r
eceive a reply. Possible causes include: the remote application did not send a r
eply, the message bus security policy blocked the reply, the reply timeout expir
ed, or the network connection was broken.
^Z
Suspended
manuel-HP-ENVY-Notebook-13-ab0XX:~/ionsat-lab-01> bg
[1]    pqiv -i x_y.png &
manuel-HP-ENVY-Notebook-13-ab0XX:~/ionsat-lab-01> gawk '{print $1,$1**3}' x_y
x_y.png  x_y.tmp
manuel-HP-ENVY-Notebook-13-ab0XX:~/ionsat-lab-01> gawk '{print $1,$1**3}' x_y.tm
p > x_x3.tmp
manuel-HP-ENVY-Notebook-13-ab0XX:~/ionsat-lab-01> gnuplot

        G N U P L O T
        Version 5.0 patchlevel 3    last modified 2016-02-21

        Copyright (C) 1986-1993, 1998, 2004, 2007-2016
        Thomas Williams, Colin Kelley and many others

        gnuplot home:     http://www.gnuplot.info
        faq, bugs, etc:   type "help FAQ"
        immediate help:   type "help"  (plot window: hit 'h')

Terminal type set to 'qt'
gnuplot> plot "x_x3.tmp" w lp
gnuplot> plot "x_x3.tmp" w lp,x**3
gnuplot> set term png
Terminal type set to 'png'
Options are 'nocrop enhanced size 640,480 font "/usr/share/fonts/truetype/libera
tion/LiberationSans-Regular.ttf,12" '
gnuplot> set output "x_x3.png"
gnuplot> replot
gnuplot> quit
manuel-HP-ENVY-Notebook-13-ab0XX:~/ionsat-lab-01> pqiv -i x_*.png
```

Open | x_x3.gnu ~/ionsat-lab-01 | Save

File Edit View Search Tools Documents Help

```
set xlabel "y"
set ylabel "x"
set grid
set title "First gnuplot script"
plot "x_x3.final" t "from hand-edited file",x**3 t "from function"
pause(-1)
set term png
set output "x_x3.final.png"
replot
```

pqiv: x_x3.final.png (640x480) 100,00% [1/1] (as user01)

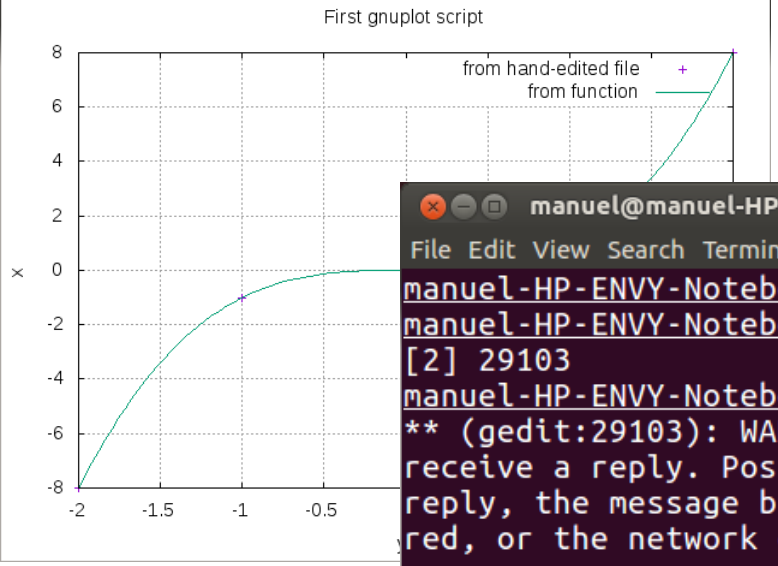

Gnuplot window 0

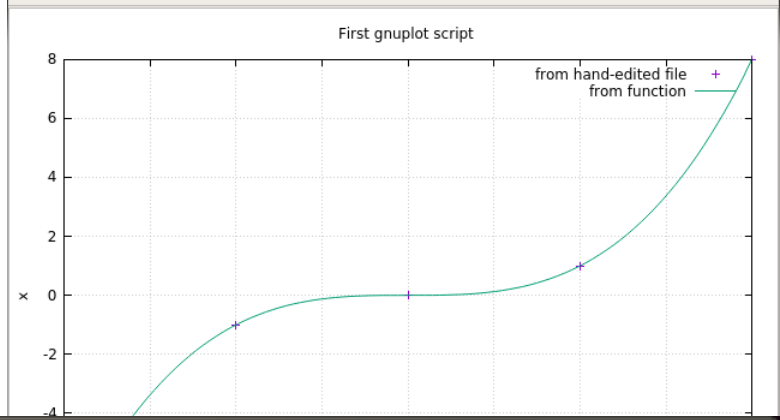

manuel@manuel-HP-ENVY-Notebook-13-ab0XX: ~

File Edit View Search Terminal Help

```
manuel-HP-ENVY-Notebook-13-ab0XX:~/ionsat-lab-01> cp x_x3.tmp x_x3.final
manuel-HP-ENVY-Notebook-13-ab0XX:~/ionsat-lab-01> gedit x_x3.gnu &
[2] 29103
manuel-HP-ENVY-Notebook-13-ab0XX:~/ionsat-lab-01>
** (gedit:29103): WARNING **: Couldn't register with accessibility bus: Did not receive a reply. Possible causes include: the remote application did not send a reply, the message bus security policy blocked the reply, the reply timeout expired, or the network connection was broken.

manuel-HP-ENVY-Notebook-13-ab0XX:~/ionsat-lab-01> gnuplot x_x3.gnu

manuel-HP-ENVY-Notebook-13-ab0XX:~/ionsat-lab-01> pqiv -i x_x3.final.png &
[3] 29176
manuel-HP-ENVY-Notebook-13-ab0XX:~/ionsat-lab-01>
** (pqiv:29176): WARNING **: Couldn't register with accessibility bus: Did not receive a reply. Possible causes include: the remote application did not send a reply, the message bus security policy blocked the reply, the reply timeout expired, or the network connection was broken.
```

Layout:

1) [**Motivation**] Precise Agriculture (PA) presentation (EU AUDITOR experiment)

2) [**Background**]: Brief introduction to main identified points of the presentation:
   a) GPS fundamentals: pseudoranges and carrier phases (optional)
   b) Ionospheric electron content
   c) Wide Area Real-Time Kinematic
   d) The International GNSS Service (*optional*)

3) [**One efficient operative system**] Quick introduction to Linux (*optional*)

4) [**New tools for learning and research**] IonSAT Tools (IT), emulating Real-Time (RT) as much as possible (presented on the PA AUDITOR experiment):
   a) *gim2vtec.v2.scr*
   b) *gimrnx2stec.v2.scr*

5) [**IT application to ECLIPSE, FLARE & GSTORM scenarios**] (*optional*).

6) [**Example of RT GPS-ionospheric system**]: UPC-IonSAT since 2012.

7) [**Monitoring of co-seismic generated ionospheric signals]:** Application of RT ionospheric sounding for potential Tsunami warnings), with GNSS dense (Tohoku and mid earthquakes, EQ) and sparse networks (Chile 2015 EQ).

8) [**Conclusions**]

New IonSAT tools: gim2vtec.v2.scr & gimrnx2stec.v2.scr

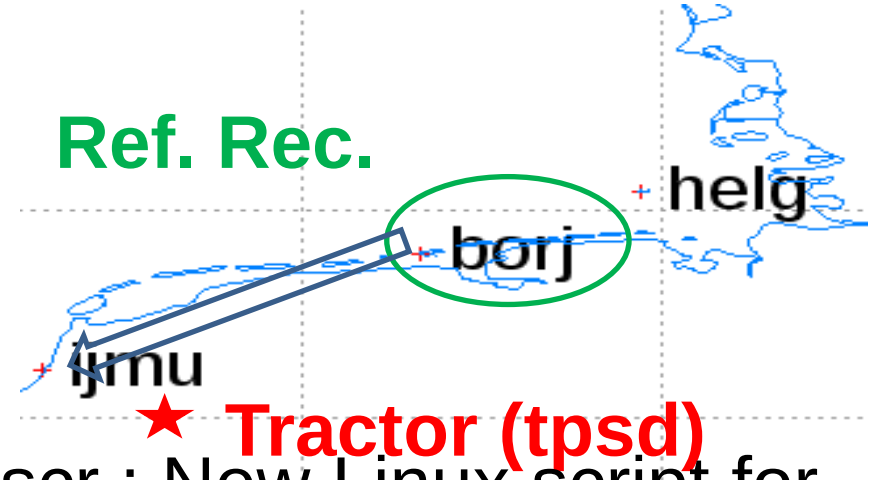

- IonSAT tool gim2vtec.v2.scr : New Linux script for Vertical Total Electron Content (VTEC) extraction from Global Ionospheric Maps (GIM).
- IonSAT tool gimrnx2stec.v2.scr: New Linux script for Slant TEC (STEC) computation from GIM-calibrated GPS meas. Carrier phase prepro.
- The first suggested application is for the *motivating* AUDITOR experiment (June 13th, 2017) described in section 1, and for the baseline between reference and permanent receiver, similar to the tractor one.

gim2vtec.v2.scr & gimrnx2stec.v2.scr @ AUDITOR

- ssh –X –p XXXXX ionsat-tools-userYY@chapman.upc.es
- Where XXXXX is the port number (see blackboard) and YY the UserId # (since 01 to 20), and the password, given to you at the beginning of the corresponding laboratory session.
- chapman:~% whoami
- chapman:~% cd ils
- chapman:~% pwd
- chapman:~% ls -l
- chapman:~% xedit run.IonSAT-lab_sessions.v4b.scr &
- Uncomment (remove the first leading #) the three command lines for AUDITOR block, save and run the script:
- chapman:~% ./run.IonSAT-lab_sessions.v4b.scr >& log.1 < /dev/null &

gim2vtec.v2.scr & gimrnx2stec.v2.scr @ AUDITOR

- chapman:~% tail -f log.1

- Once it is finished you can look at the selected results in form of plots:

- chapman:~% cd ~/ils/selected_plots
- chapman:~% ./selected_plots.scr
- chapman:~% ./selected_plots.scr ftplink AUDITOR

- **Each ftp link can be pasted on the navigator at your local computer**, for low-bandwidth connections (for high-bandwidth you may wish to replace “ftplink” by “screen”).

- You should likely find these selected plots:

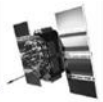

Looking at the Vertical Total Electron Content (VTEC) from Global Ionospheric Maps (GIMs)

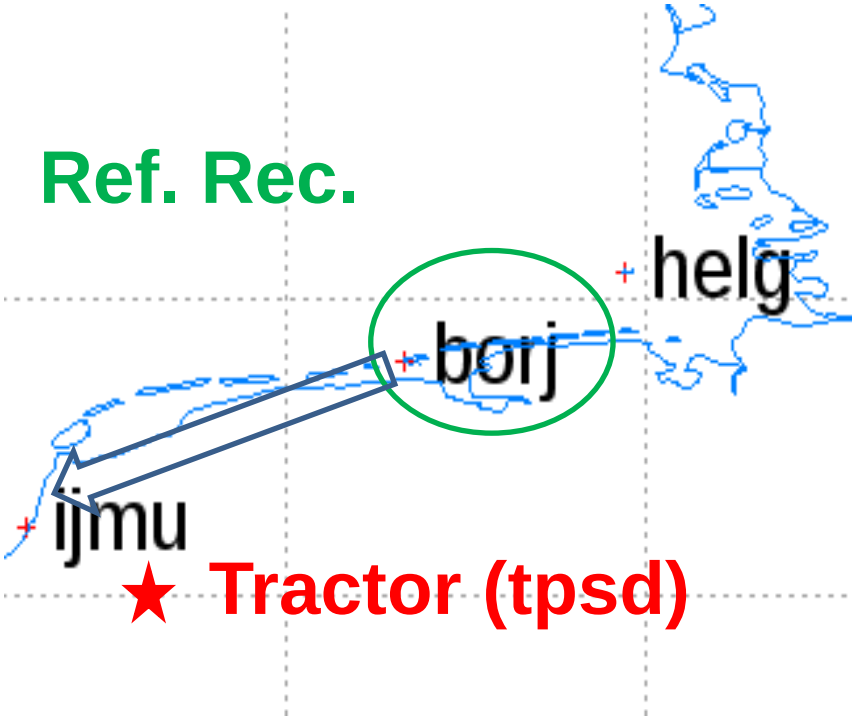

Up to higher level directory

Name	Size	Last Modified
STECs-vs-TIME.uqrg.20170612-163-to-20170614-165.borj.png	281 KB	11/18/17 6:59:39 PM GMT+1
STECs-vs-TIME.uqrg.20170612-163-to-20170614-165.ijmu.png	284 KB	11/18/17 6:59:43 PM GMT+1
VTECs-vs-TIME.uqrg.20170612-163-to-20170614-165.GIM.borj.png	171 KB	11/18/17 6:59:40 PM GMT+1
VTECs-vs-TIME.uqrg.20170612-163-to-20170614-165.GIM.ijmu.png	174 KB	11/18/17 6:59:43 PM GMT+1
VTECs-vs-TIME.uqrg.20170612-163-to-20170614-165.IG1.borj.png	228 KB	11/18/17 6:59:40 PM GMT+1
VTECs-vs-TIME.uqrg.20170612-163-to-20170614-165.IG1.ijmu.png	247 KB	11/18/17 6:59:44 PM GMT+1
VTECs-vs-TIME.uqrg.20170612-163-to-20170614-165.IG2.borj.png	212 KB	11/18/17 6:59:41 PM GMT+1
VTECs-vs-TIME.uqrg.20170612-163-to-20170614-165.IG2.ijmu.png	224 KB	11/18/17 6:59:44 PM GMT+1
VTECs-vs-TIME.uqrg.20170612-163-to-20170614-165.PI.borj.png	343 KB	11/18/17 6:59:41 PM GMT+1
VTECs-vs-TIME.uqrg.20170612-163-to-20170614-165.PI.ijmu.png	420 KB	11/18/17 6:59:45 PM GMT+1
d2LI-vs-TIME.20170612-163-to-20170614-165.PI.borj.png	139 KB	11/18/17 6:59:42 PM GMT+1
d2LI-vs-TIME.20170612-163-to-20170614-165.PI.ijmu.png	144 KB	11/18/17 6:59:46 PM GMT+1
d2VTEC300s-vs-TIME.20170612-163-to-20170614-165.PI.borj.png	123 KB	11/18/17 6:59:41 PM GMT+1
d2VTEC300s-vs-TIME.20170612-163-to-20170614-165.PI.ijmu.png	127 KB	11/18/17 6:59:45 PM GMT+1
dBw-vs-TIME.20170612-163-to-20170614-165.PI.borj.png	263 KB	11/18/17 6:59:42 PM GMT+1
dBw-vs-TIME.20170612-163-to-20170614-165.PI.ijmu.png	239 KB	11/18/17 6:59:46 PM GMT+1
ionex_2_latitudinal_VTEC_profiles_time_series.uqrg.2017.163-165.anim.gif	3431 KB	11/18/17 8:18:08 AM GMT+1
tec.output+djm.uqrg.20170612_163_to_20171650614_165.borj.png	63 KB	11/18/17 6:45:23 PM GMT+1
tec.output+djm.uqrg.20170612_163_to_20171650614_165.ijmu.png	65 KB	11/18/17 6:45:23 PM GMT+1
tec.output+djm.uqrg.20170612_163_to_20171650614_165.nama.png	75 KB	11/18/17 6:45:23 PM GMT+1
tec.output+djm.uqrg.20170612_163_to_20171650614_165.rgao.png	62 KB	11/18/17 6:45:24 PM GMT+1
tec.output+djm.uqrg.20170612_163_to_20171650614_165.tmp1.png	73 KB	11/18/17 6:45:24 PM GMT+1
tec.output+djm.uqrg.20170612_163_to_20171650614_165.valp.png	63 KB	11/18/17 6:45:24 PM GMT+1

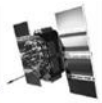

VTEC over BORJ from GIM UQRG

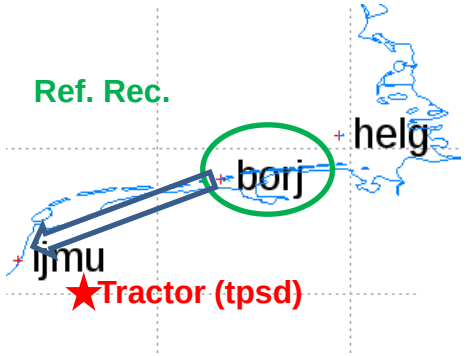

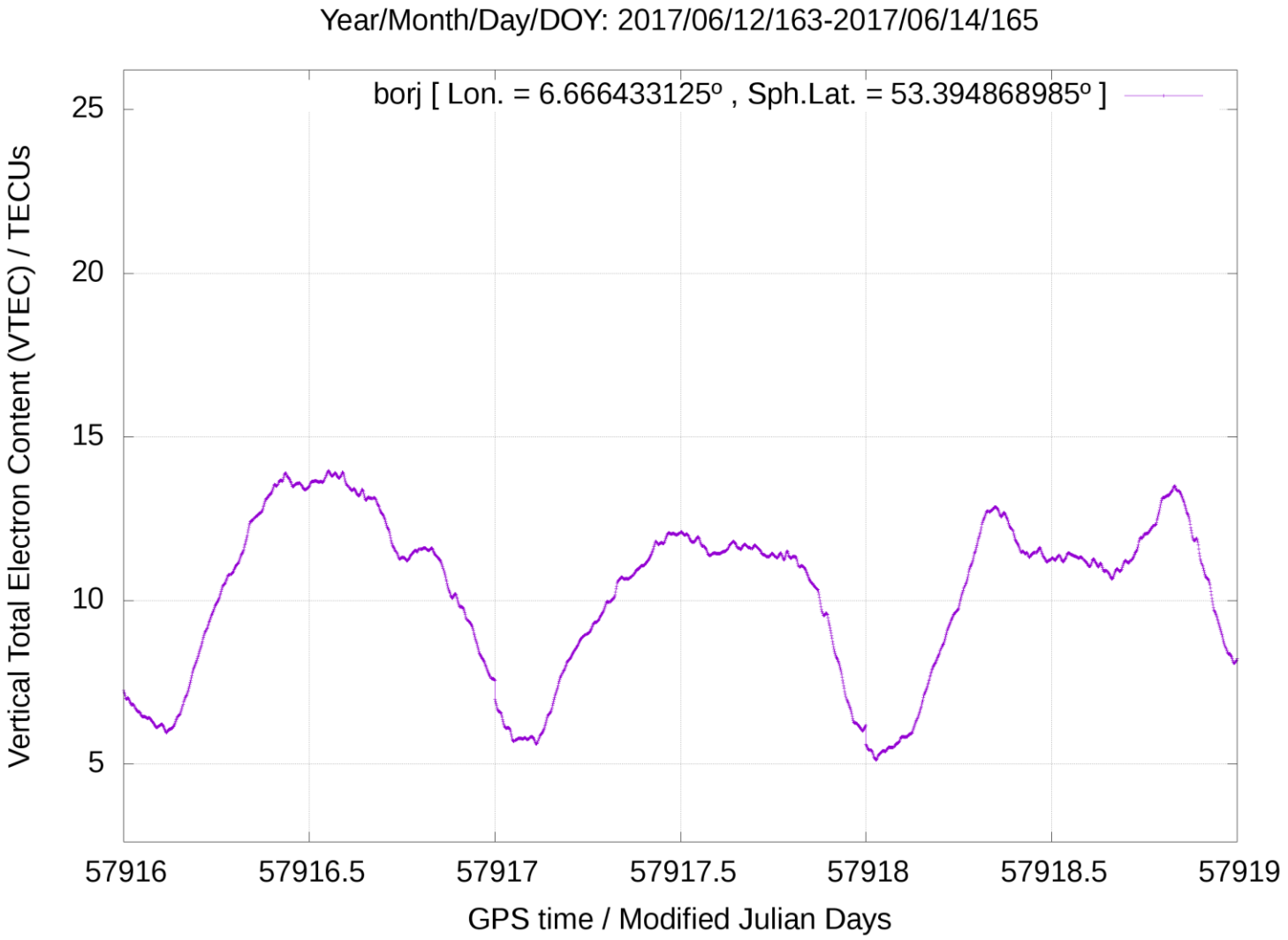

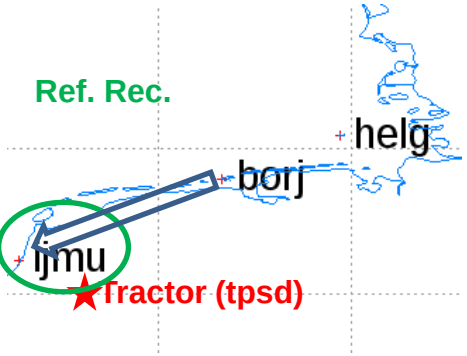

VTEC over IJMU from GIM UQRG

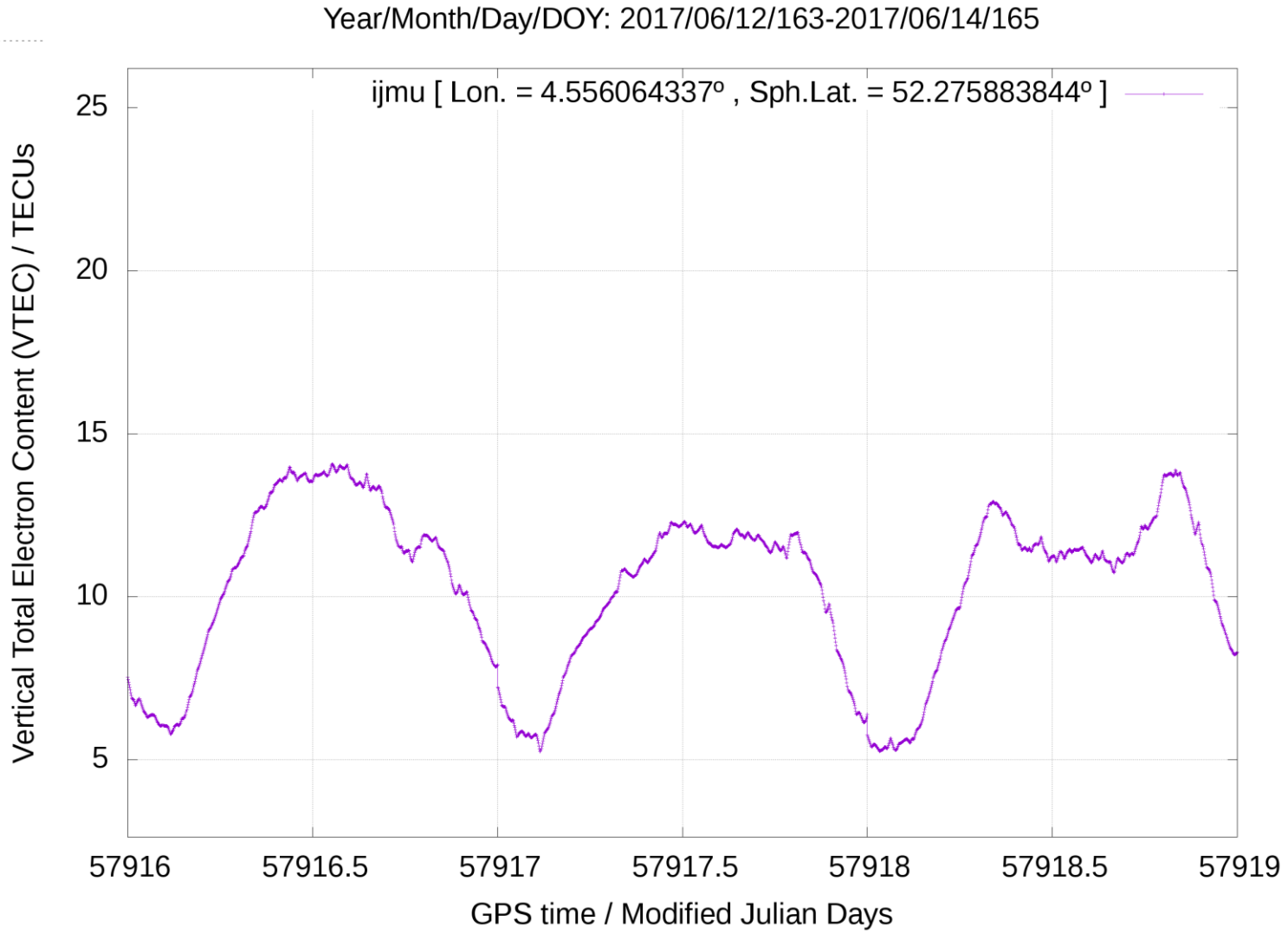

VTEC over NAMA from GIM UQRG

NAMA-TMP1 is a similar baseline to BORJ-IJMU but now at low latitude (Saudi Arabia)

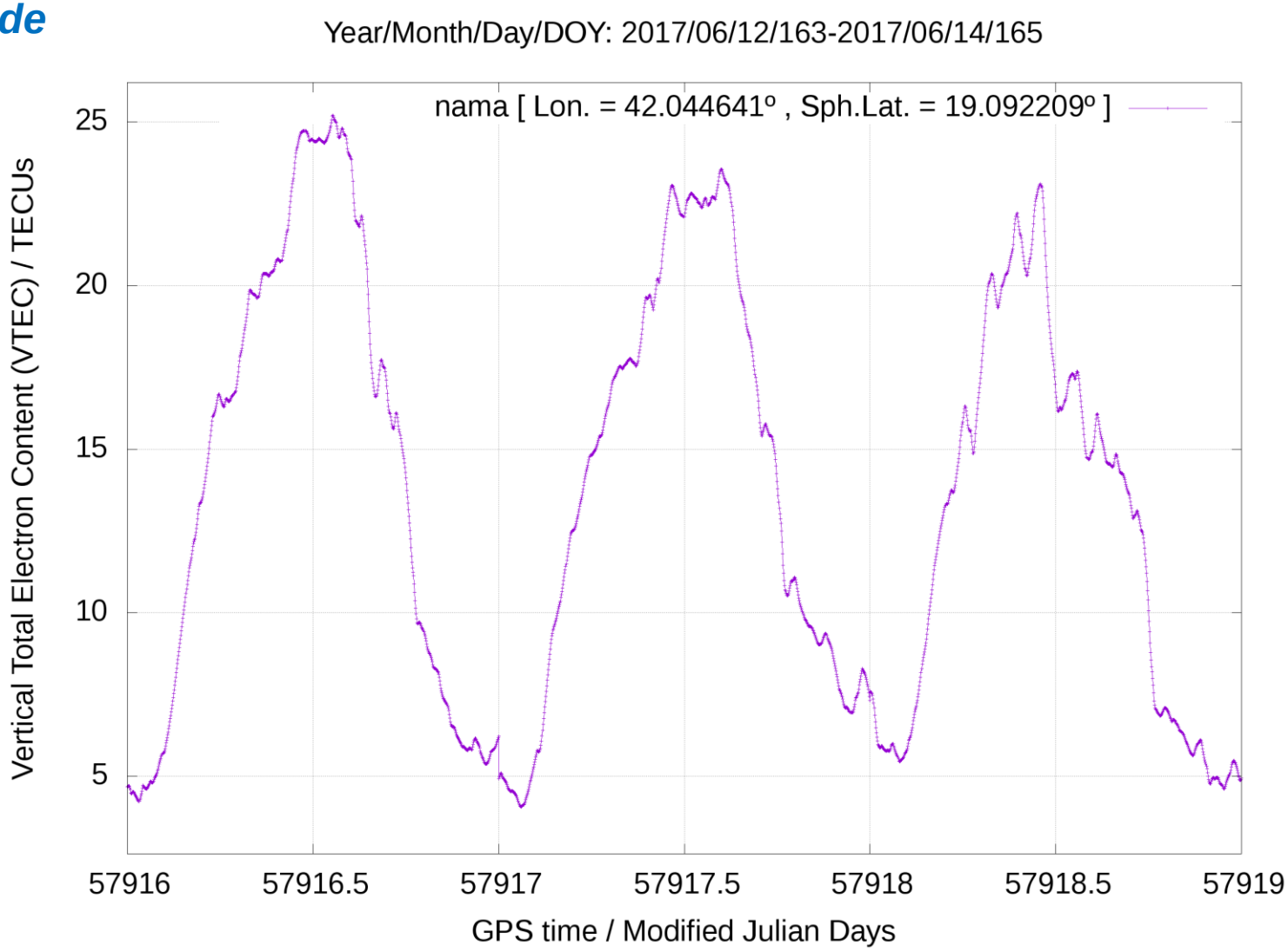

VTEC over TMP1 from GIM UQRG

NAMA-TMP1 is a similar baseline to BORJ-IJMU but now at low latitude (Saudi Arabia)

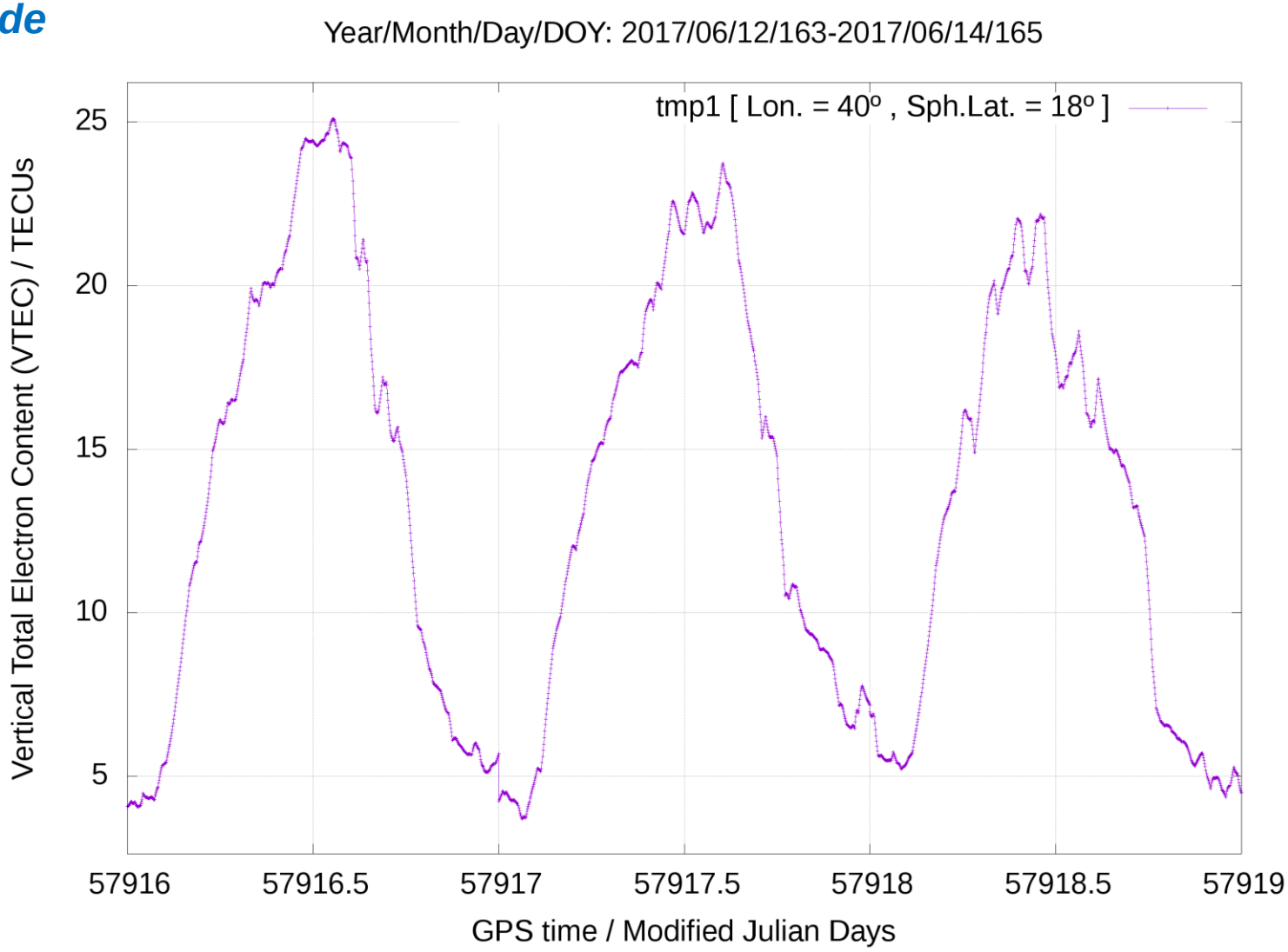

RGAO-VALP is a similar baseline to BORJ-IJMU but now at mid-low latitude in South Hemisphere (Argentina – Chile border)

VTEC over RGAO from GIM UQRG

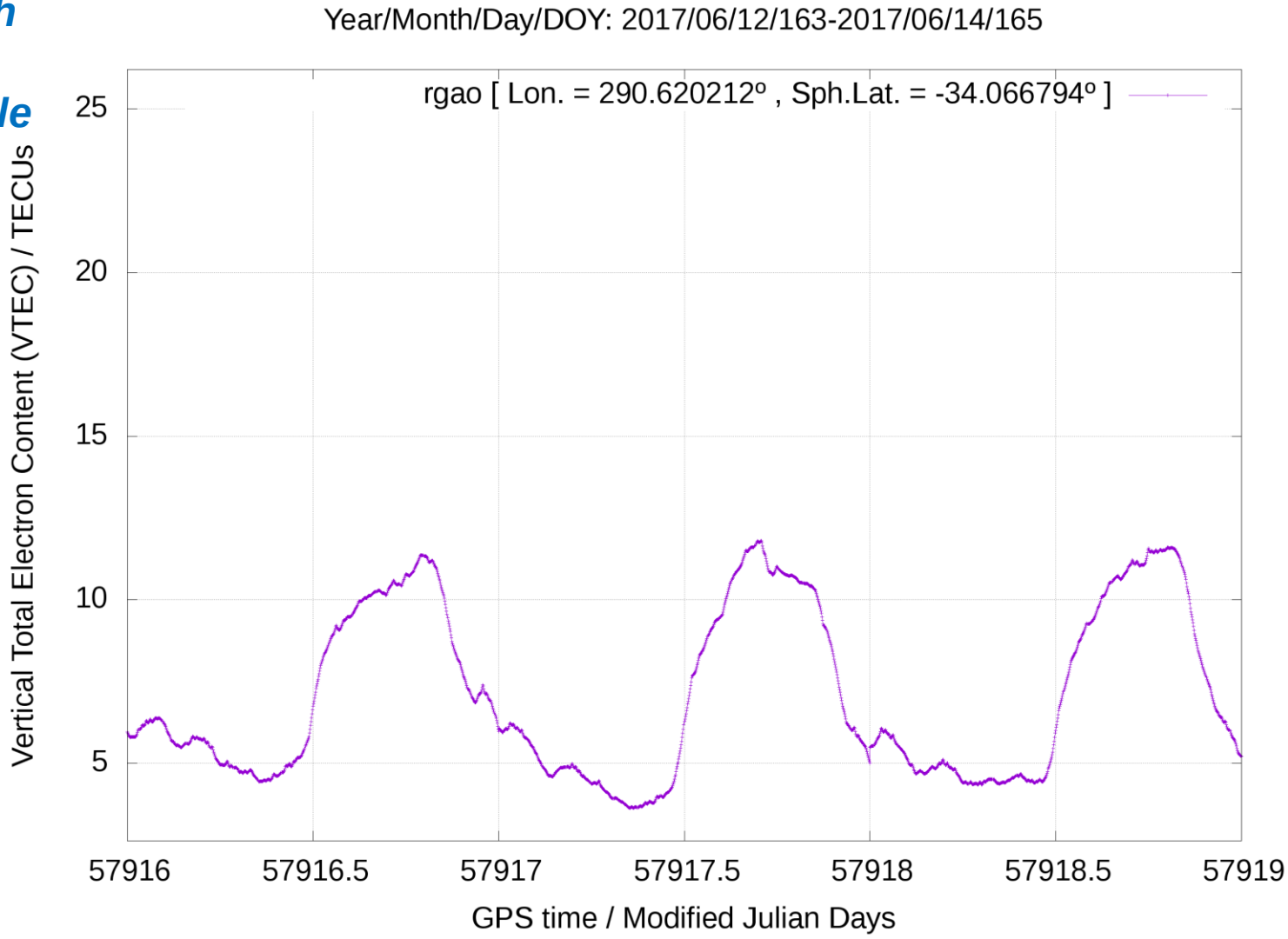

RGAO-VALP is a similar baseline to BORJ-IJMU but now at mid-low latitude in South Hemisphere (Argentina – Chile border)

VTEC over VALP from GIM UQRG

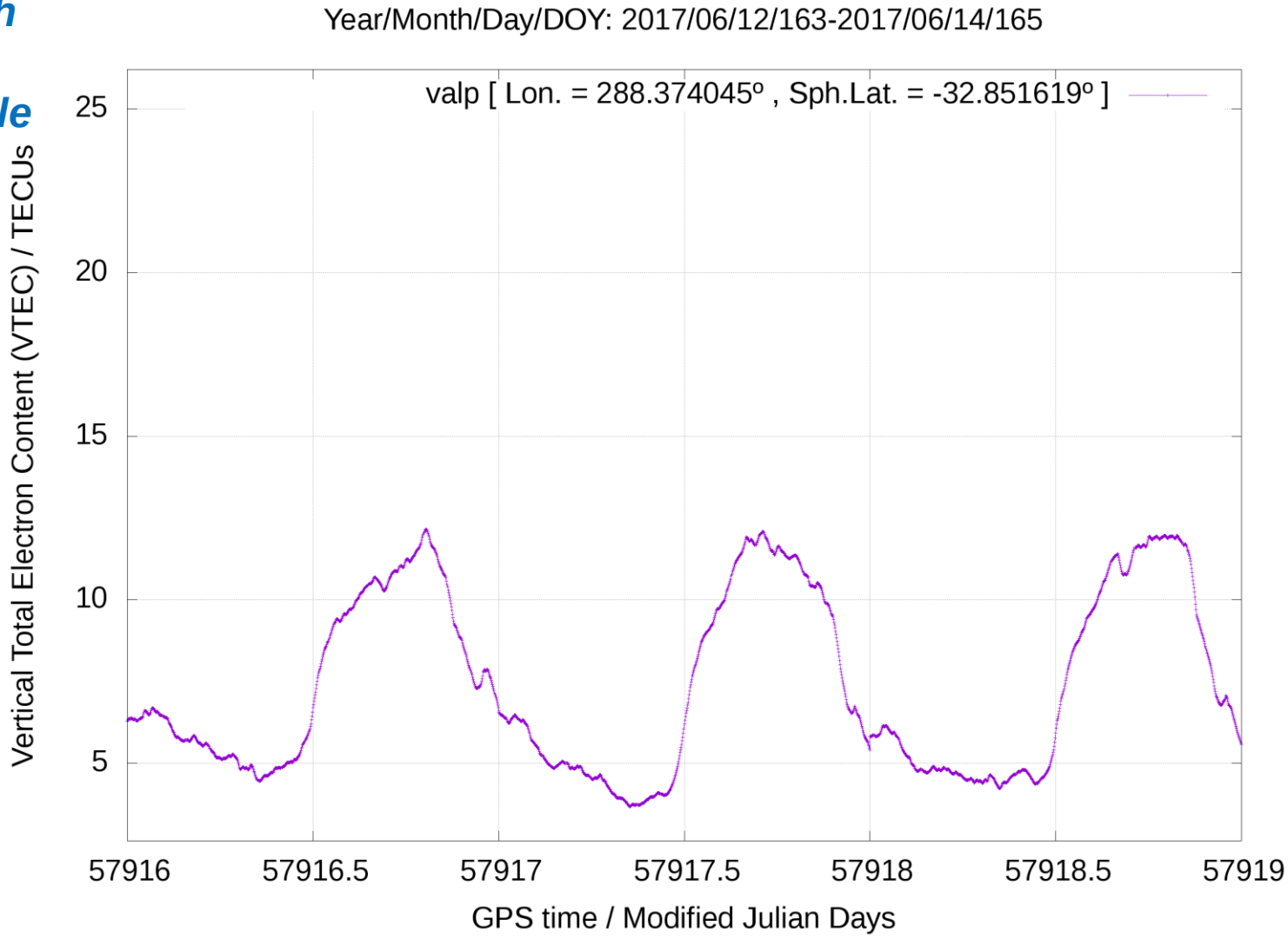

First conclusions?

➢**Exercise 1: Comment from the previous plots the temporal and spatial variability for the Vertical Ionospheric Delay and the expected ones for the Slant Ionospheric Delay** (remember 1 TECU ≃ 0.16 m in L1 and the mapping function (M=STEC/VTEC) values:

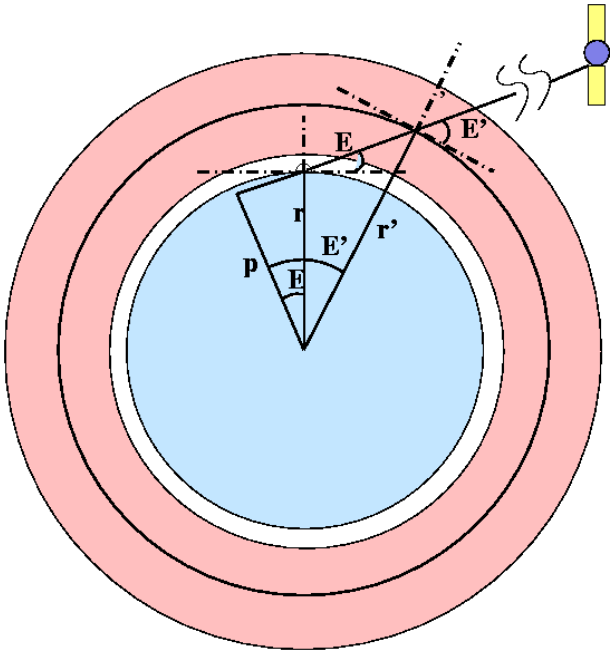

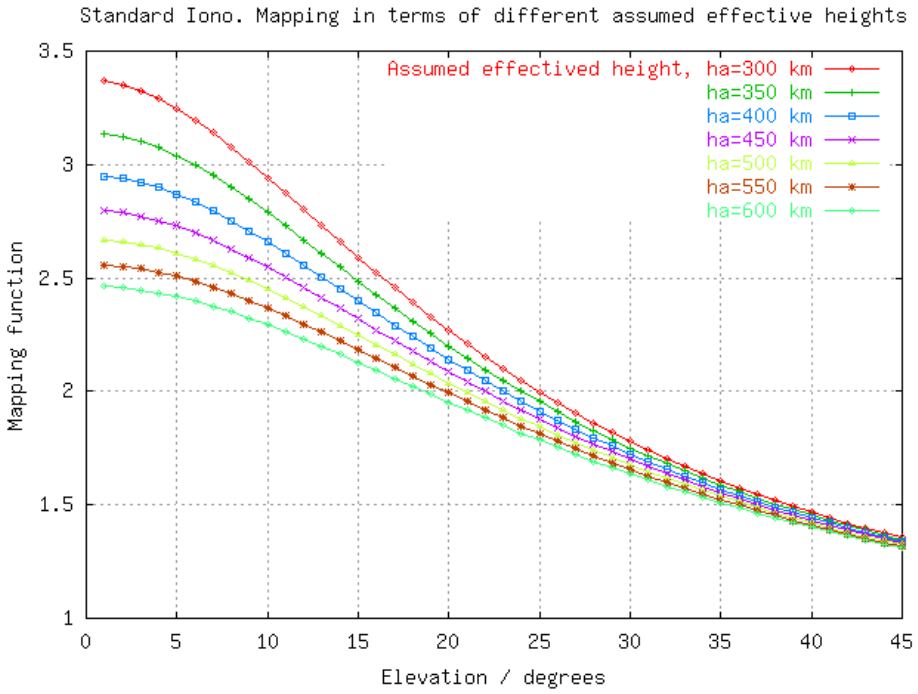

)

Looking at the Slant Total Electron Content (STEC) from dual-frequency measurements of GPS receivers (LI) calibrated with Global Ionospheric Maps (GIMs)

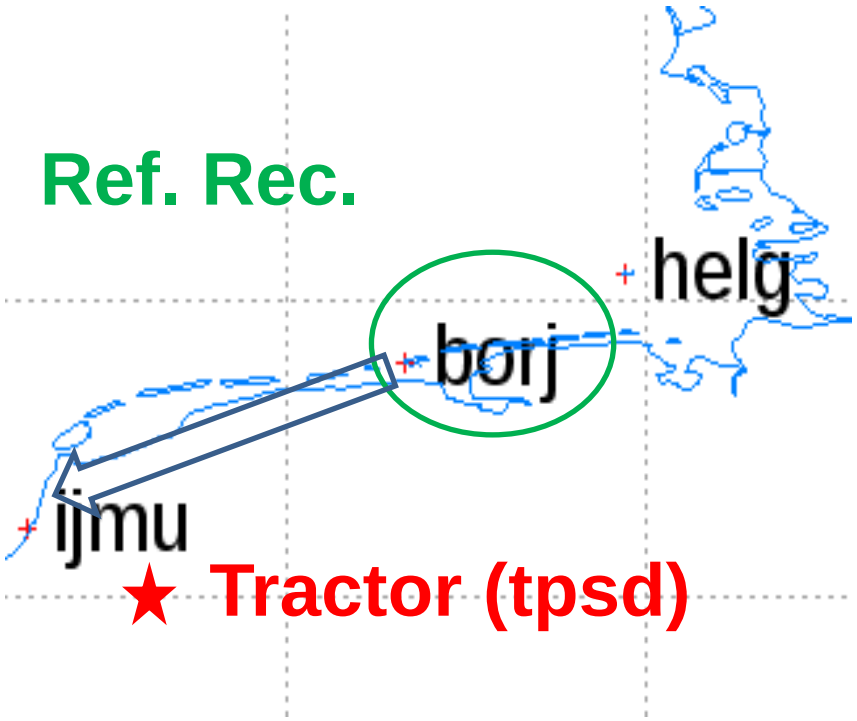

Up to higher level directory

Name	Size	Last Modified
STECs-vs-TIME.uqrg.20170612-163-to-20170614-165.borj.png	281 KB	11/18/17 6:59:39 PM GMT+1
STECs-vs-TIME.uqrg.20170612-163-to-20170614-165.ijmu.png	284 KB	11/18/17 6:59:43 PM GMT+1
VTECs-vs-TIME.uqrg.20170612-163-to-20170614-165.GIM.borj.png	171 KB	11/18/17 6:59:40 PM GMT+1
VTECs-vs-TIME.uqrg.20170612-163-to-20170614-165.GIM.ijmu.png	174 KB	11/18/17 6:59:43 PM GMT+1
VTECs-vs-TIME.uqrg.20170612-163-to-20170614-165.IG1.borj.png	228 KB	11/18/17 6:59:40 PM GMT+1
VTECs-vs-TIME.uqrg.20170612-163-to-20170614-165.IG1.ijmu.png	247 KB	11/18/17 6:59:44 PM GMT+1
VTECs-vs-TIME.uqrg.20170612-163-to-20170614-165.IG2.borj.png	212 KB	11/18/17 6:59:41 PM GMT+1
VTECs-vs-TIME.uqrg.20170612-163-to-20170614-165.IG2.ijmu.png	224 KB	11/18/17 6:59:44 PM GMT+1
VTECs-vs-TIME.uqrg.20170612-163-to-20170614-165.PI.borj.png	343 KB	11/18/17 6:59:41 PM GMT+1
VTECs-vs-TIME.uqrg.20170612-163-to-20170614-165.PI.ijmu.png	420 KB	11/18/17 6:59:45 PM GMT+1
d2LI-vs-TIME.20170612-163-to-20170614-165.PI.borj.png	139 KB	11/18/17 6:59:42 PM GMT+1
d2LI-vs-TIME.20170612-163-to-20170614-165.PI.ijmu.png	144 KB	11/18/17 6:59:46 PM GMT+1
d2VTEC300s-vs-TIME.20170612-163-to-20170614-165.PI.borj.png	123 KB	11/18/17 6:59:41 PM GMT+1
d2VTEC300s-vs-TIME.20170612-163-to-20170614-165.PI.ijmu.png	127 KB	11/18/17 6:59:45 PM GMT+1
dBw-vs-TIME.20170612-163-to-20170614-165.PI.borj.png	263 KB	11/18/17 6:59:42 PM GMT+1
dBw-vs-TIME.20170612-163-to-20170614-165.PI.ijmu.png	239 KB	11/18/17 6:59:46 PM GMT+1
ionex_2_latitudinal_VTEC_profiles_time_series.uqrg.2017.163-165.anim.gif	3431 KB	11/18/17 8:18:08 AM GMT+1
tec.output+djm.uqrg.20170612_163_to_20171650614_165.borj.png	63 KB	11/18/17 6:45:23 PM GMT+1
tec.output+djm.uqrg.20170612_163_to_20171650614_165.ijmu.png	65 KB	11/18/17 6:45:23 PM GMT+1
tec.output+djm.uqrg.20170612_163_to_20171650614_165.nama.png	75 KB	11/18/17 6:45:23 PM GMT+1
tec.output+djm.uqrg.20170612_163_to_20171650614_165.rgao.png	62 KB	11/18/17 6:45:24 PM GMT+1
tec.output+djm.uqrg.20170612_163_to_20171650614_165.tmp1.png	73 KB	11/18/17 6:45:24 PM GMT+1
tec.output+djm.uqrg.20170612_163_to_20171650614_165.valp.png	63 KB	11/18/17 6:45:24 PM GMT+1

STEC over BORJ from RINEX meas. calibrated with GIM UQRG

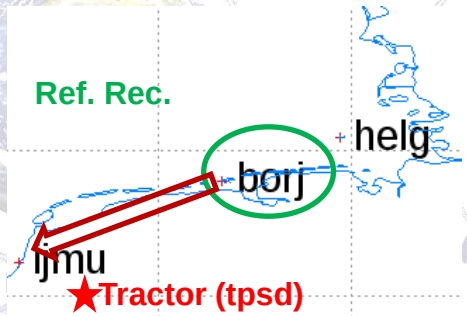

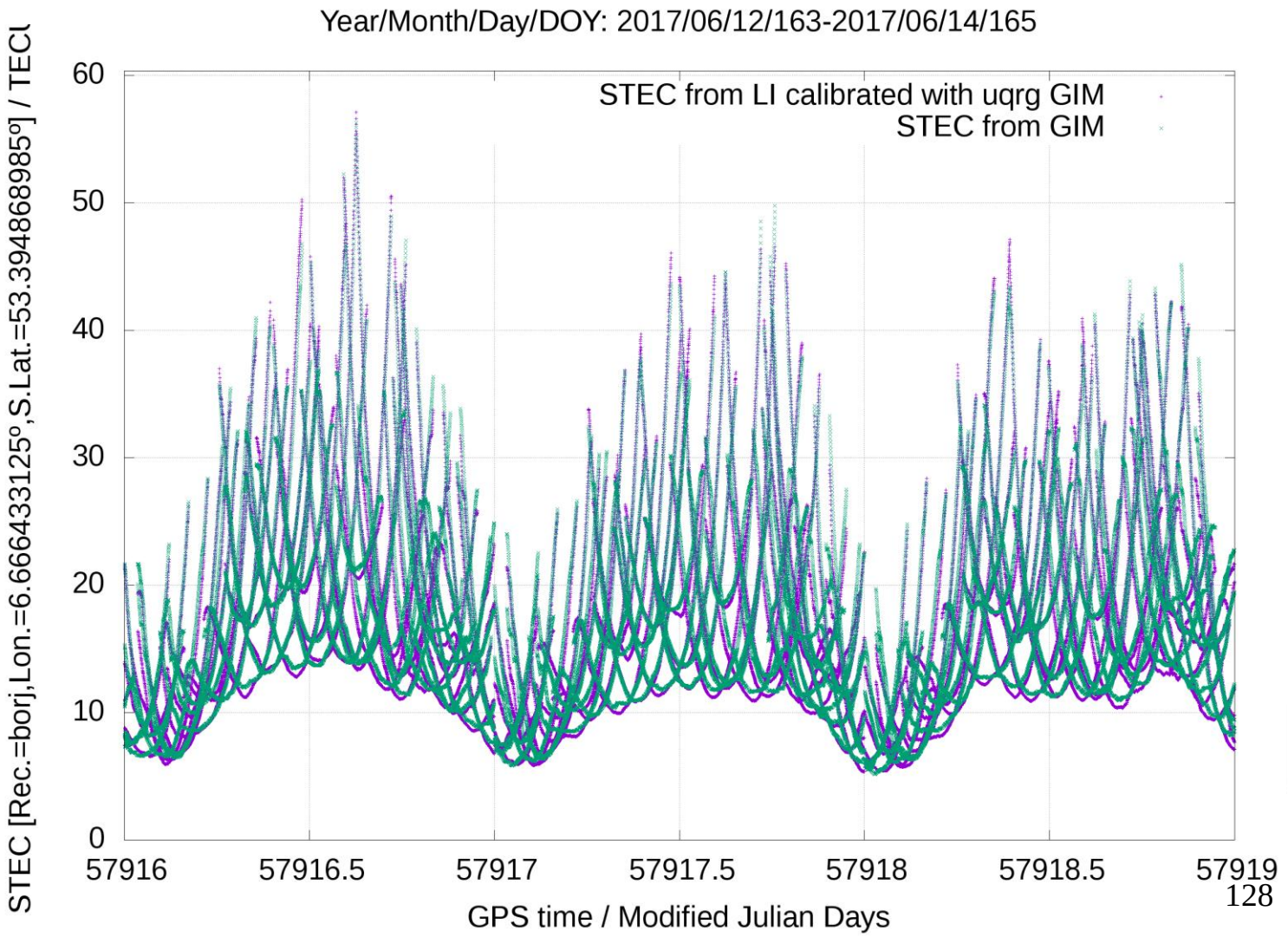

STEC over IJMU from RINEX meas. calibrated with GIM UQRG

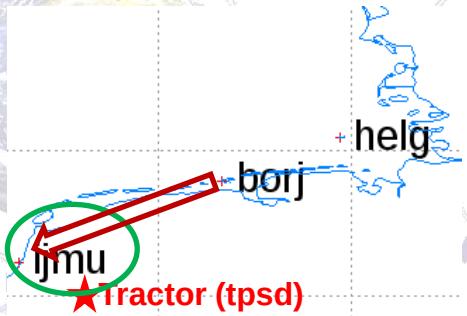

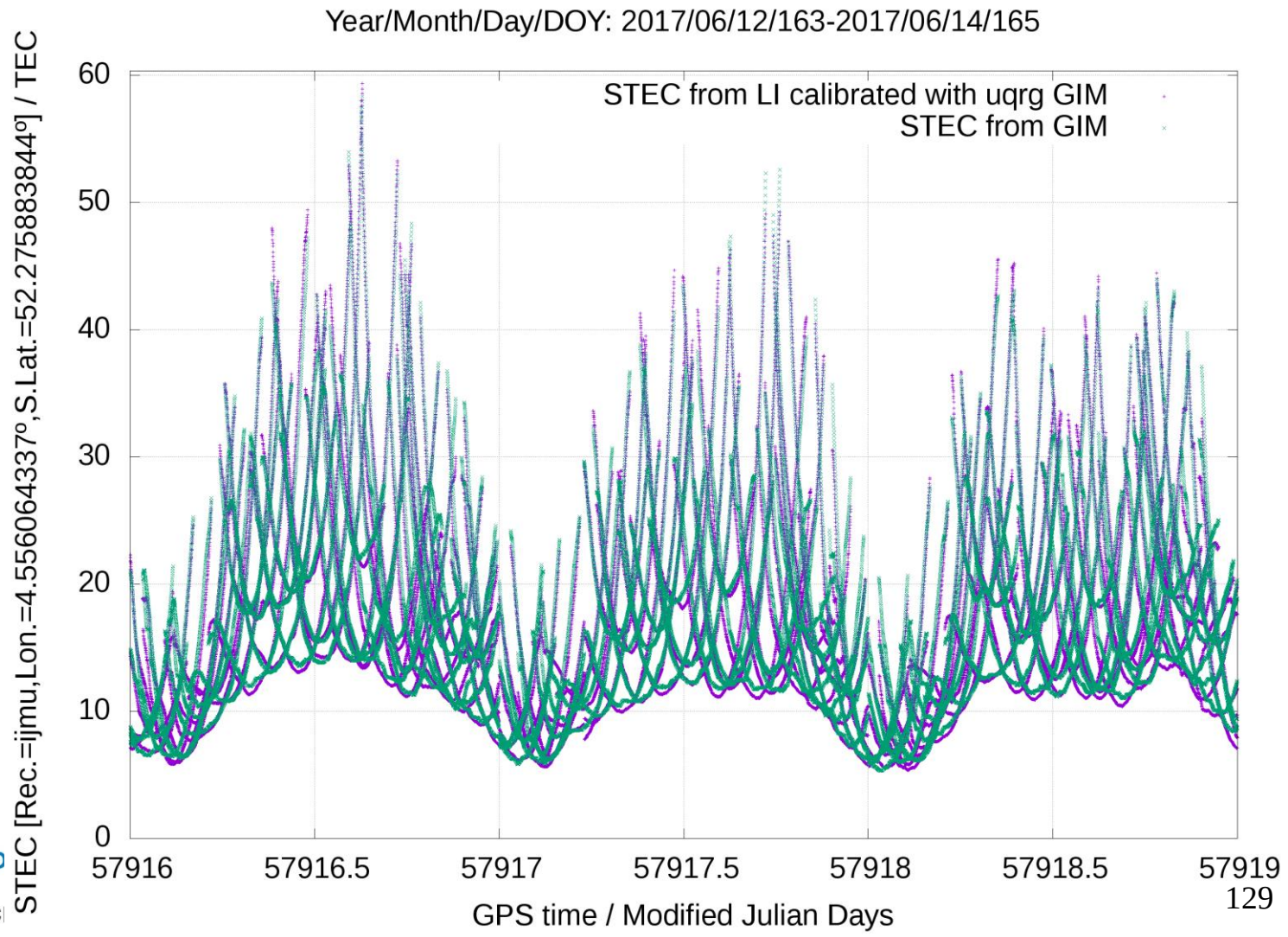

Conclusions from STEC vs time plots?

➢**Exercise 2**: Assess the answer previously provided to Exercise 1 referring to the expected range of STEC values (deduced from the VTEC ones).

➢**Questions 3:** Is the GIM able to provide the right precision? Are the dual-frequency GPS carrier phase measurements alone able to provide the right accuracy? In such a context, how could be understood the GIM-calibration of dual-frequency measurements[*]? How much b**oth** STEC differs?

$$[*]\ LI=L1-L2=\alpha \bullet S+BI+(\lambda 1-\lambda 2)\bullet \varphi \Rightarrow$$
$$\Rightarrow BI_calGIM = \langle LI-(\lambda 1-\lambda 2)\bullet \varphi-\alpha \bullet S_GIM\rangle \Rightarrow$$
$$\Rightarrow S_LIcalGIM = (LI-BI_calGIM-(\lambda 1-\lambda 2)\bullet \varphi) / \alpha$$

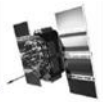

Looking at the time evolution of the meridional VTEC (VTEC vs latitude) for the approximate longitude sector (E010º) of the Argentina/Chile border during the AUDITOR experiment

Up to higher level directory

Name	Size	Last Modified
STECs-vs-TIME.uqrg.20170612-163-to-20170614-165.borj.png	281 KB	11/18/17 6:59:39 PM GMT+1
STECs-vs-TIME.uqrg.20170612-163-to-20170614-165.ijmu.png	284 KB	11/18/17 6:59:43 PM GMT+1
VTECs-vs-TIME.uqrg.20170612-163-to-20170614-165.GIM.borj.png	171 KB	11/18/17 6:59:40 PM GMT+1
VTECs-vs-TIME.uqrg.20170612-163-to-20170614-165.GIM.ijmu.png	174 KB	11/18/17 6:59:43 PM GMT+1
VTECs-vs-TIME.uqrg.20170612-163-to-20170614-165.IG1.borj.png	228 KB	11/18/17 6:59:40 PM GMT+1
VTECs-vs-TIME.uqrg.20170612-163-to-20170614-165.IG1.ijmu.png	247 KB	11/18/17 6:59:44 PM GMT+1
VTECs-vs-TIME.uqrg.20170612-163-to-20170614-165.IG2.borj.png	212 KB	11/18/17 6:59:41 PM GMT+1
VTECs-vs-TIME.uqrg.20170612-163-to-20170614-165.IG2.ijmu.png	224 KB	11/18/17 6:59:44 PM GMT+1
VTECs-vs-TIME.uqrg.20170612-163-to-20170614-165.PI.borj.png	343 KB	11/18/17 6:59:41 PM GMT+1
VTECs-vs-TIME.uqrg.20170612-163-to-20170614-165.PI.ijmu.png	420 KB	11/18/17 6:59:45 PM GMT+1
d2LI-vs-TIME.20170612-163-to-20170614-165.PI.borj.png	139 KB	11/18/17 6:59:42 PM GMT+1
d2LI-vs-TIME.20170612-163-to-20170614-165.PI.ijmu.png	144 KB	11/18/17 6:59:46 PM GMT+1
d2VTEC300s-vs-TIME.20170612-163-to-20170614-165.PI.borj.png	123 KB	11/18/17 6:59:41 PM GMT+1
d2VTEC300s-vs-TIME.20170612-163-to-20170614-165.PI.ijmu.png	127 KB	11/18/17 6:59:45 PM GMT+1
dBw-vs-TIME.20170612-163-to-20170614-165.PI.borj.png	263 KB	11/18/17 6:59:42 PM GMT+1
dBw-vs-TIME.20170612-163-to-20170614-165.PI.ijmu.png	239 KB	11/18/17 6:59:46 PM GMT+1
ionex_2_latitudinal_VTEC_profiles_time_series.uqrg.2017.163-165.anim.gif	3431 KB	11/18/17 8:18:08 AM GMT+1
tec.output+djm.uqrg.20170612_163_to_20171650614_165.borj.png	63 KB	11/18/17 6:45:23 PM GMT+1
tec.output+djm.uqrg.20170612_163_to_20171650614_165.ijmu.png	65 KB	11/18/17 6:45:23 PM GMT+1
tec.output+djm.uqrg.20170612_163_to_20171650614_165.nama.png	75 KB	11/18/17 6:45:23 PM GMT+1
tec.output+djm.uqrg.20170612_163_to_20171650614_165.rgao.png	62 KB	11/18/17 6:45:24 PM GMT+1
tec.output+djm.uqrg.20170612_163_to_20171650614_165.tmp1.png	73 KB	11/18/17 6:45:24 PM GMT+1
tec.output+djm.uqrg.20170612_163_to_20171650614_165.valp.png	63 KB	11/18/17 6:45:24 PM GMT+1

VTEC vs latitude at E290º from UQRG GIM

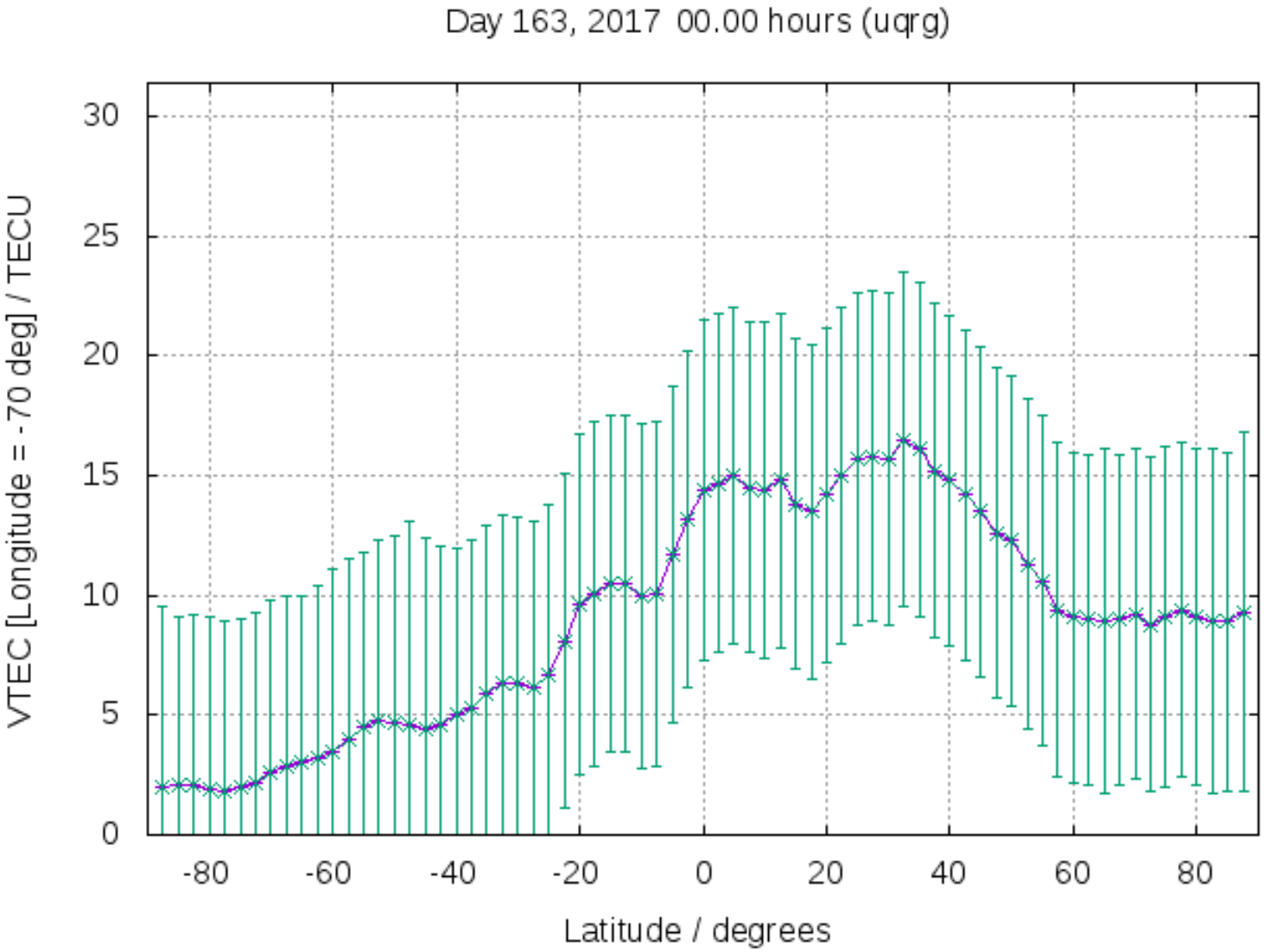

Conclusions from VTEC vs latitude plots?

- **Question 4**: Which is the approximate ratio between the highest and the lowest VTEC for different latitudes in the same meridian?
- **Question 5**: Why is systematically lower the VTEC at the South Pole than the VTEC at the North Pole?
- **Question 6:** Why the VTEC at both poles appear constant vs time?

Looking the VTEC @ IJMU deprojected from the STEC derived GIM-alone and from different ionospheric combinations of GPS measurements, after UQRG-GIM calibration, vs the LI calibrated one:

- GIM-alone and PI=P2-P1.
- Single-frequency ionospheric measurements: Iono-Graphic1, IG1=(P1-L1)/2 and Iono-Graphic2, IG2=(P2-L2)/2.

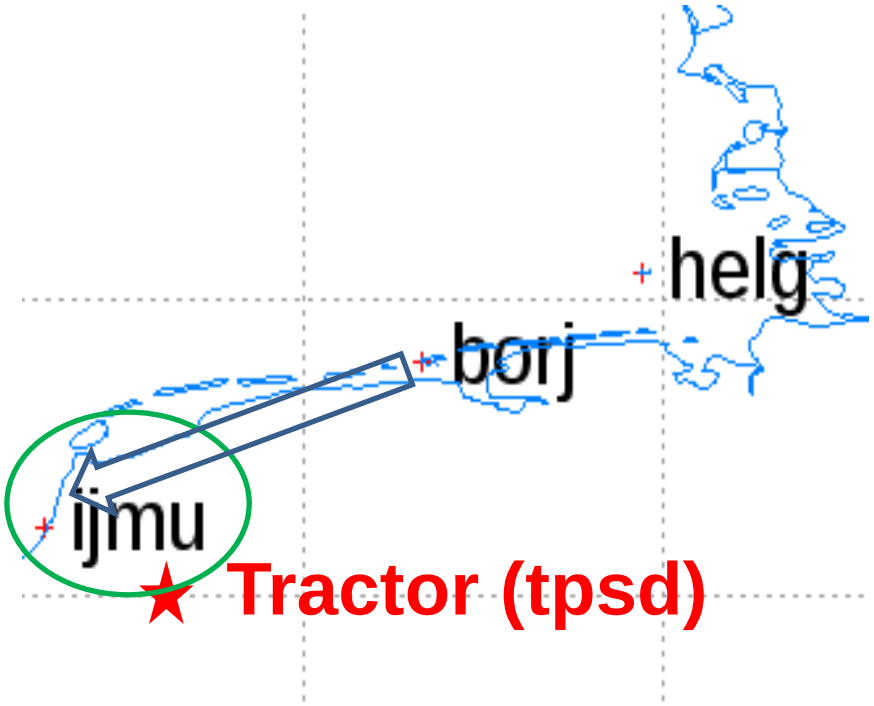

Up to higher level directory

Name	Size	Last Modified
STECs-vs-TIME.uqrg.20170612-163-to-20170614-165.borj.png	281 KB	11/18/17 6:59:39 PM GMT+1
STECs-vs-TIME.uqrg.20170612-163-to-20170614-165.ijmu.png	284 KB	11/18/17 6:59:43 PM GMT+1
VTECs-vs-TIME.uqrg.20170612-163-to-20170614-165.GIM.borj.png	171 KB	11/18/17 6:59:40 PM GMT+1
VTECs-vs-TIME.uqrg.20170612-163-to-20170614-165.GIM.ijmu.png	174 KB	11/18/17 6:59:43 PM GMT+1
VTECs-vs-TIME.uqrg.20170612-163-to-20170614-165.IG1.borj.png	228 KB	11/18/17 6:59:40 PM GMT+1
VTECs-vs-TIME.uqrg.20170612-163-to-20170614-165.IG1.ijmu.png	247 KB	11/18/17 6:59:44 PM GMT+1
VTECs-vs-TIME.uqrg.20170612-163-to-20170614-165.IG2.borj.png	212 KB	11/18/17 6:59:41 PM GMT+1
VTECs-vs-TIME.uqrg.20170612-163-to-20170614-165.IG2.ijmu.png	224 KB	11/18/17 6:59:44 PM GMT+1
VTECs-vs-TIME.uqrg.20170612-163-to-20170614-165.PI.borj.png	343 KB	11/18/17 6:59:41 PM GMT+1
VTECs-vs-TIME.uqrg.20170612-163-to-20170614-165.PI.ijmu.png	420 KB	11/18/17 6:59:45 PM GMT+1
d2LI-vs-TIME.20170612-163-to-20170614-165.PI.borj.png	139 KB	11/18/17 6:59:42 PM GMT+1
d2LI-vs-TIME.20170612-163-to-20170614-165.PI.ijmu.png	144 KB	11/18/17 6:59:46 PM GMT+1
d2VTEC300s-vs-TIME.20170612-163-to-20170614-165.PI.borj.png	123 KB	11/18/17 6:59:41 PM GMT+1
d2VTEC300s-vs-TIME.20170612-163-to-20170614-165.PI.ijmu.png	127 KB	11/18/17 6:59:45 PM GMT+1
dBw-vs-TIME.20170612-163-to-20170614-165.PI.borj.png	263 KB	11/18/17 6:59:42 PM GMT+1
dBw-vs-TIME.20170612-163-to-20170614-165.PI.ijmu.png	239 KB	11/18/17 6:59:46 PM GMT+1
ionex_2_latitudinal_VTEC_profiles_time_series.uqrg.2017.163-165.anim.gif	3431 KB	11/18/17 8:18:08 AM GMT+1
tec.output+djm.uqrg.20170612_163_to_20171650614_165.borj.png	63 KB	11/18/17 6:45:23 PM GMT+1
tec.output+djm.uqrg.20170612_163_to_20171650614_165.ijmu.png	65 KB	11/18/17 6:45:23 PM GMT+1
tec.output+djm.uqrg.20170612_163_to_20171650614_165.nama.png	75 KB	11/18/17 6:45:23 PM GMT+1
tec.output+djm.uqrg.20170612_163_to_20171650614_165.rgao.png	62 KB	11/18/17 6:45:24 PM GMT+1
tec.output+djm.uqrg.20170612_163_to_20171650614_165.tmp1.png	73 KB	11/18/17 6:45:24 PM GMT+1
tec.output+djm.uqrg.20170612_163_to_20171650614_165.valp.png	63 KB	11/18/17 6:45:24 PM GMT+1

VTEC derived from STEC over IJMU from: GIM & 2- and 1-freq. GPS meas. cal. with GIM (UQRG) vs LI=L1-L2 GIM cal.

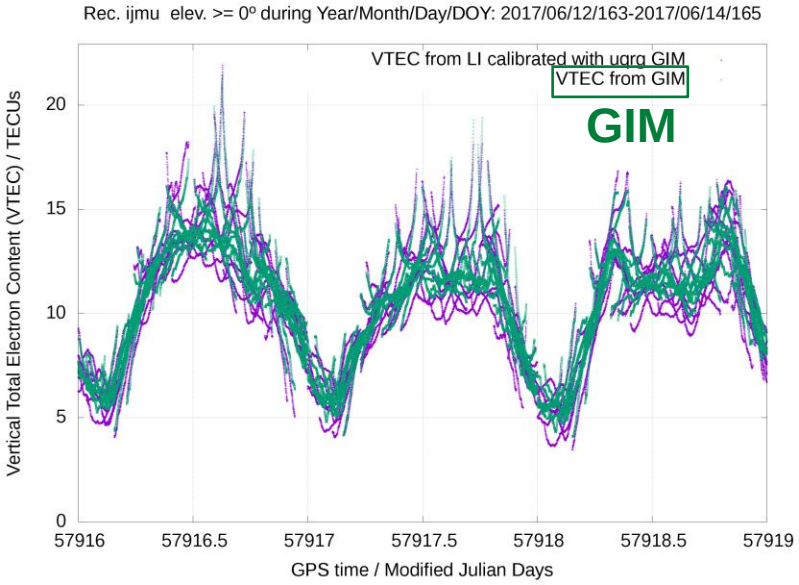

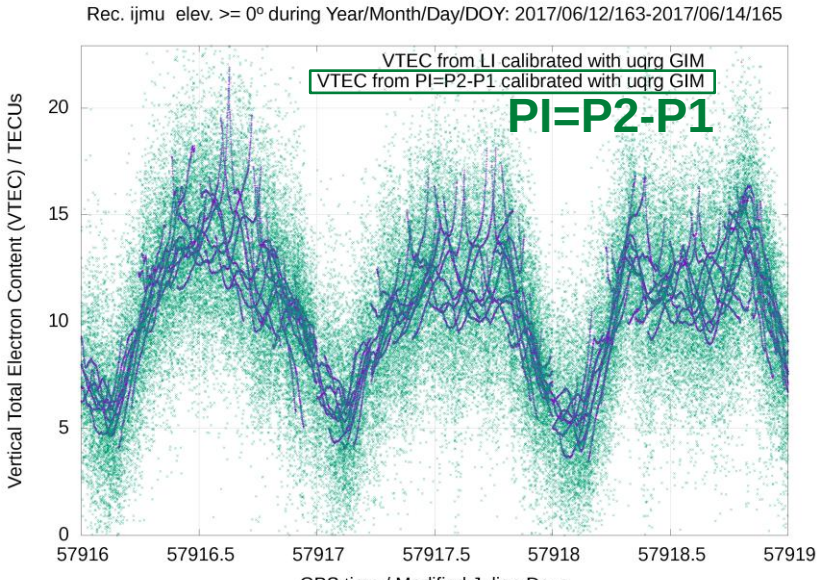

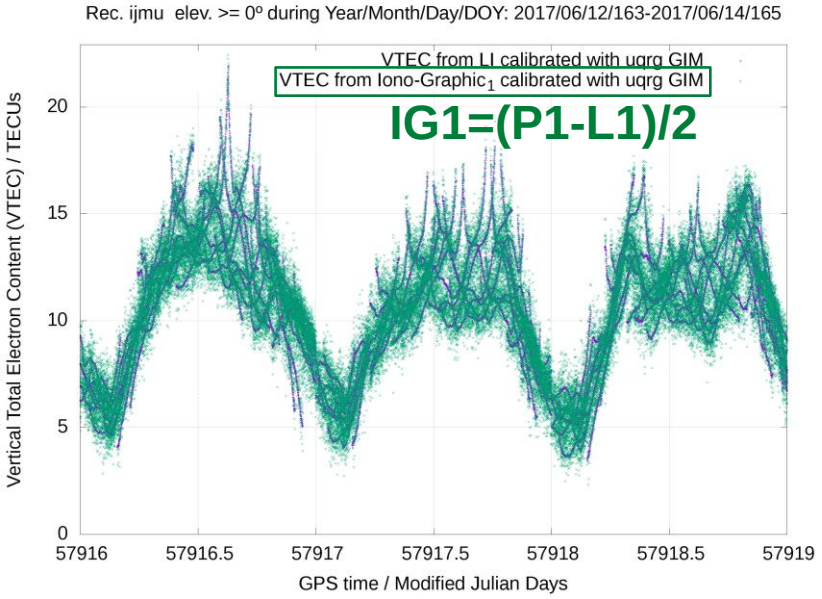

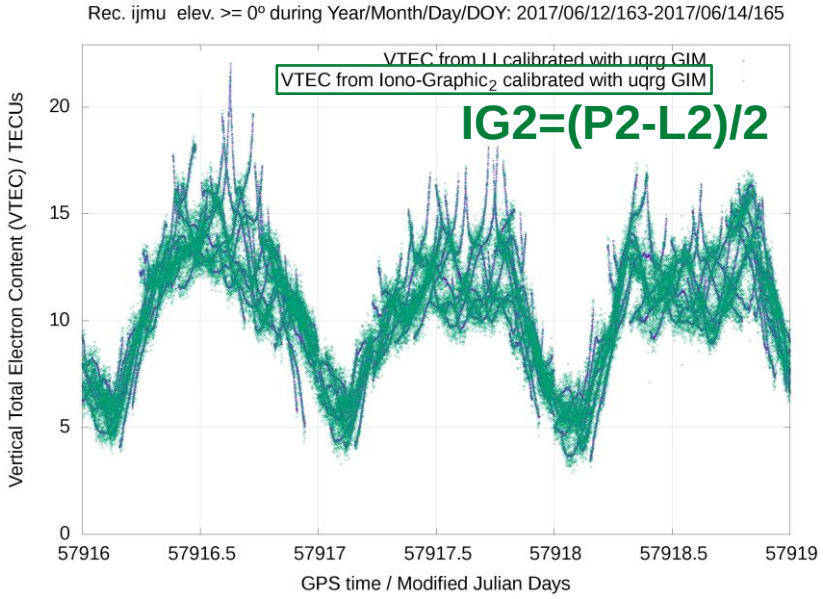

Conclusions from VTEC from STEC from GIM alone, and LI, PI, IG1 and IG2 UQRG-GIM calibrated?

- **Question 7**: Why the STEC derived from IG1 GIM calibrated is better than the corresponding PI one? The errors shown (compared with the most accurate and precise STEC from LI GIM calibrated) are compatible with the expected ones?
- **Question 8**: Why the STEC of IG2 is better than the one from IG1 in spite of the quality of P2 is worse than the quality of P1?
- **Question 9:** What would be the expected performance for IG5?

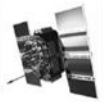

Looking for high absolute values of the double-time difference of LI=L1-L2, d2LI, and the single-time diff. of MW=Lw-Pn as a sufficient condition to declare a carrier phase cycle-slip, i.e. Blewit method (IJMU during AUDITOR experiment)

- d2LI = LI(t+dt) - LI(t) - (LI(t) - LI(t-dt)) = LI(t+dt)-2LI(t)+LI(t-dt)= -2 (LI(t) - (LI(t+dt) + LI(t-dt)) /2)
- In other words, d2LI provide a simple ionospheric detrending method, substracting to each point the linear prediction from the next and previous measurement.
- Melbourne-Wubbena does not need to be detrended (it is both ionospheric- and geometric-free, the problem is the pseudorange noise).

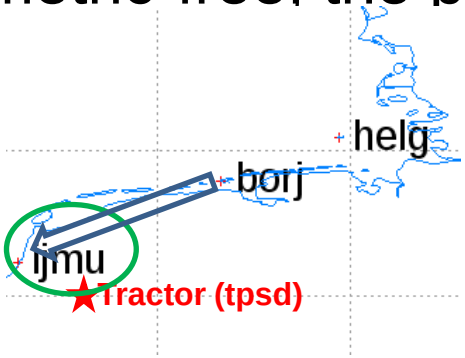

Up to higher level directory

Name	Size	Last Modified
STECs-vs-TIME.uqrg.20170612-163-to-20170614-165.borj.png	281 KB	11/18/17 6:59:39 PM GMT+1
STECs-vs-TIME.uqrg.20170612-163-to-20170614-165.ijmu.png	284 KB	11/18/17 6:59:43 PM GMT+1
VTECs-vs-TIME.uqrg.20170612-163-to-20170614-165.GIM.borj.png	171 KB	11/18/17 6:59:40 PM GMT+1
VTECs-vs-TIME.uqrg.20170612-163-to-20170614-165.GIM.ijmu.png	174 KB	11/18/17 6:59:43 PM GMT+1
VTECs-vs-TIME.uqrg.20170612-163-to-20170614-165.IG1.borj.png	228 KB	11/18/17 6:59:40 PM GMT+1
VTECs-vs-TIME.uqrg.20170612-163-to-20170614-165.IG1.ijmu.png	247 KB	11/18/17 6:59:44 PM GMT+1
VTECs-vs-TIME.uqrg.20170612-163-to-20170614-165.IG2.borj.png	212 KB	11/18/17 6:59:41 PM GMT+1
VTECs-vs-TIME.uqrg.20170612-163-to-20170614-165.IG2.ijmu.png	224 KB	11/18/17 6:59:44 PM GMT+1
VTECs-vs-TIME.uqrg.20170612-163-to-20170614-165.PI.borj.png	343 KB	11/18/17 6:59:41 PM GMT+1
VTECs-vs-TIME.uqrg.20170612-163-to-20170614-165.PI.ijmu.png	420 KB	11/18/17 6:59:45 PM GMT+1
d2LI-vs-TIME.20170612-163-to-20170614-165.PI.borj.png	139 KB	11/18/17 6:59:42 PM GMT+1
d2LI-vs-TIME.20170612-163-to-20170614-165.PI.ijmu.png	144 KB	11/18/17 6:59:46 PM GMT+1
d2VTEC300s-vs-TIME.20170612-163-to-20170614-165.PI.borj.png	123 KB	11/18/17 6:59:41 PM GMT+1
d2VTEC300s-vs-TIME.20170612-163-to-20170614-165.PI.ijmu.png	127 KB	11/18/17 6:59:45 PM GMT+1
dBw-vs-TIME.20170612-163-to-20170614-165.PI.borj.png	263 KB	11/18/17 6:59:42 PM GMT+1
dBw-vs-TIME.20170612-163-to-20170614-165.PI.ijmu.png	239 KB	11/18/17 6:59:46 PM GMT+1
ionex_2_latitudinal_VTEC_profiles_time_series.uqrg.2017.163-165.anim.gif	3431 KB	11/18/17 8:18:08 AM GMT+1
tec.output+djm.uqrg.20170612_163_to_20171650614_165.borj.png	63 KB	11/18/17 6:45:23 PM GMT+1
tec.output+djm.uqrg.20170612_163_to_20171650614_165.ijmu.png	65 KB	11/18/17 6:45:23 PM GMT+1
tec.output+djm.uqrg.20170612_163_to_20171650614_165.nama.png	75 KB	11/18/17 6:45:23 PM GMT+1
tec.output+djm.uqrg.20170612_163_to_20171650614_165.rgao.png	62 KB	11/18/17 6:45:24 PM GMT+1
tec.output+djm.uqrg.20170612_163_to_20171650614_165.tmp1.png	73 KB	11/18/17 6:45:24 PM GMT+1
tec.output+djm.uqrg.20170612_163_to_20171650614_165.valp.png	63 KB	11/18/17 6:45:24 PM GMT+1

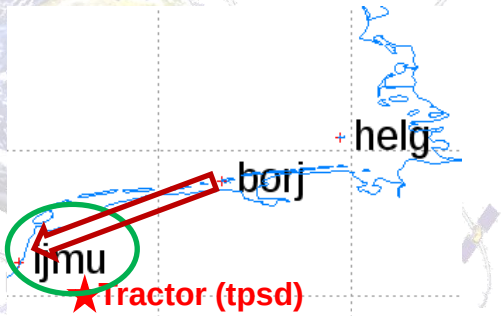

d2LI at maximum sampling rate (e.g. 30s) for IJMU from RINEX meas. marking declared potential cycle-slips

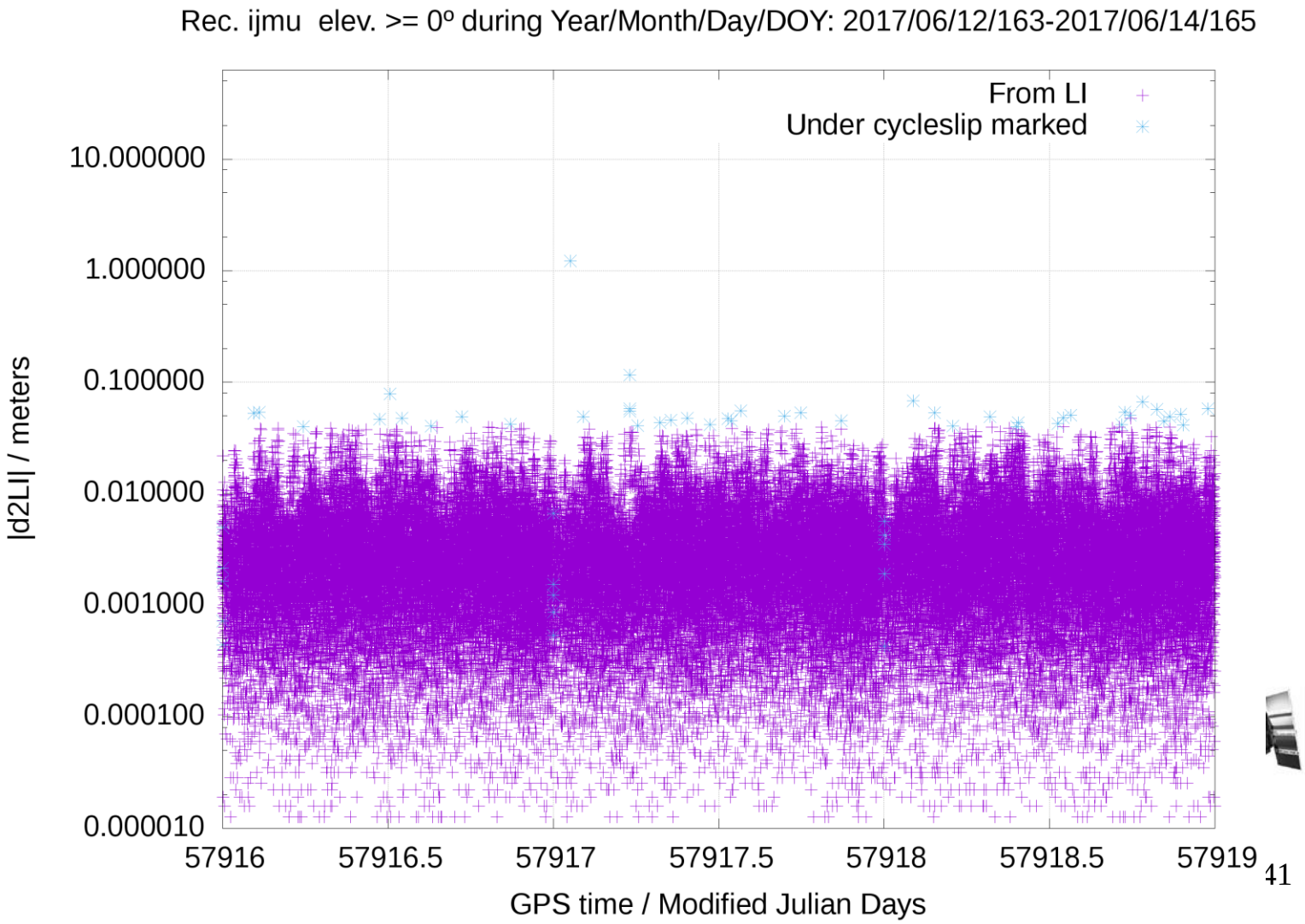

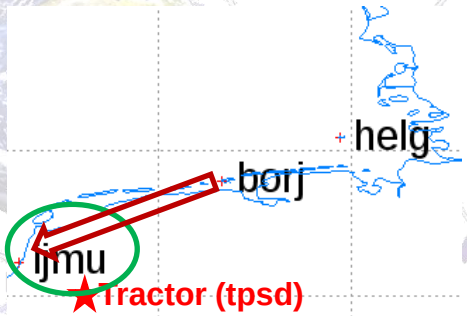

dMW=dBw at maximum sampling rate (e.g. 30s) for IJMU from RINEX meas. marking declared potential cycle-slips

Rec. ijmu elev. >= 0º during Year/Month/Day/DOY: 2017/06/12/163-2017/06/14/165

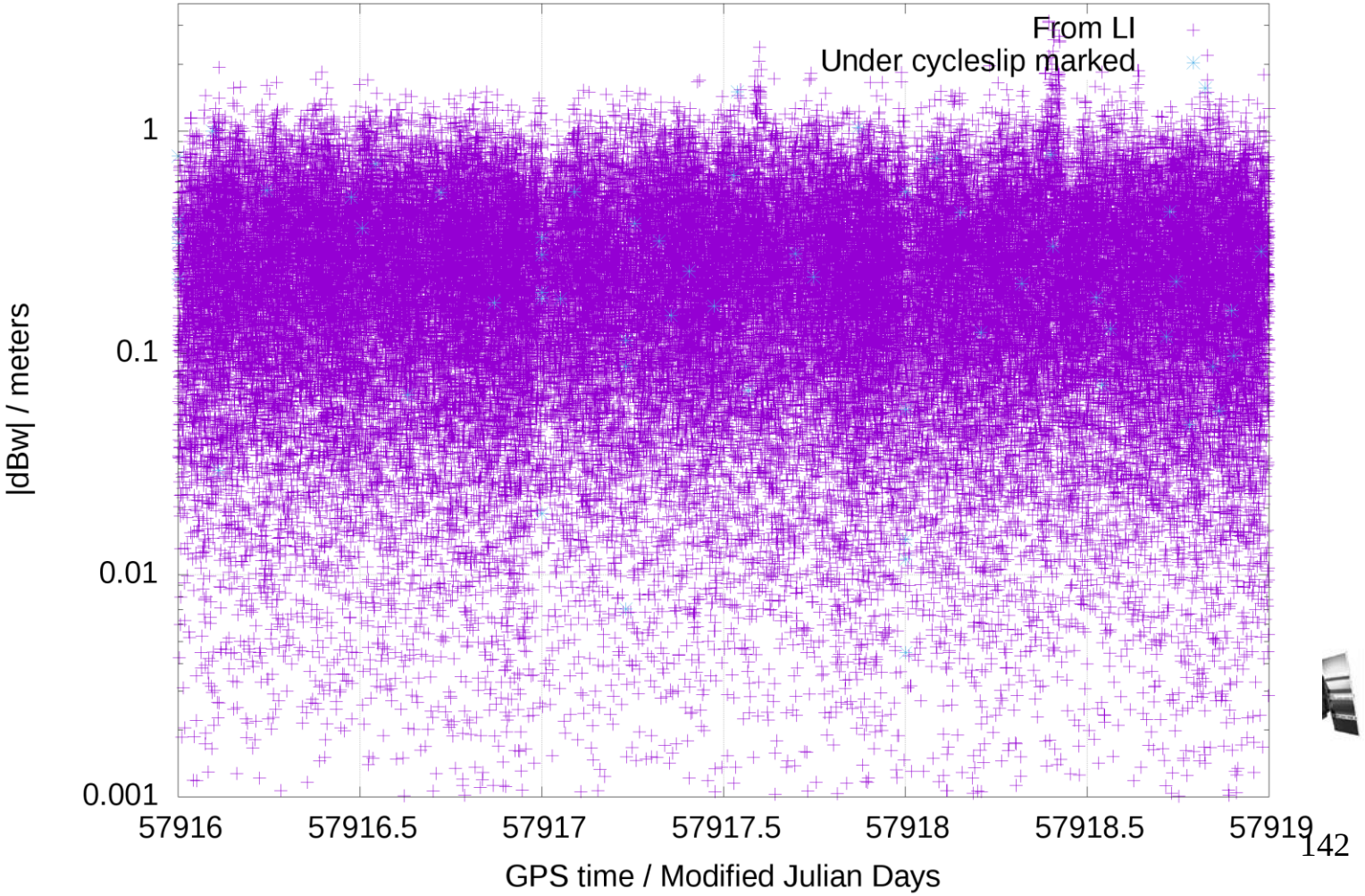

Conclusions from d2LI and dMW=dBW and marked cycle-slips?

- **Question 10**: For these receivers, are both indicators helping to detect cycle-slips in the same extent? Why?
- **Question 11**: Can all the marked cycle-slips be explained by both thresholds?

Looking for signatures of the most frequent ionospheric waves (Medium Scale Travelling Ionospheric Disturbances, MSTIDs) from d2VTEC, deprojected from d2LI with the mapping function and with time steps of 300 seconds (rec. IJMU).

- The detrending at 300 seconds maximize the sensitivity at the interval of frequencies around 1000 seconds (since hundreds to less than 2000 seconds), characteristics of MSTIDs.

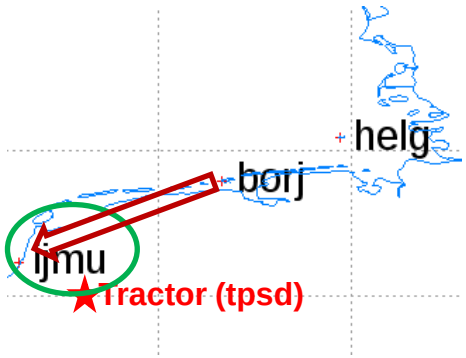

Up to higher level directory

Name	Size	Last Modified
STECs-vs-TIME.uqrg.20170612-163-to-20170614-165.borj.png	281 KB	11/18/17 6:59:39 PM GMT+1
STECs-vs-TIME.uqrg.20170612-163-to-20170614-165.ijmu.png	284 KB	11/18/17 6:59:43 PM GMT+1
VTECs-vs-TIME.uqrg.20170612-163-to-20170614-165.GIM.borj.png	171 KB	11/18/17 6:59:40 PM GMT+1
VTECs-vs-TIME.uqrg.20170612-163-to-20170614-165.GIM.ijmu.png	174 KB	11/18/17 6:59:43 PM GMT+1
VTECs-vs-TIME.uqrg.20170612-163-to-20170614-165.IG1.borj.png	228 KB	11/18/17 6:59:40 PM GMT+1
VTECs-vs-TIME.uqrg.20170612-163-to-20170614-165.IG1.ijmu.png	247 KB	11/18/17 6:59:44 PM GMT+1
VTECs-vs-TIME.uqrg.20170612-163-to-20170614-165.IG2.borj.png	212 KB	11/18/17 6:59:41 PM GMT+1
VTECs-vs-TIME.uqrg.20170612-163-to-20170614-165.IG2.ijmu.png	224 KB	11/18/17 6:59:44 PM GMT+1
VTECs-vs-TIME.uqrg.20170612-163-to-20170614-165.PI.borj.png	343 KB	11/18/17 6:59:41 PM GMT+1
VTECs-vs-TIME.uqrg.20170612-163-to-20170614-165.PI.ijmu.png	420 KB	11/18/17 6:59:45 PM GMT+1
d2LI-vs-TIME.20170612-163-to-20170614-165.PI.borj.png	139 KB	11/18/17 6:59:42 PM GMT+1
d2LI-vs-TIME.20170612-163-to-20170614-165.PI.ijmu.png	144 KB	11/18/17 6:59:46 PM GMT+1
d2VTEC300s-vs-TIME.20170612-163-to-20170614-165.PI.borj.png	123 KB	11/18/17 6:59:41 PM GMT+1
d2VTEC300s-vs-TIME.20170612-163-to-20170614-165.PI.ijmu.png	127 KB	11/18/17 6:59:45 PM GMT+1
dBw-vs-TIME.20170612-163-to-20170614-165.PI.borj.png	263 KB	11/18/17 6:59:42 PM GMT+1
dBw-vs-TIME.20170612-163-to-20170614-165.PI.ijmu.png	239 KB	11/18/17 6:59:46 PM GMT+1
ionex_2_latitudinal_VTEC_profiles_time_series.uqrg.2017.163-165.anim.gif	3431 KB	11/18/17 8:18:08 AM GMT+1
tec.output+djm.uqrg.20170612_163_to_20171650614_165.borj.png	63 KB	11/18/17 6:45:23 PM GMT+1
tec.output+djm.uqrg.20170612_163_to_20171650614_165.ijmu.png	65 KB	11/18/17 6:45:23 PM GMT+1
tec.output+djm.uqrg.20170612_163_to_20171650614_165.nama.png	75 KB	11/18/17 6:45:23 PM GMT+1
tec.output+djm.uqrg.20170612_163_to_20171650614_165.rgao.png	62 KB	11/18/17 6:45:24 PM GMT+1
tec.output+djm.uqrg.20170612_163_to_20171650614_165.tmp1.png	73 KB	11/18/17 6:45:24 PM GMT+1
tec.output+djm.uqrg.20170612_163_to_20171650614_165.valp.png	63 KB	11/18/17 6:45:24 PM GMT+1

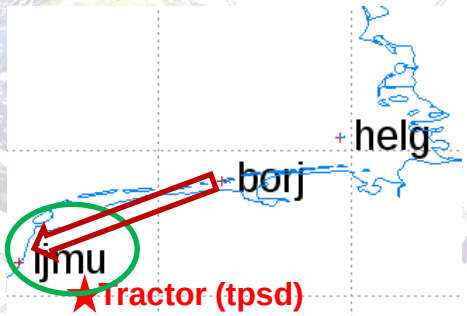

d2VTEC300s at maximum sampling rate (e.g. 30s) for IJMU from RINEX meas. marking declared potential cycle-slips

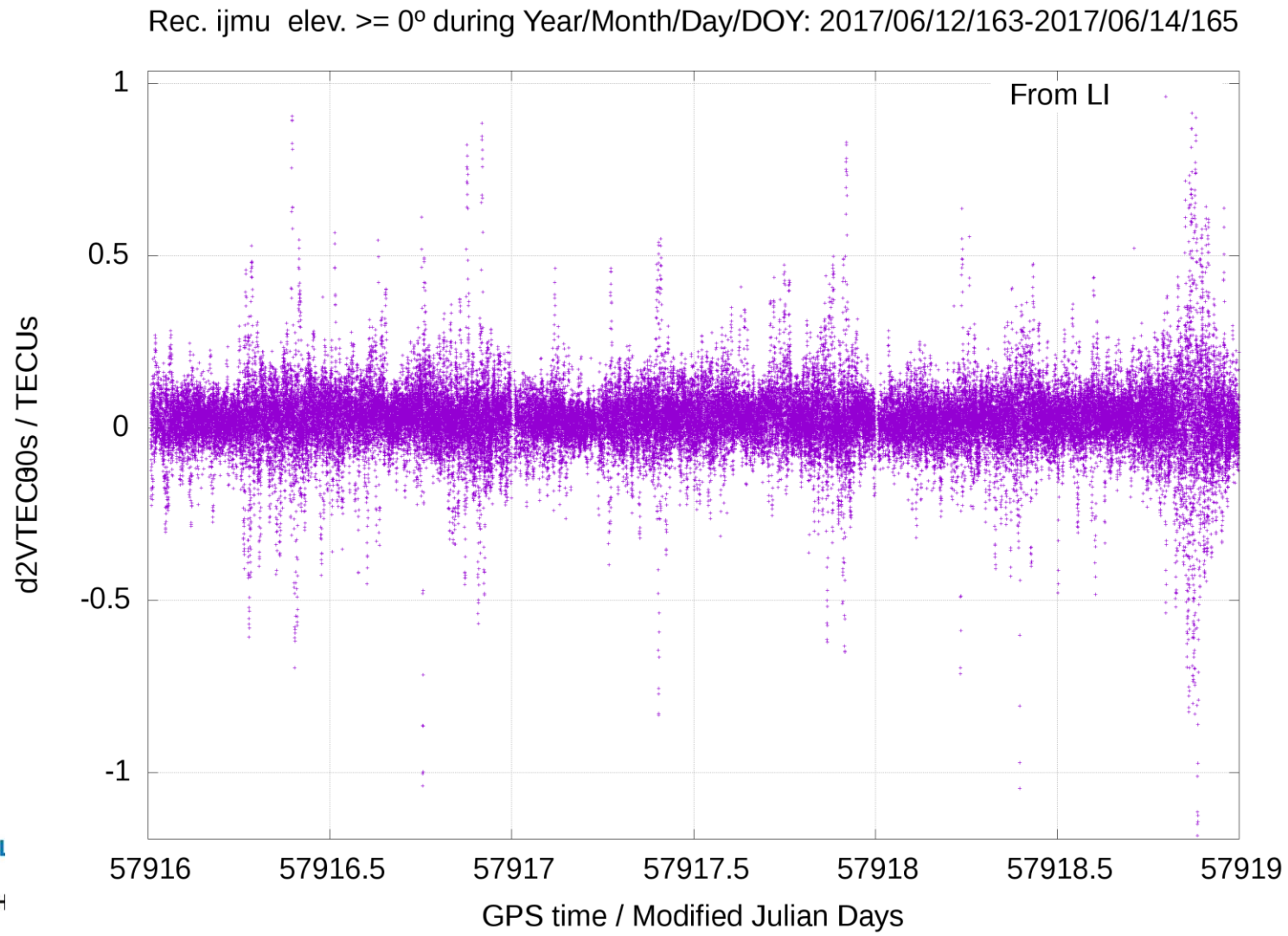

Zoom: Typical MSTID signature in the detrended VTEC (from d2VTEC300s)

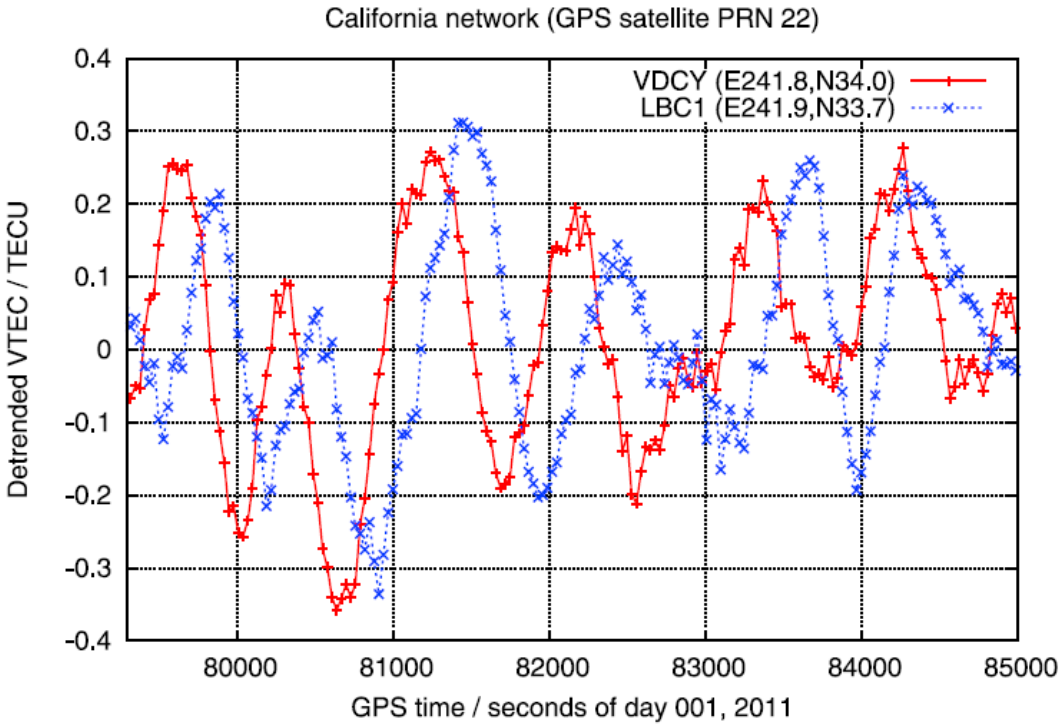

Figure 1. Example of MSTID signature in the detrended VTEC, directly obtained from the ionospheric combination of GPS carrier phases (see section 3) corresponding to an MSTID affecting GPS satellite PRN 22, advancing from receiver VDCY (E241.8,N34.0) toward LBC1 (E241.9, N33.7) in California network (CA, January 1st, 2011, see Figure 19 for more details).

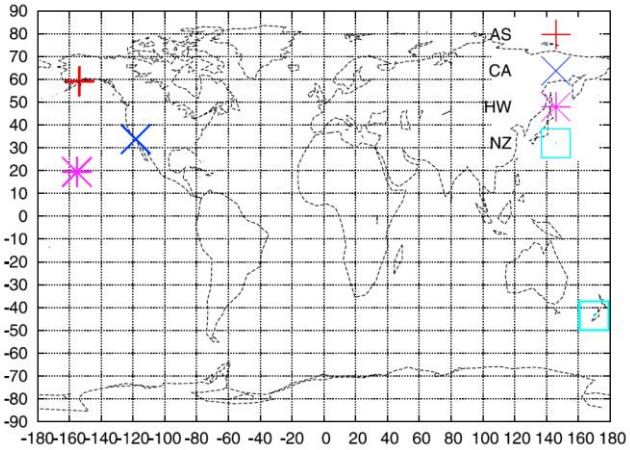

Figure 2. Global location of the local GPS networks analyzed in this work, at South of Alaska (AS), California (CA), Hawaii (HW) and New Zealand (NZ).

RADIO SCIENCE, VOL. 47, RS0K05, doi:10.1029/2011RS004951, 2012

Propagation of medium scale traveling ionospheric disturbances at different latitudes and solar cycle conditions

M. Hernández-Pajares,[1] J. M. Juan,[1] J. Sanz,[1] and A. Aragón-Àngel[1,2]

Received 2 December 2011; revised 6 April 2012; accepted 1 May 2012; published 4 July 2012.

[1] In this work, an extension in latitude range and time span with respect previous studies on Medium Scale Traveling Ionospheric Disturbances (MSTID) propagation, is presented. So far they have been basically studied at mid latitude and for limited periods (less than few years) at solar maximum conditions. This extension has been possible due to the availability of local Global Positioning System (GPS) networks at mid-north hemisphere (California), mid-south hemisphere (New Zealand), high and low latitudes (Alaska and Hawaii), for the last 13, 11, 7 and 4 years respectively. Optimal algorithms specially suitable for mass data processing have been used, such as the Single Receiver Medium Scale Traveling Ionospheric activity index (SRMTID) and the phase difference method for MSTID propagation estimation. The results reveal that several of the main MSTID climatological trends at mid latitude are also shared at low and high latitude, also modulated in intensity also by the Solar Cycle. This is the case for local fall/winter day-time equatorward propagated MSTIDs with typical velocities and wavelengths of 150–250 m/s and 100–300 km respectively. Moreover the comparison of MSTID propagation estimation using different techniques, and their implications in terms of potential origins of MSTIDs, are also discussed.

Citation: Hernández-Pajares, M., J. M. Juan, J. Sanz, and A. Aragón-Àngel (2012), Propagation of medium scale traveling ionospheric disturbances at different latitudes and solar cycle conditions, *Radio Sci.*, *47*, RS0K05, doi:10.1029/2011RS004951.

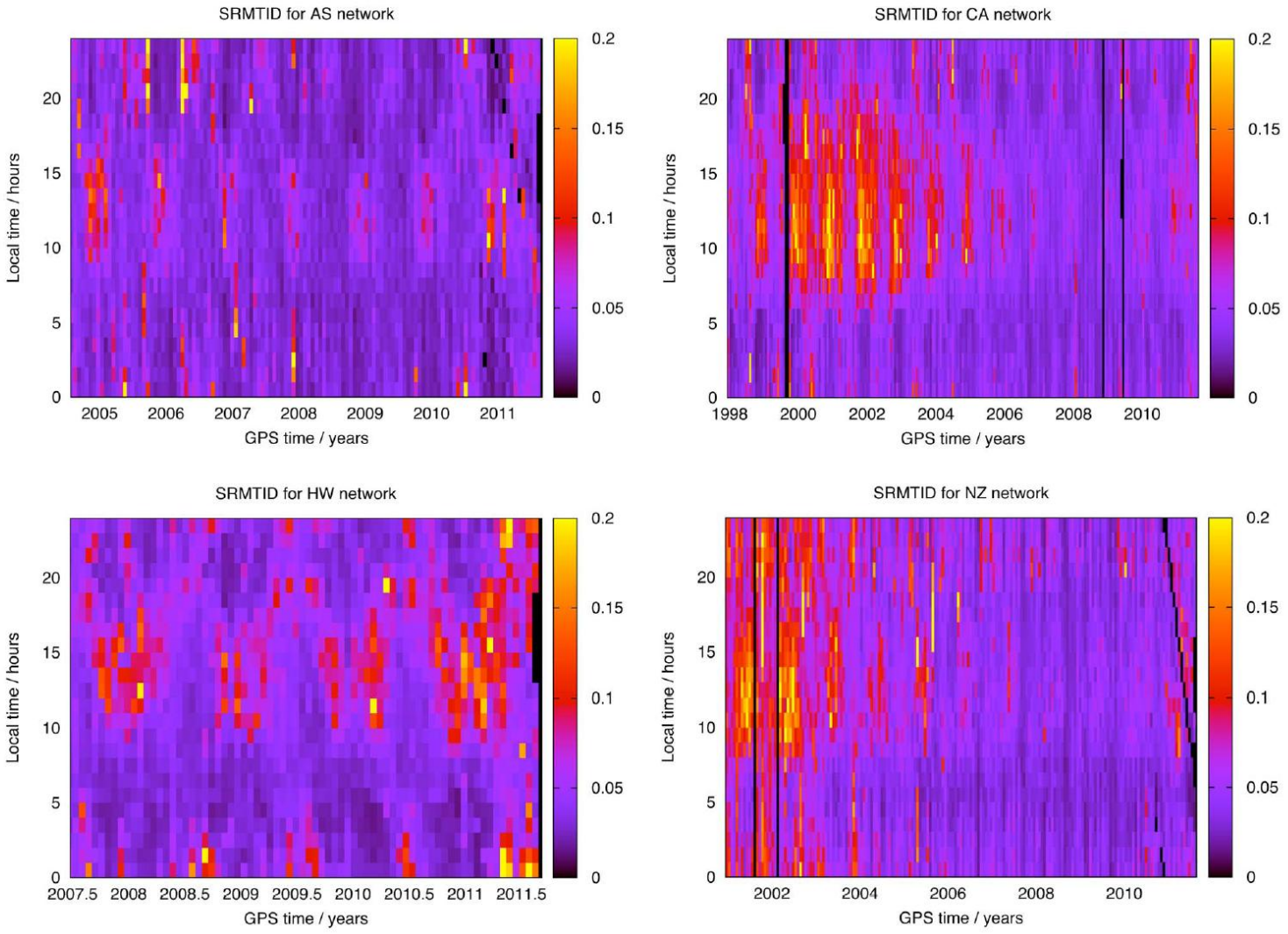

Figure 8. SRMTID index (in TECUs), in terms of GPS time (x-axis) and local time (y-axis), for the four selected networks: (top left) AS, (top right) CA, (bottom left) HW, and (bottom right) NZ.

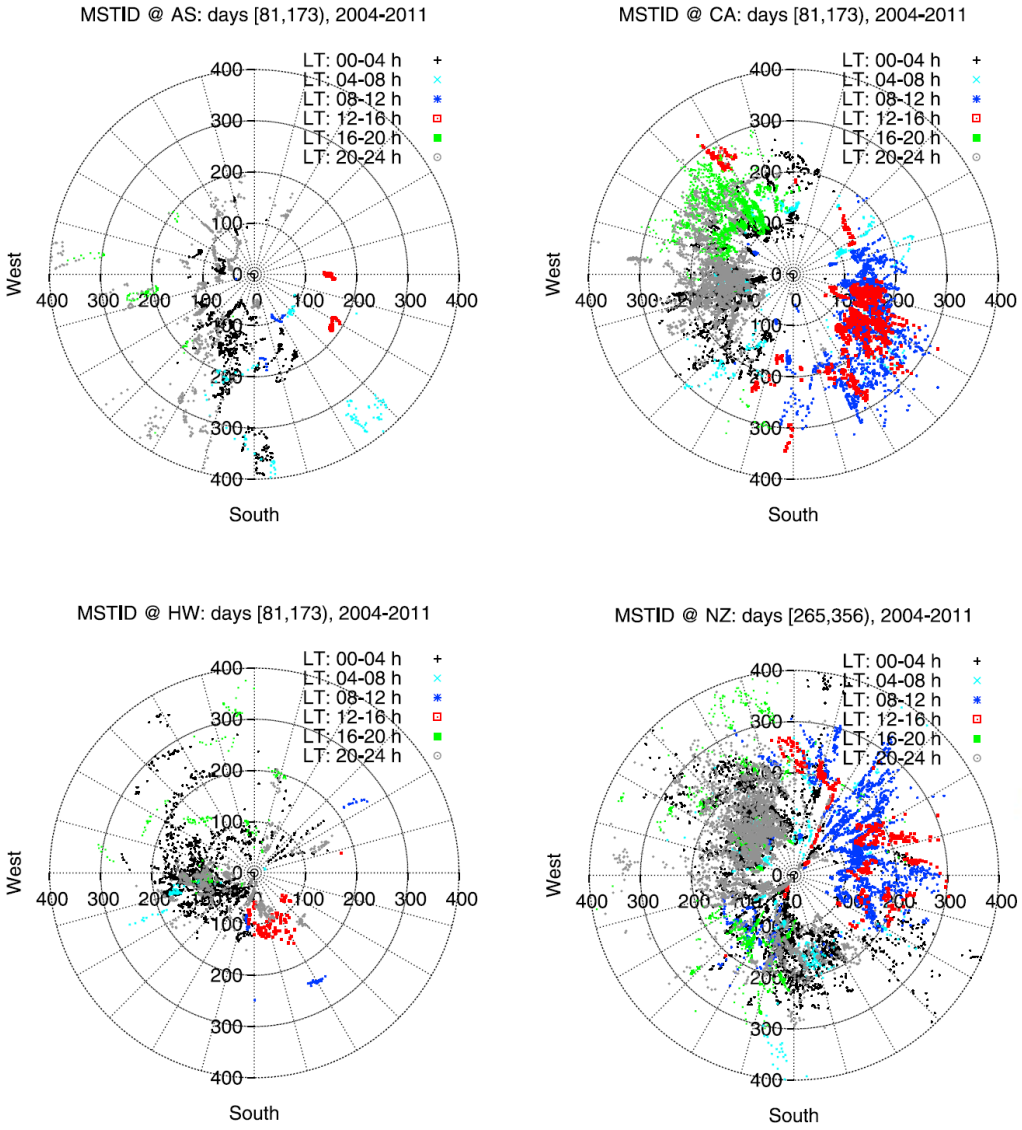

Figure 16. Polar plots representing MSTID velocities (in m/s) and azimuths, similar to Figure 14 but for local spring.

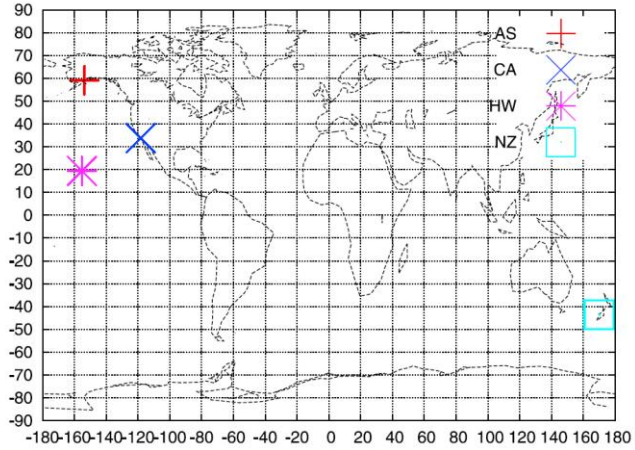

Figure 2. Global location of the local GPS networks analyzed in this work, at South of Alaska (AS), California (CA), Hawaii (HW) and New Zealand (NZ).

Conclusions from d2VTEC300s?

- **Conclusion**: The double-difference in time of LI=L1-L2, with time steps of 300 seconds (a good indicator of the most frequent ionospheric waves, difficulting the “interpolability” of the ionospheric delay from permanent GPS networks to GPS users. MSTID signature) is more intense during the night time.

- **Question 12**: Is this result in agreement with the climatology study in local networks? Why?

Recent works in MSTID: a simple RT mitigating approach for precise GPS processing

AGU PUBLICATIONS

Radio Science

RESEARCH ARTICLE

10.1002/2016RS006159

Direct MSTID mitigation in precise GPS processing

Manuel Hernández-Pajares[1], Pawel Wielgosz[2], Jacek Paziewski[2], Anna Krypiak-Gregorczyk[2], Marta Krukowska[2], Katarzyna Stepniak[2], Jan Kaplon[3], Tomasz Hadas[3], Krzysztof Sosnica[3], Jaroslaw Bosy[3], Raul Orus-Perez[4], Enric Monte-Moreno[1], Heng Yang[1], Alberto Garcia-Rigo[1], and Germán Olivares-Pulido[1]

[1]Department Mathematics, UPC-IonSAT, Barcelona, Spain, [2]University of Warmia and Mazury in Olsztyn, Olsztyn, Poland, [3]Wroclaw University of Environmental and Life Sciences, Wroclaw, Poland, [4]ESA-ESTEC, Noordwijk, Netherlands

Abstract In this paper, the authors summarize a simple and efficient approach developed to mitigate the problem in precise Global Navigation Satellite Systems (GNSS) positioning originated by the most frequent ionospheric wave signatures: the medium-scale traveling ionospheric disturbances (MSTIDs). The direct GNSS Ionospheric Interferometry technique (hereinafter dGII), presented in this paper, is applied for correcting MSTID effects on precise Real Time Kinematic (RTK) and tropospheric determination. It consists of the evolution of the former climatic Differential Delay Mitigation Model for MSTIDs (DMTID), for real-time conditions, using ionospheric data from a single permanent receiver only. The performance is demonstrated with networks of GNSS receivers in Poland, treated as users under real-time conditions, during two representative days in winter and summer seasons (days 353 and 168 of year 2013). In range domain, dGII typically reduces the ionospheric delay error up to 10–90% of the value when the MSTID mitigation model is not applied. The main dGII impact on precise positioning is that we can obtain reliable RTK position faster. In particular, the ambiguity success rate parameter increases, from 74% to 83%, with respect to the original uncorrected observations. The average of time to first fix is shortened from 30 s to 13 s. The improvement in troposphere estimaton, due to any potential impact of the MSTID mitigation model, was most difficult to demonstrate.

Key Points:
- Direct and simple MSTID mitigation technique (dGII) for GPS observations
- dGII is applicable to differential GPS processing (just one baseline is needed)
- Precise positioning is improved by means of dGII, in terms of ambiguity fixing and convergence time

Correspondence to:
M. Hernández-Pajares,
manuel.hernandez@upc.edu

Citation:
Hernández-Pajares, M., et al. (2017), Direct MSTID mitigation in precise GPS processing, *Radio Sci.*, 52, doi:10.1002/2016RS006159.

Received 9 SEP 2016
Accepted 29 JAN 2017
Accepted article online 2 FEB 2017
Corrected 5 APR 2017

This article was corrected on 5 APR 2017. See the end of the full text for details.

Recent works in MSTID: a new multi-MSTID detection and characterization technique

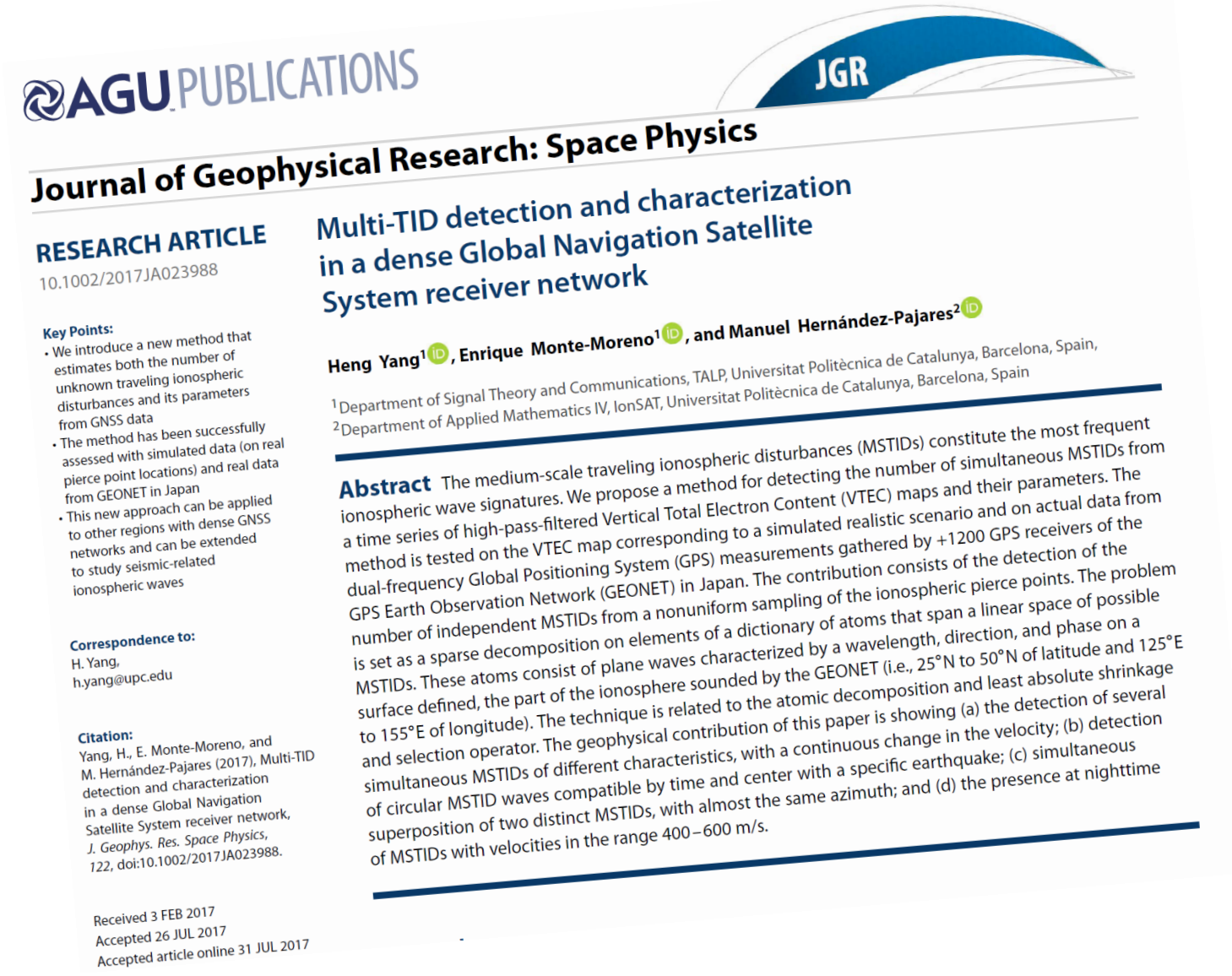

AGU PUBLICATIONS

JGR

Journal of Geophysical Research: Space Physics

RESEARCH ARTICLE

10.1002/2017JA023988

Multi-TID detection and characterization in a dense Global Navigation Satellite System receiver network

Heng Yang[1], Enrique Monte-Moreno[1], and Manuel Hernández-Pajares[2]

[1]Department of Signal Theory and Communications, TALP, Universitat Politècnica de Catalunya, Barcelona, Spain, [2]Department of Applied Mathematics IV, IonSAT, Universitat Politècnica de Catalunya, Barcelona, Spain

Key Points:

- We introduce a new method that estimates both the number of unknown traveling ionospheric disturbances and its parameters from GNSS data
- The method has been successfully assessed with simulated data (on real pierce point locations) and real data from GEONET in Japan
- This new approach can be applied to other regions with dense GNSS networks and can be extended to study seismic-related ionospheric waves

Correspondence to:
H. Yang,
h.yang@upc.edu

Citation:
Yang, H., E. Monte-Moreno, and M. Hernández-Pajares (2017), Multi-TID detection and characterization in a dense Global Navigation Satellite System receiver network, *J. Geophys. Res. Space Physics*, *122*, doi:10.1002/2017JA023988.

Received 3 FEB 2017
Accepted 26 JUL 2017
Accepted article online 31 JUL 2017

Abstract The medium-scale traveling ionospheric disturbances (MSTIDs) constitute the most frequent ionospheric wave signatures. We propose a method for detecting the number of simultaneous MSTIDs from a time series of high-pass-filtered Vertical Total Electron Content (VTEC) maps and their parameters. The method is tested on the VTEC map corresponding to a simulated realistic scenario and on actual data from dual-frequency Global Positioning System (GPS) measurements gathered by +1200 GPS receivers of the GPS Earth Observation Network (GEONET) in Japan. The contribution consists of the detection of the number of independent MSTIDs from a nonuniform sampling of the ionospheric pierce points. The problem is set as a sparse decomposition on elements of a dictionary of atoms that span a linear space of possible MSTIDs. These atoms consist of plane waves characterized by a wavelength, direction, and phase on a surface defined, the part of the ionosphere sounded by the GEONET (i.e., 25°N to 50°N of latitude and 125°E to 155°E of longitude). The technique is related to the atomic decomposition and least absolute shrinkage and selection operator. The geophysical contribution of this paper is showing (a) the detection of several simultaneous MSTIDs of different characteristics, with a continuous change in the velocity; (b) detection of circular MSTID waves compatible by time and center with a specific earthquake; (c) simultaneous superposition of two distinct MSTIDs, with almost the same azimuth; and (d) the presence at nighttime of MSTIDs with velocities in the range 400–600 m/s.

Layout:

1) [**Motivation**] Precise Agriculture (PA) presentation (EU AUDITOR experiment)

2) [**Background**]: Brief introduction to main identified points of the presentation:
   a) GPS fundamentals: pseudoranges and carrier phases (optional)
   b) Ionospheric electron content
   c) Wide Area Real-Time Kinematic
   d) The International GNSS Service (*optional*)

3) [**One efficient operative system**] Quick introduction to Linux (*optional*)

4) [**New tools for learning and research**] IonSAT Tools (IT), emulating Real-Time (RT) as much as possible (presented on the PA AUDITOR experiment):
   a) *gim2vtec.v2.scr*
   b) *gimrnx2stec.v2.scr*

5) [**IT application to ECLIPSE, FLARE & GSTORM scenarios**] (*optional*).

6) [**Example of RT GPS-ionospheric system**]: UPC-IonSAT since 2012.

7) [**Monitoring of co-seismic generated ionospheric signals]:** Application of RT ionospheric sounding for potential Tsunami warnings), with GNSS dense (Tohoku and mid earthquakes, EQ) and sparse networks (Chile 2015 EQ).

8) [**Conclusions**]

gim2vtec.v2.scr & gimrnx2stec.v2.scr @ ECLIPSE, FLARE & GSTORM

- ssh –X –p XXXXX ionsat-tools-userYY@chapman.upc.es
- Where XXXXX is the port number (see blackboard) and YY the UserId # (since 01 to 20), and the password, given to you at the beginning of the corresponding laboratory session.
- chapman:~% whoami
- chapman:~% cd ils
- chapman:~% pwd
- chapman:~% ls -l
- chapman:~% xedit run.IonSAT-lab_sessions.v4b.scr &
- Uncomment (remove the first leading #) the command lines for ECLIPSE, FLARE & GSTORM blocks, save and run the script:
- chapman:~% ./run.IonSAT-lab_sessions.v4b.scr >& log.2 < /dev/null &

gim2vtec.v2.scr & gimrnx2stec.v2.scr @ ECLIPSE, FLARE & GSTORM

- chapman:~% tail -f log.2
- Once it is finished you can look at the selected results in form of plots:
- chapman:~% cd ~/ils/selected_plots
- chapman:~% ./selected_plots.scr
- chapman:~% ./selected_plots.scr ftplink ECLIPSE
- chapman:~% ./selected_plots.scr ftplink FLARE
- chapman:~% ./selected_plots.scr ftplink GSTORM
- **Each ftp link can be pasted on the navigator at your local computer**, for low-bandwidth connections (for high-bandwidth you may wish to replace “ftplink” by “screen”).
- You should likely find these selected plots, with the navigator like for AUDITOR…

Recent example: Solar Eclipse 21 August 2017

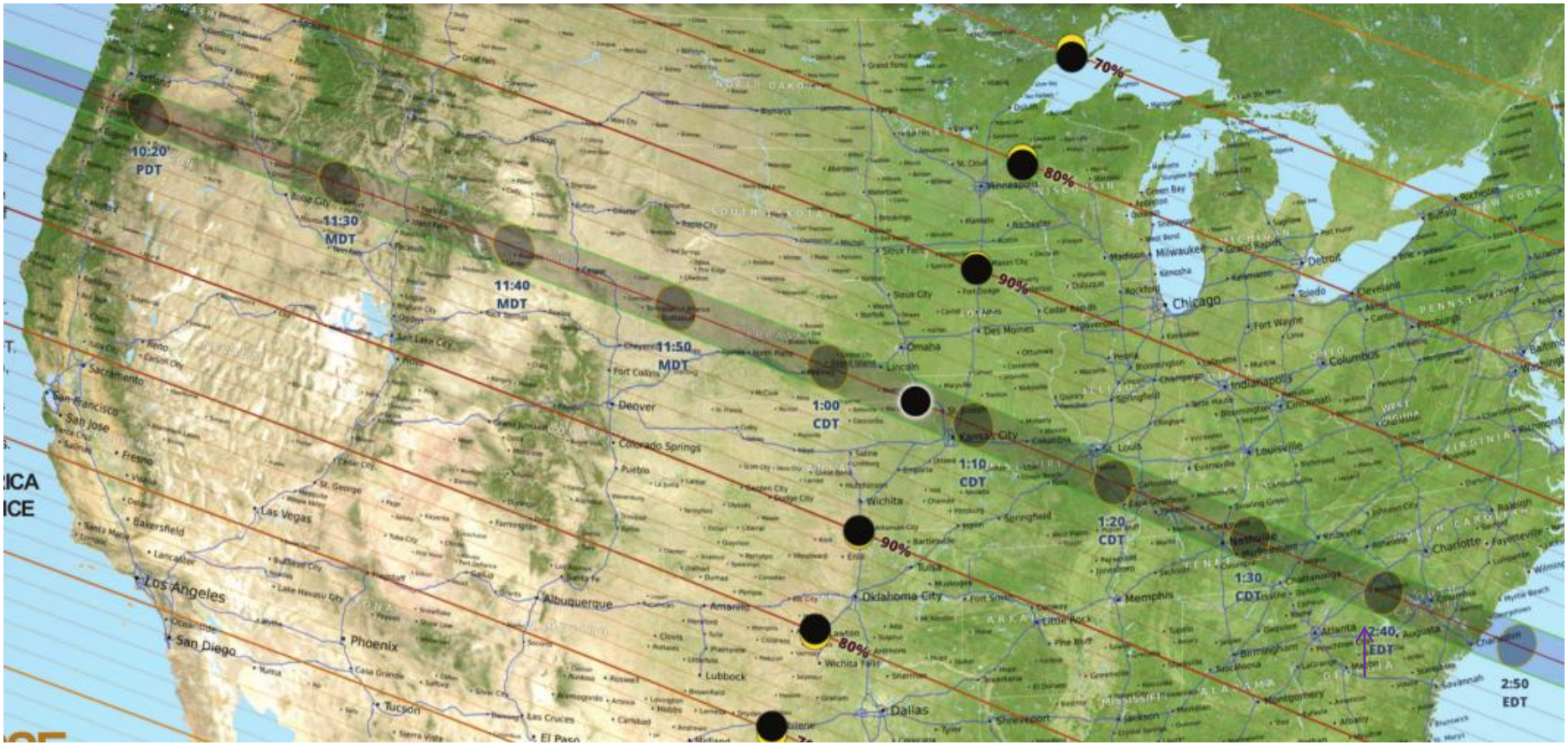

Both maps have been kindly provided by https://eclipse2017.nasa.gov

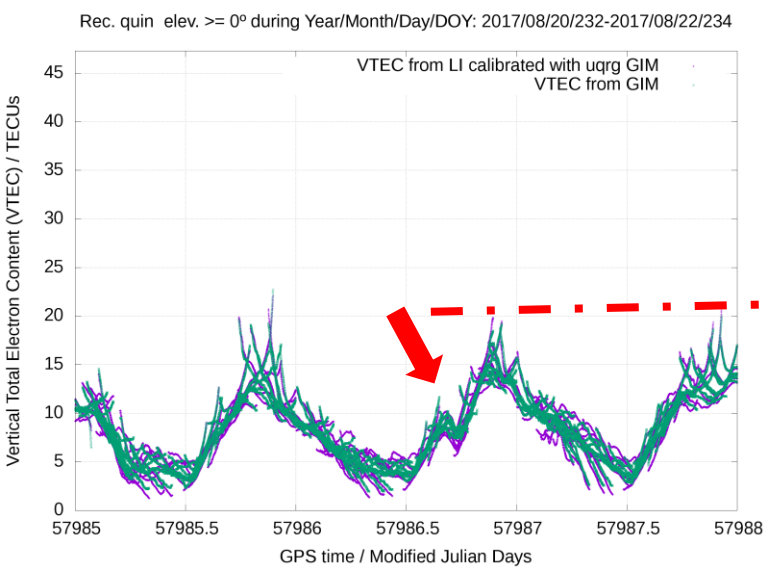

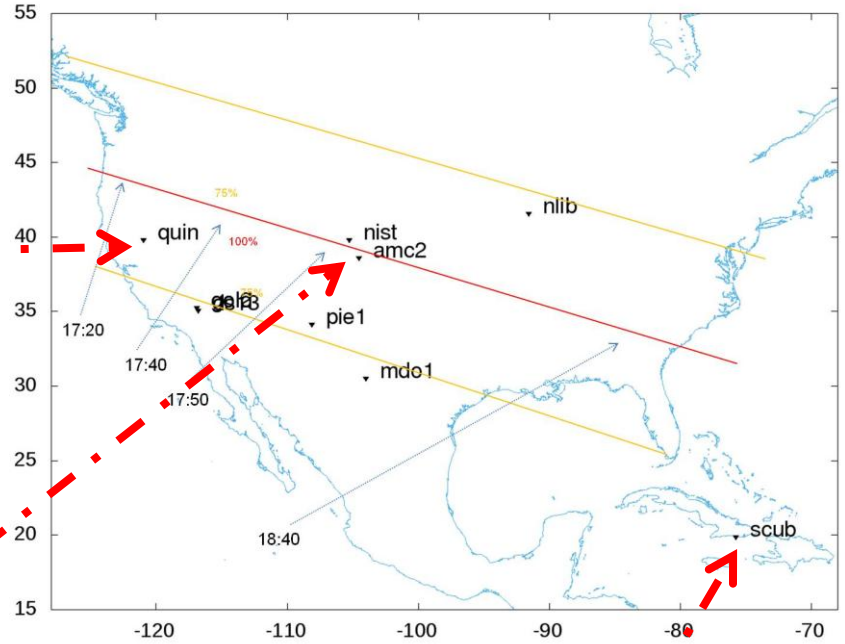

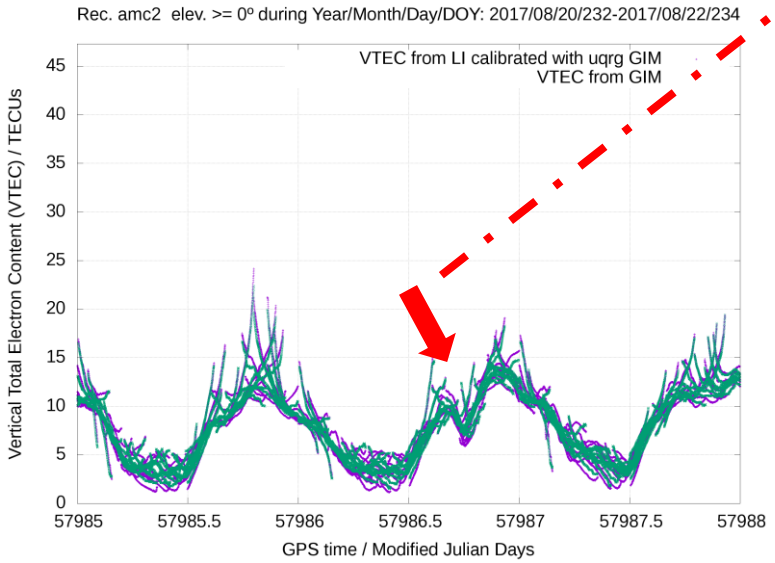

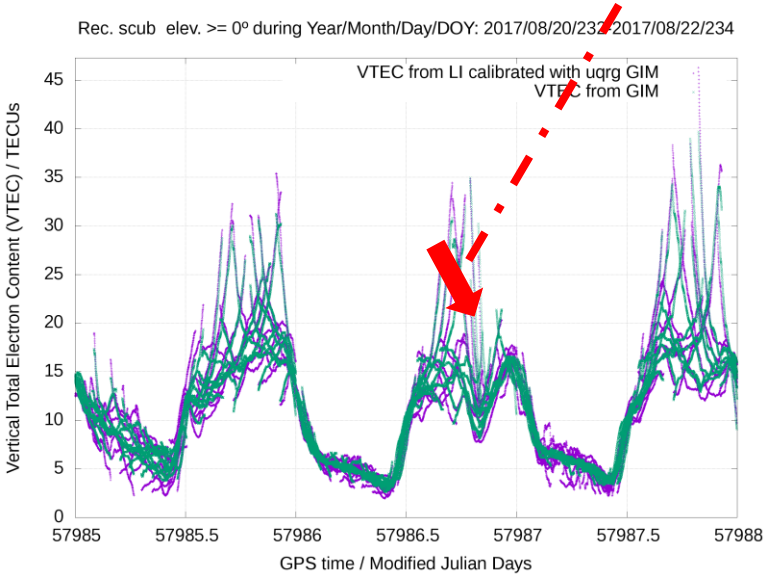

Depletion in agreement with Moon shadow timing

Solar Eclipse footprint detected with single frequency (better again with IG2 than with IG1!)

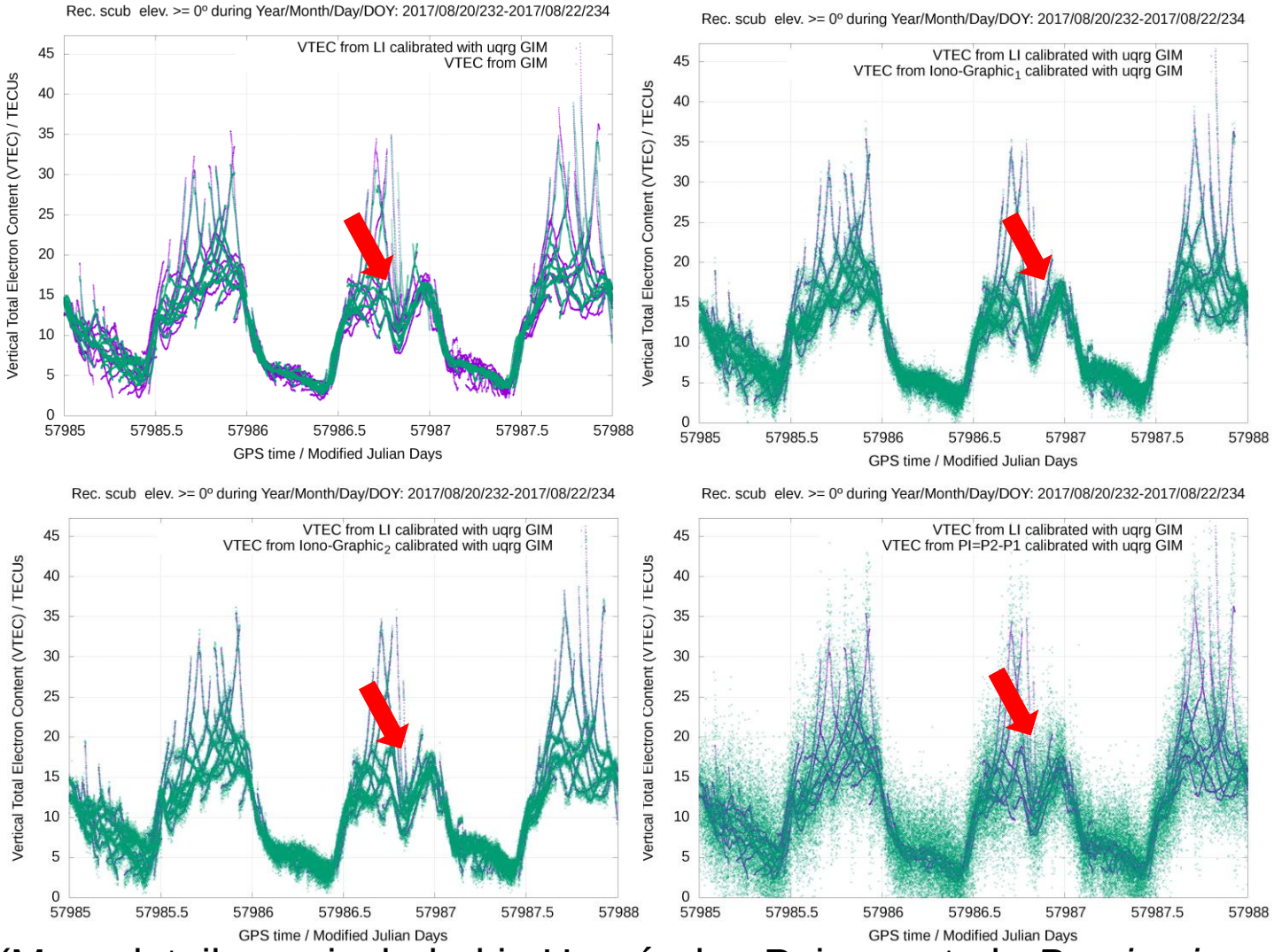

(More details are included in Hernández-Pajares et al., *Precise ionospheric determination from single-frequency GPS receivers; application during the Solar Eclipse of August 21, 2017* submitted to *GPS Solutions).*

SPACE WEATHER, VOL. 10, S12001, doi:10.1029/2012SW000826, 2012

GNSS measurement of EUV photons flux rate during strong and mid solar flares

M. Hernández-Pajares,[1] A. García-Rigo,[2] J. M. Juan,[1] J. Sanz,[1] E. Monte,[3] and A. Aragón-Àngel[1,2]

Received 6 June 2012; revised 14 October 2012; accepted 18 October 2012; published 12 December 2012.

[1] A new GNSS Solar Flare Activity Indicator (GSFLAI) is presented, given by the gradient of the ionospheric Vertical Total Electron Content (VTEC) rate, in terms of the solar-zenithal angle, measured from a global network of dual-frequency GPS receivers. It is highly correlated with the Extreme Ultraviolet (EUV) photons flux rate at the 26–34 nm spectral band, which is geo-effective in the ionization of the mono-atomic oxygen in the Earth's atmosphere. The results are supported by the comparison of GSFLAI with direct EUV observations provided by SEM instrument of SOHO spacecraft, for all the X-class solar flares occurring between 2001 and 2011 (more than 1000 direct comparisons at the 15 s SEM EUV sampling rate). The GSFLAI sensitivity enables detection of not only extreme X-class flares, but also of variations of one order of magnitude or even smaller (such as for M-class flares). Moreover, an optimal detection algorithm (SISTED), sharing the same physical fundamentals as GSFLAI, is also presented, providing 100% successful detection for all the X-class solar flares during 2000–2006 with registered location outside of the solar limb (i.e., detection of 94% of all of X-class solar-flares) and about 65% for M-class ones. As a final conclusion, GSFLAI is proposed as a new potential proxy of solar EUV photons flux rate for strong and mid solar flares, presenting high sensitivity with high temporal resolution (1 Hz, greater than previous solar EUV irradiance instruments), using existing ground GNSS facilities, and with the potential use as a solar flare detection parameter.

Citation: Hernández-Pajares, M., A. García-Rigo, J. M. Juan, J. Sanz, E. Monte, and A. Aragón-Àngel (2012), GNSS measurement of EUV photons flux rate during strong and mid solar flares, *Space Weather*, *10*, S12001, doi:10.1029/2012SW000826.

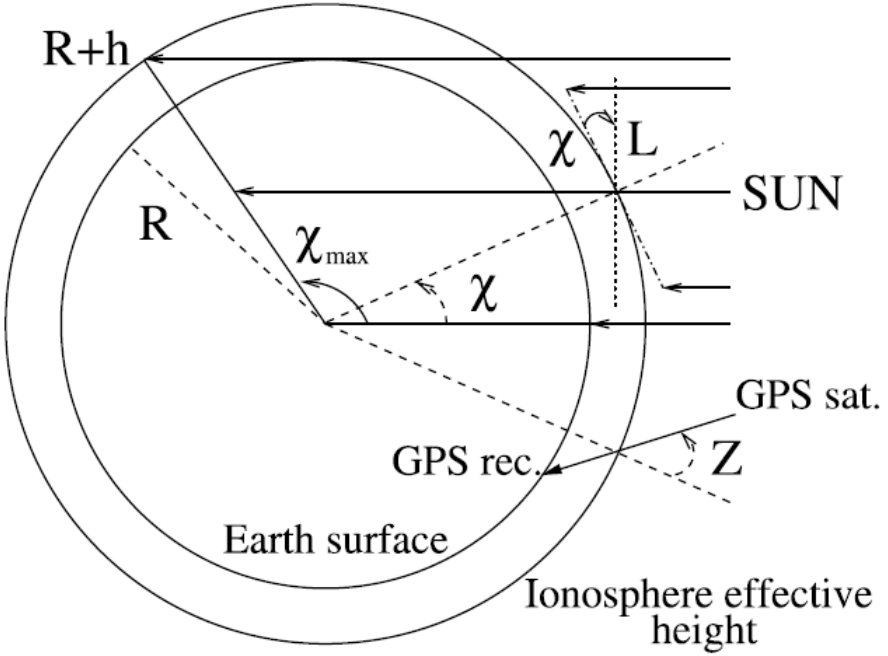

Figure 1. Layout representing the maximum solar-zenith angle illuminated by the Sun, χ_{max}, the reduction of sun illumination for a cylinder with base diameter L for a given solar-zenith angle χ, and the typical satellite receiver geometry for a satellite-zenith angle Z.

including an independent term that allows a non-zero VTEC rate at points with solar-zenith angles $\chi \geq 90°$:

$$\frac{\partial V}{\partial t} = a(t)\cos\chi + b(t) \qquad (2)$$

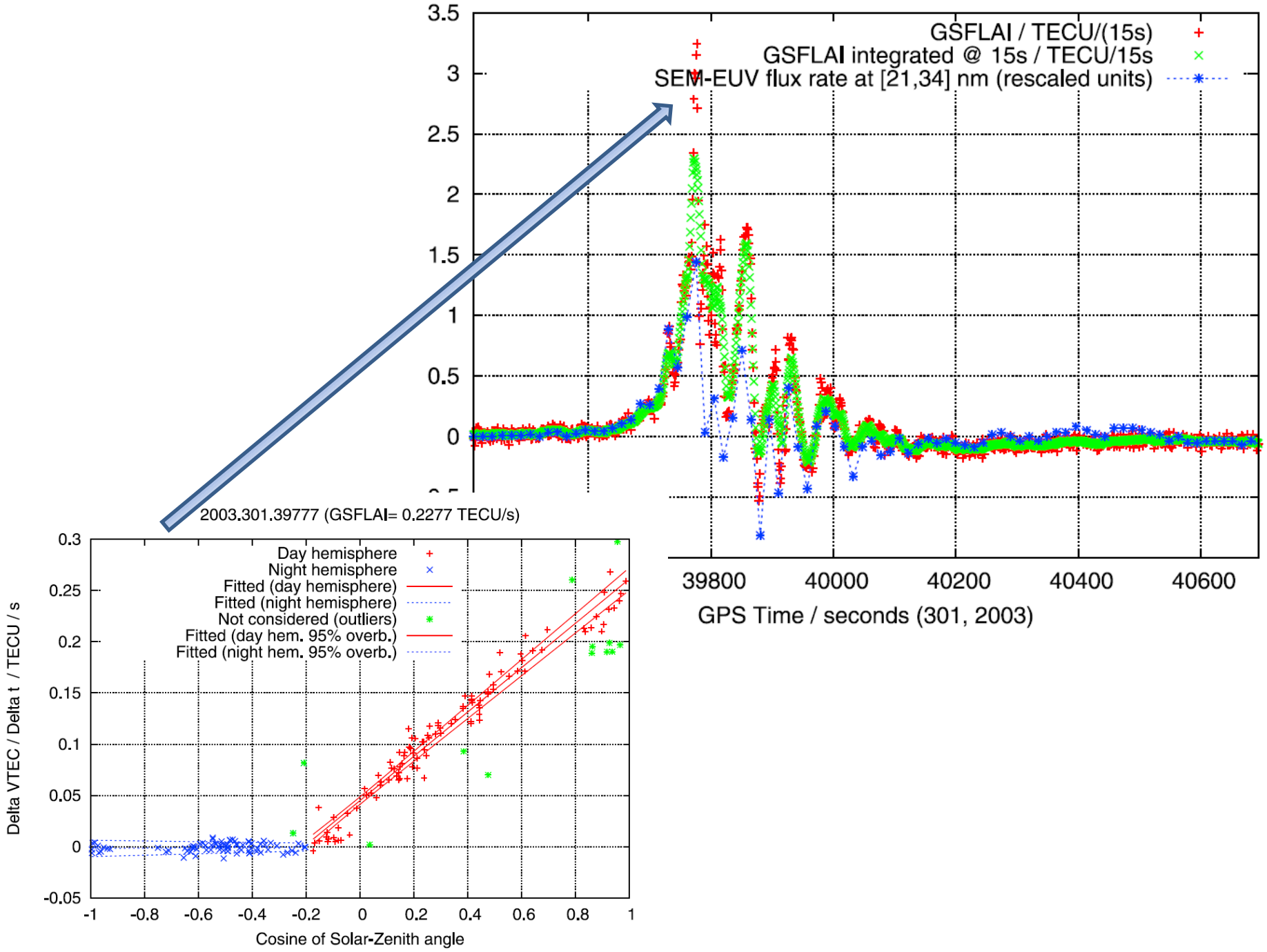
GSFLAI / TECU/(15s)
GSFLAI integrated @ 15s / TECU/15s
SEM-EUV flux rate at [21,34] nm (rescaled units)
3.5
3
2.5
2
1.5
1
0.5
0
39800
40000
40200
40400
40600
GPS Time / seconds (301, 2003)
2003.301.39777 (GSFLAI= 0.2277 TECU/s)
Day hemisphere
Night hemisphere
Fitted (day hemisphere)
Fitted (night hemisphere)
Not considered (outliers)
Fitted (day hem. 95% overb.)
Fitted (night hem. 95% overb.)
0.3
0.25
0.2
0.15
0.1
0.05
0
-0.05
-1
-0.8
-0.6
-0.4
-0.2
0
0.2
0.4
0.6
0.8
1
Delta VTEC / Delta t / TECU / s
Cosine of Solar-Zenith angle

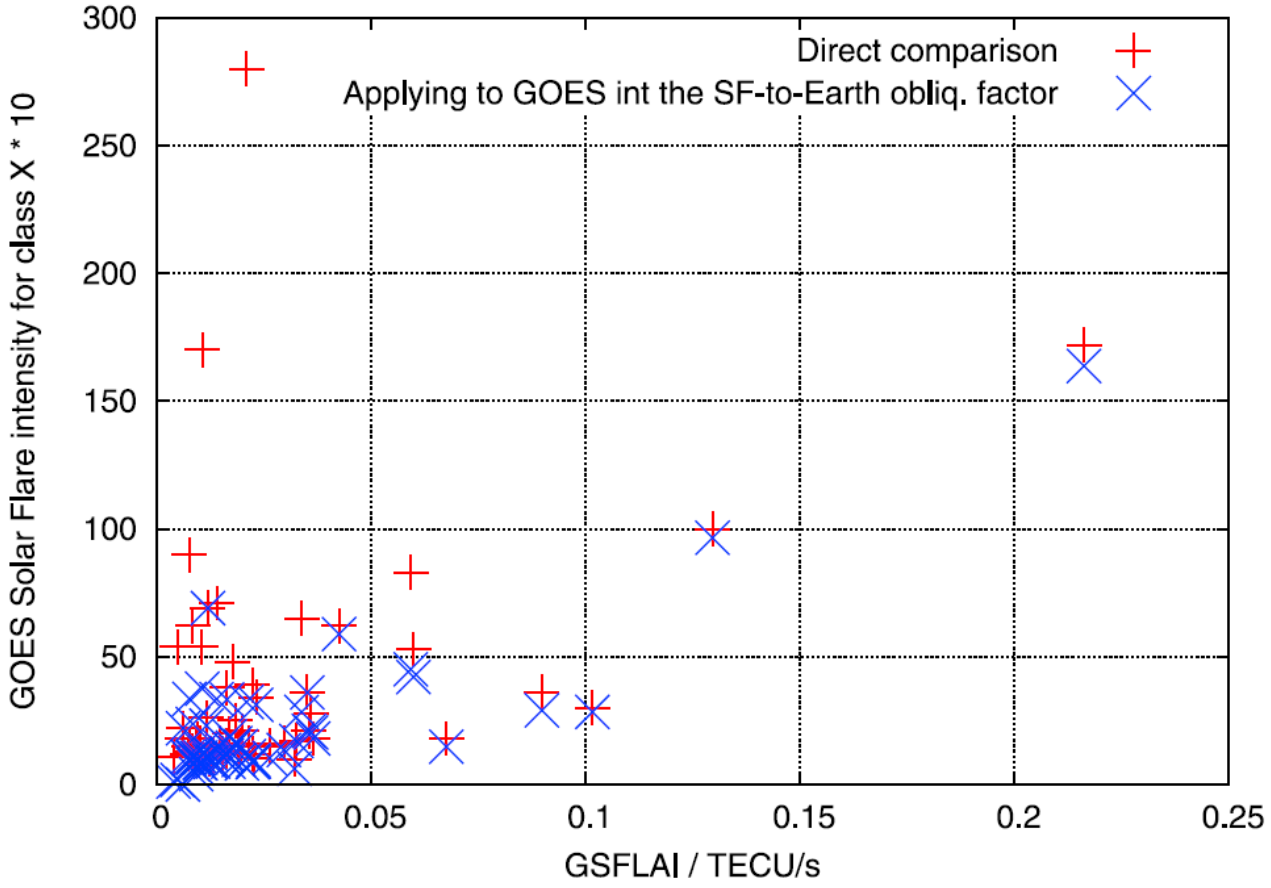

Figure 9. X-ray band solar flare intensity, corresponding to the GOES index for all the X-class flares analyzed in this work (those with available data between 2001 and 2011) represented versus the GSFLAI value at the corresponding peak. The red points represent the direct comparison, and the blue points the comparison after applying a solar-earth deprojecting factor, in terms of the solar flare occurrence location in the surface of the Sun.

Recent solar flare Sep 6th, 2017: RT detection from global RT GPS measurements with RT-TOMION @ UPC-IonSAT

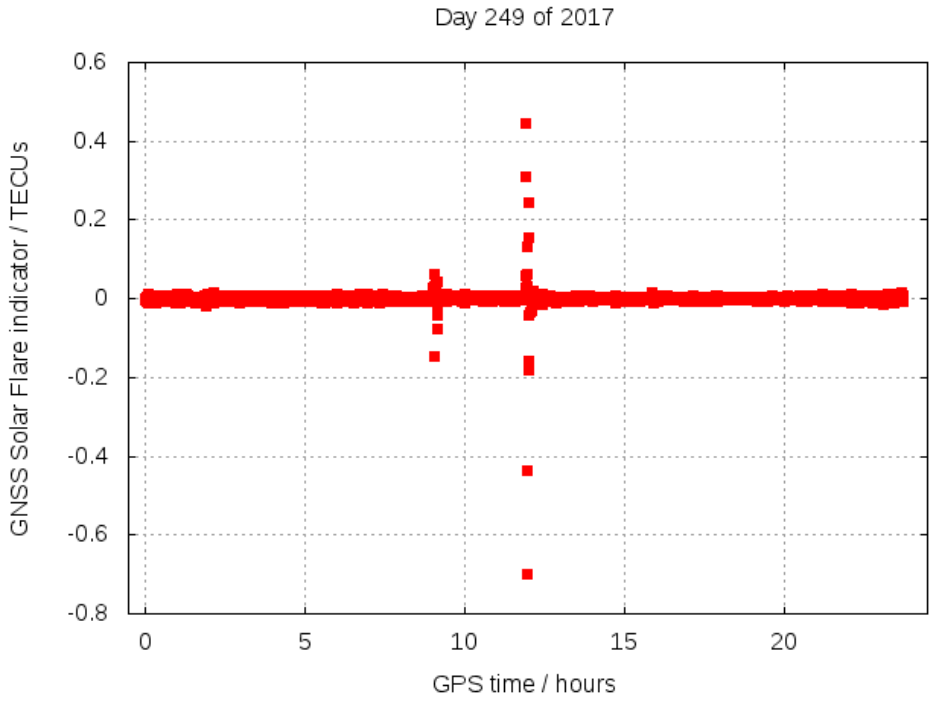

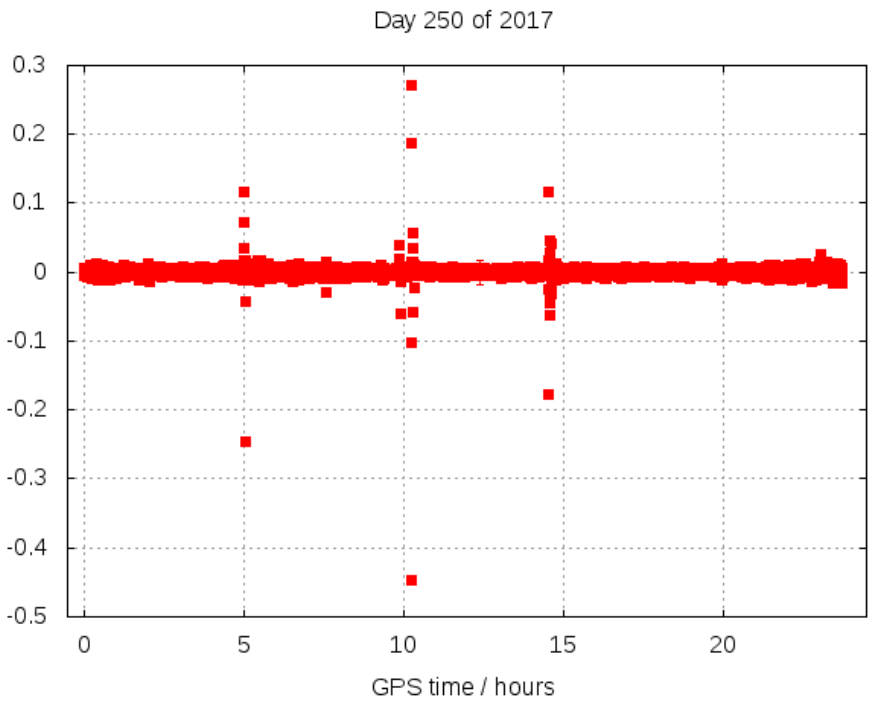

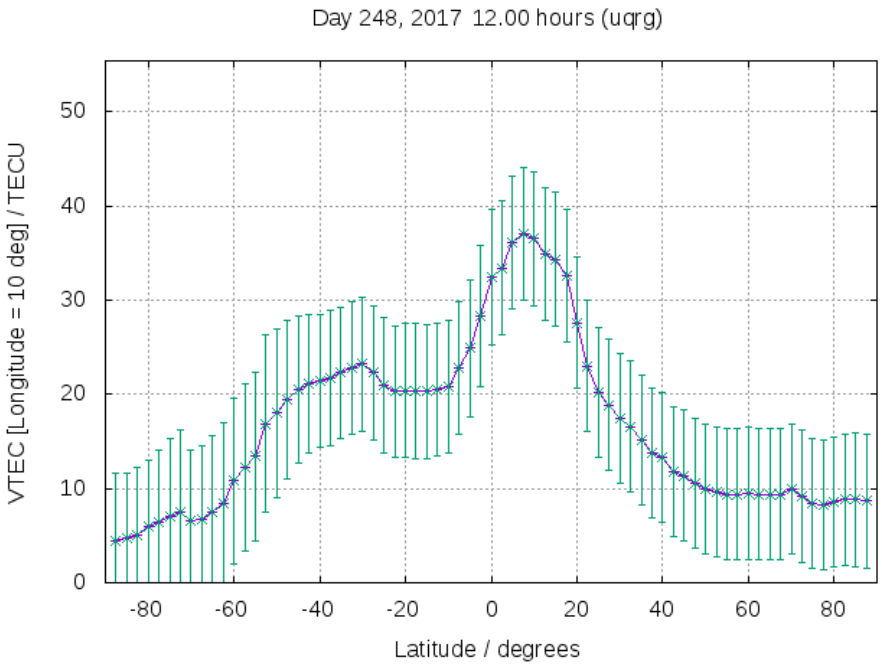

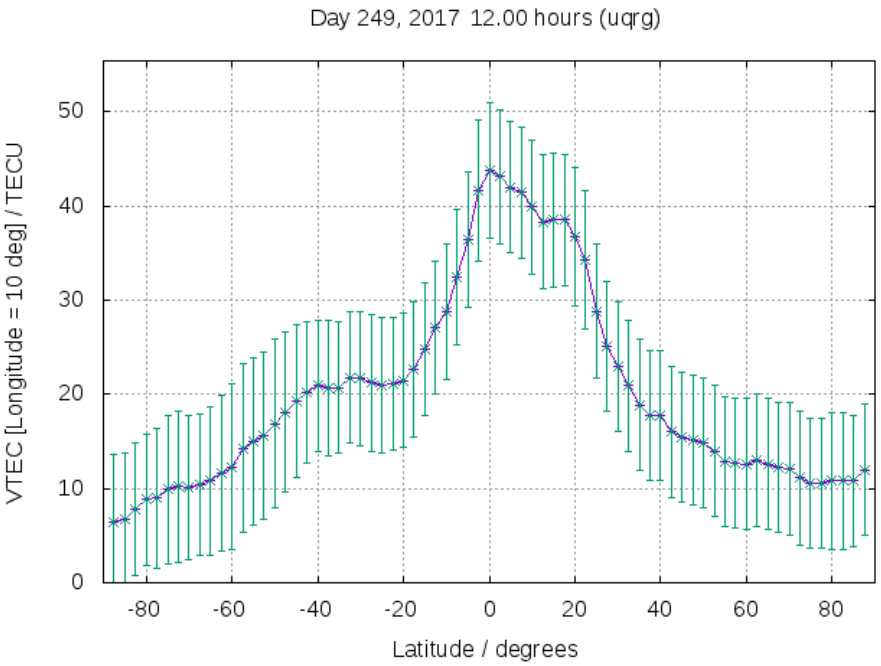

Recent solar flare Sep 6th, 2017: Meridional VTEC enhancement below solar flare compared with days before and after from UQRG GIMs

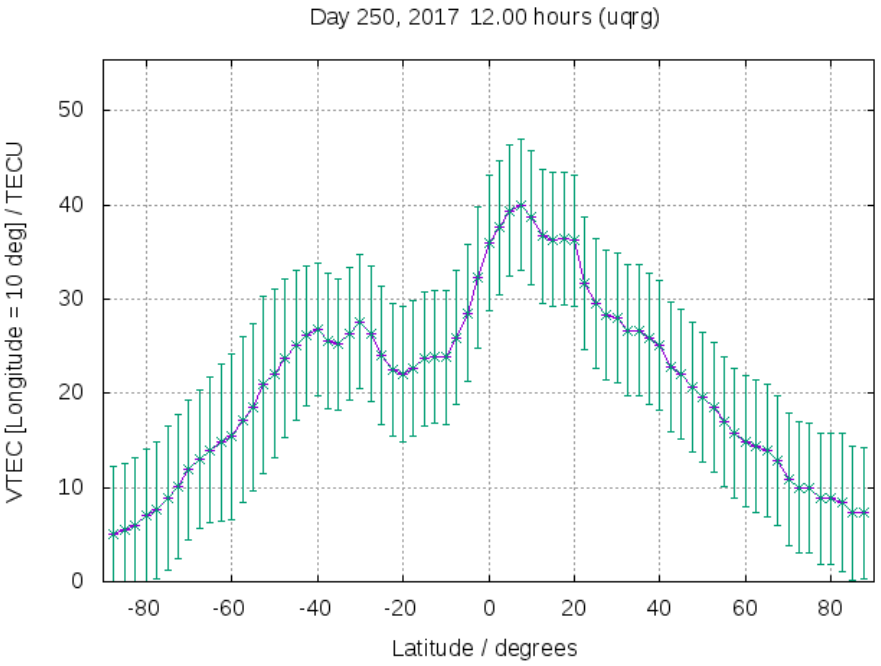

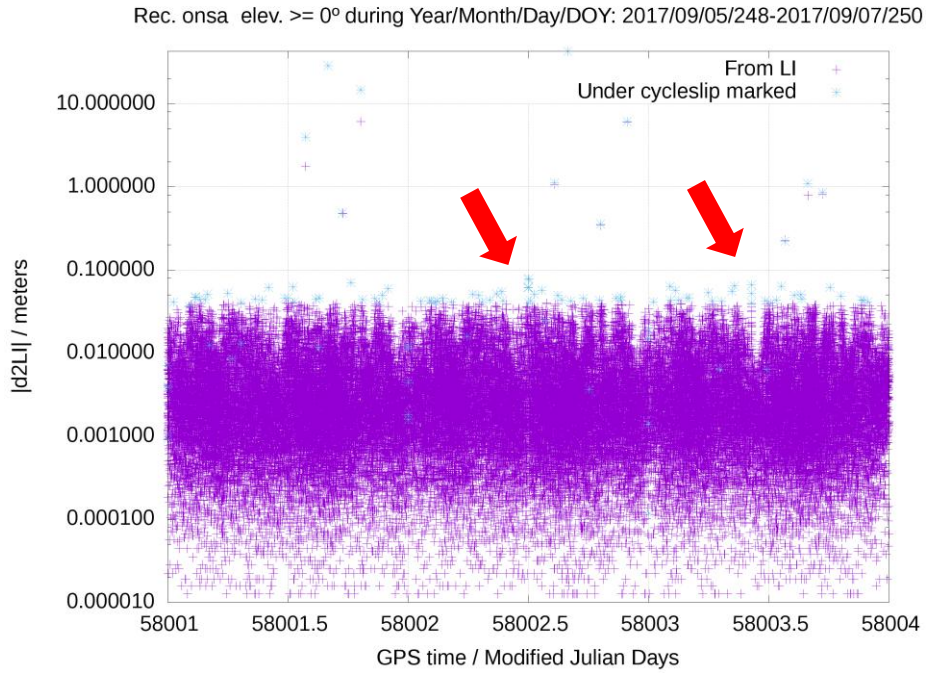
Rec. onsa elev. >= 0º during Year/Month/Day/DOY: 2017/09/05/248-2017/09/07/250
From LI
Under cycleslip marked
|d2LI| / meters
10.000000
1.000000
0.100000
0.010000
0.001000
0.000100
0.000010
58001
58001.5
58002
58002.5
58003
58003.5
58004
GPS time / Modified Julian Days

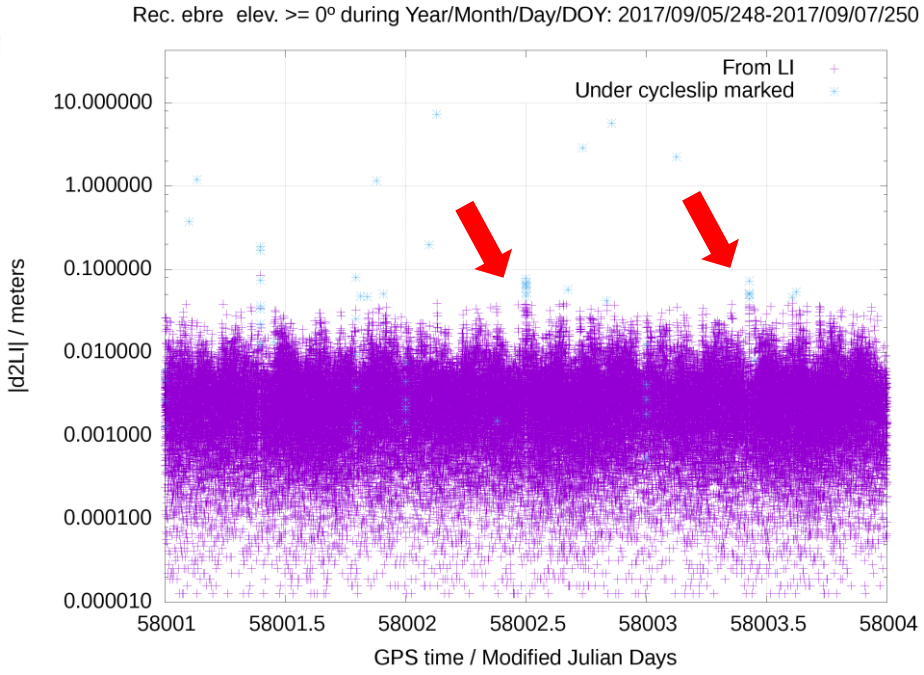
Rec. ebre elev. >= 0º during Year/Month/Day/DOY: 2017/09/05/248-2017/09/07/250
From LI
Under cycleslip marked
|d2LI| / meters
10.000000
1.000000
0.100000
0.010000
0.001000
0.000100
0.000010
58001
58001.5
58002
58002.5
58003
58003.5
58004
GPS time / Modified Julian Days

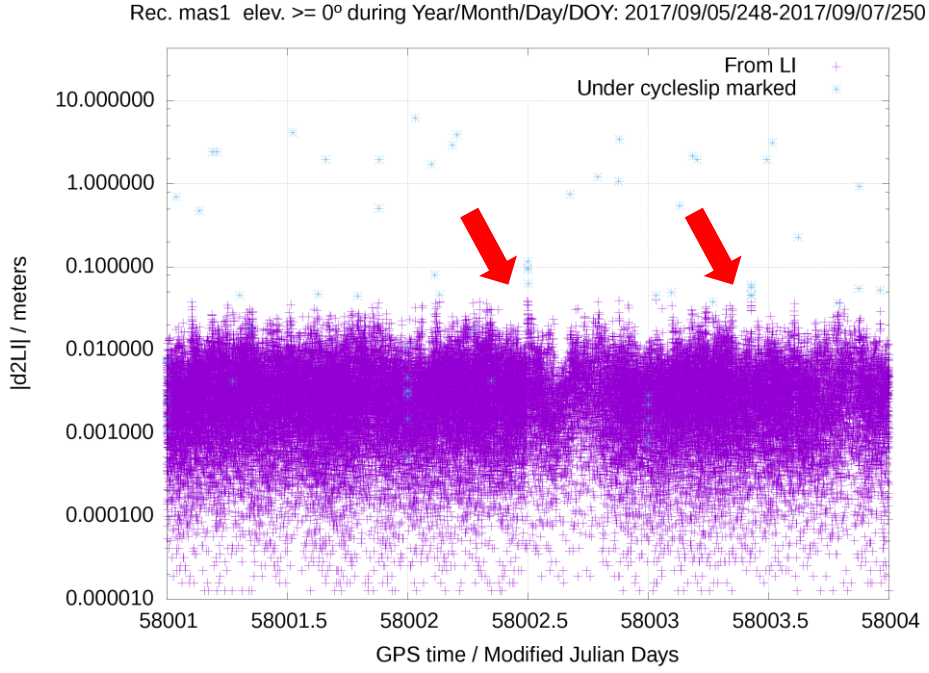
Rec. mas1 elev. >= 0º during Year/Month/Day/DOY: 2017/09/05/248-2017/09/07/250
From LI
Under cycleslip marked
|d2LI| / meters
10.000000
1.000000
0.100000
0.010000
0.001000
0.000100
0.000010
58001
58001.5
58002
58002.5
58003
58003.5
58004
GPS time / Modified Julian Days

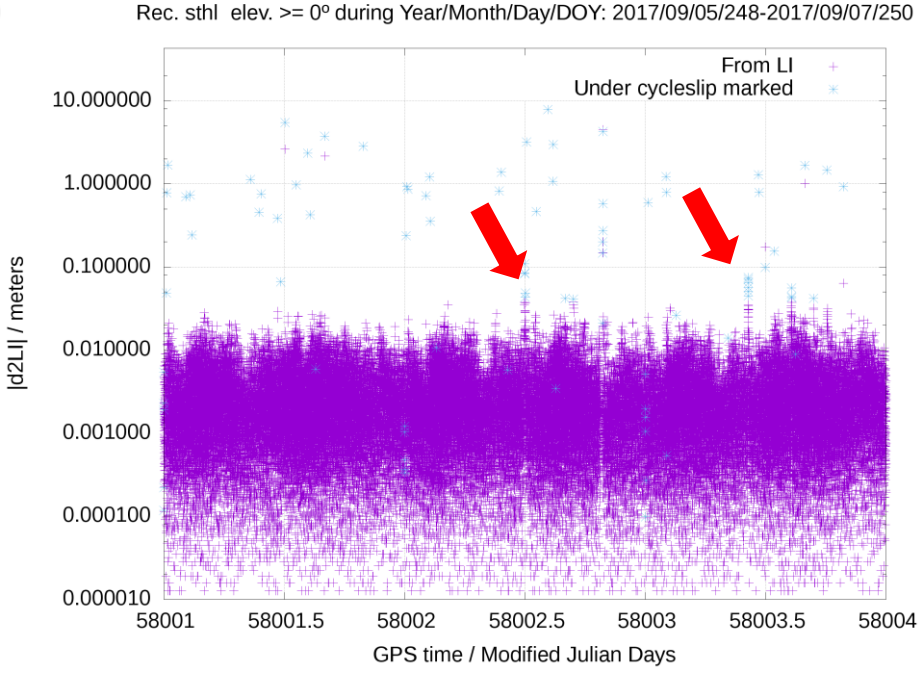
Rec. sthl elev. >= 0º during Year/Month/Day/DOY: 2017/09/05/248-2017/09/07/250
From LI
Under cycleslip marked
|d2LI| / meters
10.000000
1.000000
0.100000
0.010000
0.001000
0.000100
0.000010
58001
58001.5
58002
58002.5
58003
58003.5
58004
GPS time / Modified Julian Days

Other studies on solar flares from GPS data

AGU PUBLICATIONS

JGR

Journal of Geophysical Research: Space Physics

RESEARCH ARTICLE

10.1002/2014JA020206

Occurrence of solar flares viewed with GPS: Statistics and fractal nature

Enrique Monte-Moreno[1] and Manuel Hernández-Pajares[2]

[1]Departament de Teoria del Senyal i Comunicacions, TALP, Universitat Politècnica de Catalunya, Barcelona, Spain, [2]Departament Matemàtica Aplicada IV, IonSAT, Universitat Politècnica de Catalunya, Barcelona, Spain

Key Points:

- Statistical properties of the EUV solar flux sudden variation as a time series
- Sudden overionization studied during one solar cycle from GNSS signals
- The solar flux rate follows the Levy-Mandelbrot and fractional Brownian models

Abstract In this paper we describe the statistical properties of the EUV solar flux sudden variation. The

AGU PUBLICATIONS

JGR

Journal of Geophysical Research: Space Physics

RESEARCH ARTICLE

10.1002/2015JA021824

GPS as a solar observational instrument: Real-time estimation of EUV photons flux rate during strong, medium, and weak solar flares

Talwinder Singh[1], Manuel Hernandez-Pajares[2], Enric Monte[3], Alberto Garcia-Rigo[2], and Germán Olivares-Pulido[2]

[1]Department of Physics, Indian Institute of Technology (BHU), Varanasi, India, [2]Departament Matemàtica Aplicada IV, IonSAT res. group, Universitat Politcnica de Catalunya, Barcelona, Spain, [3]Departament de Teoria del Senyal i Comunicacions, TALP res. group, Universitat Politcnica de Catalunya, Barcelona, Spain

Key Points:

- It is shown how GPS can be efficiently used as an accurate solar observational tool
- A constant linear EUV photon flux-GSFLAI dependence is found for all kind of solar flares
- GSFLAI present advantages regarding to direct EUV photons flux measurements taken from solar probes

Ann. Geophys., 35, 377–391, 2017
www.ann-geophys.net/35/377/2017/
doi:10.5194/angeo-35-377-2017
© Author(s) 2017. CC Attribution 3.0 License.

Annales Geophysicae
Open Access
EGU

MONITOR Ionospheric Network: two case studies on scintillation and electron content variability

Yannick Béniguel[1], Iurii Cherniak[2], Alberto Garcia-Rigo[3], Pierrick Hamel[1], Manuel Hernández-Pajares[3], Roland Kameni[4], Anton Kashcheyev[5], Andrzej Krankowski[2], Michel Monnerat[8], Bruno Nava[5], Herbert Ngaya[4], Raül Orus-Perez[6], Hughes Secrétan[7], Damien Sérant[8], Stefan Schlüter[9], and Volker Wilken[10]

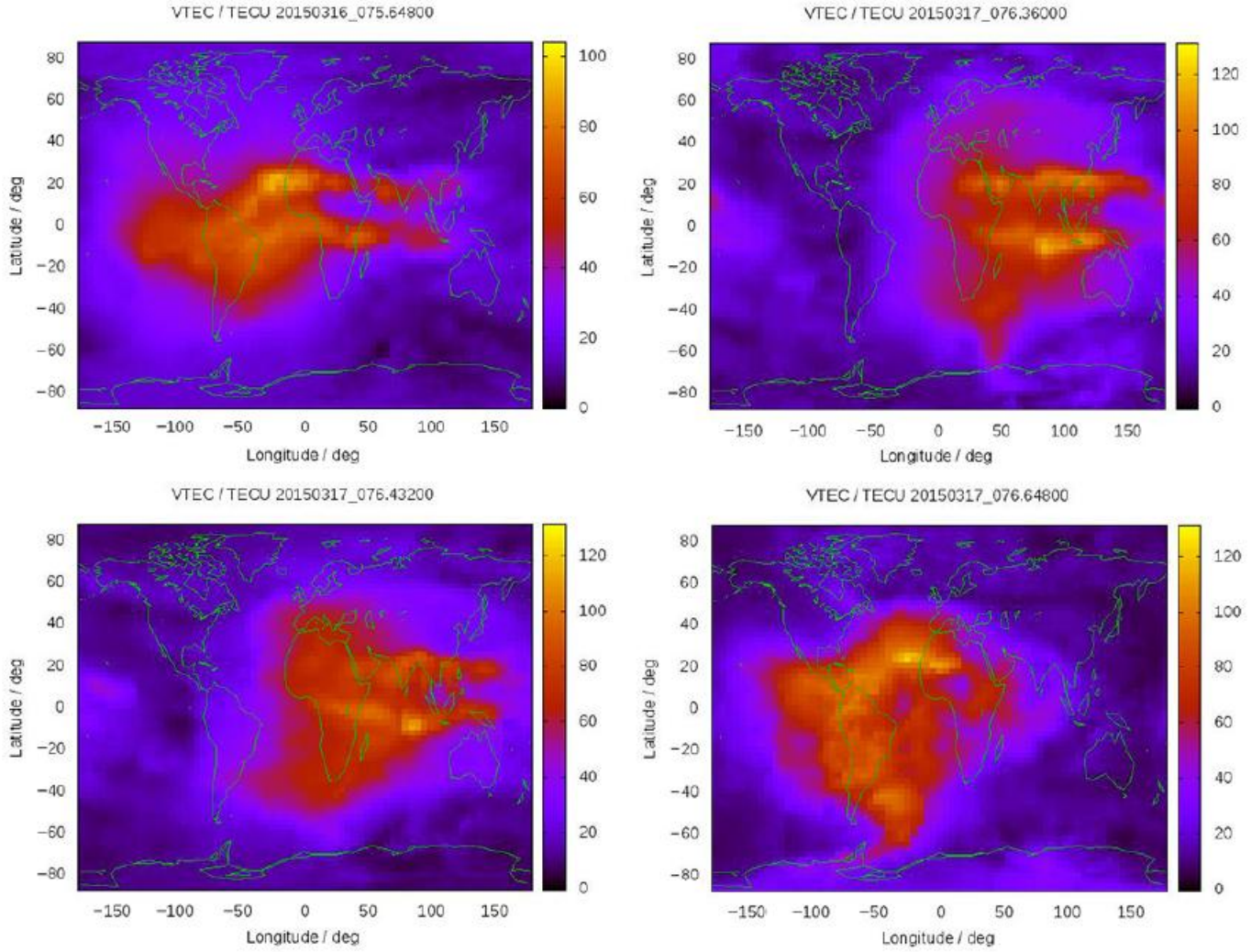

Figure 13. Rapid 15 min resolution VTEC GIMs (labelled UQRG) computed by UPC's TOMION for (from left to right, from top to bottom) 16 March at 18:00 UT and 17 March at 10:00, 12:00 and 18:00 UT.

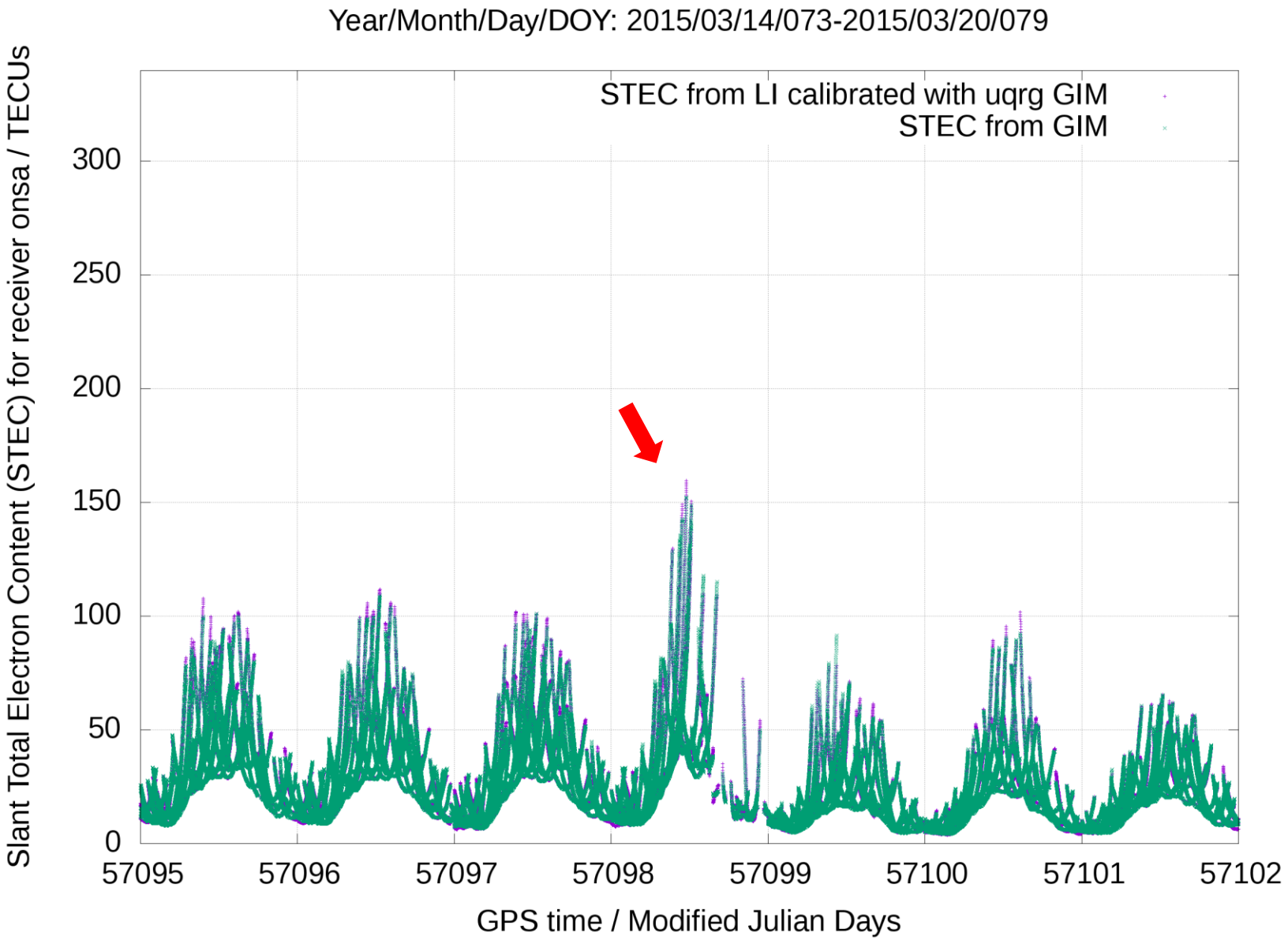
Year/Month/Day/DOY: 2015/03/14/073-2015/03/20/079
STEC from LI calibrated with uqrg GIM
STEC from GIM
Slant Total Electron Content (STEC) for receiver onsa / TECUs
0
50
100
150
200
250
300
57095
57096
57097
57098
57099
57100
57101
57102
GPS time / Modified Julian Days

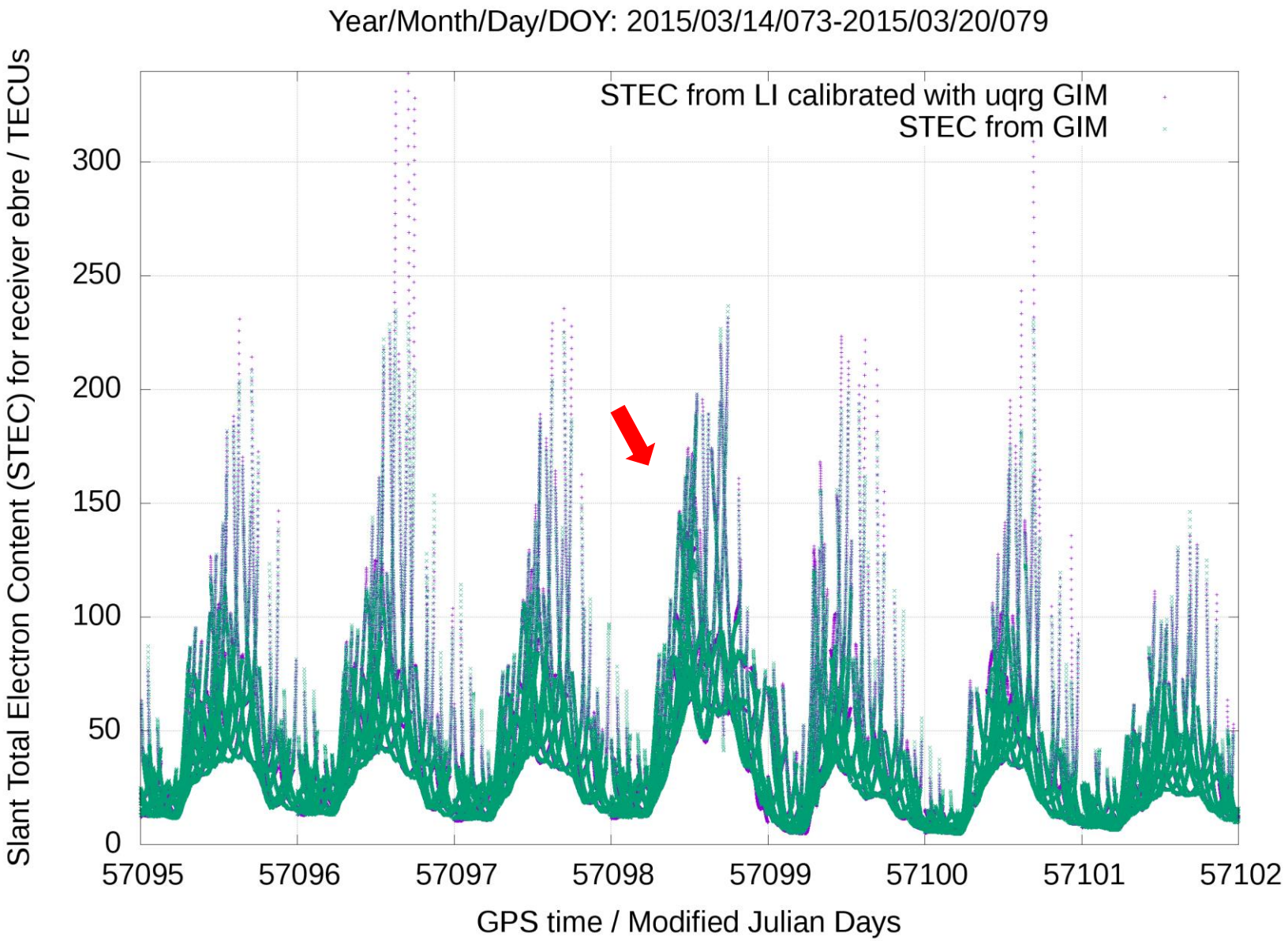
Year/Month/Day/DOY: 2015/03/14/073-2015/03/20/079
STEC from LI calibrated with uqrg GIM
STEC from GIM
Slant Total Electron Content (STEC) for receiver ebre / TECUs
0
50
100
150
200
250
300
57095
57096
57097
57098
57099
57100
57101
57102
GPS time / Modified Julian Days

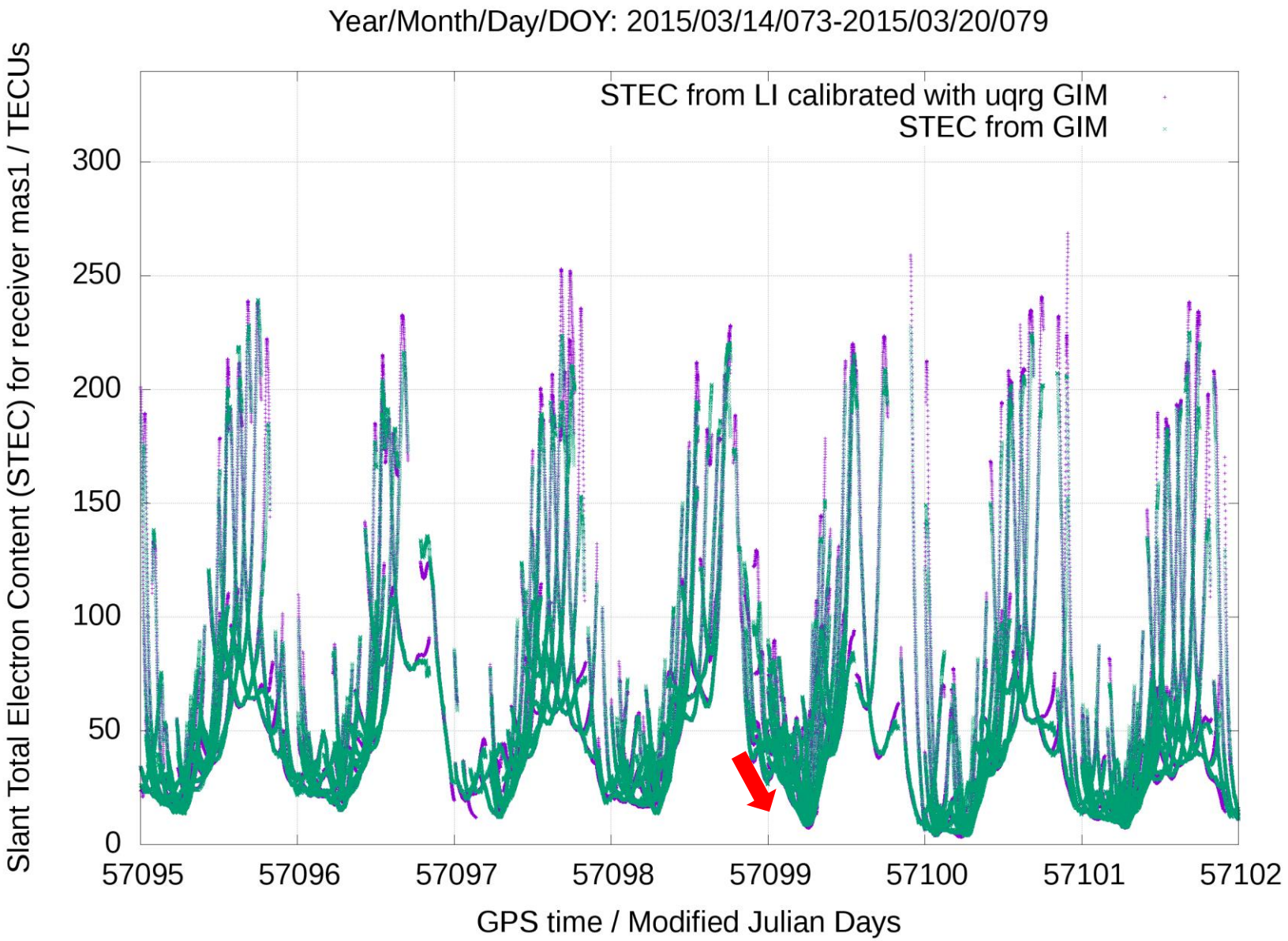
Year/Month/Day/DOY: 2015/03/14/073-2015/03/20/079
STEC from LI calibrated with uqrg GIM
STEC from GIM
Slant Total Electron Content (STEC) for receiver mas1 / TECUs
0
50
100
150
200
250
300
57095
57096
57097
57098
57099
57100
57101
57102
GPS time / Modified Julian Days

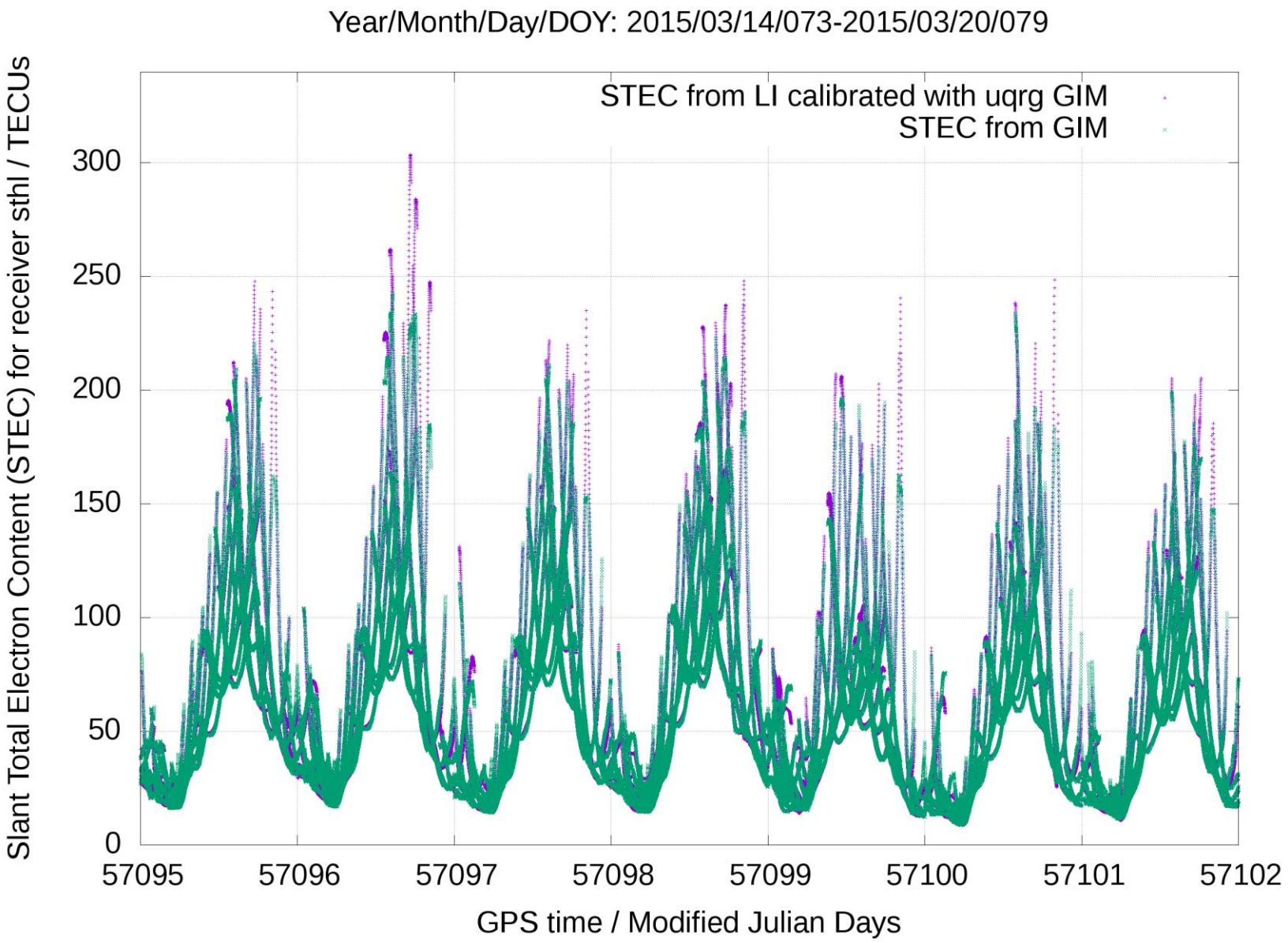
Year/Month/Day/DOY: 2015/03/14/073-2015/03/20/079
STEC from LI calibrated with uqrg GIM
STEC from GIM
Slant Total Electron Content (STEC) for receiver sthl / TECUs
0
50
100
150
200
250
300
57095
57096
57097
57098
57099
57100
57101
57102
GPS time / Modified Julian Days

Layout:

1) [**Motivation**] Precise Agriculture (PA) presentation (EU AUDITOR experiment)

2) [**Background**]: Brief introduction to main identified points of the presentation:
   a) GPS fundamentals: pseudoranges and carrier phases (optional)
   b) Ionospheric electron content
   c) Wide Area Real-Time Kinematic
   d) The International GNSS Service (*optional*)

3) [**One efficient operative system**] Quick introduction to Linux (*optional*)

4) [**New tools for learning and research**] IonSAT Tools (IT), emulating Real-Time (RT) as much as possible (presented on the PA AUDITOR experiment):
   a) *gim2vtec.v2.scr*
   b) *gimrnx2stec.v2.scr*

5) [**IT application to ECLIPSE, FLARE & GSTORM scenarios**] (*optional*).

6) [**Example of RT GPS-ionospheric system**]: UPC-IonSAT since 2012.

7) [**Monitoring of co-seismic generated ionospheric signals]:** Application of RT ionospheric sounding for potential Tsunami warnings), with GNSS dense (Tohoku and mid earthquakes, EQ) and sparse networks (Chile 2015 EQ).

8) [**Conclusions**]

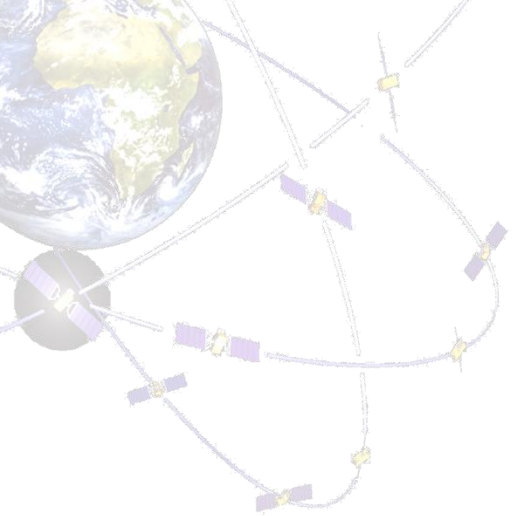

MAIN UPC RT IONOSPHERIC PRODUCTS

Acronym	Ext.Product	Sampling	Latency	Message	References
GSFLAD	GNSS Solar Flare detector in real-time (looking for significant correlation of simultaneous VTEC variation in the daylight hemisphere).	30 sec, globally	30 sec	Message MUSF	An optimized implementation for real-time conditions, evolved regarding to García-Rigo et al. 2007
SDTVAR	Sidereal day-to-day Total Electron Content variability (TECU)	30 sec, per station	30 sec	Message MUSD	Hernández-Pajares et al. 1997
SRMTID	Single Receiver Medium Latitude / Medium Scale Travelling Ionospheric Disturbance index for mid-latitude stations, the mean root square of double diff. in time of STEC for each pair GNSS transmitter-receiver, each 5 minutes (TECU/900 sec^2)	30 sec over each station	~5 min 30 sec	Message MUMT	Hernández-Pajares et al. 2006a-b
ROTI	Rate of Total Electron Content Index (TECU)	30 sec	~180 sec	Message MURO	MONITOR TN-1200

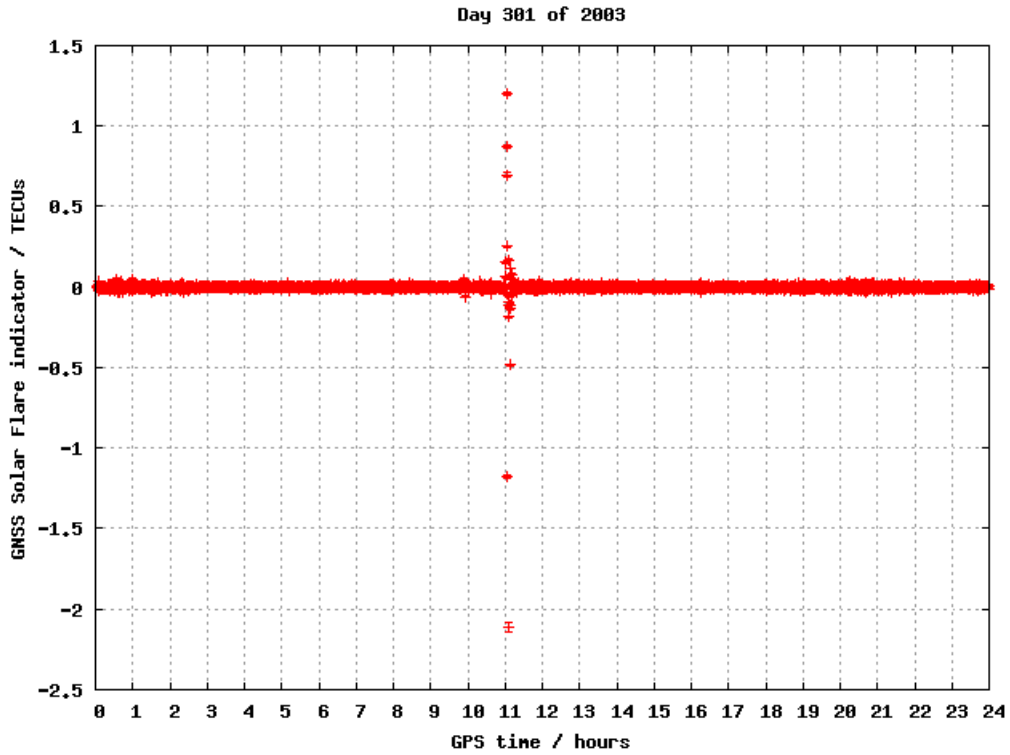

Evolution of GSFLAD index, to be provided by UPC as external MONITOR product, for the big flare triggering the Halloween ionospheric storm, during the day 301 of 2003 (file gsflad.2003.301.musf.gif, see Table 4 for details).

GSFLAD

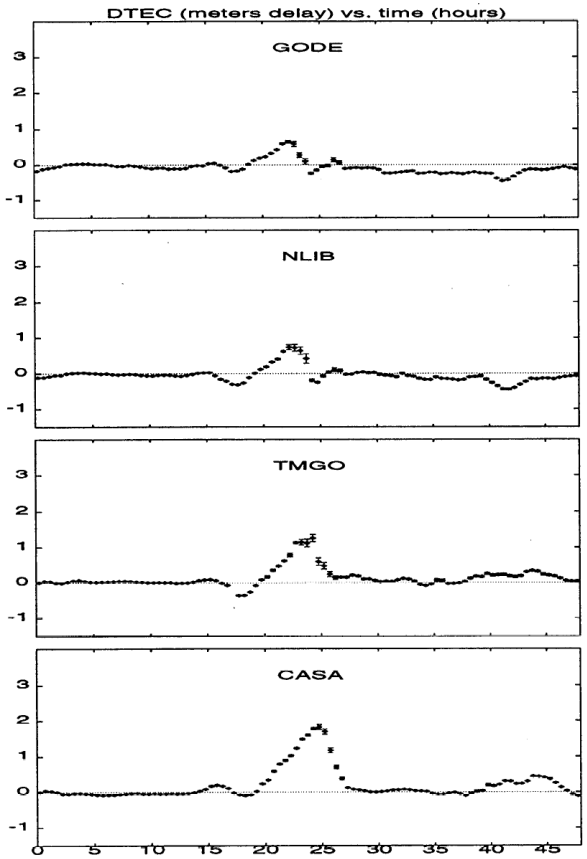

SDTVAR based detection of one ionospheric perturbation seen from four permanent GPS stations in NorthAmerica (ordered from West to East), during days 18 and 19 October 1995, referred to day 17 October (y-axis: VTEC variation in approx. tens of TECU, x-axis time in hours, referred to 18 October 0000 GPS time –source: [Hernández-Pajares et al. 1997]-).

SDTVAR

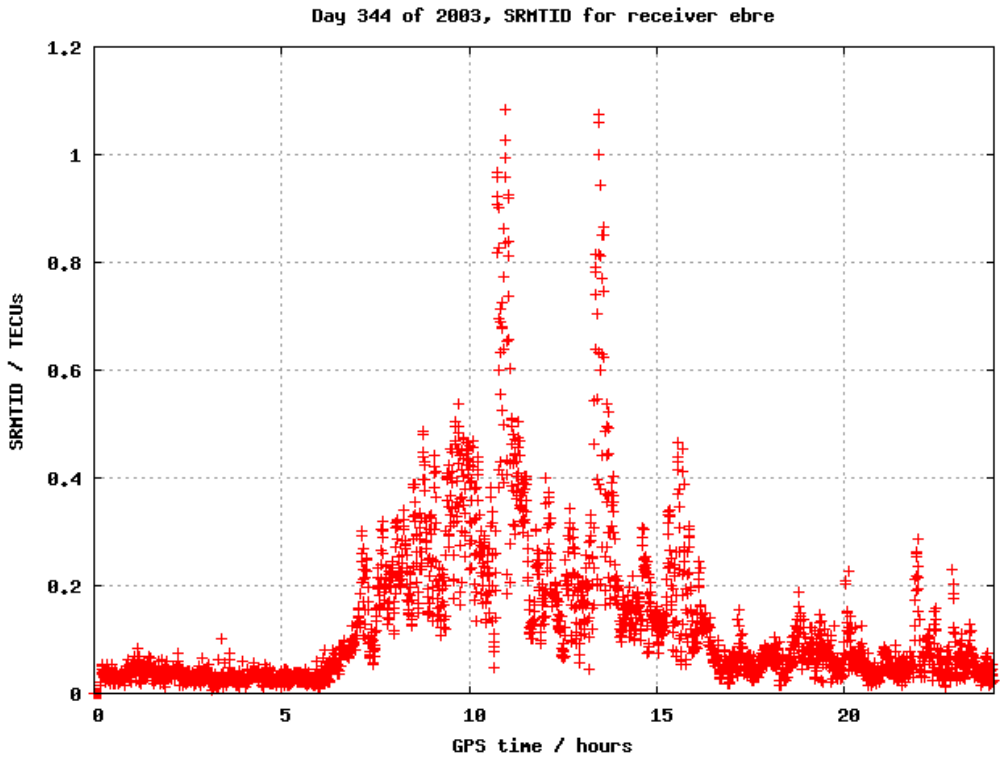

Example of SRMTID index (other external MONITOR product provided by UPC) corresponding to receiver EBRE during day 344 of 2003 (file srmtid.2003.344.mumt.ebre.gif, see Table 4 for details).

SRMTID

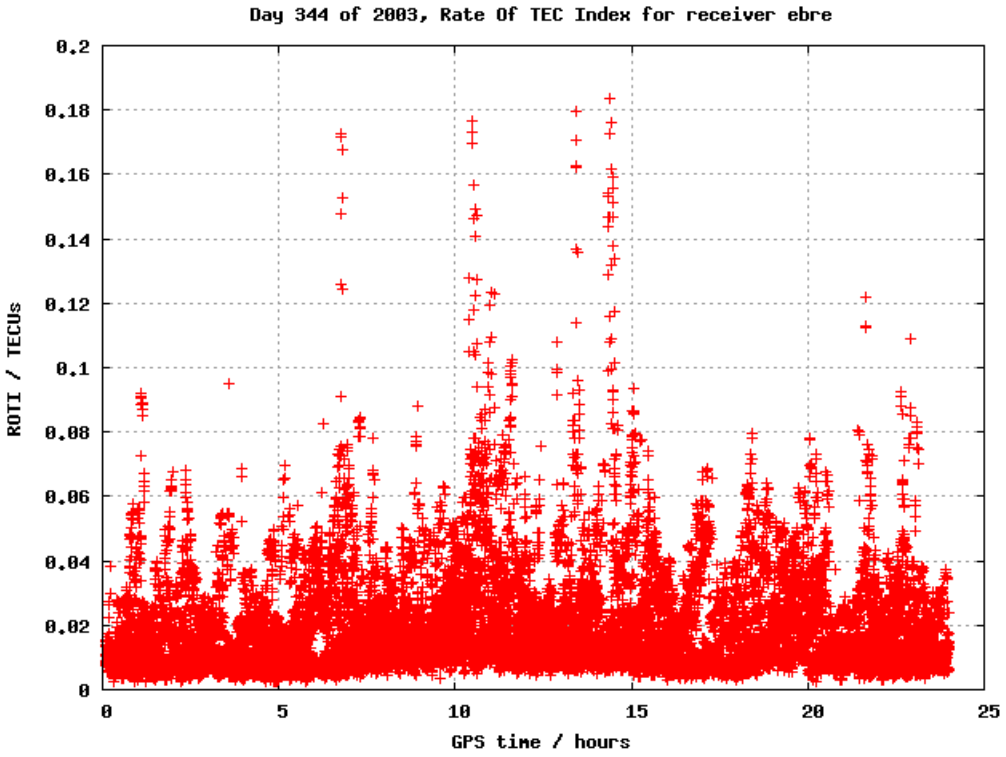

Example of ROTI evolution (additional external UPC product for MONITOR), for IGS receiver EBRE during the day 344 of 2003 (file roti.2003.344.muro.ebre.gif, see Table 4 for details).

ROTI

RT-Iono. UPC-IonSAT computed products: GSFLAI/SOLERA, Solar Flare det. & quantification

- chapman:~% firefox ftp://chapman.upc.es/.monitor/2017/327/NRT
- chapman:~% firefox ftp://chapman.upc.es/.monitor/2017/327/NRT/GSFLAD/plots/gsflad.2017.327.musf.gif

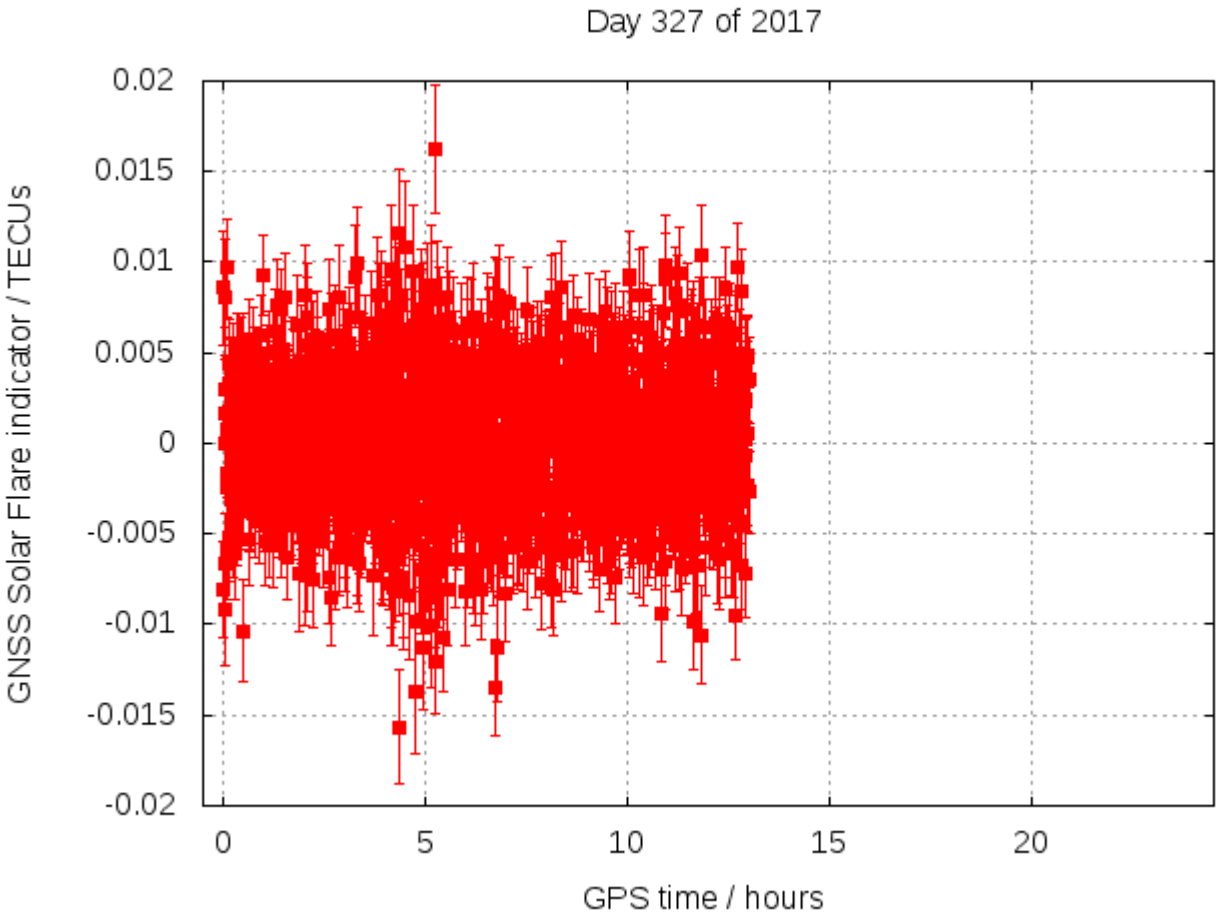

RT-Iono. UPC-IonSAT computed products: VTEC difference regarding previous sidereal day

- chapman:~% firefox

ftp://chapman.upc.es/.monitor/2017/327/NRT/SISTED/plots/sisted.2017.327.muss.gif

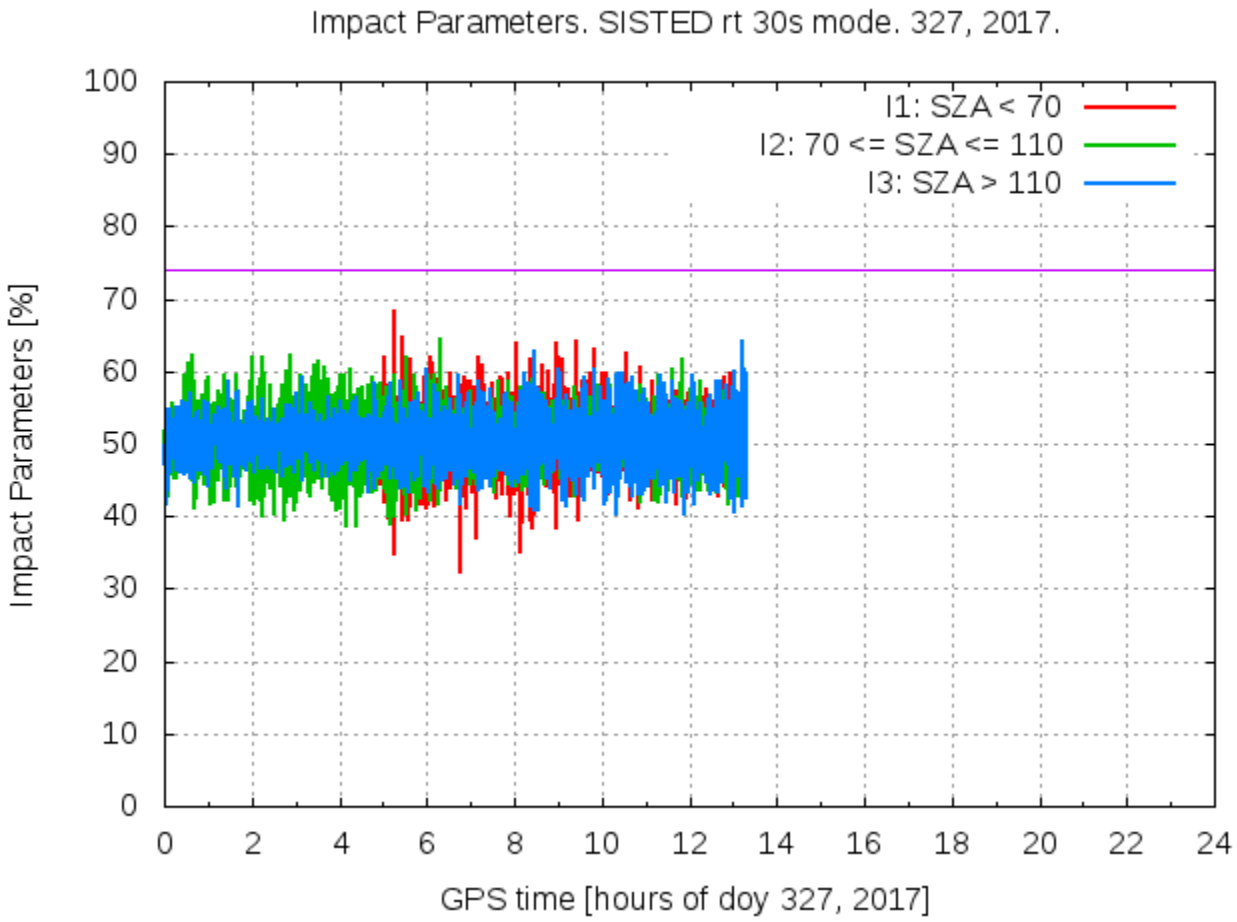

RT-Iono. UPC-IonSAT computed products: Rate Of TEC Index (ROTI) movie since last mid-night

- chapman:~% firefox ftp://chapman.upc.es/.monitor/2017/327/NRT/ROTI/global_plots/animation/w_daily_fixed_range/roti.2017.327.muro.GLOBAL_fixed_range.anim.gif

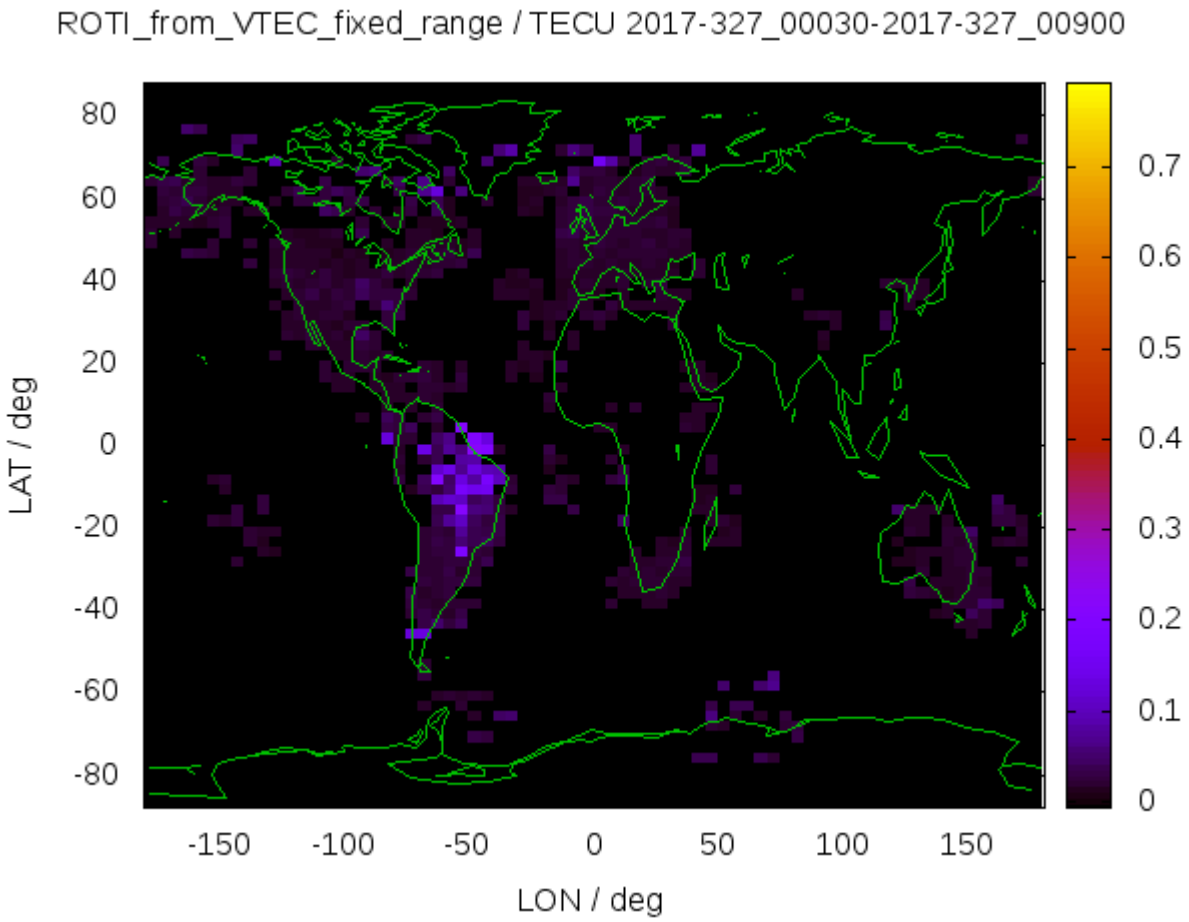

RT-Iono. UPC-IonSAT computed products: VTEC difference regarding previous sidereal day

- chapman:~% firefox

ftp://chapman.upc.es/.monitor/2017/327/NRT/SDTVAR/global_plots/animation/w_daily_fixed_range/sdtvar.2017.327.musd.GLOBAL_fixed_range.anim.gif

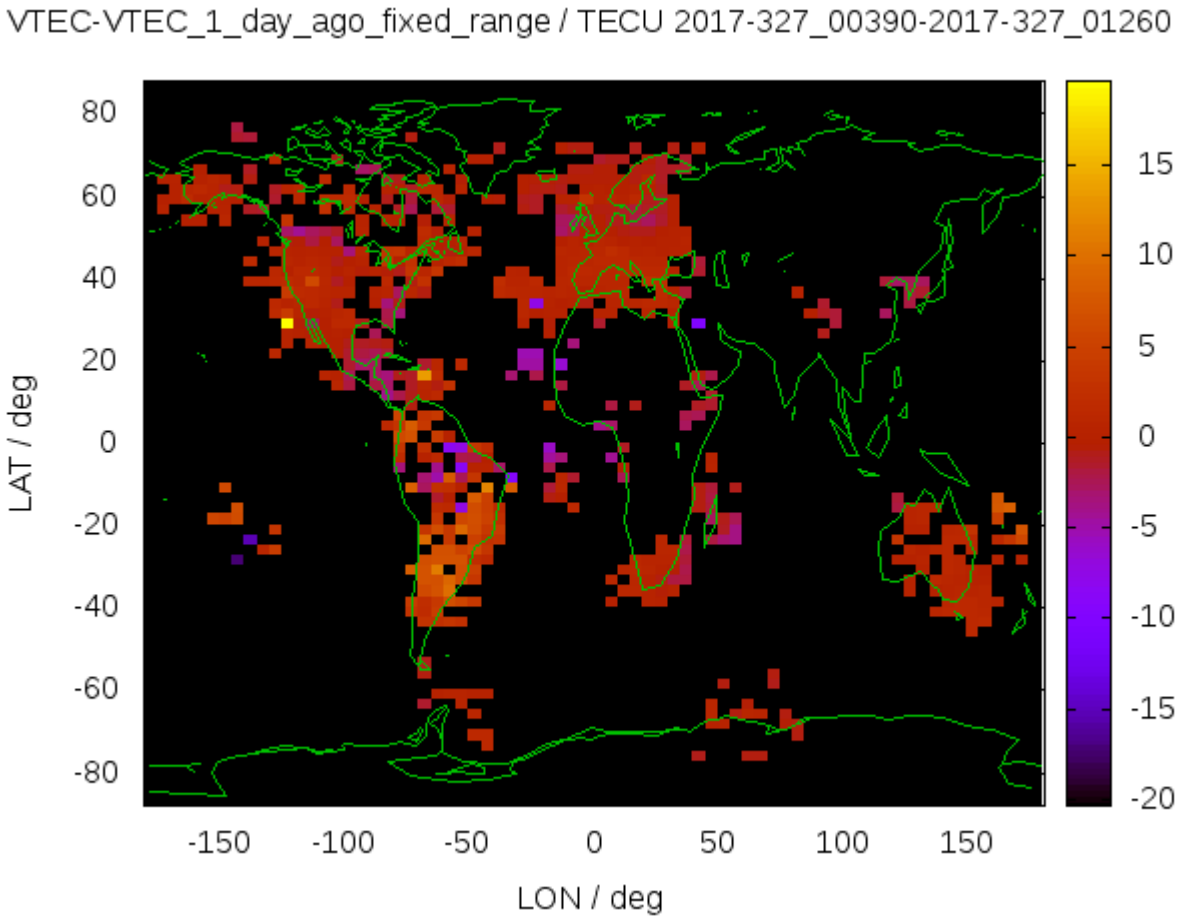

RT-Iono. UPC-IonSAT computed products: VTEC difference regarding previous sidereal day

- chapman:~% firefox

ftp://chapman.upc.es/.monitor/2017/327/NRT/SRMTID/global_plots/animation/w_daily_fixed_range/srmtid.2017.327.mumt.GLOBAL_fixed_range.anim.gif

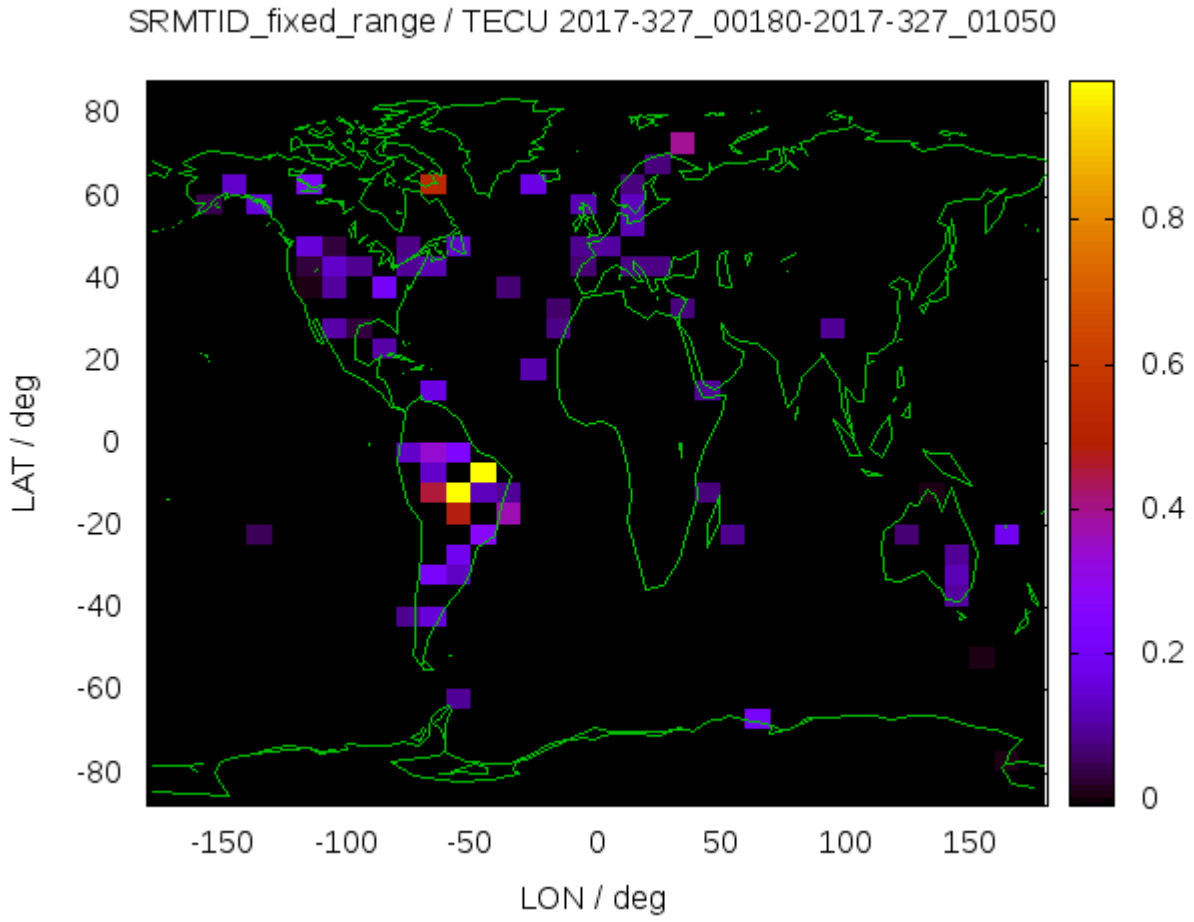

Real-time GIMs

The availability of the IGS RT datastreams with latencies of less than few seconds, containing the multi-frequency, multi-constellation GNSS measurements of hundreds of worldwide permanent receivers, is being crutial to extend the computation of ionospheric models in real-time at continental or global scale.

We are going to summarize some recent initiatives, comparison and results in this regard, since IGS2016 WS:

1) Recent comparison of some RT and NRT VTEC models (Roma-Dollase et al. 2016).
2) Questionnaire & Analysis centers already in position to contribute to a combined IGS RT-GIM soon (starting by the end of 2017, García-Rigo et al. 2017).
3) Thoughts on potential RT combination strategies.
4) Apparent limitation of present ionospheric RTCM message and simple solution.
5) Conclusions and recommendations.

UPC

IonSAT

1) Recent comparison of some RT and NRT VTEC models: *External validation vs VTEC-JASON2*

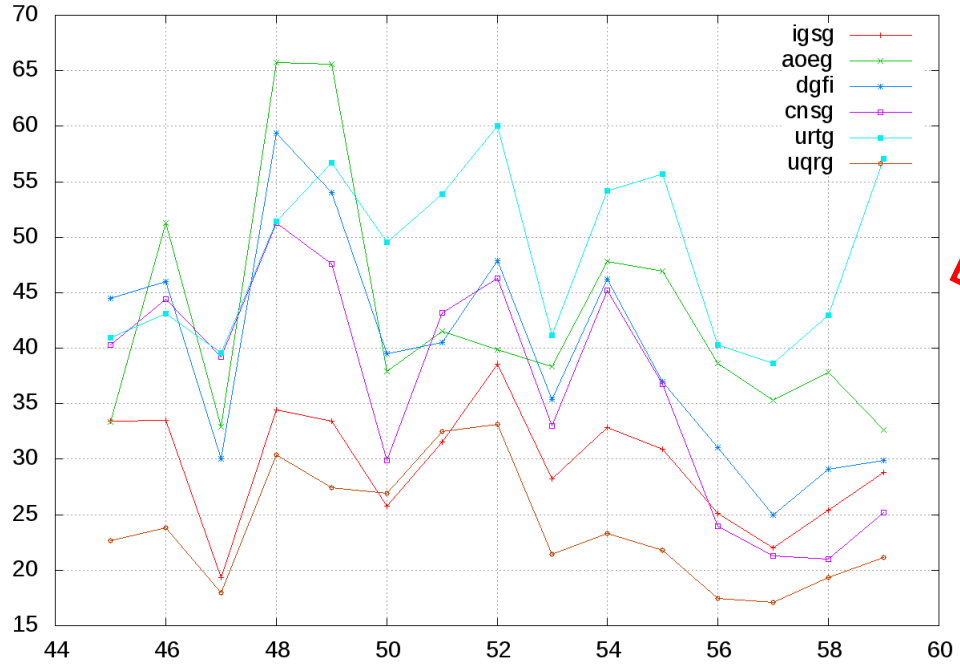

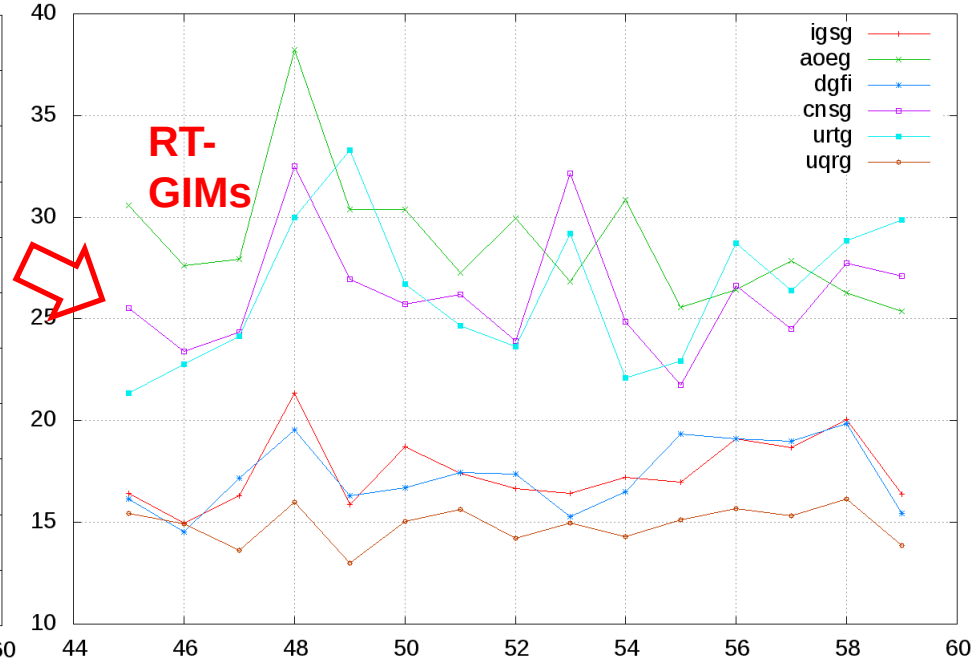

VTEC Relative RMS error (%, taken as reference VTEC-JASON2) vs day of year 2016: Left plot is only for the European region while right plot is worldwide (extracted from Roma-Dollase et al. 2016 @ BSS2016).

1) (Cont) External validation vs dSTEC-GPS @ independent receivers

GIM	RMS [TECU]	RMS max [TECU]	RMS min [TECU]	BIAS [TECU]
AOEG	11.8	22.6	4.8	-1.43
CNSG	9.2	18.8	3.0	0.21
URTG	8.2	14.9	3.4	0.30
DGFI	5.6	10.8	1.8	-0.57
IGSG	6.2	11.6	1.9	-1.01
UQRG	4.6	9.1	1.1	-0.61

RT-GIMs

35 GPS stations have been used. The dSTEC RMS has been calculated for the days of year 2016 from 45 to 59.

2) Questionnaire & Analysis centers to contribute to an IGS RT-GIM:

Questionnaire on Real Time (RT) and Near Real Time (NRT) Data Products performed in the RT-IM WG

Global and regional ionosphere maps of different parameters, available with latencies ranging from 15 minutes down to 2 minutes.

- Vertical Total Electron Content (VTEC)
- F2 layer critical frequency (foF2)
- F2 layer maximum height (hmF2)
- W index
- F2 layer bottomside thickness (B0) and shape (B2)
- Rate of TEC Index (ROTI)

(Most usual, but they may be others we are not currently aware)

2 (Cont.) RT/NRT Data Products Distribution

Only two specific formats for ionosphere data:

- IONEX
- RTCM SSR

Other general purpose formats:

- HDF5
- Web page
- Image
- General Purpose text format: HDF5, CSV, JSON
- ASCII Text data with internal formats

Distribution itself is done through:

- HTTP or web service
- FTP

And only one method exclusive for GNSS/ionosphere data: Network Transport of RTCM over Internet Protocol (NTRIP)

2 (Cont.) Analysis centers which might contribute to a combined IGS RT-GIM soon

CNES already transmits RT-GIM (RTCM iono. Messages from PRODUCTS.IGS-IP NTRIP caster)

UPC-IonSAT already transmits RT-GIM (IONEX format)

WHU already transmits RT-GIM (IONEX format)

CAS is very interested to transmit RT-GIM by the end 2017 for the RT IGS combination. Currently testing the stability of software, accuracy of RT-GIM, and trying to get more global real-time data streams (internal format, but it can be adapted).

NRCAN interested to join future RT-GIM IGS product. Currently, they produce near-real-time global vTEC maps (IONEX and spherical harmonic coefficients, no schedule yet for RTCM format). An offline comparison and comb. is suggested.

3) Thoughts on potential RT ionospheric combination strategies: *i) weighting*

RT Weighting scheme	PROS	CONS
[A] "Self-consistency" (reference: L1-L2 at the same elevation in the same phase continuous arc...)	The same which is being already applied for final and rapid combination with common mapping	We have to wait to the second (elevation-decreasing) half of each arc, i.e. half number of performance estimations...
[B] "dSTEC" (reference: L1-L2 at max. elev. ....)	Well characterized (e.g. recent paper); it only demands to store the reference LI, which is less affected by mapping errors	Same than [A] "Self-consistency"
[C] "RT-dSTEC" (The first L1-L2 measurement in the arc is taken as reference)	Full data availability, only one data stored per arc	The low elev. Ref. STEC is typically the (or one of the) very bad estimated ones, affecting all the time series.
[D] = [C] (during the ascending arc part) + [A] (during the descending part)	Full data availability, only one memory record per arc (updated at max. elevation).	Potential "overweight" of the first low-elevation reference ray (potentially mitigated with elev. mask).

dSTEC-GPS layout

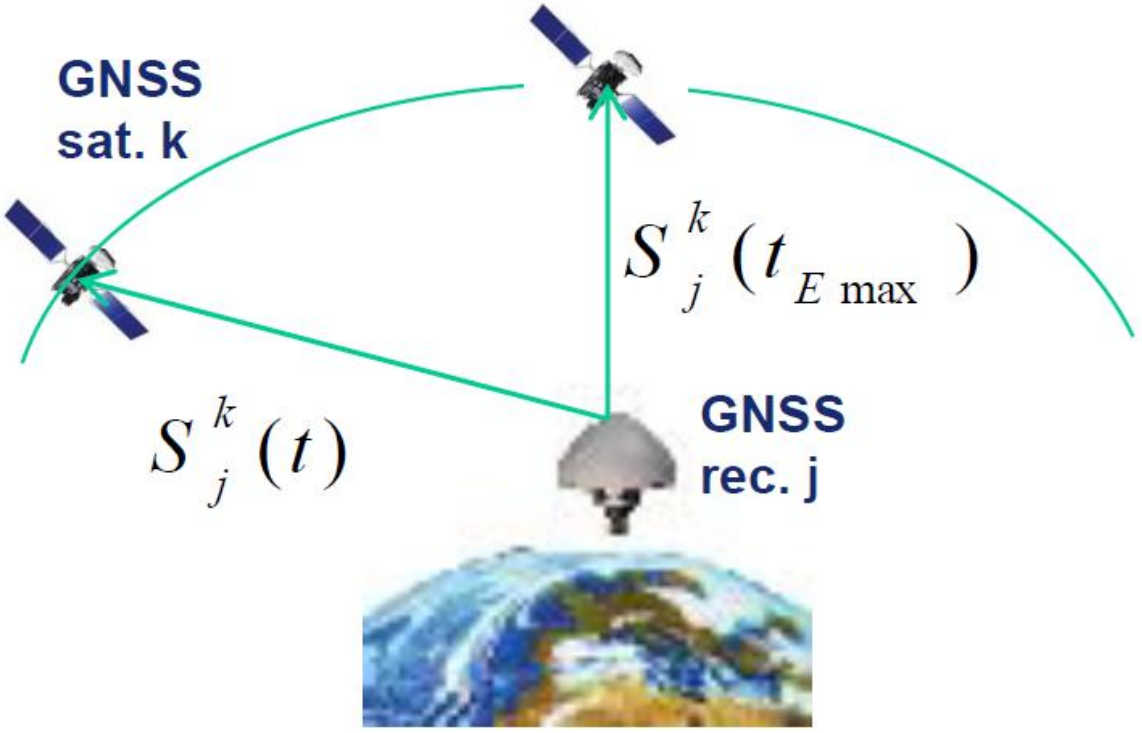

$$\Delta S_O \equiv S_j^k(t) - S_j^k(t_{E\,max})$$
$$\approx M \cdot V(t) - M_{E\,max} \cdot V(t_{E\,max})$$

3) (Cont.) Other considerations in RT ionospheric weighting strategies

ii) Weighting directly the SH coefficients (taking into account the analysis centers contributing to such order degree) seems feasible (due to the corresponding orthogonality of the basis function on the complete ionosphere) and faster.

iii) Performance temporal prediction of weights: This can be an important aid for the weight estimation, in order to avoid any latency inconvenient. A potential low / variable degree polynomial might be used for this task among other posibilities.

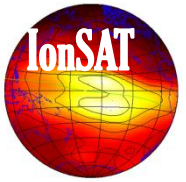

4) Apparent limitation of present ionospheric RTCM message and simple solution: *RTCM VTEC*

- RTCM currently only defines one way to provide VTEC information to the users, as a spherical harmonic series to a given order and degree (message type 1264).
- At some point at least it was under discussion as far as we know to have a message type with data representing a grid, equivalent to the IONEX file content.
- In our knowledge, the maximum order and degree allowed by the standard is 16.
- We want to analyze which is the loss of precision for the end user by using spherical harmonics instead of directly the IONEX content.

4.(Cont) *Importance of using the right SH order/degree*

ORIGINAL GIM
(UQRG1480.17i, 00UT)

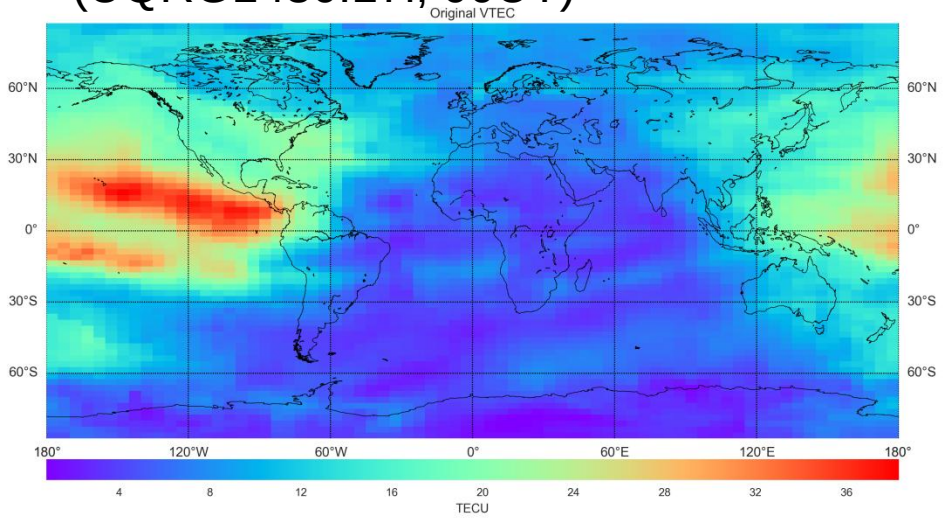

Reconstructed GIM **13% error (deg.=8 & ord.=8)**

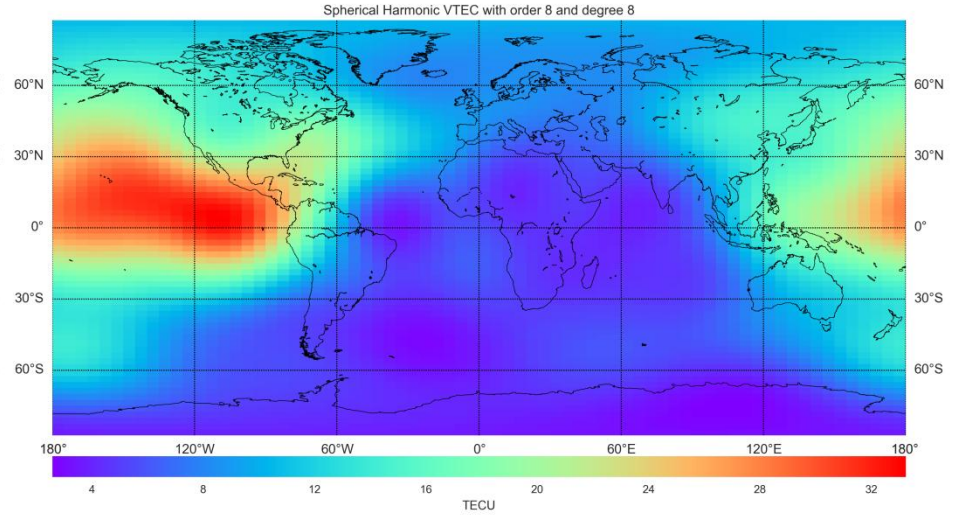

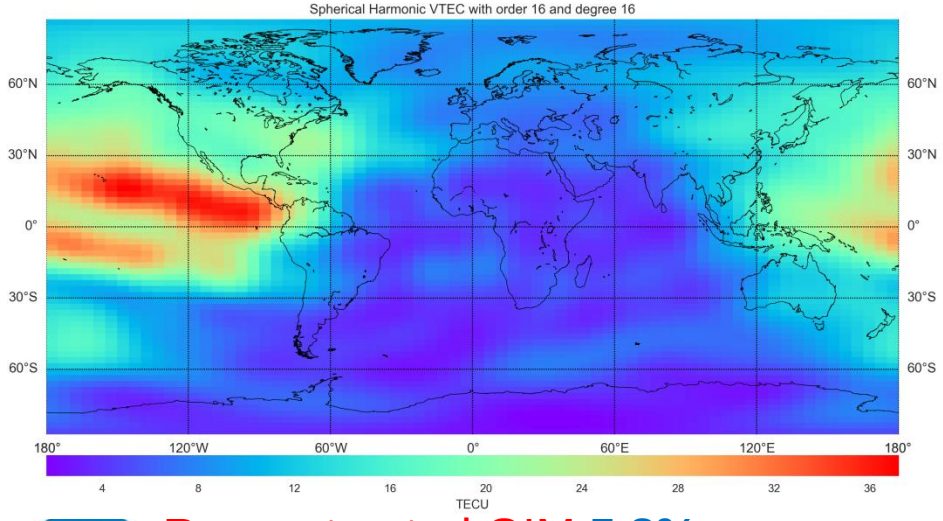

Reconstructed GIM **5.8% error (deg=16 & ord=16, max. RTCM?)**

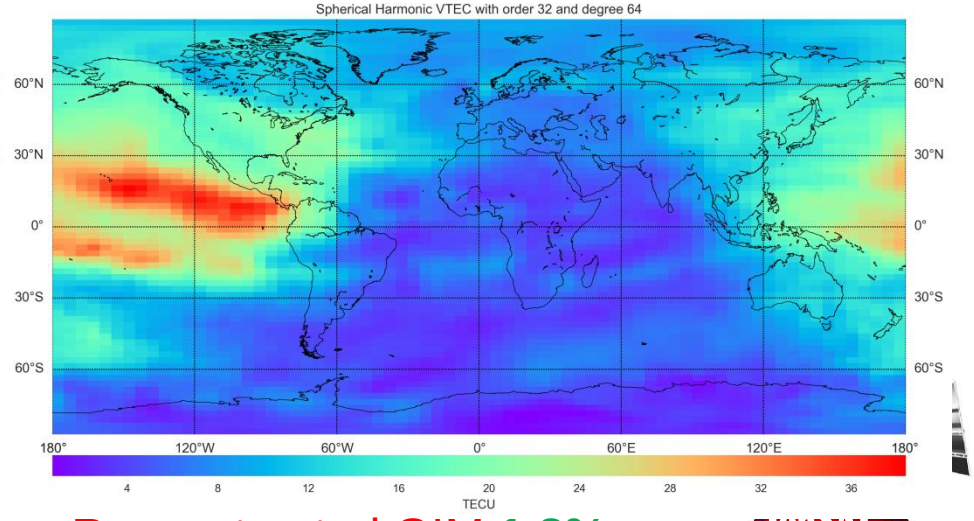

Reconstructed GIM **1.8% error (degree=64 & order=32)**

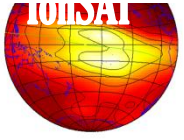

4.(Cont) *Distribution of relative errors*

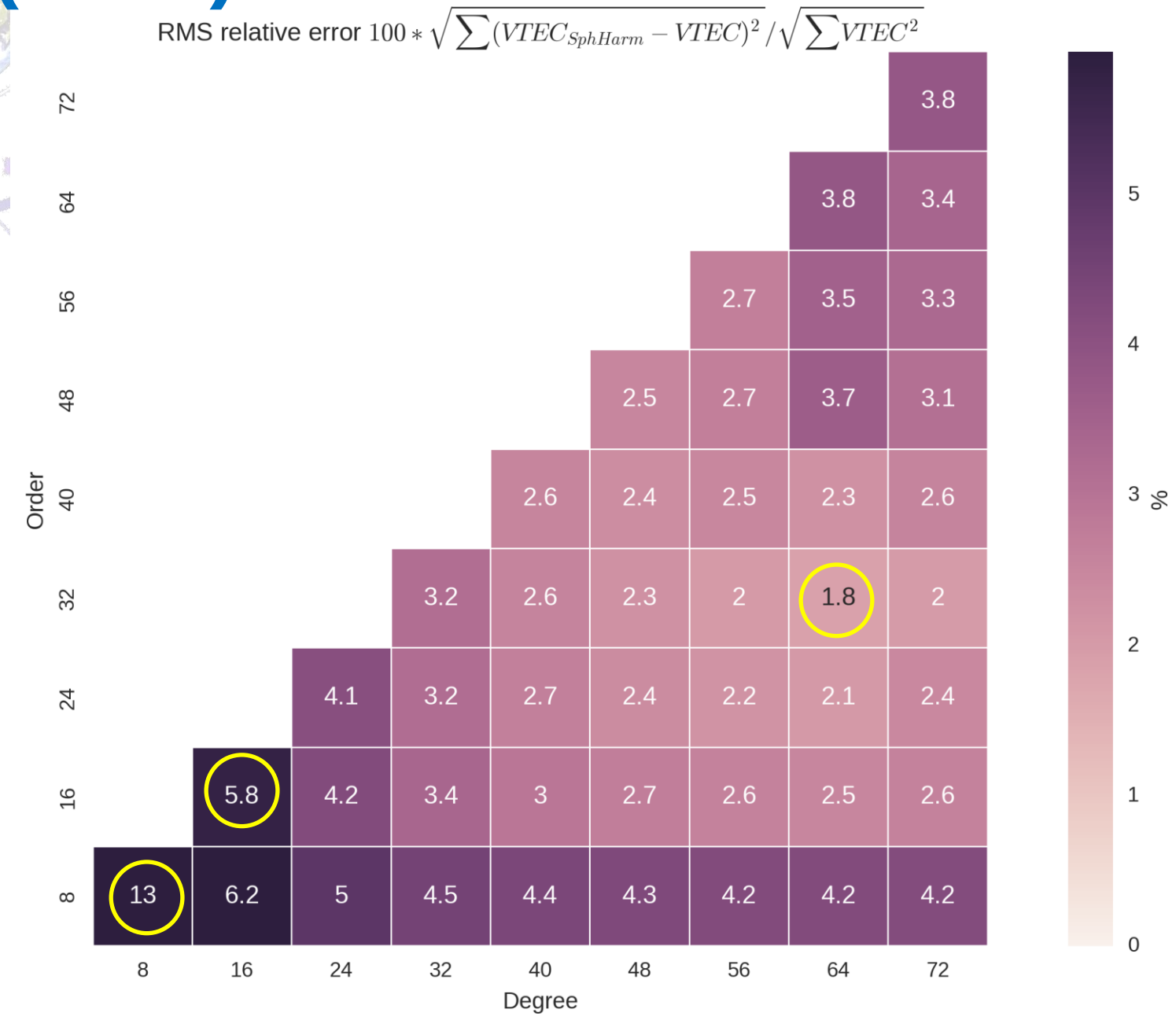

UPC

IonSAT

Conclusions / recomendation

- The availability of RT-IGS GNSS is already allowing the continuous monitoring of ionospheric electron content distribution (RT-GIMs), variability (ROTI) and Space Weather response (e.g. EUV flux rate during solar flares), among practical applications (precise farming).
- We have focused on new results which can facilitate the generation of a combined IGS RT-GIM soon:
  1) Recent comparison of some RT and NRT VTEC models.
  2) Analysis centers ready or interested to contribute to a combined IGS RT-GIM soon.
  3) Initial discussion of potential RT combination strategies.
- Apparent limitation (order & degree not larger than 16) of present ionospheric RTCM message and simple solution.
- Recommendation: to increase maximum supported RTCM SH order & degree

UPC

IonSAT

UPC-IonSAT RT-GIMs (preliminar product): Active RT datastreams

- chapman:~% firefox http://chapman.upc.es/tomion/real-time/quick/last_results/
- chapman:~% firefox http://chapman.upc.es/tomion/real-time/quick/last_results/active_stations.spherical_coordinates

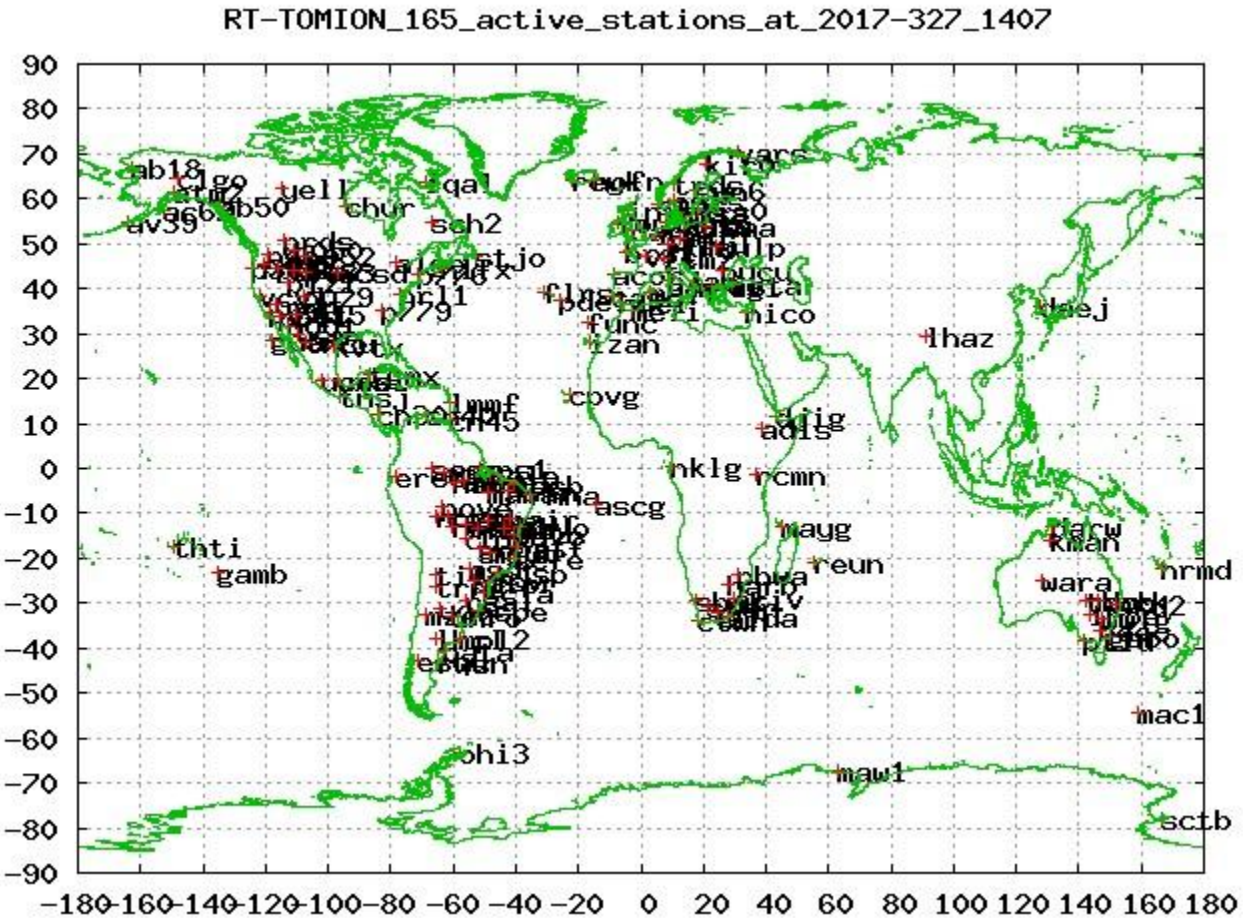

Preliminary UPC-IonSAT RT-GIMs (still under assessment and with an important room for improvement)

- chapman:~% firefox http://chapman.upc.es/tomion/real-time/quick/last_results/
- Then select the most recent (less than 30 minutes old when the system is working well)

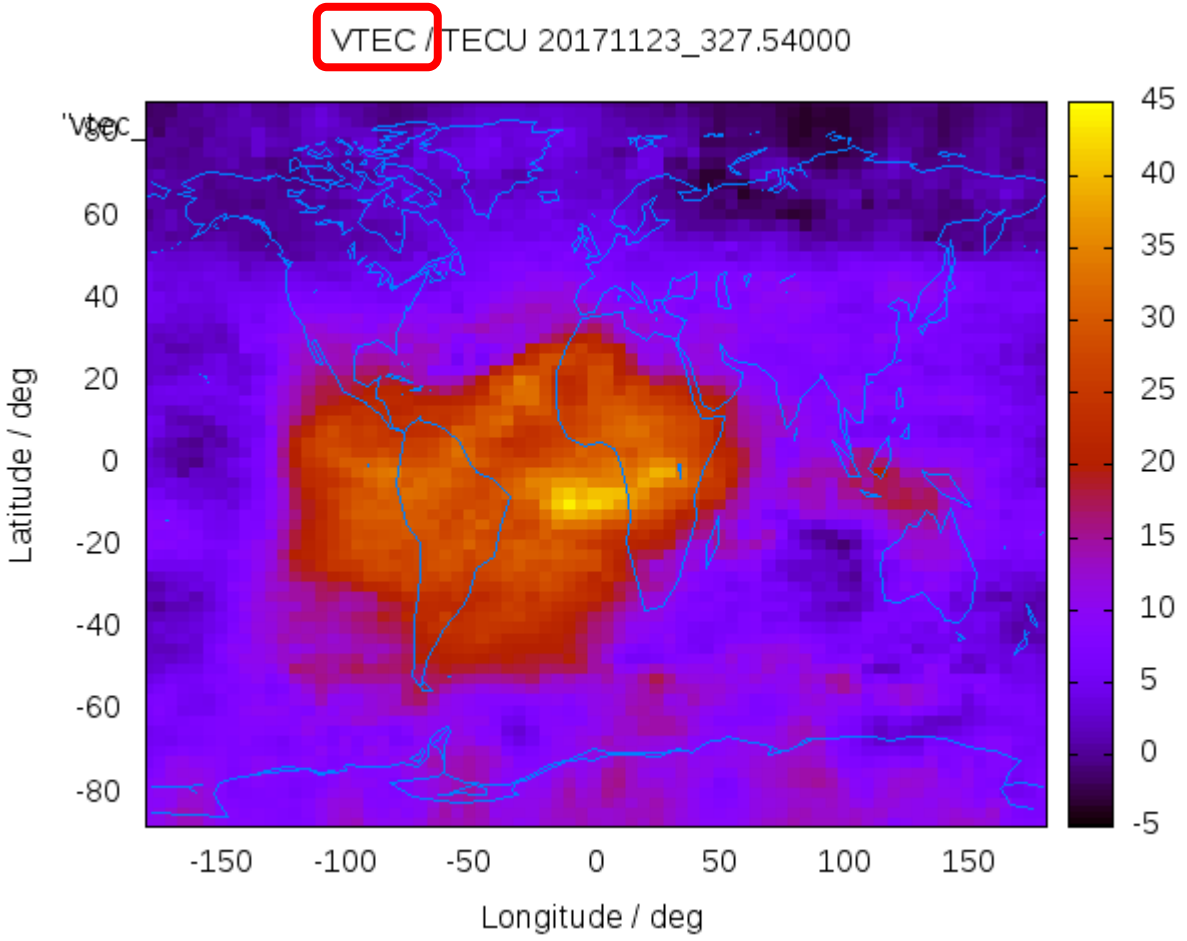

Preliminary UPC-IonSAT RT-GIMs (still under assessment and with an important room for improvement)

- chapman:~% firefox http://chapman.upc.es/tomion/real-time/quick/last_results/
- Then select the most recent (less than 30 minutes old when the system is working well)

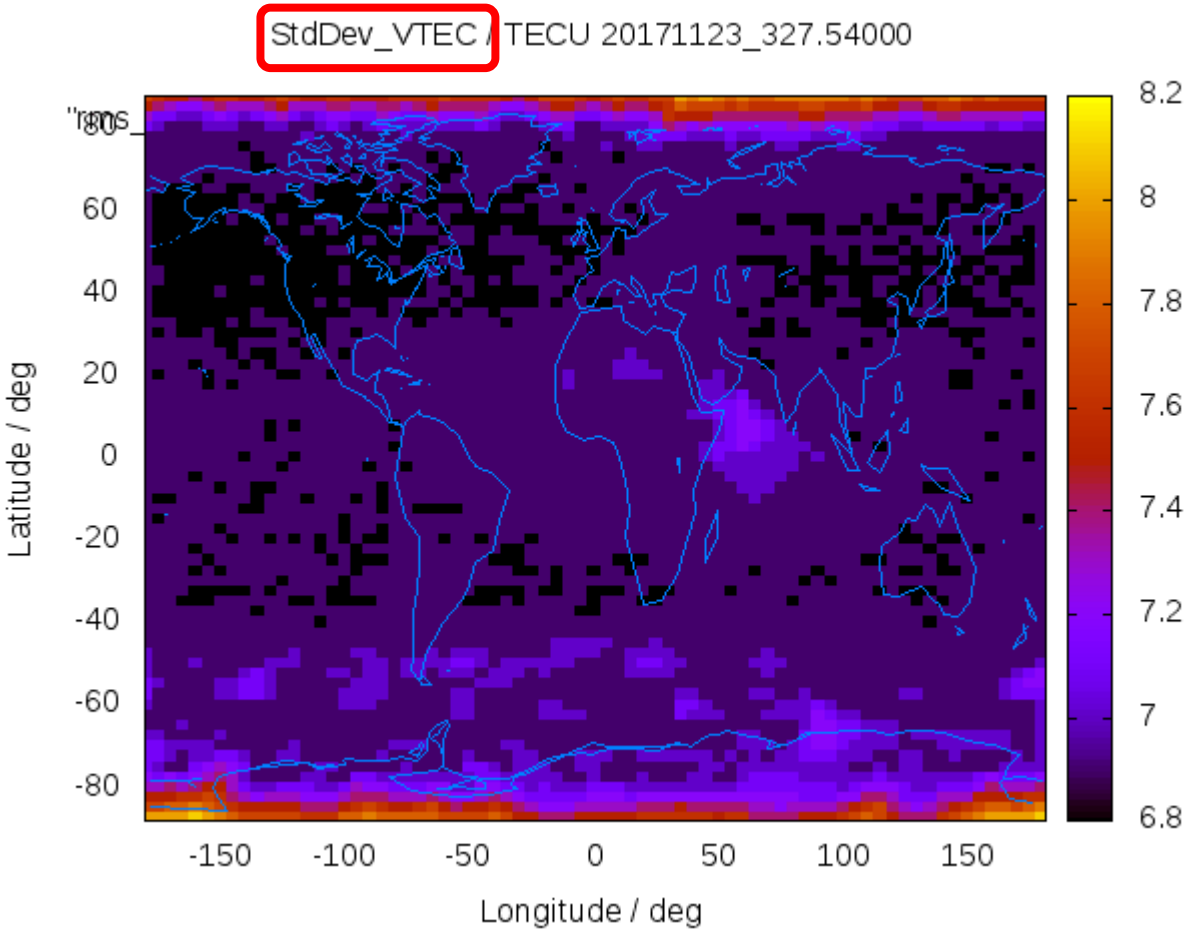

Layout:

1) [**Motivation**] Precise Agriculture (PA) presentation (EU AUDITOR experiment)

2) [**Background**]: Brief introduction to main identified points of the presentation:
   a) GPS fundamentals: pseudoranges and carrier phases (optional)
   b) Ionospheric electron content
   c) Wide Area Real-Time Kinematic
   d) The International GNSS Service (*optional*)

3) [**One efficient operative system**] Quick introduction to Linux (*optional*)

4) [**New tools for learning and research**] IonSAT Tools (IT), emulating Real-Time (RT) as much as possible (presented on the PA AUDITOR experiment):
   a) *gim2vtec.v2.scr*
   b) *gimrnx2stec.v2.scr*

5) [**IT application to ECLIPSE, FLARE & GSTORM scenarios**] (*optional*).

6) [**Example of RT GPS-ionospheric system**]: UPC-IonSAT since 2012.

7) [**Monitoring of co-seismic generated ionospheric signals]:** Application of RT ionospheric sounding for potential Tsunami warnings), with GNSS dense (Tohoku and mid earthquakes, EQ) and sparse networks (Chile 2015 EQ).

8) [**Conclusions**]

Scenario A: Dense wide networks (GEONET, SCIGN). Two case-studies of major and mid earthquakes

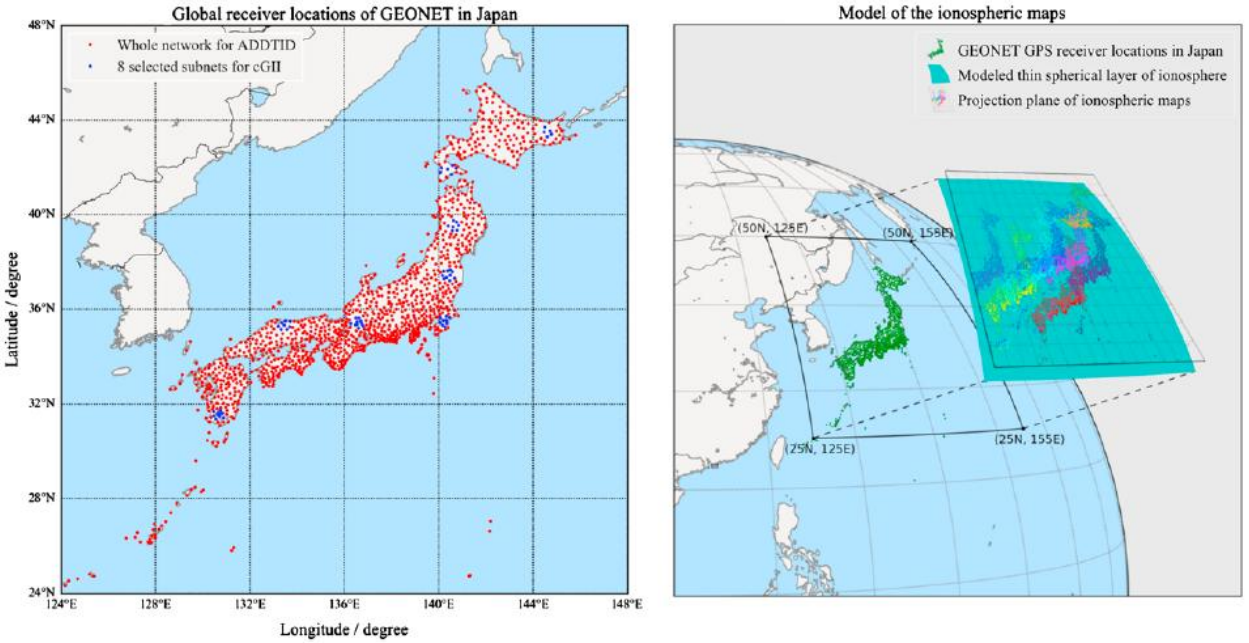

Figure 1. (left) Distribution of GPS receivers in the Japan GEONET network and (right) IPPs distribution in the ionospheric map for different satellites.

(Extracted from Yang, H., E. Monte-Moreno, and M. Hernández-Pajares (2017), *Multi-TID detection and characterization in a dense Global Navigation Satellite System receiver network,* J. Geophys. Res. Space Physics, 122, doi:10.1002/2017JA023988.)

Ionospheric signature associated to the major earthquake Tohoku / Tsunami (from d2VTEC300s)

➢firefox ftp://newg1.upc.es/.4dimitar_and_sergey/201309_30.first_study_on_Fukushima_events/d2Va_at_diff_tscales.2011.070.0300.2.gif

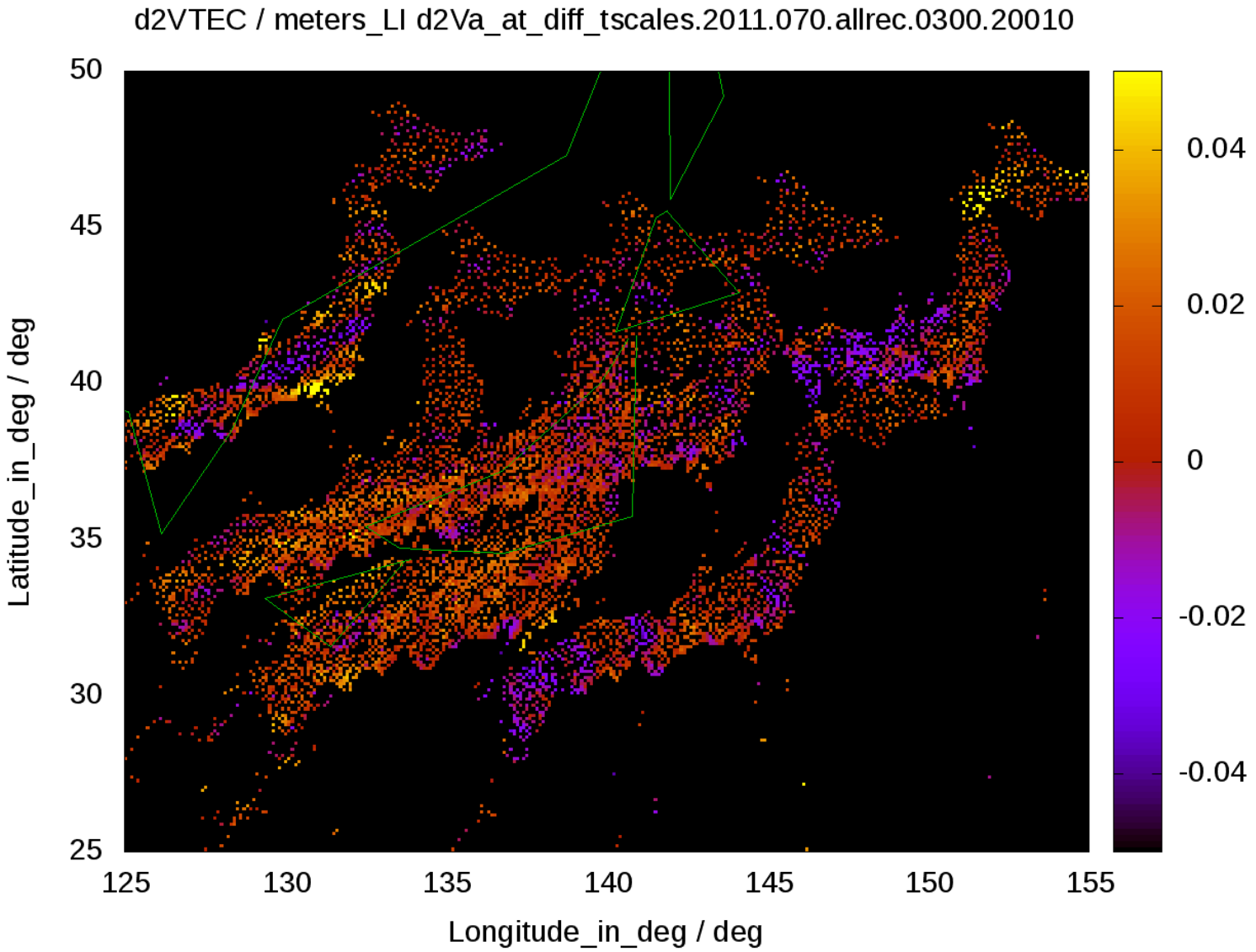

Circular ionospheric waves approx. centered in middle intensity earthquake epicenter happens few hundreds of second after

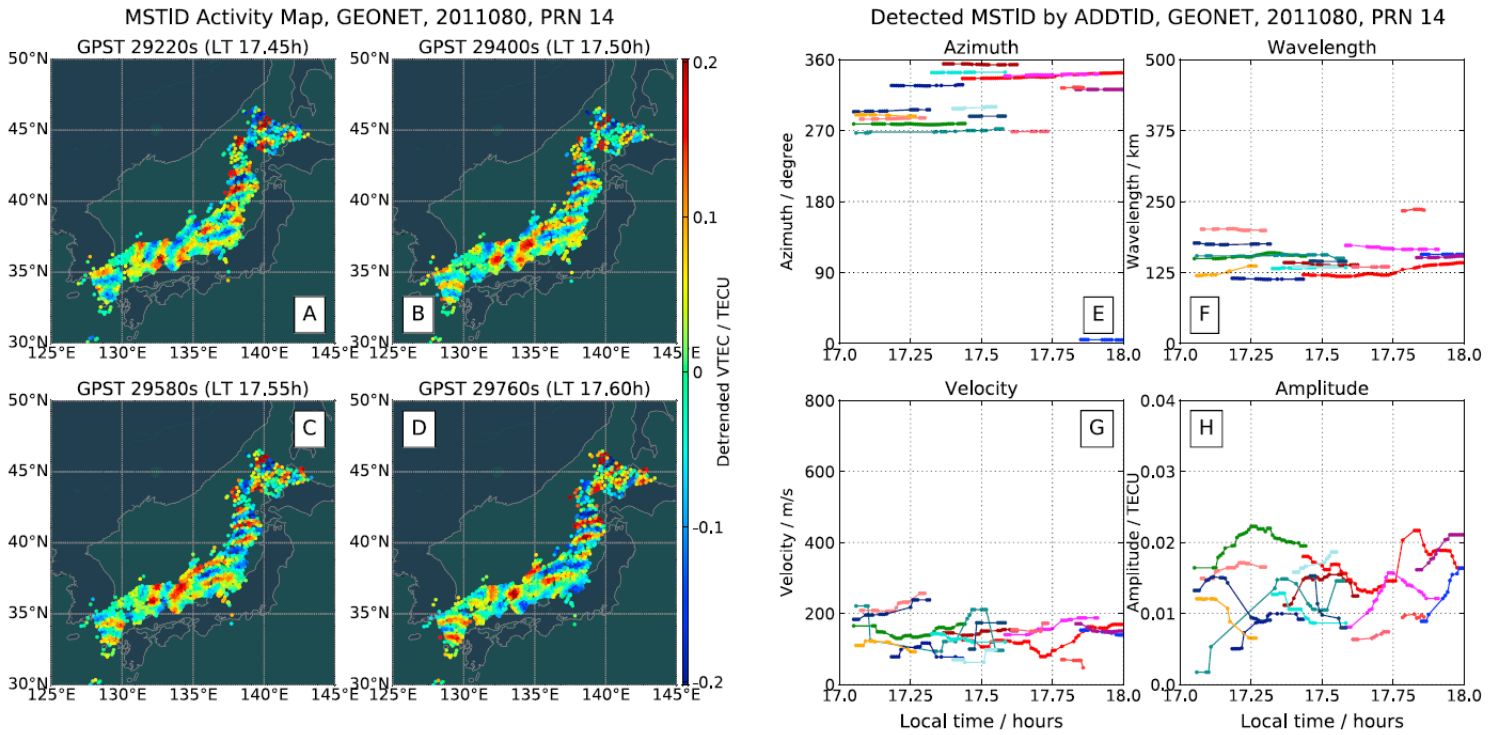

Figure 11. Circular-like MSTIDs during the evening solar terminator about 17:30 LT, from the GEONET, for satellite PRN 14, on the 80th day of 2011. (a–d) Circular MSTID in the detrended VTEC maps (in TECUs) at evening time (17:27–17:36 LT), for four snapshots at GPS time 29,220, 29,400, 29,580, and 29,760 s. (e–h) The time evolution of the estimated parameters during the time interval 17:00–18:00 LT, by azimuth, wavelength, velocity, and amplitude.

(Extracted from Yang, H., E. Monte-Moreno, and M. Hernández-Pajares (2017), *Multi-TID detection and characterization in a dense Global Navigation Satellite System receiver network,* J. Geophys. Res. Space Physics, 122, doi:10.1002/2017JA023988.)

Comments to Fig.11 of Hang et al. 2017

- This finding, obtained thanks to the extreme sensitivity of the new ADDTID technique, might be generated by two earthquakes of magnitude M4.6 and M4.9 in a 3 min interval (recorded at respectively 17:29 and 17:26 LT in U.S. Geological Surve (USGS) [2011a, 2011b]). These earthquakes occurred a few hundred seconds before the detected waves and are compatible with the center of the circular ionospheric wave. A similar precedent of a delay between occurrence of the 2011 Japan Tohoku earthquake and the circular wave disturbances detected over Japan is reported in Tsugawa et al. [2011]. In this case the delay was of about 7 min after the earthquake.

- The novelty of this finding, regarding previous works performed on major earthquakes (with magnitudes greater than 6), is the detection by the perturbation on the ionosphere despite the relative low magnitude of the earthquake.

Scenario 2: Wide not dense GPS network. Case study of major Illapel earthquake on Chile, 2015

- Eartquake happened at Chile on Sep., 16th 2015, 22:54 UTC.

- Gathered from dual-frequency GPS observations taken on few dozens of Argentina & Chile permanent GPS receivers.

- The next results were mainly computed from double-time-difference of VTEC @ 300s (i.e. d2VTEC300s, mainly focused on ionospheric periods from 400 to 1200s).

Method 1: Time evolution of map of detrended VTEC values.

- The distribution of bandwidth filtered detrended VTEC values (d2V) was not providing a direct evidence of circular waves associated with the Chile earthquake of Sep., 16th 2015[*], on the contrary than for the Tohoku earthquake of March, 11th 2011[**].
- This might be related with a simultaneous coincidence of much lower density of permanent receivers in Chile/Argentina (compared with the +1200 GNSS rec. on GEONET network on Japan), and with a lower ionospheric effect, in between the signature of the southern peak of the equatorial anomaly
- [*] ftp://newg1.upc.es/.4dimitar_and_sergey/201509_29.Chile_detrended_VTEC_maps/2015/259/d2Va_at_diff_tscales.2015.259.0300.8.gif
- [**] ftp://newg1.upc.es/.4dimitar_and_sergey/201309_30.first_study_on_Fukushima_events/d2Va_at_diff_tscales.2011.070.0300.2.gif

Method 2: detrended VTEC on a epicenter distance vs. main shock time span 3D plot

- In such situation we have reduced one dimension from (lon,lat,time,d2V) to (dtime,distance,d2V) where “dtime” is the time elapsed since the earthquake mainshock and “distance” is the distance of the ionospheric pierce point to the earthquake mainshock epicenter, following the procedure of Lognonne et al. 2006.

Reference: *Lognonné, P., Artru, J., Garcia, R., Crespon, F., Ducic, V., Jeansou, E., ... & Godet, P. E. (2006). Ground-based GPS imaging of ionospheric post-seismic signal. Planetary and Space Science, 54(5), 528-540.*

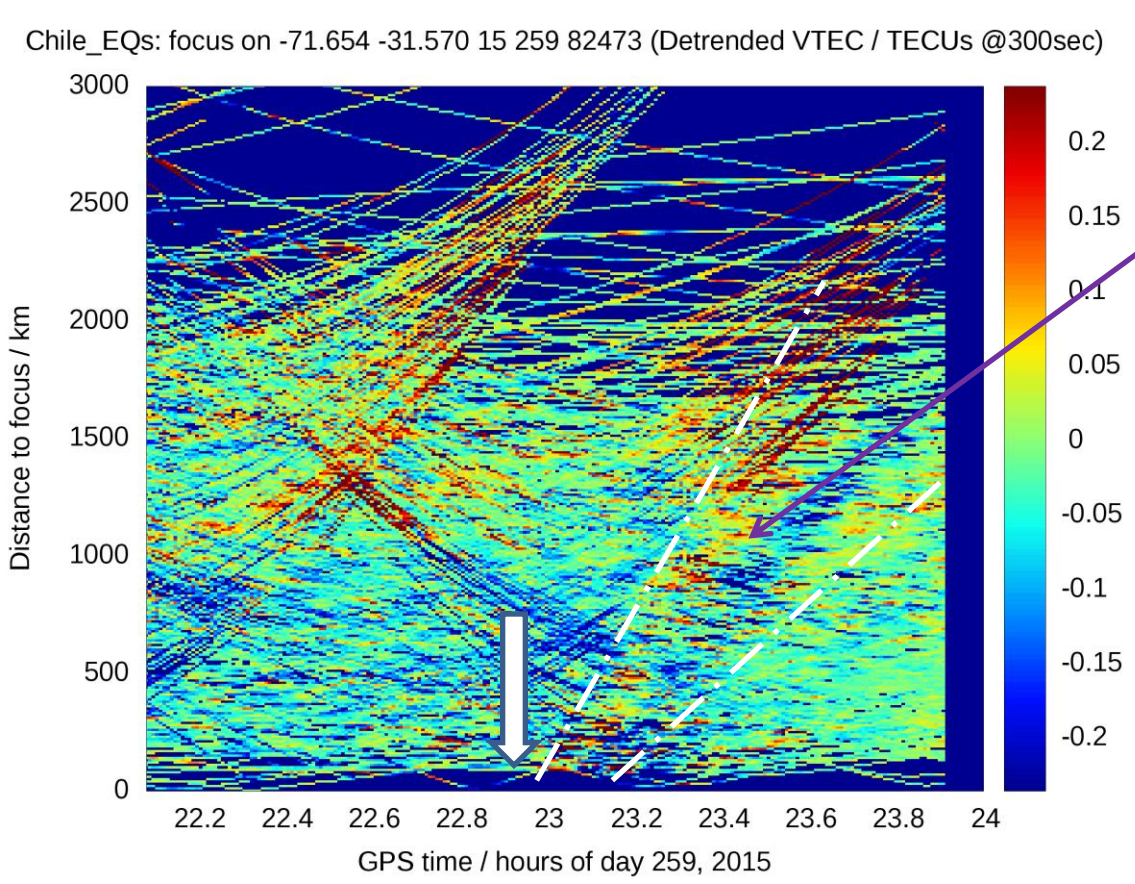

(A) Co-seismic circular wave signature with similar parameters than in previous EQs

One and half cycle of circular waves clearly seen starting at ~23:03, about 8 minutes after the Illapel EQ main shock (22:54:33 UTC = 22:54:50 GPStime = 82490 sec) , showing a range of velocities of 1000 km in 0.3 hours = 0.93 km/s to 1000 km in 0.55 hours = 0.51 km/s) and wavelength from ~100 km close to the epicenter to ~200 km at 1000 km.

Such distribution is very similar to the distribution observed at Hokkaido EQ. by Lognonné et al. (~600 s. after main shock and with velocities in between 0.74-1.5 km/s with wavelength ~500 km).

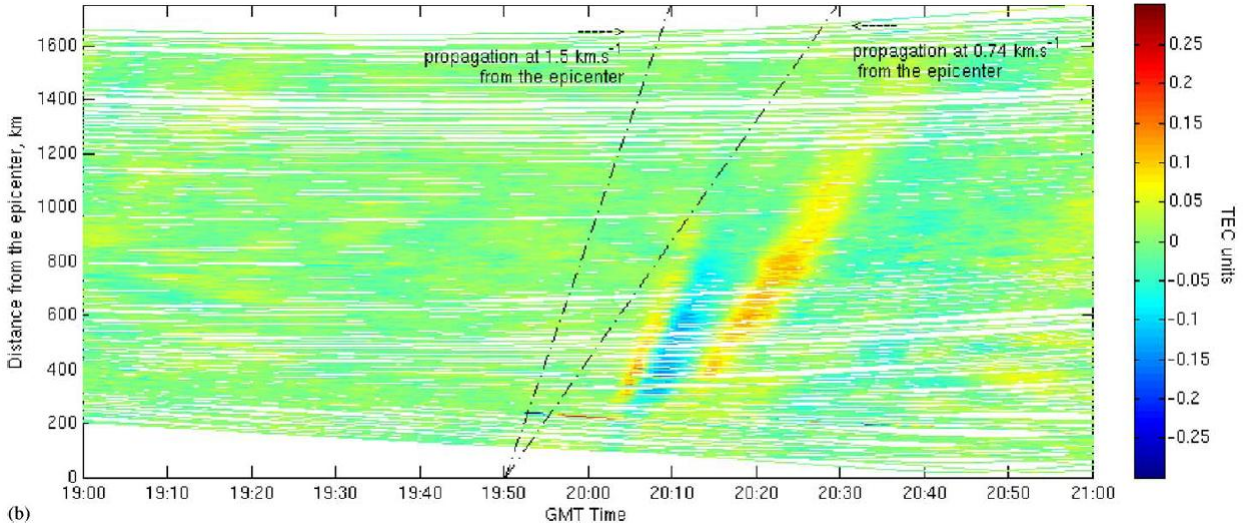

Detr. VTEC vs. EQ distance and time: Whole EQ day (259, 2015)

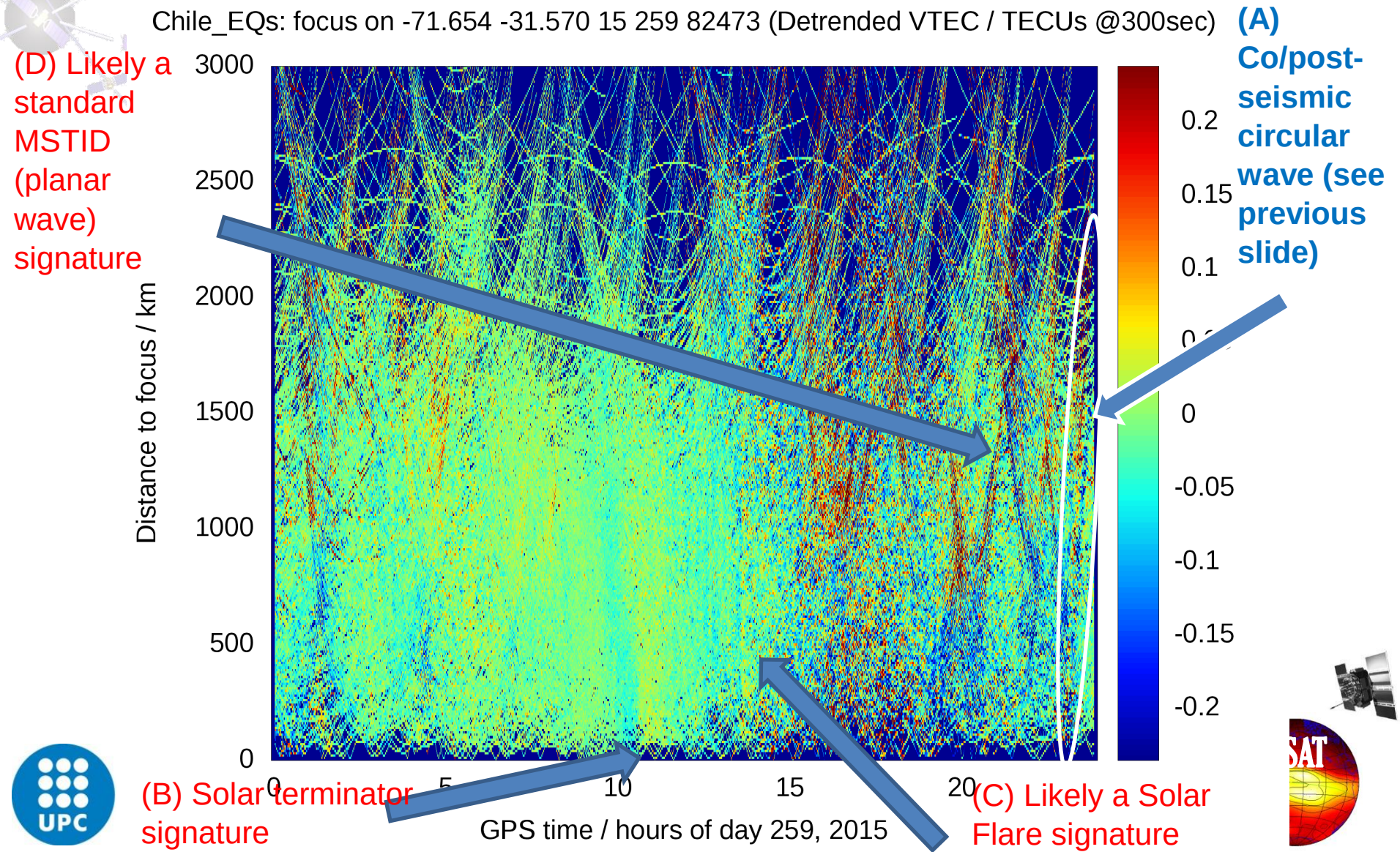

Method 1: Time evolution of map of detrended VTEC values.

- The distribution of bandwidth filtered detrended VTEC values (d2V) was not providing a direct evidence of circular waves associated with the Chile earthquake of Sep., 16th 2015[*], on the contrary than for the Tohoku earthquake of March, 11th 2011[**].
- This might be related with a simultaneous coincidence of much lower density of permanent receivers in Chile/Argentina (compared with the +1200 GNSS rec. on GEONET network on Japan), and with a lower ionospheric effect, in between the signature of the southern peak of the equatorial anomaly
- [*] ftp://newg1.upc.es/.4dimitar_and_sergey/201509_29.Chile_detrended_VTEC_maps/2015/259/d2Va_at_diff_tscales.2015.259.0300.8.gif
- [**] ftp://newg1.upc.es/.4dimitar_and_sergey/201309_30.first_study_on_Fukushima_events/d2Va_at_diff_tscales.2011.070.0300.2.gif

Method 2: detrended VTEC on a epicenter distance vs. main shock time span 3D plot

- In such situation we have reduced one dimension from (lon,lat,time,d2V) to (dtime,distance,d2V) where “dtime” is the time elapsed since the earthquake mainshock and “distance” is the distance of the ionospheric pierce point to the earthquake mainshock epicenter, following the procedure of Lognonne et al. 2006.

Reference: *Lognonné, P., Artru, J., Garcia, R., Crespon, F., Ducic, V., Jeansou, E., ... & Godet, P. E. (2006). Ground-based GPS imaging of ionospheric post-seismic signal. Planetary and Space Science, 54(5), 528-540.*

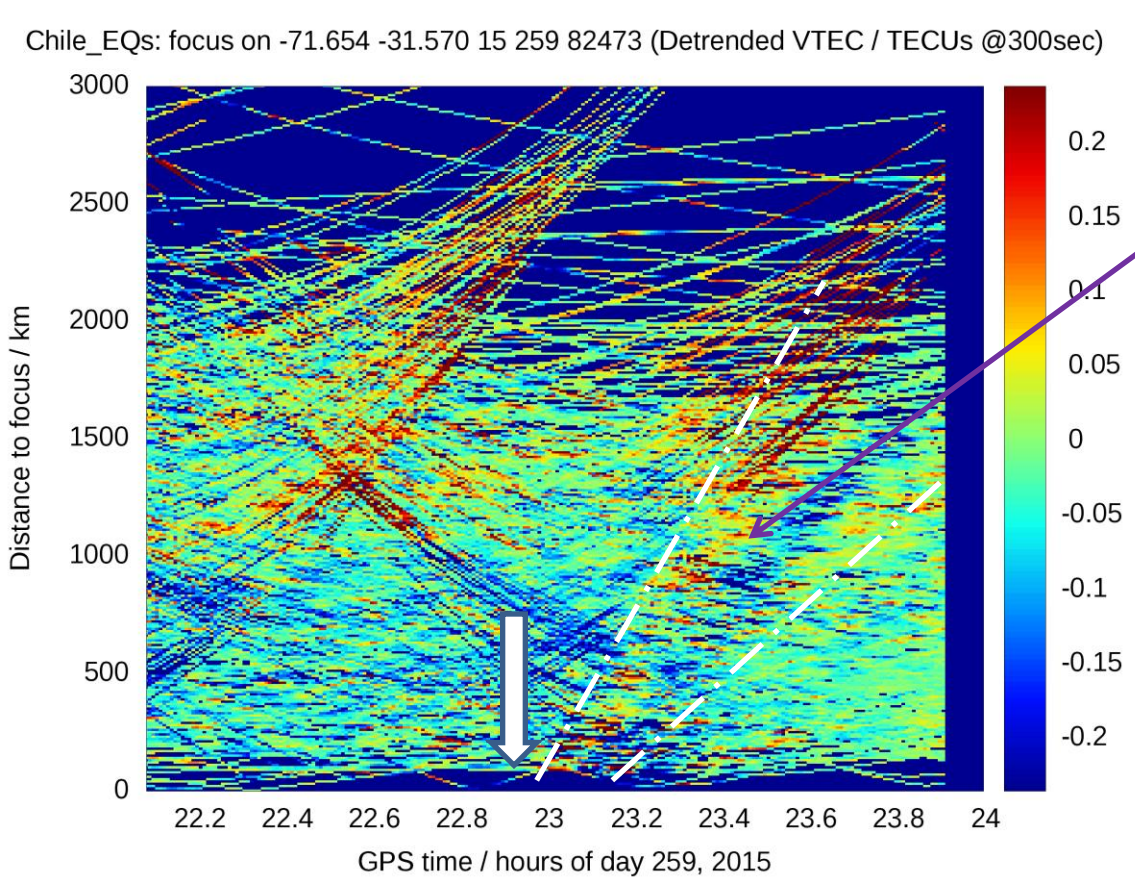

(A) Co-seismic circular wave signature with similar parameters than in previous EQs

One and half cycle of circular waves clearly seen starting at ~23:03, about 8 minutes after the Illapel EQ main shock (22:54:33 UTC = 22:54:50 GPStime = 82490 sec) , showing a range of velocities of 1000 km in 0.3 hours = 0.93 km/s to 1000 km in 0.55 hours = 0.51 km/s) and wavelength from ~100 km close to the epicenter to ~200 km at 1000 km.

Such distribution is very similar to the distribution observed at Hokkaido EQ. by Lognonné et al. (~600 s. after main shock and with velocities in between 0.74-1.5 km/s with wavelength ~500 km).

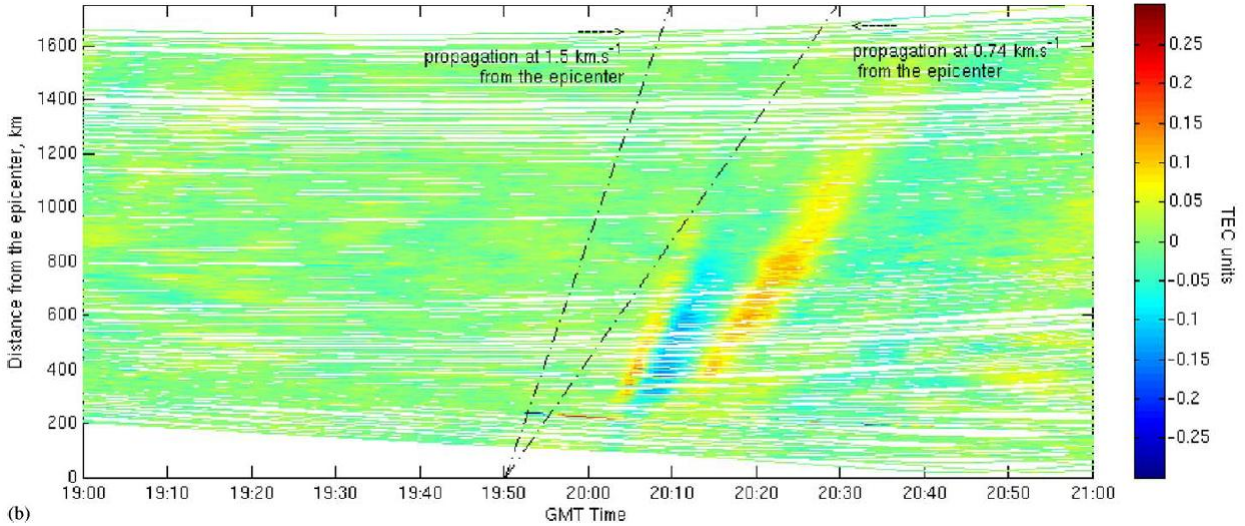

Detr. VTEC vs. EQ distance and time: Whole EQ day (259, 2015)

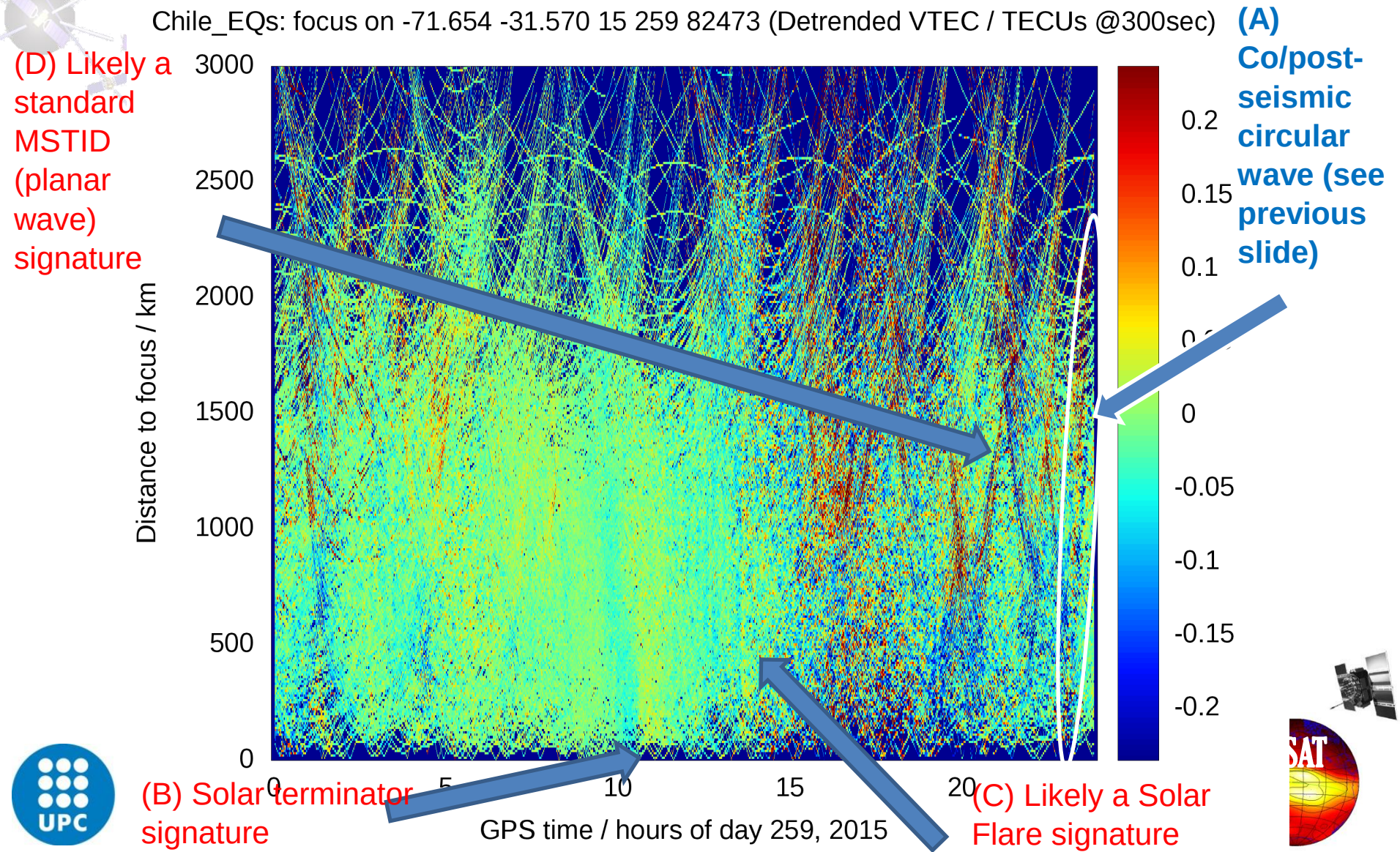

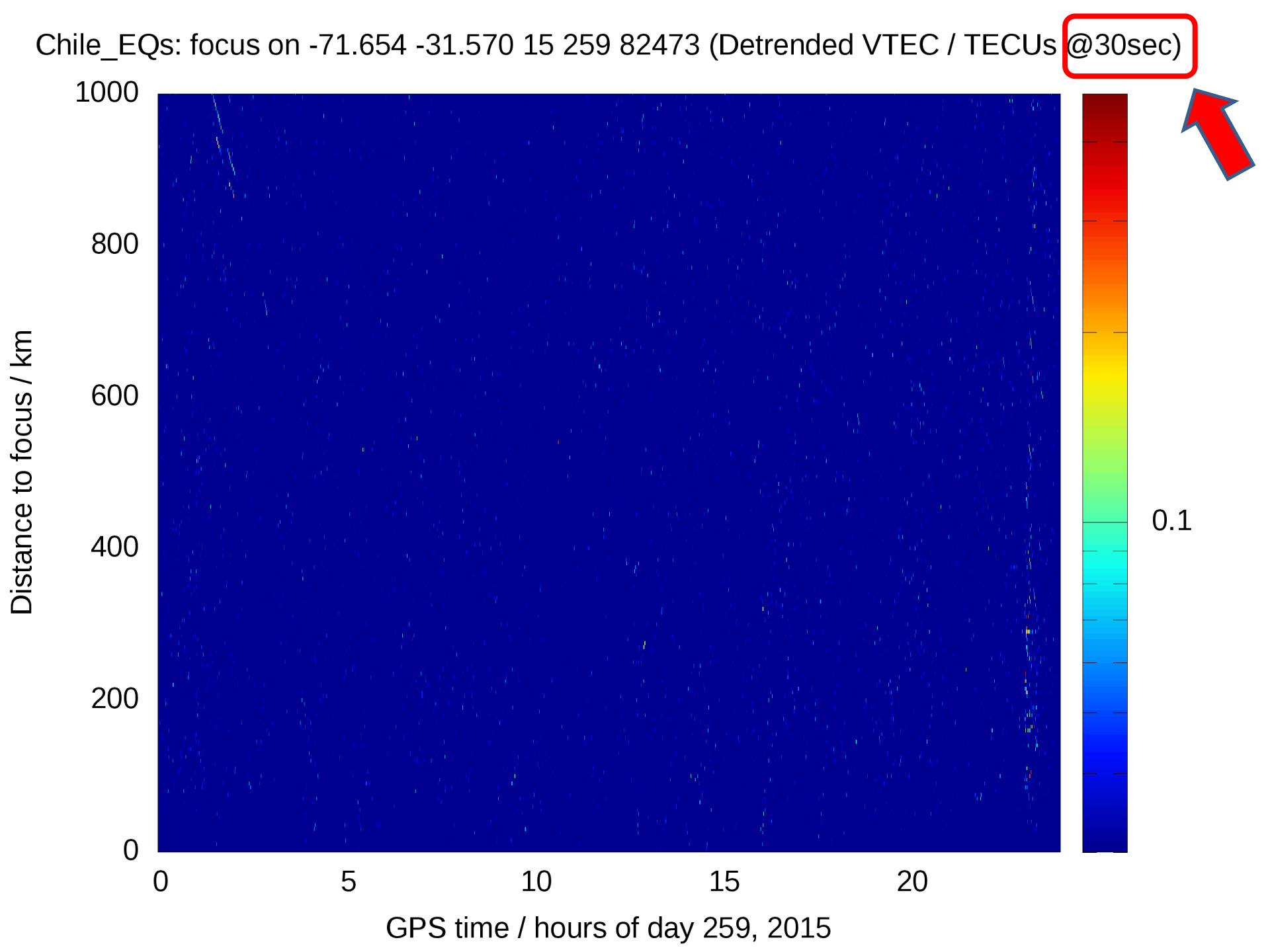
Chile_EQs: focus on -71.654 -31.570 15 259 82473 (Detrended VTEC / TECUs @30sec)
1000
800
600
400
200
0
Distance to focus / km
0
5
10
15
20
GPS time / hours of day 259, 2015
0.1

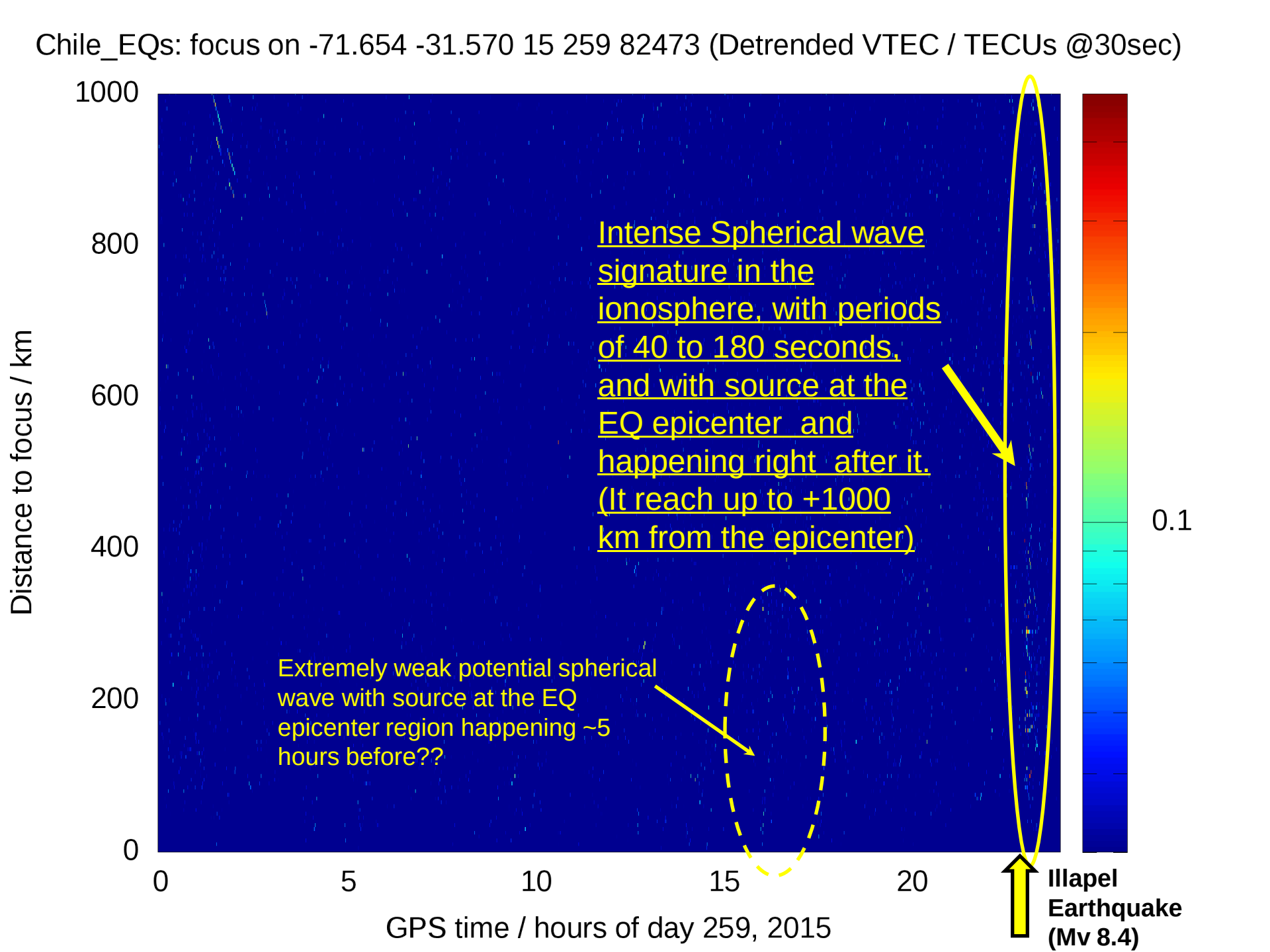
Chile_EQs: focus on -71.654 -31.570 15 259 82473 (Detrended VTEC / TECUs @30sec)
1000
800
600
400
200
0
Distance to focus / km
0
5
10
15
20
GPS time / hours of day 259, 2015
Intense Spherical wave signature in the ionosphere, with periods of 40 to 180 seconds, and with source at the EQ epicenter and happening right after it. (It reach up to +1000 km from the epicenter)
Extremely weak potential spherical wave with source at the EQ epicenter region happening ~5 hours before??
0.1
Illapel Earthquake (Mv 8.4)

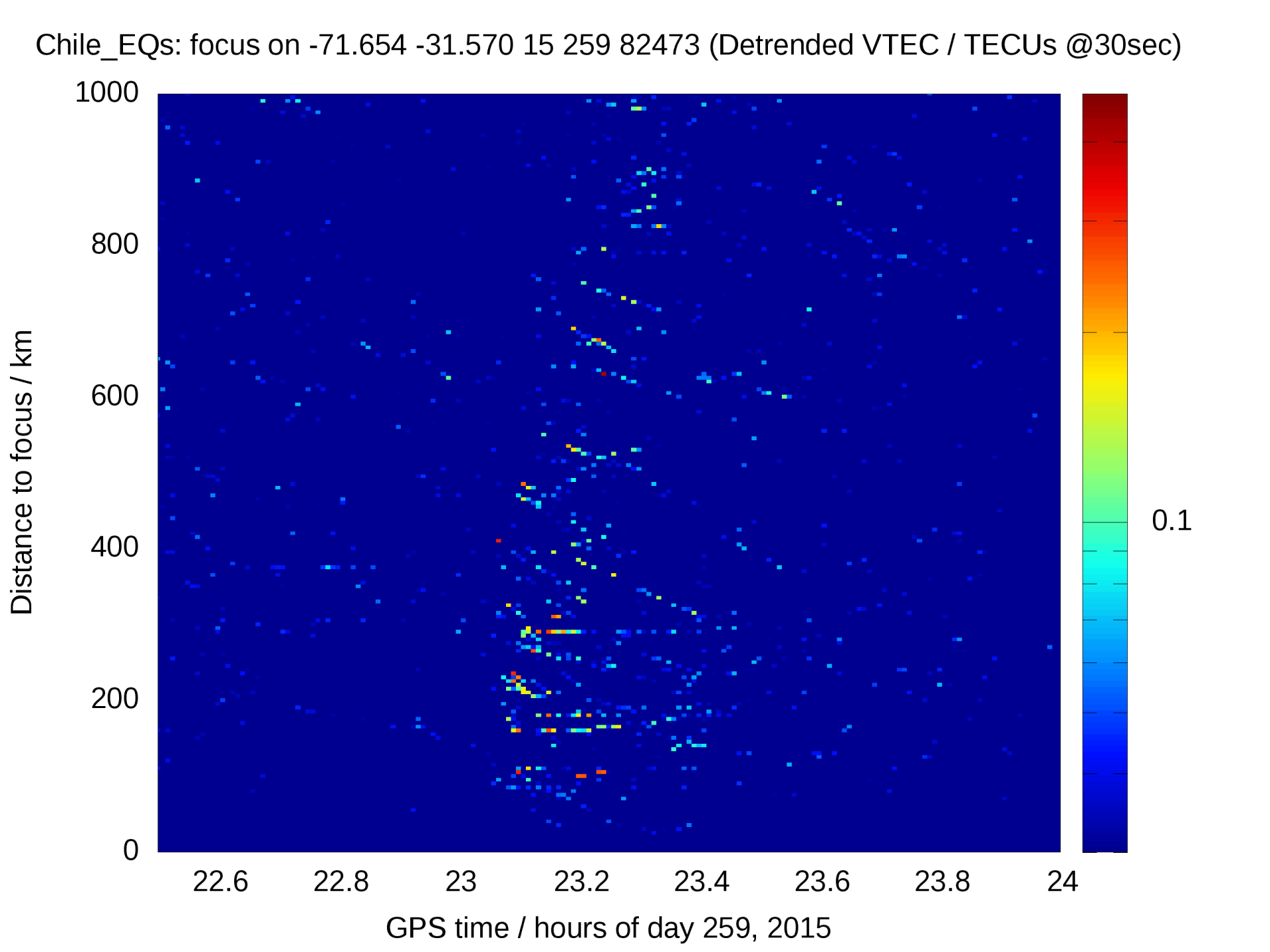
Chile_EQs: focus on -71.654 -31.570 15 259 82473 (Detrended VTEC / TECUs @30sec)
1000
800
600
400
200
0
Distance to focus / km
22.6
22.8
23
23.2
23.4
23.6
23.8
24
GPS time / hours of day 259, 2015
0.1

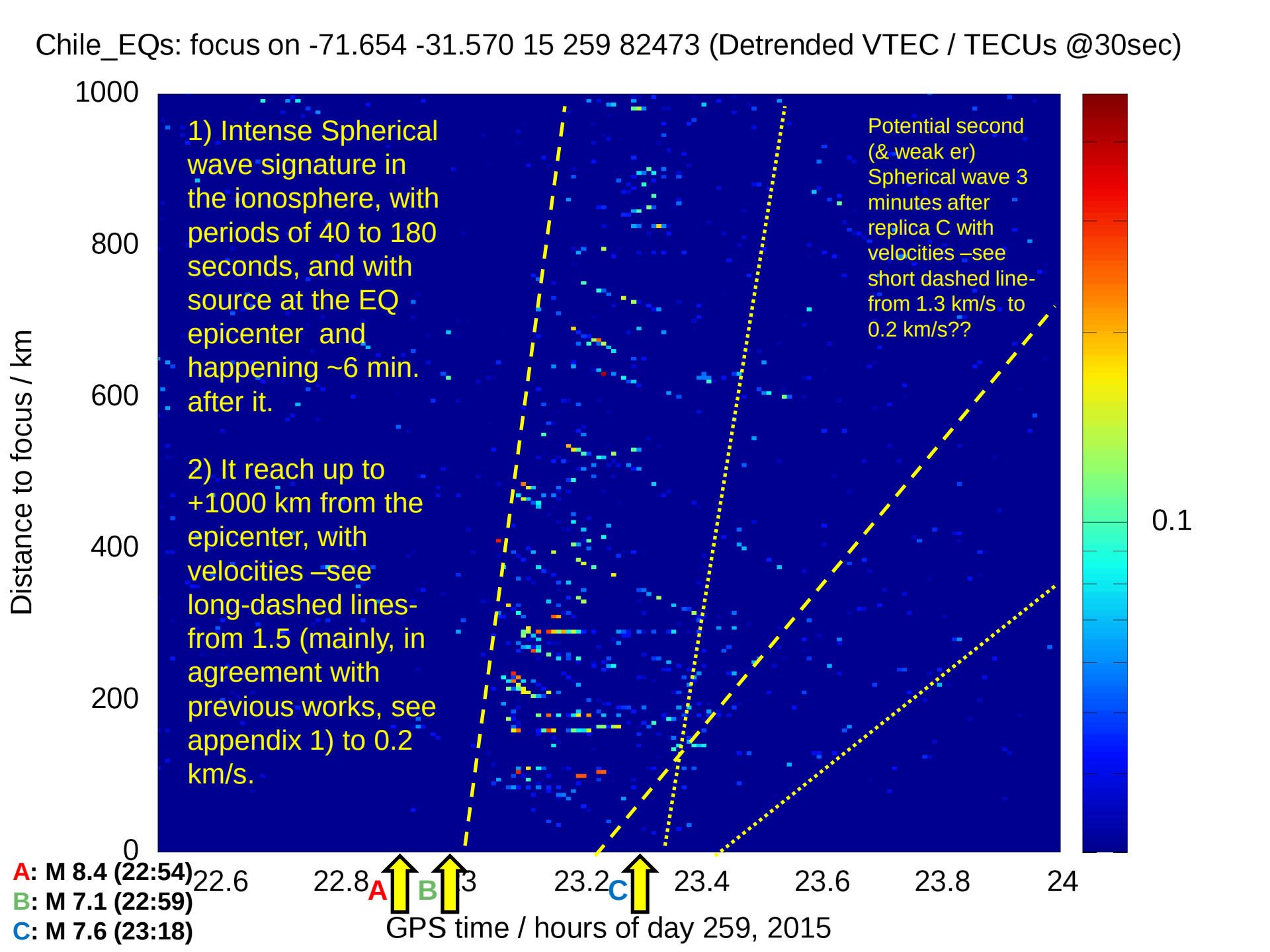
Chile_EQs: focus on -71.654 -31.570 15 259 82473 (Detrended VTEC / TECUs @30sec)
1) Intense Spherical wave signature in the ionosphere, with periods of 40 to 180 seconds, and with source at the EQ epicenter and happening ~6 min. after it.
2) It reach up to +1000 km from the epicenter, with velocities –see long-dashed lines- from 1.5 (mainly, in agreement with previous works, see appendix 1) to 0.2 km/s.
Potential second (& weak er) Spherical wave 3 minutes after replica C with velocities –see short dashed line- from 1.3 km/s to 0.2 km/s??
Distance to focus / km
1000
800
600
400
200
0
0.1
22.6
22.8
23
23.2
23.4
23.6
23.8
24
A
B
C
GPS time / hours of day 259, 2015
A: M 8.4 (22:54)
B: M 7.1 (22:59)
C: M 7.6 (23:18)

Layout:

1) [**Motivation**] Precise Agriculture (PA) presentation (EU AUDITOR experiment)

2) [**Background**]: Brief introduction to main identified points of the presentation:
   a) GPS fundamentals: pseudoranges and carrier phases (optional)
   b) Ionospheric electron content
   c) Wide Area Real-Time Kinematic
   d) The International GNSS Service (*optional*)

3) [**One efficient operative system**] Quick introduction to Linux (*optional*)

4) [**New tools for learning and research**] IonSAT Tools (IT), emulating Real-Time (RT) as much as possible (presented on the PA AUDITOR experiment):
   a) *gim2vtec.v2.scr*
   b) *gimrnx2stec.v2.scr*

5) [**IT application to ECLIPSE, FLARE & GSTORM scenarios**] (*optional*).

6) [**Example of RT GPS-ionospheric system**]: UPC-IonSAT since 2012.

7) [**Monitoring of co-seismic generated ionospheric signals]:** Application of RT ionospheric sounding for potential Tsunami warnings), with GNSS dense (Tohoku and mid earthquakes, EQ) and sparse networks (Chile 2015 EQ).

8) [**Conclusions**]

Conclusions

- The real-time ionospheric sounding with GNSS is playing an increasing role in improving different areas, such as precise real-time positioning, space weather monitoring, earthquake signatures and potential tsunami detection, among others.

- Many of the above mentioned contributions can be easily implemented in real-time.

MANY THANKS FOR YOUR ATTENTION!